EUROPEAN ORGANIZATION FOR NUCLEAR RESEARCH (CERN)

CERN-EP-2019-028
2020/10/06

CMS-TOP-18-004

Measurement of $\mathrm{t\bar{t}}$ normalised multi-differential cross sections in pp collisions at $\sqrt{s} = 13\,\mathrm{TeV}$, and simultaneous determination of the strong coupling strength, top quark pole mass, and parton distribution functions

The CMS Collaboration*

Abstract

Normalised multi-differential cross sections for top quark pair ($\mathrm{t\bar{t}}$) production are measured in proton-proton collisions at a centre-of-mass energy of 13 TeV using events containing two oppositely charged leptons. The analysed data were recorded with the CMS detector in 2016 and correspond to an integrated luminosity of $35.9\,\mathrm{fb}^{-1}$. The double-differential $\mathrm{t\bar{t}}$ cross section is measured as a function of the kinematic properties of the top quark and of the $\mathrm{t\bar{t}}$ system at parton level in the full phase space. A triple-differential measurement is performed as a function of the invariant mass and rapidity of the $\mathrm{t\bar{t}}$ system and the multiplicity of additional jets at particle level. The data are compared to predictions of Monte Carlo event generators that complement next-to-leading-order (NLO) quantum chromodynamics (QCD) calculations with parton showers. Together with a fixed-order NLO QCD calculation, the triple-differential measurement is used to extract values of the strong coupling strength α_S and the top quark pole mass ($m_\mathrm{t}^\mathrm{pole}$) using several sets of parton distribution functions (PDFs). The measurement of $m_\mathrm{t}^\mathrm{pole}$ exploits the sensitivity of the $\mathrm{t\bar{t}}$ invariant mass distribution to $m_\mathrm{t}^\mathrm{pole}$ near the production threshold. Furthermore, a simultaneous fit of the PDFs, α_S, and $m_\mathrm{t}^\mathrm{pole}$ is performed at NLO, demonstrating that the new data have significant impact on the gluon PDF, and at the same time allow an accurate determination of α_S and $m_\mathrm{t}^\mathrm{pole}$. The values $\alpha_\mathrm{S}(m_\mathrm{Z}) = 0.1135^{+0.0021}_{-0.0017}$ and $m_\mathrm{t}^\mathrm{pole} = 170.5 \pm 0.8\,\mathrm{GeV}$ are extracted, which account for experimental and theoretical uncertainties, the latter being estimated from NLO scale variations. Possible effects from Coulomb and soft-gluon resummation near the $\mathrm{t\bar{t}}$ production threshold are neglected in these parameter extractions. A rough estimate of these effects indicates an expected correction of $m_\mathrm{t}^\mathrm{pole}$ of the order of $+1\,\mathrm{GeV}$, which can be regarded as additional theoretical uncertainty in the current $m_\mathrm{t}^\mathrm{pole}$ extraction.

*See Appendix D for the list of collaboration members

"Published in the European Physical Journal C as doi:10.1140/epjc/s10052-020-7917-7."

1 Introduction

Measurements of top quark pair ($\mathrm{t\bar{t}}$) production are important for checking the validity of the standard model (SM) and searching for new phenomena. In particular, the large data set delivered by the CERN LHC allows precise measurements of the $\mathrm{t\bar{t}}$ production cross section as a function of $\mathrm{t\bar{t}}$ kinematic observables. These can be used to check the most recent predictions of perturbative quantum chromodynamics (QCD) and to constrain input parameters, some of which are fundamental to the SM. At the LHC, top quarks are predominantly produced via gluon-gluon fusion. Using measurements of the production cross section in a global fit of parton distribution functions (PDFs) can help determine the gluon distribution at large values of x [1–3], where x is the fraction of the proton momentum carried by a parton. Furthermore, measurements of the cross section as a function of the $\mathrm{t\bar{t}}$ invariant mass, from the threshold to the TeV region, provide high sensitivity for constraining the top quark pole mass, $m_{\mathrm{t}}^{\mathrm{pole}}$, which is defined as the pole of the top quark propagator (see e.g. Refs. [4–6]). At LHC energies, a large fraction of $\mathrm{t\bar{t}}$ events is produced with additional hard jets in the final state. Events containing such additional jets constitute important backgrounds for interesting but rare SM processes such as the associated production of a Higgs boson and $\mathrm{t\bar{t}}$, as well as for searches for new physics associated with $\mathrm{t\bar{t}}$ production, and must therefore be well understood. Within the SM, processes with extra jets can also be used to constrain the strong coupling strength, α_{S}, at the scale of the top quark mass. Furthermore, the production of $\mathrm{t\bar{t}}$ in association with extra jets provides additional sensitivity to $m_{\mathrm{t}}^{\mathrm{pole}}$ since gluon radiation depends on $m_{\mathrm{t}}^{\mathrm{pole}}$ through threshold and cone effects [7].

Differential cross sections for $\mathrm{t\bar{t}}$ production have been measured previously in proton-antiproton collisions at the Tevatron at a centre-of-mass energy of 1.96 TeV [8, 9] and in proton-proton (pp) collisions at the LHC at $\sqrt{s} = 7$ TeV [10–14], 8 TeV [14–21], and 13 TeV [22–27]. A milestone was reached in three CMS analyses [20, 22, 23], where the $\mathrm{t\bar{t}}$ production dynamics was probed with double-differential cross sections. The first analysis [20] used data recorded at $\sqrt{s} = 8$ TeV by the CMS experiment in 2012. Only $\mathrm{t\bar{t}}$ decays where, after the decay of each top quark into a bottom quark and a W boson, both of the W bosons decay leptonically were considered. Specifically, the $\mathrm{e}^{\pm}\mu^{\mp}$ decay mode ($\mathrm{e}\mu$) was selected, requiring two oppositely charged leptons and at least two jets. Our present paper provides a new measurement, following the procedures of Ref. [20]. It is based on data taken by the CMS experiment in 2016 at $\sqrt{s} = 13$ TeV, corresponding to an integrated luminosity of $35.9 \pm 0.9\,\mathrm{fb}^{-1}$. In addition to $\mathrm{e}\mu$, the decay modes $\mathrm{e^+e^-}$ (ee) and $\mu^+\mu^-$ ($\mu\mu$) are also selected, roughly doubling thereby the total number of expected $\mathrm{t\bar{t}}$ signal events. Our latest measurement complements the analyses [22, 23], based on data taken at $\sqrt{s} = 13$ TeV, but using $\mathrm{t\bar{t}}$ decays in the ℓ+jets ($\ell = \mathrm{e}, \mu$) final state.

As in the previous work [20], measurements are performed of the normalised double-differential $\mathrm{t\bar{t}}$ production cross section as a function of observables describing the kinematic properties of the top quark, top antiquark, and the $\mathrm{t\bar{t}}$ system: the transverse momentum of the top quark, $p_{\mathrm{T}}(\mathrm{t})$, rapidity of the top quark, $y(\mathrm{t})$; the transverse momentum, $p_{\mathrm{T}}(\mathrm{t\bar{t}})$, the rapidity, $y(\mathrm{t\bar{t}})$, and invariant mass, $M(\mathrm{t\bar{t}})$, of the $\mathrm{t\bar{t}}$ system; the pseudorapidity difference between the top quark and antiquark, $\Delta\eta(\mathrm{t}, \bar{\mathrm{t}})$, and the angle between the top quark and antiquark in the transverse plane, $\Delta\phi(\mathrm{t}, \bar{\mathrm{t}})$. When referring to the kinematic variables $p_{\mathrm{T}}(\mathrm{t})$ and $y(\mathrm{t})$, we use only the parameters of the top quark and not of the top antiquark, to avoid double counting of events. In all, the double-differential $\mathrm{t\bar{t}}$ cross section is measured as a function of six different pairs of kinematic variables. As demonstrated in Ref. [20], the different combinations of kinematic variables are sensitive to different aspects of the QCD calculations.

For the first time at the LHC, the triple-differential cross section is measured as a function of $M(\mathrm{t\bar{t}})$, $y(\mathrm{t\bar{t}})$, and N_{jet}, where N_{jet} is the number of extra jets not arising from the decay of the $\mathrm{t\bar{t}}$ system. For this purpose, the kinematic reconstruction algorithm is optimised to determine the invariant mass of the $\mathrm{t\bar{t}}$ system in an unbiased way. As will be shown below, the triple-differential measurements provide tight constraints on the parametrised gluon PDF, as well as on α_{S}, and $m_{\mathrm{t}}^{\mathrm{pole}}$. Previous studies of additional jet activity in $\mathrm{t\bar{t}}$ events at the LHC can be found in Refs. [23, 28, 29]. The α_{S} and $m_{\mathrm{t}}^{\mathrm{pole}}$ parameters were also extracted from measurements of the total inclusive $\mathrm{t\bar{t}}$ production cross sections in Refs. [30–35].

The measurements are defined at parton level and must therefore be corrected for effects of hadronisation, and detector resolution and inefficiency. A regularised unfolding process is performed simultaneously in bins of the two or three variables in which the cross sections are measured. The normalised differential $\mathrm{t\bar{t}}$ cross section is determined by dividing the distributions by the measured total inclusive $\mathrm{t\bar{t}}$ production cross section, where the latter is evaluated by integrating over all bins in the respective observables.

The parton-level results are compared with theoretical predictions obtained with the generators POWHEG (version 2) [36, 37] and MG5_aMC@NLO [38], interfaced to PYTHIA [39, 40] for parton showering, hadronisation, and multiple-parton interactions (MPIs). They are also compared to theoretical predictions obtained at next-to-leading-order (NLO) QCD using several sets of PDFs,t after applying corrections for non-perturbative (NP) effects.

The structure of the paper is as follows: Section 2 contains a brief description of the CMS detector. Details of the event simulation are given in Section 3. The event selection, kinematic reconstruction, and comparison between data and simulation are described in Section 4. The unfolding procedure is detailed in Section 5, the method to determine the differential cross sections is presented in Section 6, and the assessment of the systematic uncertainties is discussed in Section 7. We show the results of the measurement and their comparison to theoretical predictions in Section 8. Section 9 presents the extraction of α_{S} and $m_{\mathrm{t}}^{\mathrm{pole}}$ from the measured $\mathrm{t\bar{t}}$ cross section, using several sets of PDFs, and Section 10 presents the simultaneous fit of the PDFs, α_{S}, and $m_{\mathrm{t}}^{\mathrm{pole}}$ to the data. Finally, Section 11 provides a summary.

2 The CMS detector

The central feature of the CMS apparatus is a superconducting solenoid of 6 m internal diameter, providing a magnetic field of 3.8 T. Within the solenoid volume are a silicon pixel and strip tracker, a lead tungstate crystal electromagnetic calorimeter (ECAL), and a brass and scintillator hadron calorimeter, each composed of a barrel and two endcap sections. Forward calorimeters extend the η coverage provided by the barrel and endcap detectors. Muons are measured in gas-ionisation detectors embedded in the steel flux-return yoke outside the solenoid. Events of interest are selected using a two-tiered trigger system [41]. The first level, composed of custom hardware processors, uses information from the calorimeters and muon detectors to select events at a rate of around 100 kHz within a time interval of less than 4 μs. The second level, known as the high-level trigger (HLT), consists of a farm of processors running a version of the full event reconstruction software optimised for fast processing, and reduces the event rate to around 1 kHz before data storage. A more detailed description of the CMS detector, together with a definition of the coordinate system used and the relevant kinematic variables, can be found in Ref. [42].

3 Event simulation

Simulations of physics processes are performed with Monte Carlo (MC) event generators and serve three purposes: firstly, to obtain representative SM predictions of $\mathrm{t\bar{t}}$ production cross sections to be compared to the results of this analysis. Secondly, when interfacing generated $\mathrm{t\bar{t}}$ signal events with a detector simulation, to determine corrections for the effects of hadronisation, reconstruction and selection efficiencies, and resolutions that are to be applied to the data. Thirdly, when interfacing generated background processes to the detector simulation, to obtain predictions for the backgrounds. All MC programs used in this analysis perform the event generation in several steps: matrix-element (ME) level, parton showering matched to ME, hadronisation, and underlying event, including multiparton interaction (MPI). The $\mathrm{t\bar{t}}$ signal processes are simulated with ME calculations at NLO in QCD. For all simulations the proton structure is described by the NNPDF 3.0 NLO PDF set with $\alpha_S(m_Z) = 0.118$ [43] where $m_Z = 91\,\text{GeV}$ is the Z boson mass [44], and the value of the top quark mass parameter is fixed to $m_t^{MC} = 172.5\,\text{GeV}$. For the default signal simulation, the POWHEG (version 2) [36, 45, 46] generator is taken. The h_{damp} parameter of POWHEG, which regulates the damping of real emissions in the NLO calculation when matching to the parton shower, is set to $h_{damp} = 1.581 m_t^{MC}$ [47]. The PYTHIA program (version 8.2) [40] with the CUETP8M2T4 tune [47–49] is used to model parton showering, hadronisation and MPIs. An alternative sample is generated using the MG5_aMC@NLO (version 2.2.2) [38] generator, including up to two extra partons at the ME level at NLO. In this setup, referred to as MG5_aMC@NLO + PYTHIA, MADSPIN [50] is used to model the decays of the top quarks while preserving their spin correlation. The events are matched to PYTHIA using the FxFx prescription [51]. A second alternative sample is generated with POWHEG and interfaced with HERWIG++ (version 2.7.1) [52] using the EE5C tune [53].

The main background contributions originate from single top quarks produced in association with a W boson (tW), Z/γ^* bosons produced with additional jets (Z +jets), W boson production with additional jets (W +jets) and diboson (W W, W Z, and Z Z) events. Other backgrounds are negligible. For all background samples, the NNPDF3.0 [43] PDF set is used and parton showering, hadronisation, and MPIs are simulated with PYTHIA. Single top quark production is simulated with POWHEG (version 1) [37, 54] using the CUETP8M2T4 tune in PYTHIA with the h_{damp} parameter set to 172.5 GeV in POWHEG. The Z +jets process is simulated at NLO using MG5_aMC@NLO with up to two additional partons at ME level and matched to PYTHIA using the FxFx prescription. The W +jets process is simulated at leading order (LO) using MG5_aMC@NLO with up to four additional partons at ME level and matched to PYTHIA using the MLM prescription [55]. Diboson events are simulated with PYTHIA. Predictions are normalised based on their theoretical cross sections and the integrated luminosity of the data sample. The cross sections are calculated to approximate next-to-NLO (NNLO) for single top quark in the tW channel [56], NNLO for Z +jets and W +jets [57], and NLO for diboson production [58]. The $\mathrm{t\bar{t}}$ simulation is normalised to a cross section of $832\,^{+20}_{-29}(\text{scale}) \pm 35(\text{PDF}+\alpha_S)\,\text{pb}$ calculated with the TOP++ (version 2.0) program [59] at NNLO including resummation of next-to-next-to-leading-logarithm (NNLL) soft-gluon terms assuming $m_t^{pole} = 172.5\,\text{GeV}$ and the proton structure described by the CT14 NNLO PDF set [60].

To model the effect of additional pp interactions within the same bunch crossing (pileup), simulated minimum bias interactions are added to the simulated data. Events in the simulation are then weighted to reproduce the pileup distribution in the data, which is estimated from the measured bunch-to-bunch instantaneous luminosity assuming a total inelastic pp cross section of 69.2 mb [61].

In all cases, the interactions of particles with the CMS detector are simulated using GEANT4

(version 9.4) [62].

4 Event selection and $t\bar{t}$ kinematic reconstruction

The event selection procedure follows closely the one reported in Ref. [27]. Events are selected that correspond to the decay topology where both top quarks decay into a W boson and a b quark, and each of the W bosons decays directly into an electron or a muon and a neutrino. This defines the signal, while all other $t\bar{t}$ events, including those with at least one electron or muon originating from the decay of a τ lepton are regarded as background. The signal comprises three distinct final state channels: the same-flavour channels corresponding to two electrons (e^+e^-) or two muons ($\mu^+\mu^-$) and the different-flavour channel corresponding to one electron and one muon ($e^\pm\mu^\mp$). Final results are derived by combining the three channels.

At HLT level, events are selected either by single-lepton or dilepton triggers. The former require the presence of at least one electron or muon and the latter the presence of either two electrons, two muons, or an electron and a muon. For the single-electron and -muon triggers, p_T thresholds of 27 and 24 GeV are applied, respectively. The same-flavour dilepton triggers require either an electron pair with $p_T > 23$ GeV for the leading electron and $p_T > 12$ GeV for the subleading electron or a muon pair with $p_T > 17$ GeV for the leading muon and $p_T > 8$ GeV for the subleading muon. Here leading and subleading refers to the electron or muon with the highest and second-highest p_T, respectively, in the event. The different-flavour dilepton triggers require either an electron with $p_T > 23$ GeV and a muon with $p_T > 8$ GeV, or a muon with $p_T > 23$ GeV and an electron with $p_T > 8$ GeV.

Events are reconstructed using a particle-flow (PF) algorithm [63], which aims to identify and reconstruct each individual particle in an event with an optimised combination of information from the various elements of the CMS detector. Charged hadrons from pileup are subtracted on an event-by-event basis. Subsequently, the remaining neutral-hadron component from pileup is accounted for through jet energy corrections [64].

Electron candidates are reconstructed from a combination of the track momentum at the main interaction vertex, the corresponding energy deposition in the ECAL, and the energy sum of all bremsstrahlung photons associated with the track [65]. The electron candidates are required to have $p_T > 25$ GeV for the leading candidate and $p_T > 20$ GeV for the subleading candidate and $|\eta| < 2.4$. Electron candidates with ECAL clusters in the region between the barrel and endcap ($1.44 < |\eta_{\text{cluster}}| < 1.57$) are excluded, because the reconstruction of an electron object in this region is not optimal. A relative isolation criterion $I_{\text{rel}} < 0.06$ is applied, where I_{rel} is defined as the p_T sum of all neutral hadron, charged hadron, and photon candidates within a distance of 0.3 from the electron in η–ϕ space, divided by the p_T of the electron candidate. In addition, electron identification requirements are applied to reject misidentified electron candidates and candidates originating from photon conversions. Muon candidates are reconstructed using the track information from the tracker and the muon system. They are required to have $p_T > 25$ GeV for the leading candidate and $p_T > 20$ GeV for the subleading candidate and $|\eta| < 2.4$. An isolation requirement of $I_{\text{rel}} < 0.15$ is applied to muon candidates, including particles within a distance of 0.4 from the muon in η–ϕ space. In addition, muon identification requirements are applied to reject misidentified muon candidates and candidates originating from in-flight decay processes. For both electron and muon candidates, a correction is applied to I_{rel} to suppress residual pileup effects.

Jets are reconstructed by clustering the PF candidates using the anti-k_T clustering algorithm [66, 67] with a distance parameter $R = 0.4$. The jet energies are corrected following the procedures

described in Ref. [68] and applied to the data taken by the CMS experiment in 2016. After correcting for all residual energy depositions from charged and neutral particles from pileup, p_T- and η-dependent jet energy corrections are applied to correct for the detector response. A jet is selected if it has $p_T > 30\,\text{GeV}$ and $|\eta| < 2.4$. Jets are rejected if the distance in η–ϕ space between the jet and the closest lepton is less than 0.4. Jets originating from the hadronisation of b quarks (b jets) are identified with an algorithm [69] that uses secondary vertices together with track-based lifetime information to construct a b tagging discriminant. The chosen working point has a b jet tagging efficiency of ≈80–90% and a mistagging efficiency of ≈10% for jets originating from gluons, as well as u, d, or s quarks, and ≈30–40% for jets originating from c quarks.

The missing transverse momentum vector $\vec{p}_T^{\,\text{miss}}$ is defined as the projection on the plane perpendicular to the beams of the negative vector sum of the momenta of all PF candidates in an event. Its magnitude is referred to as p_T^{miss}. Jet energy corrections are propagated to improve the determination of $\vec{p}_T^{\,\text{miss}}$.

Events are selected offline if they contain exactly two isolated electrons or muons of opposite electric charge. Furthermore, they need to contain at least two jets and at least one of these jets must be b tagged. Events with an invariant mass of the lepton pair, $M(\ell\ell)$, smaller than 20 GeV are removed in order to suppress contributions from heavy-flavour resonance decays and low-mass Drell–Yan processes. Backgrounds from Z +jets processes in the e^+e^- and $\mu^+\mu^-$ channels are further suppressed by requiring $|m_Z - M(\ell\ell)| > 15\,\text{GeV}$, and $p_T^{\text{miss}} > 40\,\text{GeV}$. The remaining background contribution from tW, Z +jets, W +jets, diboson and $t\bar{t}$ events from decay channels other than that of the signal are estimated from the simulation.

In this analysis, the $t\bar{t}$ production cross section is also measured as a function of the extra jet multiplicity, N_{jet}. Extra jets (also referred to as additional jets) are jets arising primarily from hard QCD radiation and not from the top quark decays. At generator level, the extra jets are defined in dilepton $t\bar{t}$ events as jets with $p_T > 30\,\text{GeV}$, $|\eta| < 2.4$, built of particles except neutrinos using the anti-k_T clustering algorithm [66, 67] with a distance parameter $R = 0.4$, and isolated from the charged leptons (i.e. e or μ) and b quarks originating from the top quark decays by a minimal distance of 0.4 in η–ϕ space. The charged leptons and b quarks are taken directly after W and top quark decays, respectively. At reconstruction level the extra jets are defined in dilepton $t\bar{t}$ candidate events as jets with $p_T > 30\,\text{GeV}$, $|\eta| < 2.4$, and isolated from the leptons and b jets originating from the top quark decays by the same minimal distance in η–ϕ space.

The $t\bar{t}$ kinematic properties are determined from the four-momenta of the decay products using a kinematic reconstruction method [15]. The three-momenta of the neutrino (ν) and of the antineutrino ($\bar{\nu}$) are not directly measured, but they can be reconstructed by imposing the following six kinematic constraints: the conservation in the event of the total transverse momentum vector, and the masses of the W bosons, top quark, and top antiquark. The reconstructed top quark and antiquark masses are required to be 172.5 GeV. The $\vec{p}_T^{\,\text{miss}}$ in the event is assumed to originate solely from the two neutrinos in the top quark and antiquark decay chains. To resolve the ambiguity due to multiple algebraic solutions of the equations for the neutrino momenta, the solution with the smallest invariant mass of the $t\bar{t}$ system is taken. The reconstruction is performed 100 times, each time randomly smearing the measured energies and directions of the reconstructed leptons and jets within their resolution. This smearing procedure recovers certain events that initially yield no solution because of measurement uncertainties. The three-momenta of the two neutrinos are determined as a weighted average over all smeared solutions. For each solution, the weight is calculated based on the expected true spectrum of

the invariant mass of a lepton and a b jet stemming from the decay of a top quark and taking the product of the two weights for the top quark and antiquark decay chains. All possible lepton-jet combinations in the event that satisfy the requirement on the invariant mass of the lepton and jet $M_{\ell b} < 180\,\text{GeV}$ are considered. Combinations are ranked based on the presence of b-tagged jets in the assignments, i.e. a combination with both leptons assigned to b-tagged jets is preferred over those with one or no b-tagged jet. Among assignments with equal number of b-tagged jets, the one with the highest sum of weights is chosen. Events with no solution after smearing are discarded. The efficiency of the kinematic reconstruction, defined as the number of events where a solution is found divided by the total number of selected $\mathrm{t\bar{t}}$ events, is studied in data and simulation and consistent results are observed. The efficiency is about 90% for signal events. After applying the full event selection and the kinematic reconstruction of the $\mathrm{t\bar{t}}$ system, 150 410 events are observed in the $\mathrm{e}^{\pm}\mu^{\mp}$ channel, 34 890 events in the $\mathrm{e}^{+}\mathrm{e}^{-}$ channel, and 70 346 events in the $\mu^{+}\mu^{-}$ channel. Combining all decay channels, the estimated signal fraction in data is 80.6%. Figure 1 shows the distributions of the reconstructed top quark and $\mathrm{t\bar{t}}$ kinematic variables and of the multiplicity of additional jets in the events. In general, the data are reasonably well described by the simulation, however some trends are visible, in particular for $p_{\mathrm{T}}(\mathrm{t})$, where the simulation predicts a somewhat harder spectrum than that observed in data, as reported in previous differential $\mathrm{t\bar{t}}$ cross section measurements [15, 18, 20, 22, 23, 26, 27].

The $M(\mathrm{t\bar{t}})$ value obtained using the full kinematic reconstruction described above is highly sensitive to the value of the top quark mass used as a kinematic constraint. Since one of the objectives of this analysis is to extract the top quark mass from the differential $\mathrm{t\bar{t}}$ measurements, exploiting the $M(\mathrm{t\bar{t}})$ distribution in particular, an alternative algorithm is employed, which reconstructs the $\mathrm{t\bar{t}}$ kinematic variables without using the top quark mass constraint. This algorithm is referred to as the "loose kinematic reconstruction". In this algorithm, the $\nu\overline{\nu}$ system is reconstructed rather than the ν and $\overline{\nu}$ separately. Consequently, it can only be used to reconstruct the total $\mathrm{t\bar{t}}$ system but not the top quark and antiquark separately. As in the full kinematic reconstruction, all possible lepton-jet combinations in the event that satisfy the requirement on the invariant mass of the lepton and jet $M_{\ell b} < 180\,\text{GeV}$ are considered. Combinations are ranked based on the presence of b-tagged jets in the assignments, but among combinations with equal number of b-tagged jets, the ones with the highest-p_{T} jets are chosen. The kinematic variables of the $\nu\overline{\nu}$ system are derived as follows: its $\vec{p}_{\mathrm{T}}$ is set equal to $\vec{p}_{\mathrm{T}}^{\,\mathrm{miss}}$, while its unknown longitudinal momentum and energy are set equal to the longitudinal momentum and energy of the lepton pair. Additional constraints are applied on the invariant mass of the neutrino pair, $M(\nu\overline{\nu}) \geq 0$, and on the invariant mass of the W bosons, $M(\mathrm{W}^{+}\mathrm{W}^{-}) \geq 2M_{\mathrm{W}}$, which have only minor effects on the performance of the reconstruction. The method yields similar $\mathrm{t\bar{t}}$ kinematic resolutions and reconstruction efficiency as for the full kinematic reconstruction. In this analysis, the loose kinematic reconstruction is exclusively used to measure triple-differential cross sections as a function of $M(\mathrm{t\bar{t}})$, $y(\mathrm{t\bar{t}})$, and extra jet multiplicity, which are exploited to determine QCD parameters, as well as the distributions used to cross-check the results. Figure 2 shows the distributions of the reconstructed $\mathrm{t\bar{t}}$ invariant mass and rapidity using the loose kinematic reconstruction. These distributions are similar to the ones obtained using the full kinematic reconstruction (as shown in Fig. 1). Towards forward rapidities $|y(\mathrm{t\bar{t}})| \geq 1.5$ a trend is visible in which the MC simulations predict more events than observed in the data. However, the differences between simulations and data are still compatible within the estimated shape uncertainties in the signal and backgrounds.

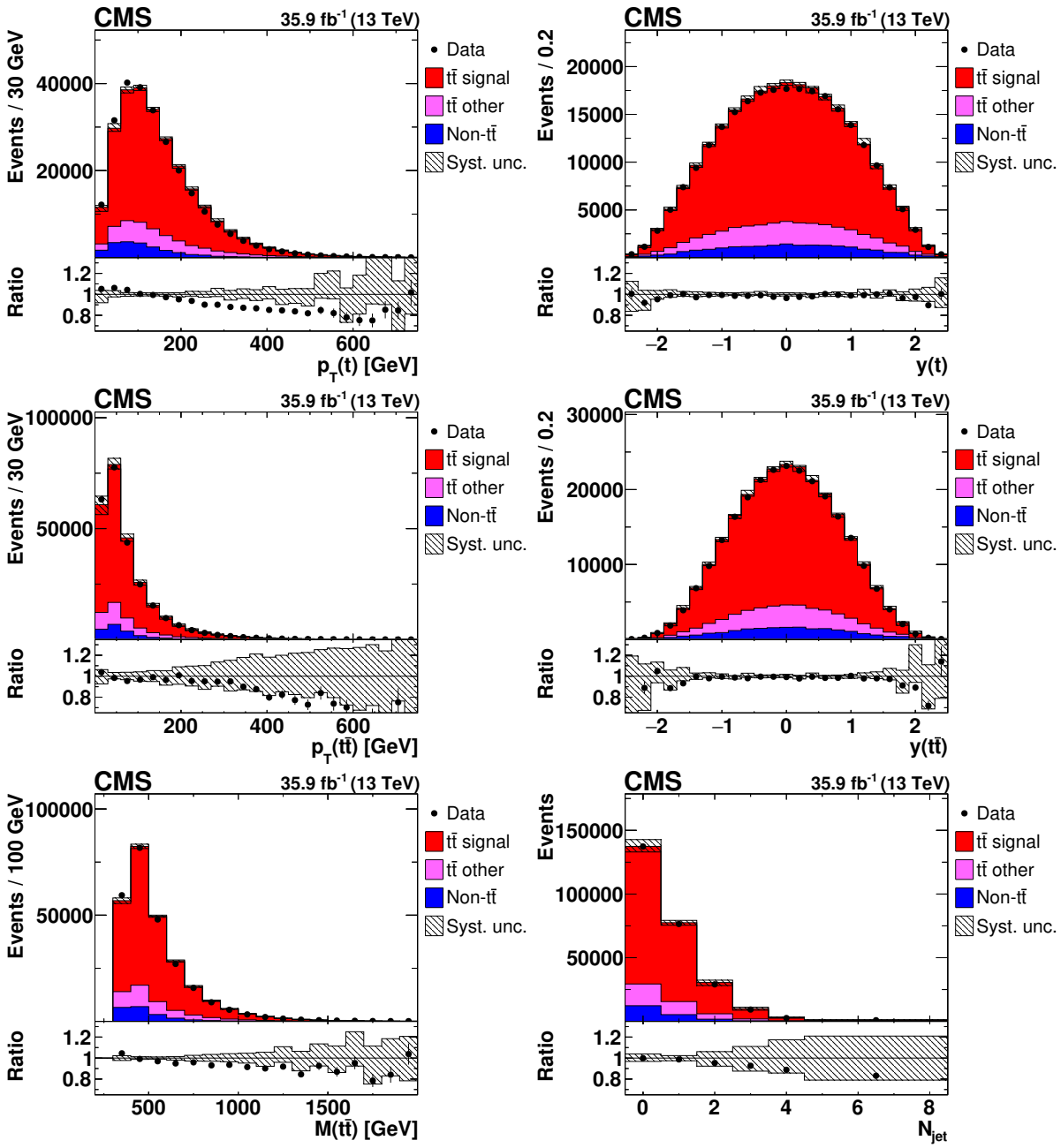

Figure 1: Distributions of $p_{\mathrm{T}}(\mathrm{t})$ (upper left), $y(\mathrm{t})$ (upper right), $p_{\mathrm{T}}(\mathrm{t\bar{t}})$ (middle left), $y(\mathrm{t\bar{t}})$ (middle right), $M(\mathrm{t\bar{t}})$ (lower left), and N_{jet} (lower right) in selected events after the kinematic reconstruction, at detector level. The experimental data with the vertical bars corresponding to their statistical uncertainties are plotted together with distributions of simulated signal and different background processes. The hatched regions correspond to the estimated shape uncertainties in the signal and backgrounds (as detailed in Section 7). The lower panel in each plot shows the ratio of the observed data event yields to those expected in the simulation.

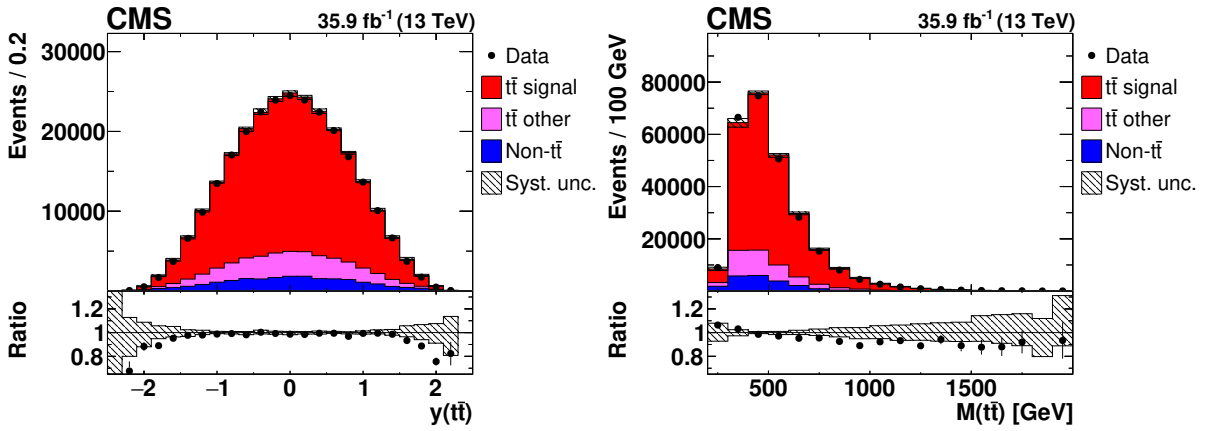

Figure 2: Distributions of $y(\mathrm{t\bar{t}})$ (left) and $M(\mathrm{t\bar{t}})$ (right) in selected events after the loose kinematic reconstruction. Details can be found in the caption of Fig. 1.

5 Signal extraction and unfolding

The number of signal events in data is extracted by subtracting the expected number of background events from the observed number of events for each bin of the observables. All expected background numbers are obtained directly from the MC simulations (see Section 3) except for $\mathrm{t\bar{t}}$ final states other than the signal. The latter are dominated by events in which one or both of the intermediate W bosons decay into τ leptons with subsequent decay into an electron or muon. These events arise from the same $\mathrm{t\bar{t}}$ production process as the signal and thus the normalisation of this background is fixed to that of the signal. For each bin the number of events obtained after the subtraction of other background sources is multiplied by the ratio of the number of selected $\mathrm{t\bar{t}}$ signal events to the total number of selected $\mathrm{t\bar{t}}$ events (i.e. the signal and all other $\mathrm{t\bar{t}}$ events) in simulation.

The numbers of signal events obtained after background subtraction are corrected for detector effects, using the TUNFOLD package [70]. The event yields in the $\mathrm{e^+e^-}$, $\mu^+\mu^-$ and $\mathrm{e^\pm}\mu^\mp$ channels are added together, and the unfolding is performed. It is verified that the measurements in the separate channels yield consistent results. The response matrix plays a key role in this unfolding procedure. An element of this matrix specifies the probability for an event originating from one bin of the true distribution to be observed in a specific bin of the reconstructed observables. The response matrix includes the effects of acceptance, detector efficiencies, and resolutions. The response matrix is defined such that the true level corresponds to the full phase space (with no kinematic restrictions) for $\mathrm{t\bar{t}}$ production at parton level. At the detector level, the number of bins used is typically a few times larger than the number of bins used at generator level. The response matrix is taken from the signal simulation. The generalised inverse of the response matrix is used to obtain the distribution of unfolded event numbers from the measured distribution by applying a χ^2 minimisation technique. An additional χ^2 term is included representing Tikhonov regularisation [71]. The regularisation reduces the effect of the statistical fluctuations present in the measured distribution on the high-frequency content of the unfolded spectrum. The regularisation strength is chosen such that the global correlation coefficient is minimal [72]. For the measurements presented here, this choice results in a small contribution from the regularisation term to the total χ^2, on the order of a few percent. The unfolding of multidimensional distributions is performed by internally mapping the multi-dimensional arrays to one-dimensional arrays [70].

6 Cross section determination

The normalised cross sections for $t\bar{t}$ production are measured in the full $t\bar{t}$ kinematic phase space at parton level. The number of unfolded signal events $\hat{M}_i^{\text{unf}}$ in bins i of kinematic variables is used to define the normalised cross sections as a function of several (two or three) variables

$$\frac{\sigma_i}{\sigma} = \frac{1}{\sigma} \frac{\hat{M}_i^{\text{unf}}}{\mathcal{B}\,\mathcal{L}}, \tag{1}$$

where the total cross section σ is evaluated by summing σ_i over all bins, $\mathcal{B}$ is the branching ratio of $t\bar{t}$ into e^+e^- , $\mu^+\mu^-$, and $e^\pm\mu^\mp$ final states and $\mathcal{L}$ is the integrated luminosity of the data sample. For presentation purposes, the measured cross sections are divided by the bin width of the first variable. They present single-differential cross sections as a function of the first variable in different ranges of the second or second and third variables and are referred to as double- or triple-differential cross sections, respectively. The bin widths are chosen based on the resolutions of the kinematic variables, such that the purity and the stability of each bin is generally above 20%. For a given bin, the purity is defined as the fraction of events in the $t\bar{t}$ signal simulation that are generated and reconstructed in the same bin with respect to the total number of events reconstructed in that bin. To evaluate the stability, the number of events in the $t\bar{t}$ signal simulation that are generated and reconstructed in a given bin are divided by the total number of reconstructed events generated in the bin.

The cross section determination based on the signal extraction and unfolding described in Section 5 has been validated with closure tests. Large numbers of pseudo-data sets were generated from the $t\bar{t}$ signal MC simulations and analysed as if they were real data. The normalised differential cross sections are found to be unbiased and the confidence intervals based on the nominal measurements and the estimated $\pm1\sigma$ uncertainties provide correct coverage probability. Any residual non-closure between generated and measured cross sections is found to be small compared to the statistical uncertainties of the measurements and is therefore neglected. A further closure test has been performed by unfolding pseudo-data sets generated using reweighted signal MCs for the detector corrections. The reweighting is performed as a function of the differential cross section kinematic observables and is used to introduce controlled shape variations, e.g. making the $p_{\text{T}}(\text{t})$ spectrum harder or softer. This test is sensitive to the stability of the unfolding with respect to the underlying physics model in the simulation. The effect on the unfolded cross sections is negligible for reweightings that lead to shape changes that are comparable to the observed differences between data and nominal MC distributions.

7 Systematic uncertainties

The systematic uncertainties in the measured differential cross sections are categorised into two classes: experimental uncertainties arising from imperfect modelling of the detector response, and theoretical uncertainties arising from the modelling of the signal and background processes. Each source of systematic uncertainty is assessed by changing in the simulation the corresponding efficiency, resolution, or scale by its uncertainty, using a prescription similar to the one followed in Ref. [27]. For each change made, the cross section determination is repeated, and the difference with respect to the nominal result in each bin is taken as the systematic uncertainty.

7.1 Experimental uncertainties

To account for the pileup uncertainty, the value of the total pp inelastic cross section, which is used to estimate the mean number of additional pp interactions, is varied by $\pm4.6\%$, corre-

sponding to the uncertainty in the measurement of this cross section [61].

The efficiencies of the dilepton triggers are measured with independent triggers based on a $p_{\mathrm{T}}^{\mathrm{miss}}$ requirement. Scale factors, defined as the ratio of the trigger efficiencies in data and simulation, are calculated in bins of lepton η and p_{T}. They are applied to the simulation and varied within their uncertainties. The uncertainties from the modelling of lepton identification and isolation efficiencies are determined using the "tag-and-probe" method with Z +jets event samples [73, 74]. The differences of these efficiencies between data and simulation in bins of η and p_{T} are generally less than 10% for electrons, and negligible for muons. The uncertainty is estimated by varying the corresponding scale factors in the simulation within their uncertainties. An implicit assumption made in the analysis is that the scale factors derived from the Z +jets sample are applicable for the $\mathrm{t\bar{t}}$ samples, where the efficiency for lepton isolation is reduced due to the typically larger number of jets present in the events. An additional uncertainty of 1% is added to take into account a possible violation of this assumption. This uncertainty is verified with studies with $\mathrm{t\bar{t}}$ enriched samples using a similar event selection as for the present analysis. In these studies the lepton isolation criteria are relaxed for one lepton and the efficiency for passing the criteria is measured both in data and simulation.

The uncertainty arising from the jet energy scale (JES) is determined by varying the twenty-six sources of uncertainty in the JES in bins of p_{T} and η and taking the quadrature sum of the effects [68]. These uncertainties also include several sources related to pileup, that contribute a smaller part of all JES related uncertainties. The JES variations are also propagated to the uncertainties in $\vec{p}_{\mathrm{T}}^{\,\mathrm{miss}}$. The uncertainty from the jet energy resolution (JER) is determined by the variation of the simulated JER by $\pm$ 1 standard deviation in different η regions [68]. An additional uncertainty in the calculation of $\vec{p}_{\mathrm{T}}^{\,\mathrm{miss}}$ is estimated by varying the energies of reconstructed particles not clustered into jets.

The uncertainty due to imperfect modelling of the b tagging efficiency is determined by varying the measured scale factor for b tagging efficiencies within its uncertainties [69].

The uncertainty in the integrated luminosity of the 2016 data sample recorded by CMS is 2.5% [75] and is applied simultaneously to the normalisation of all simulated distributions.

7.2 Theoretical uncertainties

The uncertainties of the modelling of the $\mathrm{t\bar{t}}$ signal events are evaluated with appropriate variations of the nominal simulation based on POWHEG + PYTHIA and the CUETP8M2T4 tune (see Section 3 for details). The studies presented in [47] show that the nominal simulation provides a reasonable prediction of differential $\mathrm{t\bar{t}}$ production cross sections at $\sqrt{s} = 8\,\mathrm{TeV}$ and $\sqrt{s} = 13\,\mathrm{TeV}$, also for events with additional jets, and thus can be used as a solid basis for evaluating theoretical uncertainties in the present analysis.

The uncertainty arising from missing higher-order terms in the simulation of the signal process at ME level is assessed by varying the renormalisation, μ_{r}, and factorisation, μ_{f}, scales in the POWHEG simulation up and down by factors of two with respect to the nominal values. In the POWHEG sample, the nominal scales are defined as $\mu_{\mathrm{r}} = \mu_{\mathrm{f}} = \sqrt{m_{\mathrm{t}}^2 + p_{\mathrm{T,t}}^2}$, where $p_{\mathrm{T,t}}$ denotes the p_{T} of the top quark in the $\mathrm{t\bar{t}}$ rest frame. In total, three variations are applied: one with the factorisation scale fixed, one with the renormalisation scale fixed, and one with both scales varied up and down coherently together. The maximum of the resulting measurement variations is taken as the final uncertainty. In the parton-shower simulation, the corresponding uncertainty is estimated by varying the scale up and down by factors of 2 for initial-state radiation and $\sqrt{2}$ for final-state radiation, as suggested in Ref. [49].

The uncertainty from the choice of PDF is assessed by reweighting the signal simulation according to the prescription provided for the CT14 NLO set [60]. An additional uncertainty is independently derived by varying the α_S value within its uncertainty in the PDF set. The dependence of the measurement on the assumed top quark mass parameter m_t^{MC} value is estimated by varying m_t^{MC} in the simulation by ± 1 GeV around the central value of 172.5 GeV.

The uncertainty originating from the scheme used to match the ME-level calculation to the parton-shower simulation is derived by varying the h_{damp} parameter in POWHEG in the range $0.996 m_t^{MC} < h_{damp} < 2.239 m_t^{MC}$, according to the tuning results from Ref. [47].

The uncertainty related to modelling of the underlying event is estimated by varying the parameters used to derive the CUETP8M2T4 tune in the default setup. The default setup in PYTHIA includes a model of colour reconnection based on MPIs with early resonance decays switched off. The analysis is repeated with three other models of colour reconnection within PYTHIA: the MPI-based scheme with early resonance decays switched on, a gluon-move scheme [76], and a QCD-inspired scheme [77]. The total uncertainty from colour reconnection modelling is estimated by taking the maximum deviation from the nominal result.

The uncertainty from the knowledge of the b quark fragmentation function is assessed by varying the Bowler–Lund function within its uncertainties [78]. In addition, the analysis is repeated using the Peterson model for b quark fragmentation [79], and the final uncertainty is determined, separately for each measurement bin, as an envelope of the variations of the normalised cross section resulting from all variations of the b quark fragmentation function. An uncertainty from the semileptonic branching ratios of b hadrons is estimated by varying them according to the world average uncertainties [44]. As $t\bar{t}$ events producing electrons or muons originating from the decay of τ leptons are considered to be background, the measured differential cross sections are sensitive to the branching ratios of τ leptons decaying into electrons or muons assumed in the simulation. Hence, an uncertainty is determined by varying the branching ratios by 1.5% [44] in the simulation.

The normalisations of all non-$t\bar{t}$ backgrounds are varied up and down by $\pm 30\%$ taken from measurements as explained in Ref. [74].

The total systematic uncertainty in each measurement bin is estimated by adding all the contributions described above in quadrature, separately for positive and negative cross section variations. If a systematic uncertainty results in two cross section variations of the same sign, the largest one is taken, while the opposite variation is set to zero.

8 Results of the measurement

The normalised differential cross sections of $t\bar{t}$ production are measured in the full phase space at parton level for top quarks (after radiation and before the top quark and antiquark decays) and at particle level for additional jets in the events, for the following variables:

1. double-differential cross sections as a function of pair of variables:
   - $|y(t)|$ and $p_T(t)$,
   - $M(t\bar{t})$ and $|y(t)|$,
   - $M(t\bar{t})$ and $|y(t\bar{t})|$,
   - $M(t\bar{t})$ and $\Delta\eta(t,\bar{t})$,
   - $M(t\bar{t})$ and $\Delta\phi(t,\bar{t})$,

- $M(\mathrm{t\bar{t}})$ and $p_{\mathrm{T}}(\mathrm{t\bar{t}})$ and
- $M(\mathrm{t\bar{t}})$ and $p_{\mathrm{T}}(\mathrm{t})$.

These cross sections are denoted in the following as $[y(\mathrm{t}), p_{\mathrm{T}}(\mathrm{t})]$, etc.

2. triple-differential cross sections as a function of N_{jet}, $M(\mathrm{t\bar{t}})$, and $y(\mathrm{t\bar{t}})$. These cross sections are measured separately using two ($N_{\mathrm{jet}} = 0$ and $N_{\mathrm{jet}} \geq 1$) and three ($N_{\mathrm{jet}} = 0$, $N_{\mathrm{jet}} = 1$, and $N_{\mathrm{jet}} \geq 2$) bins of N_{jet}, for the particle-level jets. These cross sections are denoted as $[N_{\mathrm{jet}}^{0,1+}, M(\mathrm{t\bar{t}}), y(\mathrm{t\bar{t}})]$ and $[N_{\mathrm{jet}}^{0,1,2+}, M(\mathrm{t\bar{t}}), y(\mathrm{t\bar{t}})]$, respectively.

The pairs of variables for the double-differential cross sections are chosen in order to obtain representative combinations that are sensitive to different aspects of the $\mathrm{t\bar{t}}$ production dynamics, mostly following the previous measurement [20]. The variables for the triple-differential cross sections are chosen in order to enhance sensitivity to the PDFs, α_{S}, and $m_{\mathrm{t}}^{\mathrm{pole}}$. In particular, the combination of $y(\mathrm{t\bar{t}})$ and $M(\mathrm{t\bar{t}})$ variables provides sensitivity for the PDFs, as demonstrated in [20], the N_{jet} distribution for α_{S} and $M(\mathrm{t\bar{t}})$ for $m_{\mathrm{t}}^{\mathrm{pole}}$.

The numerical values of the measured cross sections and their uncertainties are provided in Appendix A. In general, the total uncertainties for all measured cross sections are about 5–10%, but exceed 20% in some regions of phase space, such as the last N_{jet} range of the $[N_{\mathrm{jet}}^{0,1,2+}, M(\mathrm{t\bar{t}}), y(\mathrm{t\bar{t}})]$ distribution. The total uncertainties are dominated by the systematic uncertainties receiving similar contributions from the experimental and theoretical systematic sources. The largest experimental systematic uncertainty is associated with the JES. Both the JES and signal modelling systematic uncertainties are also affected by the statistical uncertainties in the simulated samples that are used for the evaluation of these uncertainties. The cross sections measured in the $\mathrm{e^+e^-}$, $\mu^+\mu^-$ and $\mathrm{e^\pm}\mu^\mp$ channels separately are compatible with each other.

In Figs. 3–11, the measured cross sections are compared to three theoretical predictions based on MC simulations: POWHEG + PYTHIA ('POW+PYT'), POWHEG + HERWIG++ ('POW+HER'), and MG5_aMC@NLO + PYTHIA ('MG5+PYT'). The 'POW+PYT' and 'POW+HER' theoretical predictions differ by the parton-shower method, hadronisation and event tune (p_{T}-ordered parton showering, string hadronisation model and CUETP8M2T4 tune in 'POW+PYT', or angular ordered parton showering, cluster hadronisation model and EE5C tune in 'POW+HER'), while the 'POW+PYT' and 'MG5+PYT' predictions adopt different matrix elements (inclusive $\mathrm{t\bar{t}}$ production at NLO in 'POW+PYT', or $\mathrm{t\bar{t}}$ with up to two extra partons at NLO in 'MG5+PYT') and different methods for matching with parton shower (correcting the first parton shower emission to the NLO result in 'POW+PYT', or subtracting from the exact NLO result its parton shower approximation in 'MG5+PYT'). For each comparison, a χ^2 and the number of degrees of freedom (dof) are reported. The χ^2 value is calculated taking into account the statistical and systematic data uncertainties, while ignoring uncertainties of the predictions:

$$\chi^2 = \mathbf{R}_{N-1}^T \mathbf{Cov}_{N-1}^{-1} \mathbf{R}_{N-1}, \tag{2}$$

where $\mathbf{R}_{N-1}$ is the column vector of the residuals calculated as the difference of the measured cross sections and the corresponding predictions obtained by discarding one of the N bins, and $\mathbf{Cov}_{N-1}$ is the $(N-1) \times (N-1)$ submatrix obtained from the full covariance matrix by discarding the corresponding row and column. The matrix $\mathbf{Cov}_{N-1}$ obtained in this way is invertible, while the original covariance matrix $\mathbf{Cov}$ is singular because for normalised cross sections one degree of freedom is lost, as can be deduced from Eq. (1). The covariance matrix

Cov is calculated as:

$$\mathbf{Cov} = \mathbf{Cov}^{\text{unf}} + \mathbf{Cov}^{\text{syst}}, \tag{3}$$

where $\mathbf{Cov}^{\text{unf}}$ and $\mathbf{Cov}^{\text{syst}}$ are the covariance matrices corresponding to the statistical uncertainties from the unfolding, and the systematic uncertainties, respectively. The systematic covariance matrix $\mathbf{Cov}^{\text{syst}}$ is calculated as:

$$\mathbf{Cov}_{ij}^{\text{syst}} = \sum_{k,l} \frac{1}{N_k} C_{j,k,l} C_{i,k,l}, \quad 1 \leq i \leq N, \quad 1 \leq j \leq N, \tag{4}$$

where $C_{i,k,l}$ stands for the systematic uncertainty from variation l of source k in the ith bin, and N_k is the number of variations for source k. The sums run over all sources of the systematic uncertainties and all corresponding variations. Most of the systematic uncertainty sources in this analysis consist of positive and negative variations and thus have $N_k = 2$, whilst several model uncertainties (the model of colour reconnection and the b quark fragmentation function) consist of more than two variations, a property which is accounted for in Eq. (4). All systematic uncertainties are treated as additive, i.e. the relative uncertainties are used to scale the corresponding measured value in the construction of $\mathbf{Cov}^{\text{syst}}$. This treatment is consistent with the cross section normalisation and makes the χ^2 in Eq. (2) independent of which of the N bins is excluded. A multiplicative treatment of uncertainties has been tested as well, and consistent results were obtained. The cross section measurements for different multi-differential distributions are statistically and systematically correlated. No attempt is made to quantify the correlations between bins from different multi-differential distributions. Thus, quantitative comparisons between theoretical predictions and the data can only be made for each single set of multi-differential cross sections.

In Fig. 3, the $p_{\text{T}}(\text{t})$ distribution is compared in different ranges of $|y(\text{t})|$ to predictions from 'POW+PYT', 'POW+HER', and 'MG5+PYT'. The data distribution is softer than that of the predictions over the entire $y(\text{t})$ range. Only 'POW+HER' describes the data well, while the other two simulations predict a harder $p_{\text{T}}(\text{t})$ distribution than measured in the data over the entire $y(\text{t})$ range. The disagreement is strongest for 'POW+PYT'.

Figures 4 and 5 illustrate the distributions of $|y(\text{t})|$ and $|y(\text{t}\bar{\text{t}})|$ in different $M(\text{t}\bar{\text{t}})$ ranges compared to the same set of MC models. The shapes of the $y(\text{t})$ and $y(\text{t}\bar{\text{t}})$ distributions are reasonably well described by all models, except for the largest $M(\text{t}\bar{\text{t}})$ range, where all theoretical predictions are more central than the data for $y(\text{t})$ and less central for $y(\text{t}\bar{\text{t}})$. The $M(\text{t}\bar{\text{t}})$ distribution is softer in the data than in the theoretical predictions. The latter trend is the strongest for 'POW+PYT', being consistent with the disagreement for the $p_{\text{T}}(\text{t})$ distribution (as shown in Fig. 3). The best agreement for both $[M(\text{t}\bar{\text{t}}), y(\text{t})]$ and $[M(\text{t}\bar{\text{t}}), y(\text{t}\bar{\text{t}})]$ cross sections is provided by 'POW+HER'.

In Fig. 6, the $\Delta\eta(\text{t}, \bar{\text{t}})$ distribution is compared in the same $M(\text{t}\bar{\text{t}})$ ranges to the theoretical predictions. For all generators, there is a discrepancy between the data and simulation for the medium and high $M(\text{t}\bar{\text{t}})$ bins, where the predicted $\Delta\eta(\text{t}, \bar{\text{t}})$ values are too low. The disagreement is the strongest for 'MG5+PYT'.

Figures 7 and 8 illustrate the comparison of the distributions of $\Delta\phi(\text{t}, \bar{\text{t}})$ and $p_{\text{T}}(\text{t}\bar{\text{t}})$ in the same $M(\text{t}\bar{\text{t}})$ ranges to the theoretical predictions. Both these distributions are sensitive to gluon radiation. All MC models describe the data well within uncertainties, except for 'MG5+PYT', which predicts a $p_{\text{T}}(\text{t}\bar{\text{t}})$ distribution in the last $M(\text{t}\bar{\text{t}})$ bin of the $[M(\text{t}\bar{\text{t}}), p_{\text{T}}(\text{t}\bar{\text{t}})]$ cross sections that is too hard.

In Fig. 9, the $p_{\text{T}}(\text{t})$ distribution is compared in different $M(\text{t}\bar{\text{t}})$ ranges to the theoretical predictions. None of the MC generators is able to describe the data, generally predicting a too hard

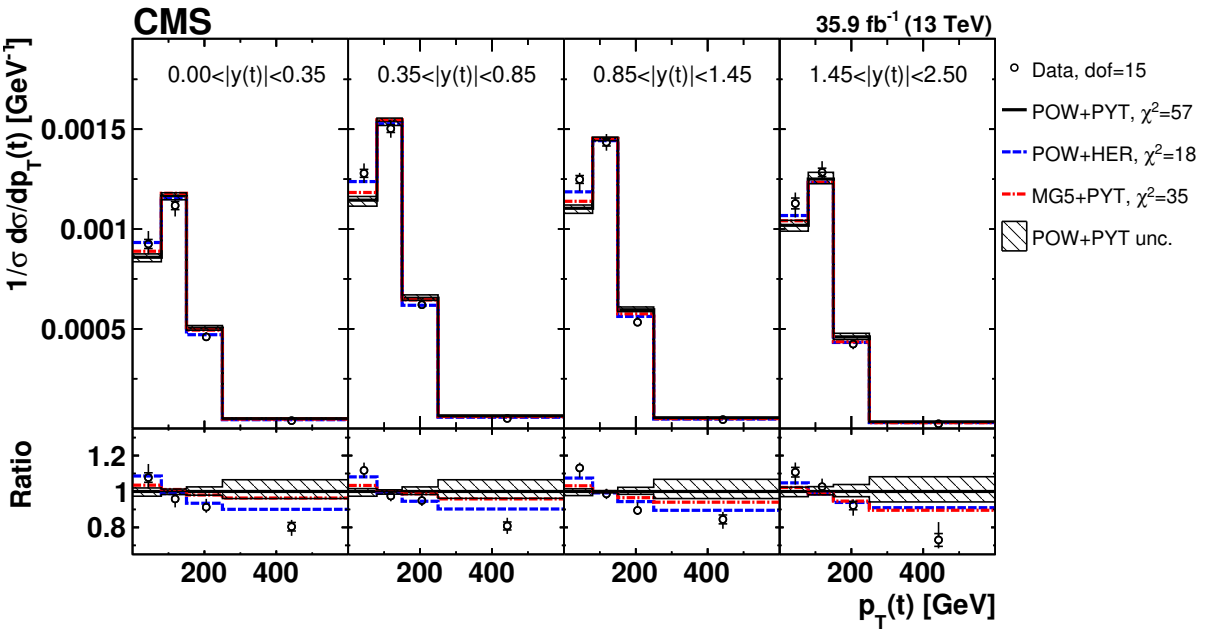

Figure 3: Comparison of the measured $[y(t), p_T(t)]$ cross sections to the theoretical predictions calculated using POWHEG + PYTHIA ('POW+PYT'), POWHEG + HERWIG++ ('POW+HER'), and MG5_aMC@NLO + PYTHIA ('MG5+PYT') event generators. The inner vertical bars on the data points represent the statistical uncertainties and the full bars include also the systematic uncertainties added in quadrature. For each MC model, values of χ^2 which take into account the bin-to-bin correlations and dof for the comparison with the data are reported. The hatched regions correspond to the theoretical uncertainties in POWHEG + PYTHIA (see Section 7). In the lower panel, the ratios of the data and other simulations to the 'POW+PYT' predictions are shown.

$p_T(t)$ distribution. The discrepancy is larger at high $M(t\bar{t})$ values where the softer $p_T(t)$ spectrum in the data must be kinematically correlated with the larger $\Delta\eta(t,\bar{t})$ values (as shown in Fig. 6), compared to the predictions. The disagreement is the strongest for 'POW+PYT'. While the 'POW+HER' simulation is able to reasonably describe the $p_T(t)$ distribution in the entire range of $y(t\bar{t})$ (as shown in Fig. 3), it does not provide a good description in all ranges of $M(t\bar{t})$, in particular predicting a too hard $p_T(t)$ distribution at high $M(t\bar{t})$.

Figures 10 and 11 illustrate the triple-differential cross sections as a function of $|y(t\bar{t})|$ in different $M(t\bar{t})$ and N_{jet} ranges, measured using two or three bins of N_{jet}. For the $[N_{jet}^{0,1+}, M(t\bar{t}), y(t\bar{t})]$ measurement, all MC models describe the data well. For the $[N_{jet}^{0,1,2+}, M(t\bar{t}), y(t\bar{t})]$ measurement, only 'POW+PYT' is in satisfactory agreement with the data. In particular, 'POW+HER' predicts too high a cross section for $N_{jet} > 1$, while 'MG5+PYT' provides the worst description of the $M(t\bar{t})$ distribution for $N_{jet} = 1$.

All obtained χ^2 values, ignoring theoretical uncertainties, are listed in Table 1. The corresponding p-values are visualised in Fig. 12. From these values one can conclude that none of the central predictions of the considered MC generators is able to provide predictions that correctly describe all distributions. In particular, for $[M(t\bar{t}), \Delta\eta(t,\bar{t})]$ and $[M(t\bar{t}), p_T(t)]$ the χ^2 values are relatively large for all MC generators. In total, the best agreement with the data is provided by 'POW+PYT' and 'POW+HER', with 'POW+PYT' better describing the measurements probing N_{jet} and radiation, and 'POW+HER' better describing the ones involving probes of the p_T distribution.

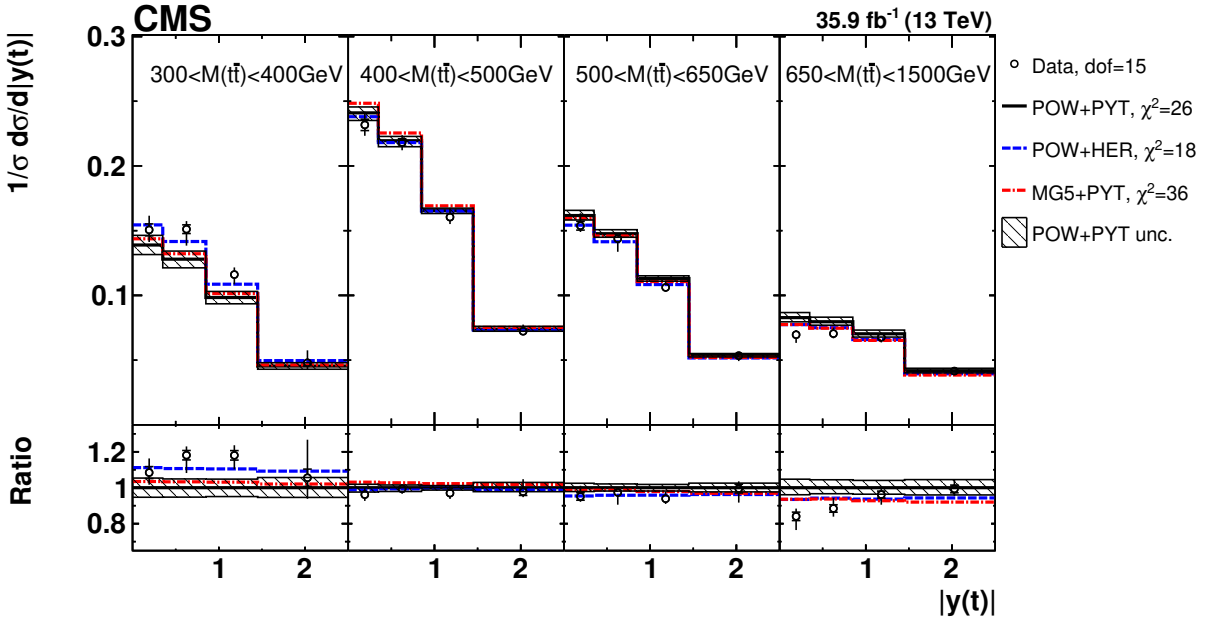

Figure 4: Comparison of the measured $[M(\mathrm{t\bar{t}}), y(\mathrm{t})]$ cross sections to the theoretical predictions calculated using MC event generators (further details can be found in the Fig. 3 caption).

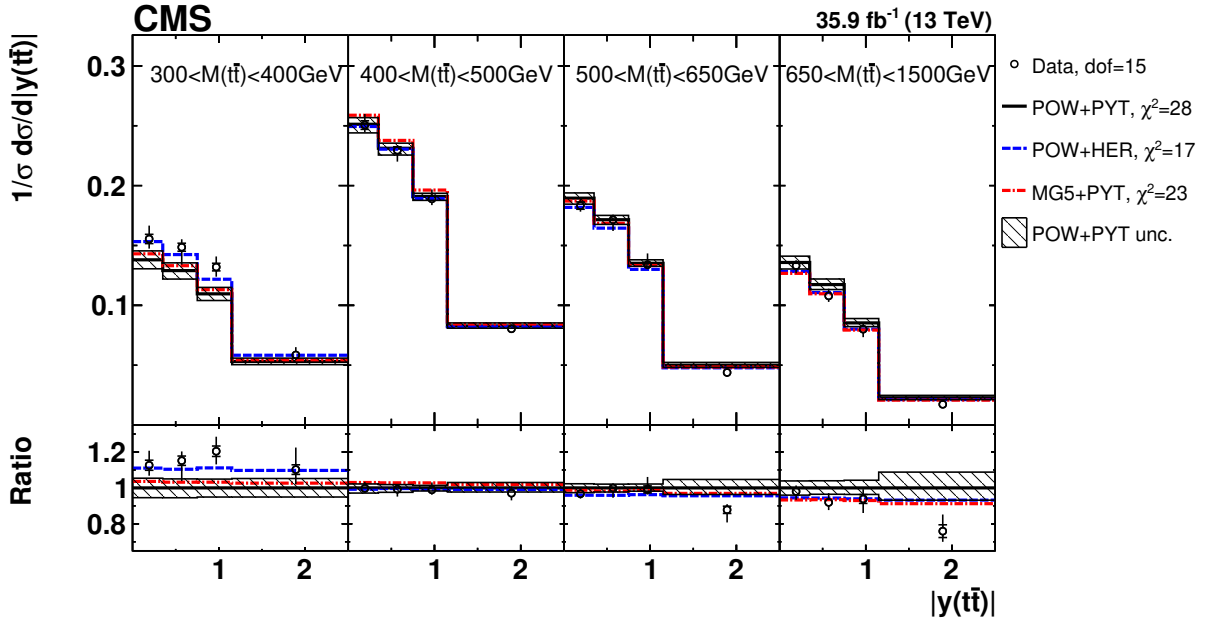

Figure 5: Comparison of the measured $[M(\mathrm{t\bar{t}}), y(\mathrm{t\bar{t}})]$ cross sections to the theoretical predictions calculated using MC event generators (further details can be found in the Fig. 3 caption).

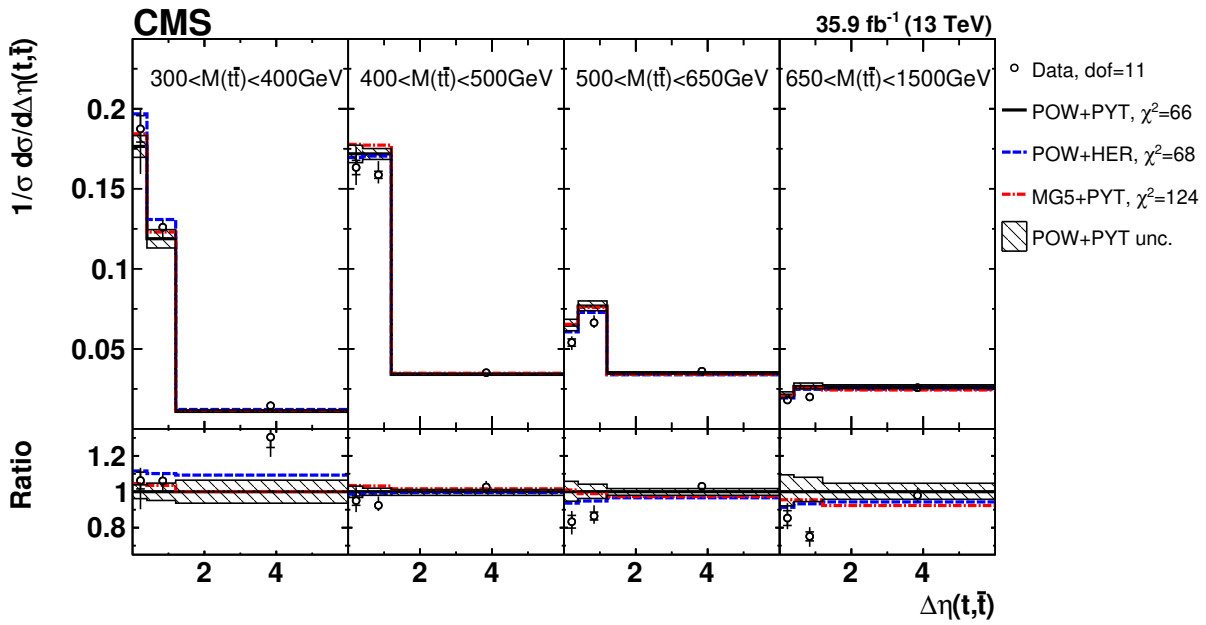

Figure 6: Comparison of the measured $[M(\mathrm{t\bar{t}}), \Delta\eta(\mathrm{t}, \bar{\mathrm{t}})]$ cross sections to the theoretical predictions calculated using MC event generators (further details can be found in the Fig. 3 caption).

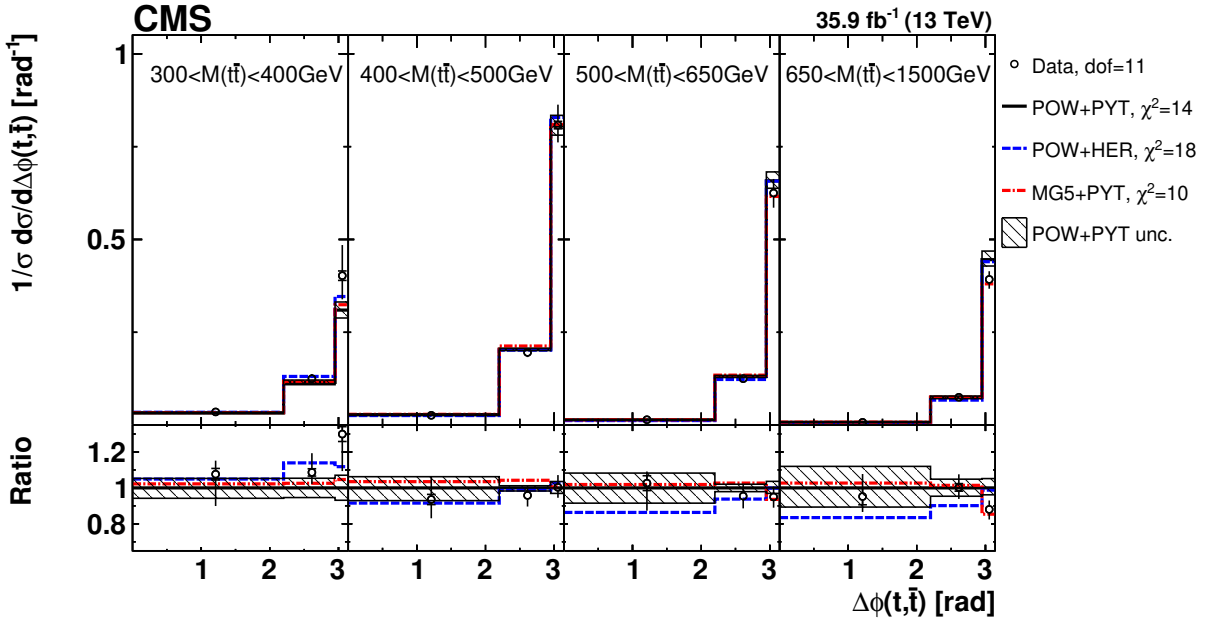

Figure 7: Comparison of the measured $[M(\mathrm{t\bar{t}}), \Delta\phi(\mathrm{t}, \bar{\mathrm{t}})]$ cross sections to the theoretical predictions calculated using MC event generators (further details can be found in the Fig. 3 caption).

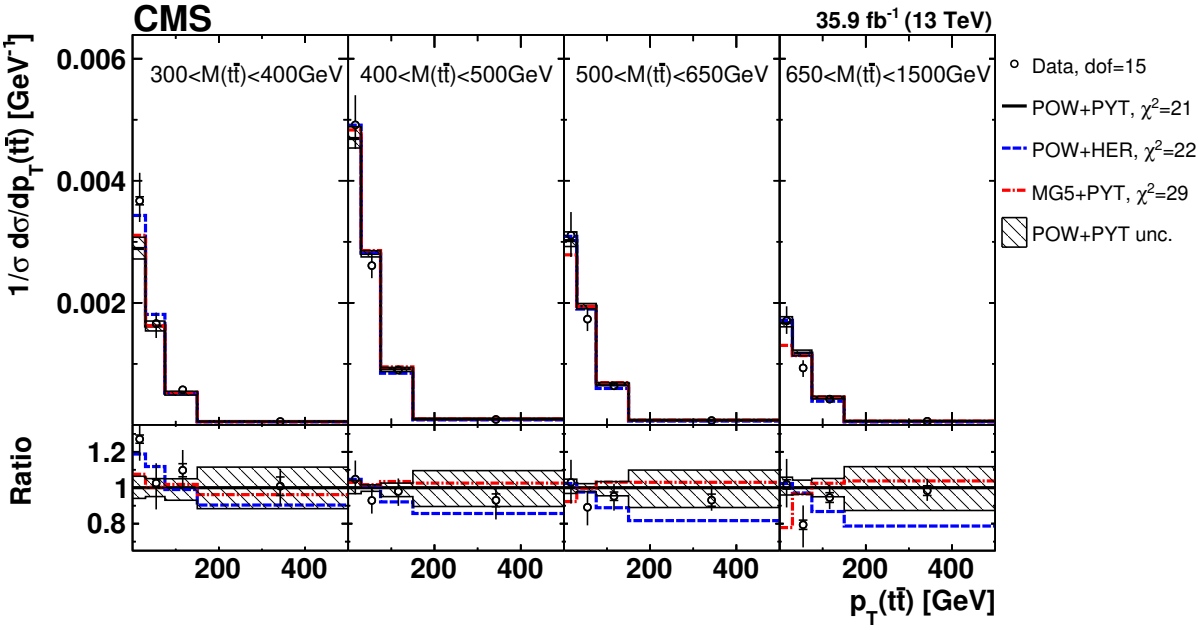

Figure 8: Comparison of the measured $[M(\mathrm{t\bar{t}}), p_{\mathrm{T}}(\mathrm{t\bar{t}})]$ cross sections to the theoretical predictions calculated using MC event generators (further details can be found in the Fig. 3 caption).

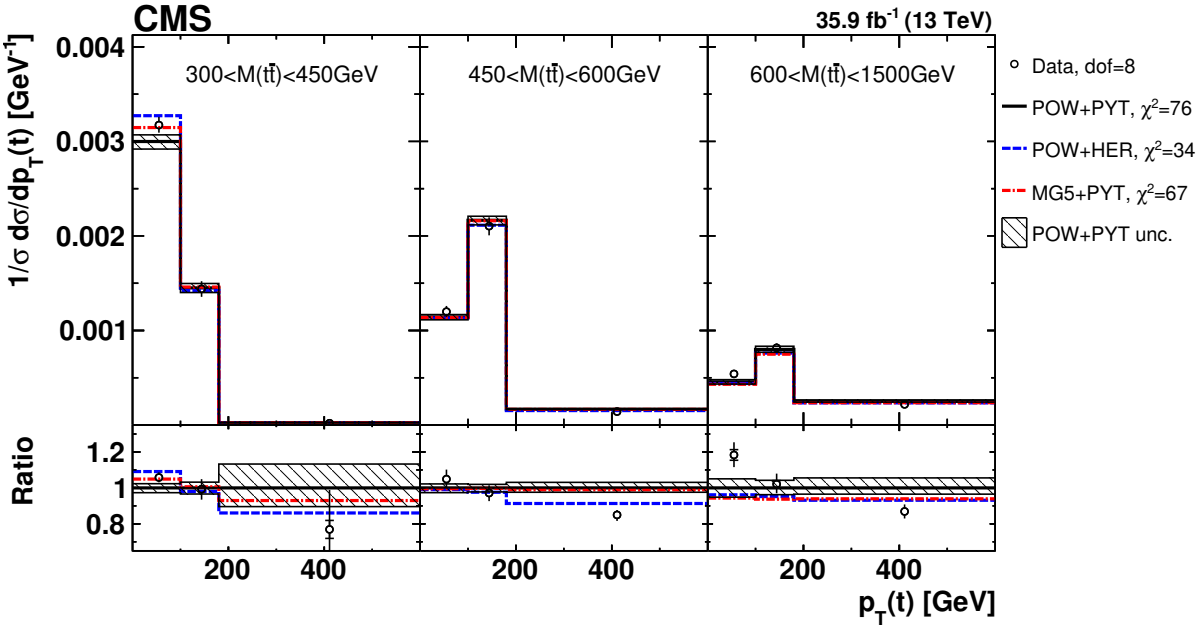

Figure 9: Comparison of the measured $[M(\mathrm{t\bar{t}}), p_{\mathrm{T}}(\mathrm{t})]$ cross sections to the theoretical predictions calculated using MC event generators (further details can be found in the Fig. 3 caption).

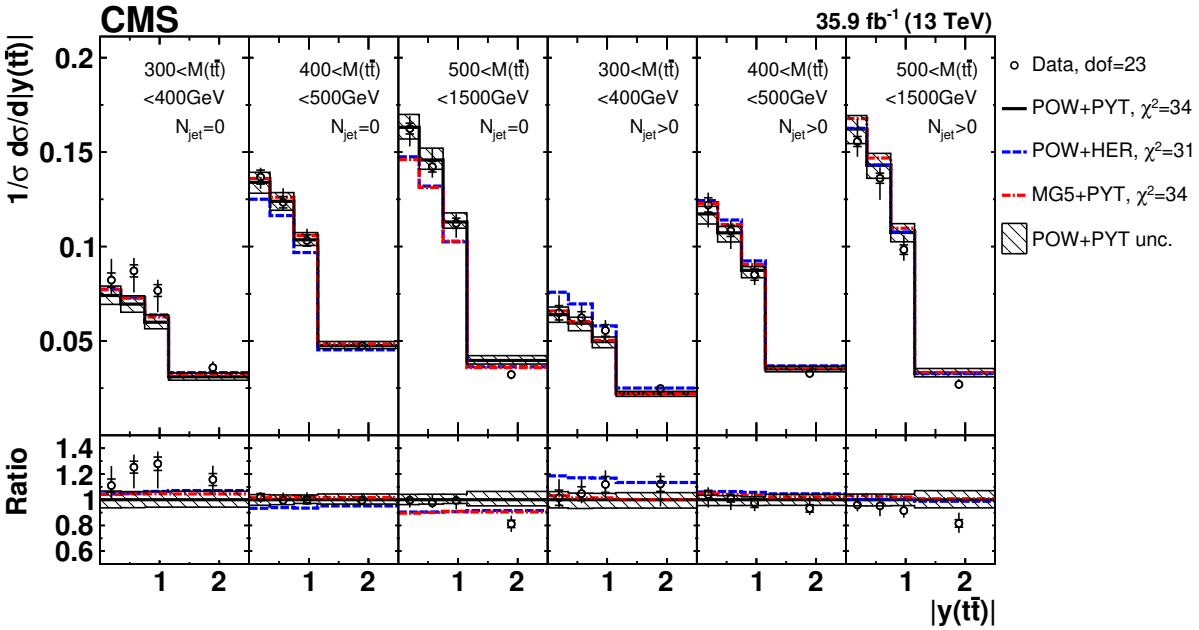

Figure 10: Comparison of the measured $[N_{\text{jet}}^{0,1+}, M(\text{t}\bar{\text{t}}), y(\text{t}\bar{\text{t}})]$ cross sections to the theoretical predictions calculated using MC event generators (further details can be found in the Fig. 3 caption).

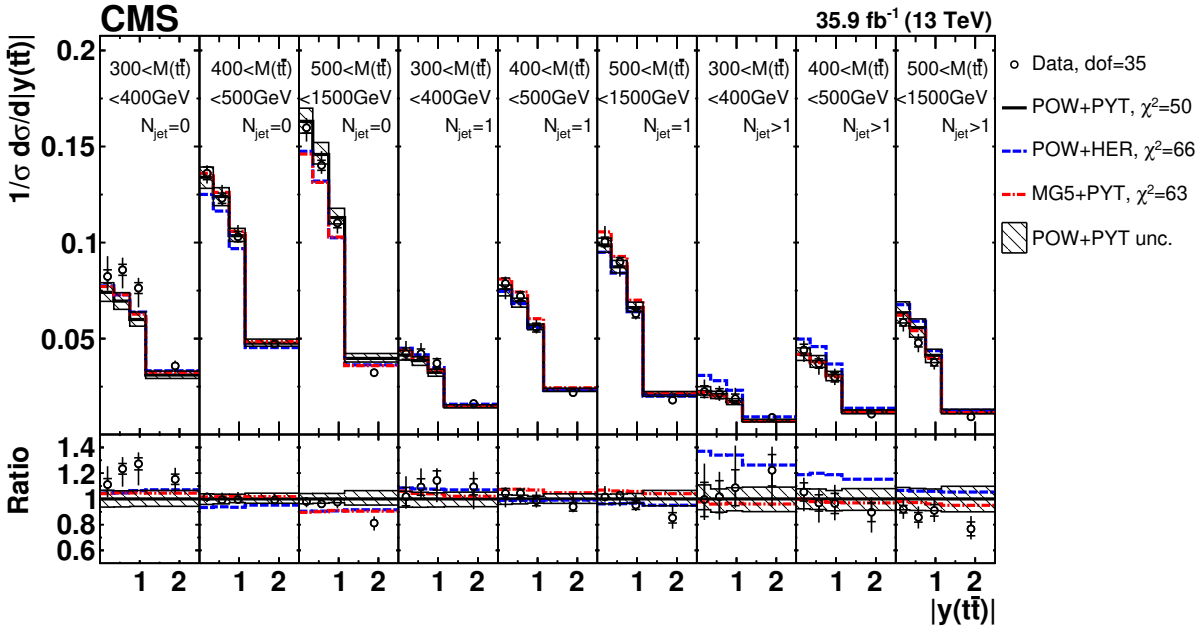

Figure 11: Comparison of the measured $[N_{\text{jet}}^{0,1,2+}, M(\text{t}\bar{\text{t}}), y(\text{t}\bar{\text{t}})]$ cross sections to the theoretical predictions calculated using MC event generators (further details can be found in the Fig. 3 caption).

Table 1: The χ^2 values (taking into account data uncertainties and ignoring theoretical uncertainties) and dof of the measured cross sections with respect to the predictions of various MC generators.

Cross section variables	dof	χ^2		
		'POW+PYT'	'POW+HER'	'MG5+PYT'
$[y(\mathrm{t}), p_{\mathrm{T}}(\mathrm{t})]$	15	57	18	35
$[M(\mathrm{t\bar{t}}), y(\mathrm{t})]$	15	26	18	36
$[M(\mathrm{t\bar{t}}), y(\mathrm{t\bar{t}})]$	15	28	17	23
$[M(\mathrm{t\bar{t}}), \Delta\eta(\mathrm{t}, \bar{\mathrm{t}})]$	11	66	68	124
$[M(\mathrm{t\bar{t}}), \Delta\phi(\mathrm{t}, \bar{\mathrm{t}})]$	15	14	18	10
$[M(\mathrm{t\bar{t}}), p_{\mathrm{T}}(\mathrm{t\bar{t}})]$	15	21	22	29
$[M(\mathrm{t\bar{t}}), p_{\mathrm{T}}(\mathrm{t})]$	15	77	34	68
$[N_{\mathrm{jet}}^{0,1+}, M(\mathrm{t\bar{t}}), y(\mathrm{t\bar{t}})]$	23	34	31	34
$[N_{\mathrm{jet}}^{0,1,2+}, M(\mathrm{t\bar{t}}), y(\mathrm{t\bar{t}})]$	35	50	66	63

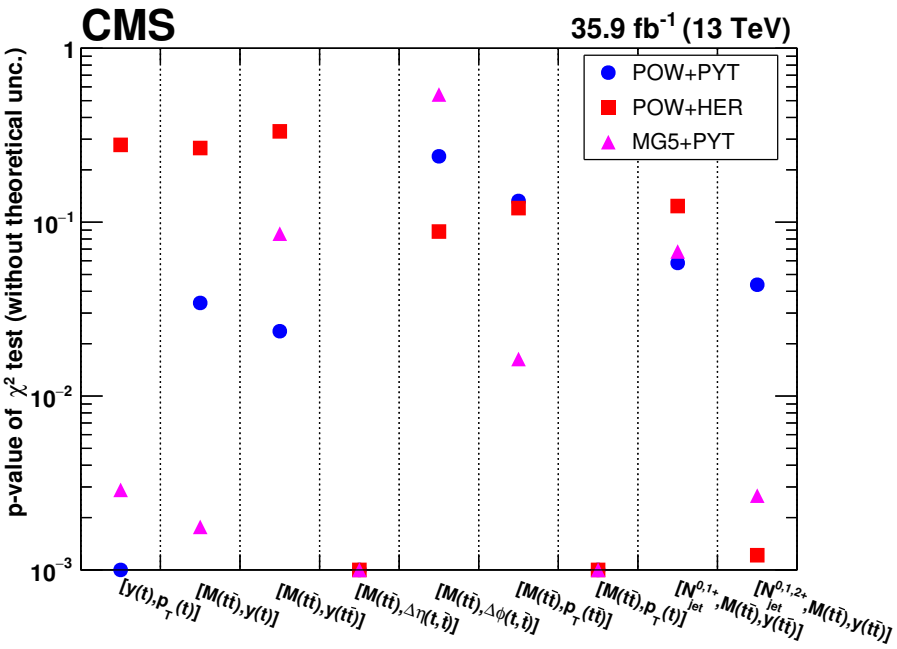

Figure 12: Assessment of compatibility of various MC predictions with the data. The plot show the p-values of χ^2-tests between data and predictions. Only the data uncertainties are taken into account in the χ^2-tests while uncertainties on the theoretical calculations are ignored. Points with $p \leq 0.001$ are shown at $p = 0.001$.

9 Extraction of α_S and m_t^{pole} from $[N_{jet}^{0,1+}, M(t\bar{t}), y(t\bar{t})]$ cross sections using external PDFs

To extract α_S and m_t^{pole}, the measured triple-differential cross sections are compared to fixed-order NLO predictions that do not have variable parameters, except for the factorisation and renormalisation scales. These predictions provide a simpler assessment of theoretical uncertainties than predictions from MC event generators. The latter complement fixed-order computations with parton showers, thus accounting for important QCD corrections beyond fixed order, but complicating thereby the interpretation of the extracted parameters, because the modelling of the showers can involve different PDFs and α_S values. Furthermore, for PDF fits using these data (to be discussed in Section 10), fast computation techniques are required that are currently available only for fixed-order calculations.

Fixed-order theoretical calculations for fully differential cross sections for inclusive $t\bar{t}$ production are publicly available at NLO $O(\alpha_S^3)$ in the fixed-flavour number scheme [80], and for $t\bar{t}$ production with one (NLO $O(\alpha_S^4)$) [81] and two (NLO $O(\alpha_S^5)$) [82, 83] additional jets. These calculations are used in the present analysis. Furthermore, NLO predictions for $t\bar{t}$ production with three additional jets exist [84], but are not used in this paper because the sample of events with three additional jets is not large enough to allow us to measure multi-differential cross sections. The exact fully differential NNLO $O(\alpha_S^4)$ calculations for inclusive $t\bar{t}$ production have recently appeared in the literature [85, 86], but these predictions have not been published yet for multi-differential cross sections. The NNLO calculations for $t\bar{t}$ production with additional jets have not been performed yet.

In the case of the $[N_{jet}^{0,1+}, M(t\bar{t}), y(t\bar{t})]$ measurement, cross sections for inclusive $t\bar{t}$ and $t\bar{t}+1$ jet production in each bin of $M(t\bar{t})$ and $y(t\bar{t})$ are obtained in the following way. The cross sections for inclusive $t\bar{t}+1$ jet production are taken from the $N_{jet} \geq 1$ bins of the $[N_{jet}^{0,1+}, M(t\bar{t}), y(t\bar{t})]$ measurements. The cross sections for inclusive $t\bar{t}$ jet production are calculated from the sum of the cross sections in the $N_{jet} = 0$ and $N_{jet} \geq 1$ bins. Statistical and systematic uncertainties and all correlations are obtained using error propagation. Finally, the cross sections obtained for inclusive $t\bar{t}$ and $t\bar{t}+1$ jet production are compared to the NLO $O(\alpha_S^3)$ and NLO $O(\alpha_S^4)$ calculations, respectively. For these processes, the ratios of NLO over LO predictions are about 1.5 on average, and the requirement $p_T > 30\,\text{GeV}$ for the jets ensures that logarithms of the ratio p_T/m_t^{pole} are not large, thereby demonstrating good convergence of the perturbation series. Similarly, cross sections for inclusive $t\bar{t}$, $t\bar{t}+1$, and $t\bar{t}+2$ jets production are obtained using the $[N_{jet}^{0,1,2+}, M(t\bar{t}), y(t\bar{t})]$ measurement and compared to the NLO $O(\alpha_S^3)$, NLO $O(\alpha_S^4)$, and NLO $O(\alpha_S^5)$ calculations, respectively. Thus, all cross sections are compared to calculations of the order in α_S required for NLO accuracy. For presentation purposes, the cross sections are shown in Figs. 14–16 in the $N_{jet} = 0$ and $N_{jet} \geq 1$ bins used before for the $[N_{jet}^{0,1+}, M(t\bar{t}), y(t\bar{t})]$ measurements, one with $N_{jet} = 0$ and another with $N_{jet} \geq 1$. The measured cross sections for $N_{jet} \geq 1$ are compared to the NLO calculation for inclusive $t\bar{t}+1$ jet production, while those for $N_{jet} = 0$ are compared to the difference of the NLO calculations for inclusive $t\bar{t}$ and inclusive $t\bar{t}+1$ jet production. The normalisation cross section is evaluated by integrating the differential cross sections over all bins, i.e. it is given by the inclusive $t\bar{t}$ cross section. As discussed below, χ^2 values are calculated for the comparisons of data and NLO predictions and are also used for the extraction of parameter values. The total χ^2 values obtained are identical for the comparisons based on inclusive $t\bar{t}$ and $t\bar{t}+1$ jet production cross sections and the ones based on the $[N_{jet}^{0,1+}, M(t\bar{t}), y(t\bar{t})]$ results, shown in Figs. 14–16, because the χ^2 values are invariant

under invertible linear transformations of the set of cross section values.

The NLO predictions are obtained using the MG5_aMC@NLO framework running in the fixed-order mode. A number of the latest proton NLO PDF sets are used, namely: ABMP16 [87], CJ15 [88], CT14 [60], HERAPDF2.0 [89], JR14 [90], MMHT2014 [91], and NNPDF3.1 [92], available via the LHAPDF interface (version 6.1.5) [93]. No $\mathrm{t\bar{t}}$ data were used in the determination of the CJ15, CT14, HERAPDF2.0 and JR14 PDF sets; only total $\mathrm{t\bar{t}}$ production cross section measurements were used to determine the ABMP16 and MMHT2014 PDFs, and both total and differential (from LHC Run 1) $\mathrm{t\bar{t}}$ cross sections were used in the NNPDF3.1 extraction. The number of active flavours is set to $n_\mathrm{f} = 5$, an $m_\mathrm{t}^\mathrm{pole} = 172.5\,\mathrm{GeV}$ is used, and α_S is set to the value used for the corresponding PDF extraction. The renormalisation and factorisation scales are chosen to be $\mu_\mathrm{r} = \mu_\mathrm{f} = H'/2, H' = \sum_i m_{\mathrm{t},i}$. Here the sum is running over all final-state partons (t, $\bar{\mathrm{t}}$, and up to three light partons in the $\mathrm{t\bar{t}} + 2$ jet calculations) and m_t denotes a transverse mass, defined as $m_\mathrm{t} = \sqrt{m^2 + p_\mathrm{T}^2}$. The theoretical uncertainty is estimated by varying μ_r and μ_f independently up and down by a factor of 2, with the additional restriction that the ratio $\mu_\mathrm{r}/\mu_\mathrm{f}$ stays between 0.5 and 2 [94]. Additionally, an alternative scale choice $\mu_\mathrm{r} = \mu_\mathrm{f} = H/2, H = \sum_i m_{\mathrm{t},i}$, with the sum running only over t and $\bar{\mathrm{t}}$ [86], is considered. The scales are varied coherently in the predictions with different N_jet. The final uncertainty is determined as an envelope of all scale variations on the normalised cross sections. This uncertainty is referred to hereafter as a scale uncertainty and is supposed to estimate the impact of missing higher-order terms. The PDF uncertainties are taken into account in the theoretical predictions for each PDF set. The PDF uncertainties of CJ15 [88] and CT14 [60], evaluated at 90% confidence level (CL), are rescaled to the 68% CL for consistency with other PDF sets. The uncertainties in the normalised $\mathrm{t\bar{t}}$ cross sections originating from α_S and $m_\mathrm{t}^\mathrm{pole}$ are estimated by varying them within $\alpha_\mathrm{S}(m_\mathrm{Z}) = 0.118 \pm 0.001$ and $m_\mathrm{t}^\mathrm{pole} = 172.5 \pm 1.0\,\mathrm{GeV}$, respectively (for presentation purposes, in some figures larger variations of $\alpha_\mathrm{S}(m_\mathrm{Z})$ and $m_\mathrm{t}^\mathrm{pole}$ by ± 0.005 and $\pm 5.0\,\mathrm{GeV}$, respectively, are shown).

To compare the measured cross sections to the NLO QCD calculations, the latter are further corrected from parton to particle level. The NLO QCD calculations are provided for parton-level jets and stable top quarks, therefore the corrections (further referred to as NP) are determined using additional POWHEG + PYTHIA MC simulations for $\mathrm{t\bar{t}}$ production with and without MPI, hadronisation and top quark decays, and defined as:

$$C_\mathrm{NP} = \frac{\sigma^\mathrm{particle}_{\text{isolated from } \mathrm{t} \to \ell, \mathrm{b}}}{\sigma^\mathrm{parton}_{\text{no MPI, no had., no } \mathrm{t\bar{t}} \text{ decays}}}. \tag{5}$$

Here $\sigma^\mathrm{particle}_{\text{isolated from } \mathrm{t} \to \ell, \mathrm{b}}$ is the cross section with MPI and hadronisation for jets built of particles excluding neutrinos and isolated from charged leptons and b quarks from the top quark decays, as defined in Section 4, and $\sigma^\mathrm{parton}_{\text{no MPI, no had., no } \mathrm{t\bar{t}} \text{ decays}}$ is the cross section without MPI and hadronisation for jets built of partons excluding t and $\bar{\mathrm{t}}$. Both cross sections are calculated at NLO matched with parton showers. The C_NP factors are used to correct the NLO predictions to particle level. The NP corrections are determined in bins of the triple-differential cross sections as a function of N_jet, $M(\mathrm{t\bar{t}})$, and $y(\mathrm{t\bar{t}})$, even though they depend primarily on N_jet and have only weak dependence on the $\mathrm{t\bar{t}}$ kinematic properties. For the cross sections with up to two extra jets measured in this analysis, the estimated NP corrections are close to 1, within 5%. The dependence of the NP corrections on MC modelling was studied using MC samples with varied hadronisation model, underlying event tune, and ME and parton-shower scales, as detailed

in Section 7. All resulting variations of C_{NP} were found to be $\lesssim$1%, therefore no uncertainties on the determined NP corrections are assigned. To compare to the measured cross sections, the normalised multi-differential cross sections of the theoretical predictions are obtained by dividing the cross sections in specific bins by the total cross section summed over all bins.

The theoretical uncertainties for the $[N_{\mathrm{jet}}^{0,1+}, M(\mathrm{t\bar{t}}), y(\mathrm{t\bar{t}})]$ and $[N_{\mathrm{jet}}^{0,1,2+}, M(\mathrm{t\bar{t}}), y(\mathrm{t\bar{t}})]$ cross sections are illustrated in Fig. 13. The CT14 PDF set with $\alpha_{\mathrm{S}}(m_{\mathrm{Z}}) = 0.118$, $m_{\mathrm{t}}^{\mathrm{pole}} = 172.5\,\mathrm{GeV}$ is used as the nominal calculation. The contributions arising from the PDF, $\alpha_{\mathrm{S}}(m_{\mathrm{Z}})$ ($\pm$0.005), and $m_{\mathrm{t}}^{\mathrm{pole}}$ ($\pm$1 GeV) uncertainties are shown separately. The total theoretical uncertainties are obtained by adding the effects from PDF, $\alpha_{\mathrm{S}}(m_{\mathrm{Z}})$, $m_{\mathrm{t}}^{\mathrm{pole}}$, and scale variations in quadrature. On average, the total theoretical uncertainties are 5–10%. They receive similar contributions from PDF, $\alpha_{\mathrm{S}}(m_{\mathrm{Z}})$, $m_{\mathrm{t}}^{\mathrm{pole}}$, and scale variations. This shows that the measured $[N_{\mathrm{jet}}^{0,1+}, M(\mathrm{t\bar{t}}), y(\mathrm{t\bar{t}})]$ cross sections can be used for reliable and precise extraction of the PDFs and QCD parameters. In this analysis the PDFs, $\alpha_{\mathrm{S}}(m_{\mathrm{Z}})$, and $m_{\mathrm{t}}^{\mathrm{pole}}$ are extracted from the $[N_{\mathrm{jet}}^{0,1+}, M(\mathrm{t\bar{t}}), y(\mathrm{t\bar{t}})]$ cross sections. These results are considered to be the nominal ones and are checked by repeating the analysis using the $[N_{\mathrm{jet}}^{0,1,2+}, M(\mathrm{t\bar{t}}), y(\mathrm{t\bar{t}})]$ cross sections.

In Figs. 14–16 the $[N_{\mathrm{jet}}^{0,1+}, M(\mathrm{t\bar{t}}), y(\mathrm{t\bar{t}})]$ cross sections are compared to the predictions obtained using different PDFs, $\alpha_{\mathrm{S}}(m_{\mathrm{Z}})$, and $m_{\mathrm{t}}^{\mathrm{pole}}$ values. For each comparison, a χ^2 is calculated, taking into account the uncertainties of the data but ignoring uncertainties of the predictions. For the comparison in Fig. 14, additional χ^2 values are determined, taking also PDF uncertainties in the predictions into account, i.e. Eq. (3) becomes $\mathbf{Cov} = \mathbf{Cov}^{\mathrm{unf}} + \mathbf{Cov}^{\mathrm{syst}} + \mathbf{Cov}^{\mathrm{PDF}}$, where $\mathbf{Cov}^{\mathrm{PDF}}$ is a covariance matrix that accounts for the PDF uncertainties. Theoretical uncertainties from scale, $\alpha_{\mathrm{S}}(m_{\mathrm{Z}})$, and $m_{\mathrm{t}}^{\mathrm{pole}}$ variations are not included in this χ^2 calculation. Sizeable differences of the χ^2 values are observed for the predictions obtained using different PDFs. These differences can be attributed to the different input data and methodologies that were used to extract these sets of PDFs as discussed elsewhere [95, 96]. Among the PDF sets considered, the best description of the data is provided by the ABMP16 PDFs. This comparison also shows that the data prefer lower $\alpha_{\mathrm{S}}(m_{\mathrm{Z}})$ and $m_{\mathrm{t}}^{\mathrm{pole}}$ value than in the nominal calculation using CT14. The largest sensitivity to $m_{\mathrm{t}}^{\mathrm{pole}}$ is observed in the lowest $M(\mathrm{t\bar{t}})$ region close to the threshold, while the sensitivity in the other $M(\mathrm{t\bar{t}})$ bins occurs mainly because of the cross section normalisation.

The values of $\alpha_{\mathrm{S}}(m_{\mathrm{Z}})$ and $m_{\mathrm{t}}^{\mathrm{pole}}$ are extracted by calculating a χ^2 between data and NLO predictions as a function of the input $\alpha_{\mathrm{S}}(m_{\mathrm{Z}})$ or $m_{\mathrm{t}}^{\mathrm{pole}}$ value, and approximating the dependence with a parabola. The minimum of the parabola is taken as the extracted $\alpha_{\mathrm{S}}(m_{\mathrm{Z}})$ or $m_{\mathrm{t}}^{\mathrm{pole}}$ value, while its uncertainty is estimated from the $\Delta\chi^2 = 1$ variation. This extraction is performed separately using different PDF sets, as well as different scale values. As for the additional χ^2 values in Fig. 14, the PDF uncertainties in the predictions are taken into account in these χ^2 calculations. Among the available PDF sets, only CT14, HERAPDF2.0, and ABMP16 provide PDF sets for enough different $\alpha_{\mathrm{S}}(m_{\mathrm{Z}})$ values and are suitable for $\alpha_{\mathrm{S}}(m_{\mathrm{Z}})$ extraction. Because the dependence of the measured $[N_{\mathrm{jet}}^{0,1+}, M(\mathrm{t\bar{t}}), y(\mathrm{t\bar{t}})]$ cross sections on the $m_{\mathrm{t}}^{\mathrm{MC}}$ value (as well as on PDFs and α_{S}) is much smaller than the sensitivity of the theoretical predictions to $m_{\mathrm{t}}^{\mathrm{pole}}$ (more details are given in Appendix C), it is not taken into account in the extraction procedure.

The $\alpha_{\mathrm{S}}(m_{\mathrm{Z}})$ and $m_{\mathrm{t}}^{\mathrm{pole}}$ scans for different PDF sets are shown in Fig. 17. The extracted $\alpha_{\mathrm{S}}(m_{\mathrm{Z}})$ and $m_{\mathrm{t}}^{\mathrm{pole}}$ values are reported in the plots. Furthermore, the $\alpha_{\mathrm{S}}(m_{\mathrm{Z}})$ ($m_{\mathrm{t}}^{\mathrm{pole}}$) scans were per-

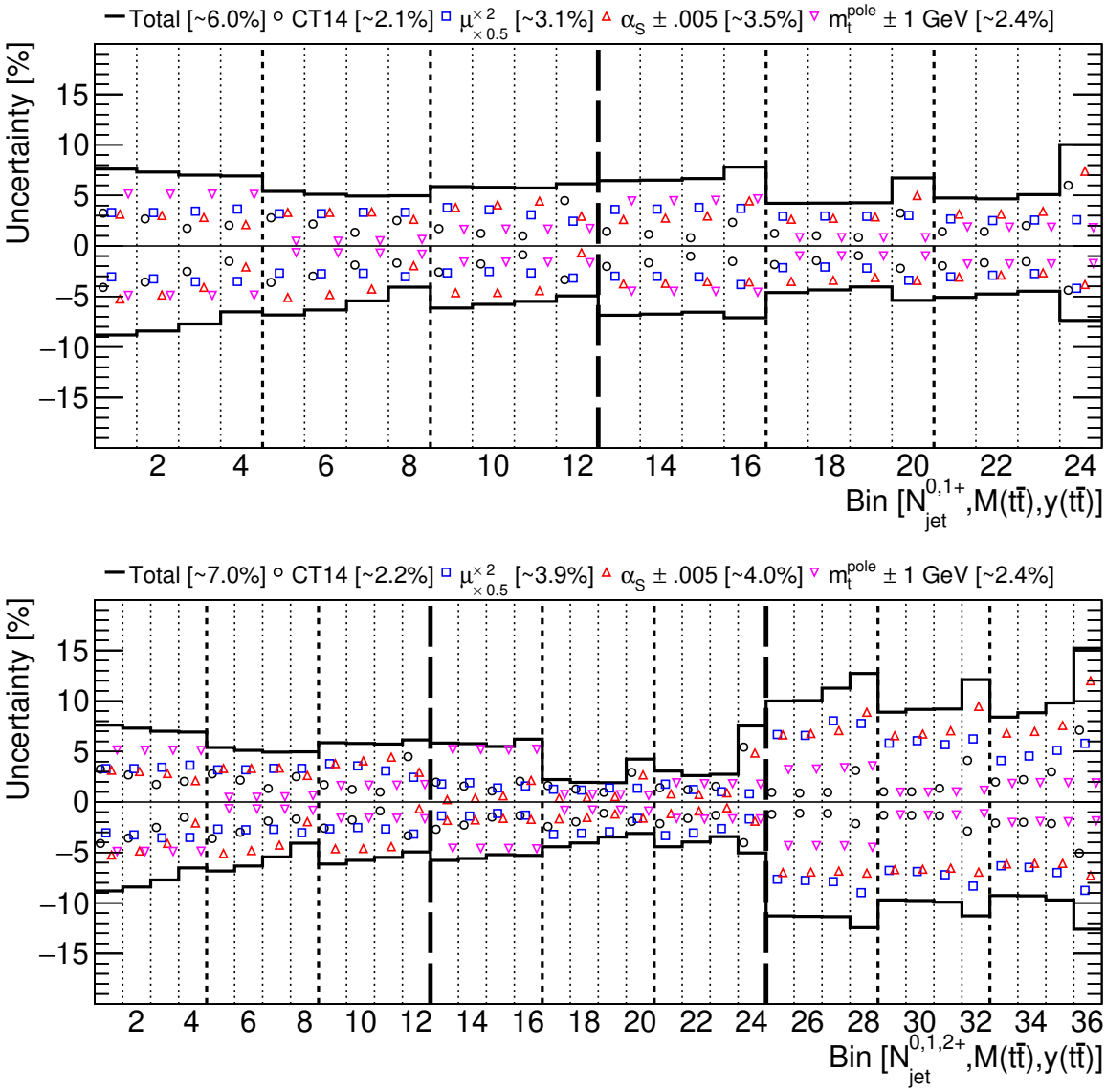

Figure 13: The theoretical uncertainties for $[N_{\text{jet}}^{0,1+}, M(\text{t}\bar{\text{t}}), y(\text{t}\bar{\text{t}})]$ (upper) and $[N_{\text{jet}}^{0,1,2+}, M(\text{t}\bar{\text{t}}), y(\text{t}\bar{\text{t}})]$ (lower) cross sections, arising from PDF, $\alpha_S(m_Z)$, and m_t^{pole} variations, as well as the total theoretical uncertainties, with their bin-averaged values shown in brackets. The bins are the same as in Figs. 10 and 11.

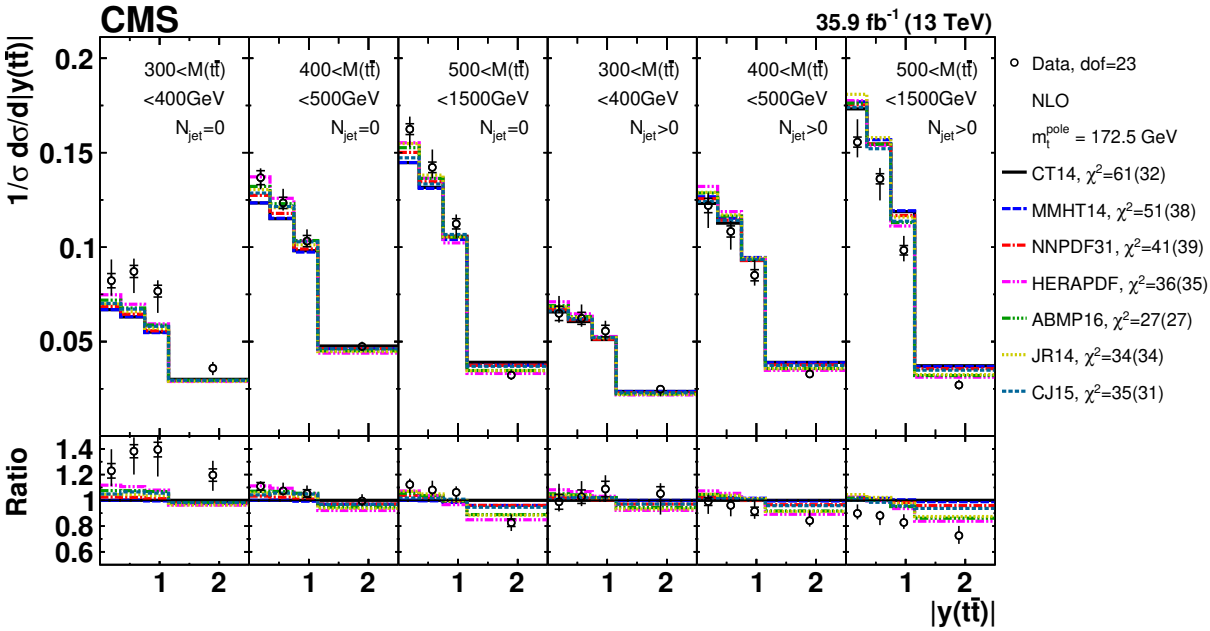

Figure 14: Comparison of the measured $[N_{\text{jet}}^{0,1+}, M(\text{t}\bar{\text{t}}), y(\text{t}\bar{\text{t}})]$ cross sections to NLO predictions obtained using different PDF sets (further details can be found in Fig. 3). For each theoretical prediction, values of χ^2 and dof for the comparison to the data are reported, while additional χ^2 values that include PDF uncertainties are shown in parentheses.

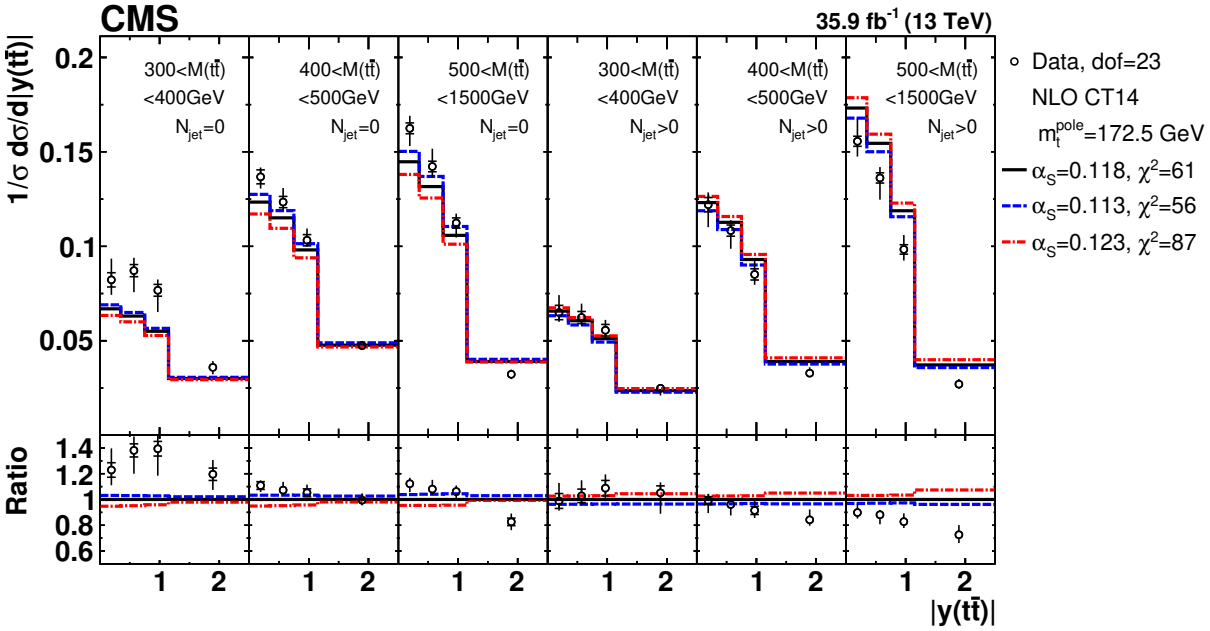

Figure 15: Comparison of the measured $[N_{\text{jet}}^{0,1+}, M(\text{t}\bar{\text{t}}), y(\text{t}\bar{\text{t}})]$ cross sections to NLO predictions obtained using different $\alpha_S(m_Z)$ values (further details can be found in Fig. 3). For each theoretical prediction, values of χ^2 and dof for the comparison to the data are reported.

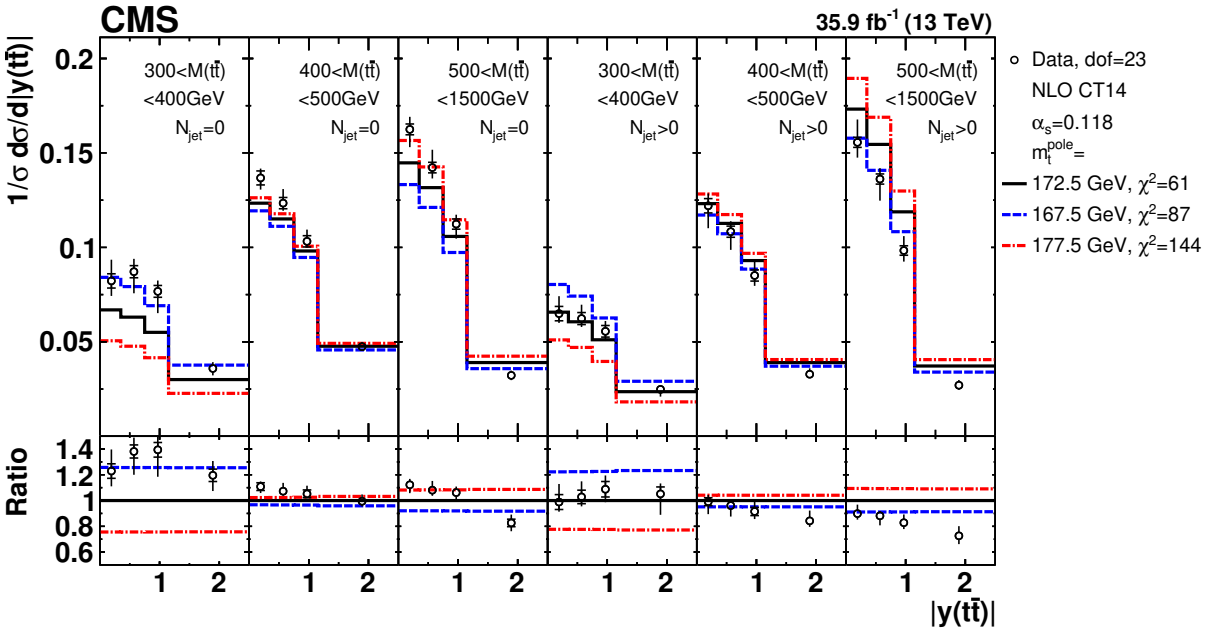

Figure 16: Comparison of the measured $[N_{\text{jet}}^{0,1+}, M(\text{t}\bar{\text{t}}), y(\text{t}\bar{\text{t}})]$ cross sections to NLO predictions obtained using different $m_{\text{t}}^{\text{pole}}$ values (further details can be found in Fig. 3). For each theoretical prediction, values of χ^2 and dof for the comparison to the data are reported.

formed using altered scale and $m_{\text{t}}^{\text{pole}}$ ($\alpha_{\text{S}}(m_{\text{Z}})$) settings and different PDF sets. For all input PDF sets, the impact of the scale variations is moderate and a weak positive correlation (∼30%) between $\alpha_{\text{S}}(m_{\text{Z}})$ and $m_{\text{t}}^{\text{pole}}$ is observed (the distributions are shown in Figs. B.1 and B.2 in Appendix B).

The values of $\alpha_{\text{S}}(m_{\text{Z}})$ and $m_{\text{t}}^{\text{pole}}$, extracted at NLO, are compared in Fig. 18 to the world average [97] and reported in Tables 2 and 3. The contributions to the total uncertainty arising from the data and from the theoretical prediction due to PDF, scale, and $m_{\text{t}}^{\text{pole}}$ or $\alpha_{\text{S}}(m_{\text{Z}})$ uncertainties are shown separately. For the extraction of $\alpha_{\text{S}}(m_{\text{Z}})$, the experimental, PDF, scale, and $m_{\text{t}}^{\text{pole}}$ uncertainties are comparable in magnitude. The size of the PDF uncertainties varies significantly for different PDF sets, and the extracted $\alpha_{\text{S}}(m_{\text{Z}})$ values depend on the input PDFs because of a strong correlation between α_{S} and the gluon distribution. This illustrates that precise and reliable $\alpha_{\text{S}}(m_{\text{Z}})$ extractions from the observed data can be obtained only in a simultaneous PDF and $\alpha_{\text{S}}(m_{\text{Z}})$ fit. For the $m_{\text{t}}^{\text{pole}}$ extraction, the total uncertainty is dominated by the data uncertainties. The world average [97] is computed based on extractions of $m_{\text{t}}^{\text{pole}}$ from inclusive $\text{t}\bar{\text{t}}$ cross sections at NNLO+NNLL and differential distributions at NLO, and dominated by the inclusive cross section measurement and a measurement from leptonic distributions. For the combination, correlations were not taken into account. The world average α_{S} value [97] is based on (at least) full NNLO QCD predictions.

Near the mass threshold, relevant for the $m_{\text{t}}^{\text{pole}}$ extraction, the fixed-order perturbation series should be improved with Coloumb and soft-gluon resummation that, however, is not available in the tools used to obtain theoretical predictions in this work. In Ref. [98] these effects are found to be relevant only very close to the threshold (within a few GeV) and give a correction of about +1% to the total $\text{t}\bar{\text{t}}$ cross section. A more recent study for the total cross section shows that these corrections are presently known only with a large relative uncertainty [99].

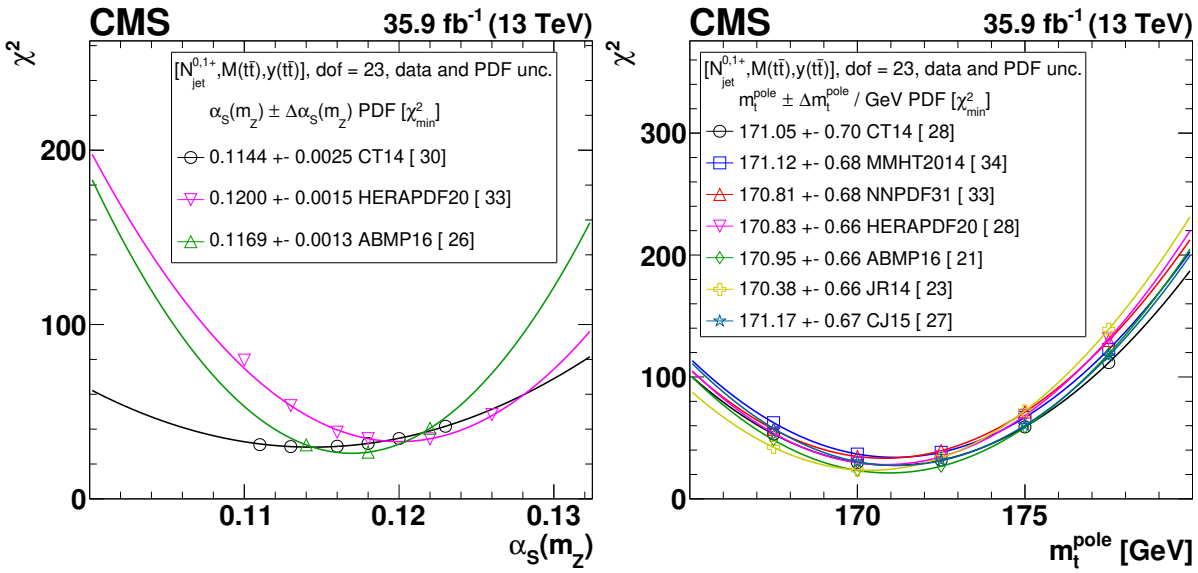

Figure 17: The $\alpha_S(m_Z)$ (left) and m_t^{pole} (right) extraction at NLO from the measured $[N_{jet}^{0,1+}, M(t\bar{t}), y(t\bar{t})]$ cross sections using different PDF sets. The extracted $\alpha_S(m_Z)$ and m_t^{pole} values are reported for each PDF set, and the estimated minimum χ^2 value is shown in brackets. Further details are given in the text.

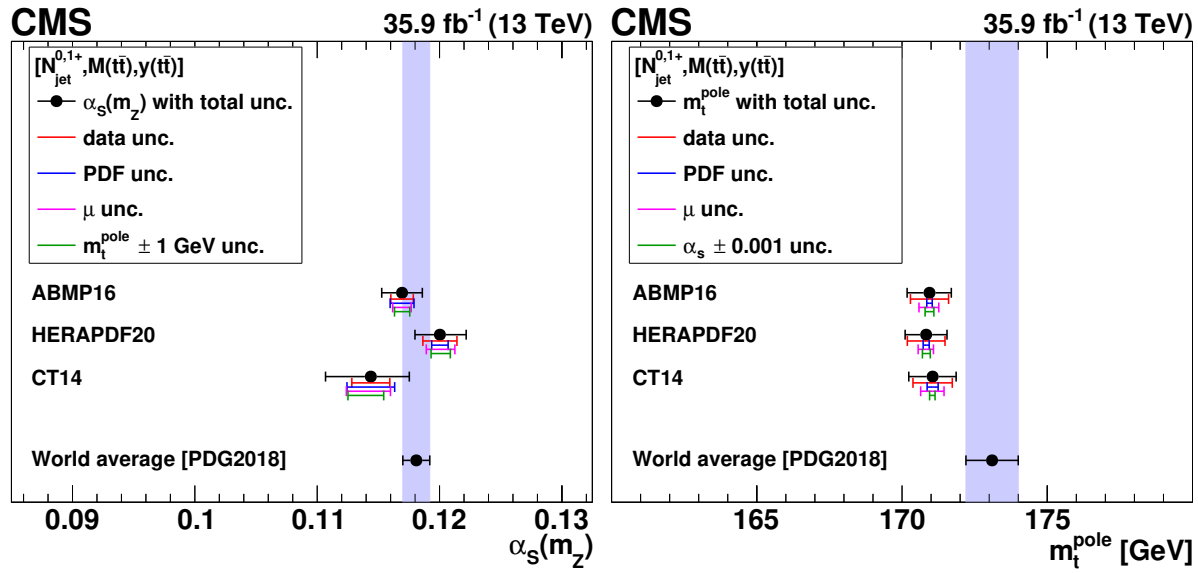

Figure 18: The $\alpha_S(m_Z)$ (left) and m_t^{pole} (right) values extracted at NLO using different PDFs. The contributions to the total uncertainty arising from the data and from the theory prediction due to PDF, scale, and m_t^{pole} or $\alpha_S(m_Z)$ uncertainties are shown separately. An additional theoretical uncertainty in the extracted m_t^{pole} (right) value of the order of +1 GeV, due to missing Coulomb and soft-gluon resummation near the $t\bar{t}$ production threshold, is not shown. The world average values $\alpha_S(m_Z) = 0.1181 \pm 0.0011$ and $m_t^{pole} = 173.1 \pm 0.9$ GeV from Ref. [97] are shown for reference.

Table 2: The $\alpha_S(m_Z)$ values extracted at NLO using different PDFs, together with their fit, PDF, scale (μ), and m_t^{pole} uncertainties.

PDF set	$\alpha_S(m_Z)$
CT14	$0.1144 \pm 0.0016(\text{fit}) \pm 0.0019(\text{PDF})^{+0.0020}_{-0.0016}(\mu)^{+0.0019}_{-0.0011}(m_t^{pole})$
HERAPDF2.0	$0.1200 \pm 0.0014(\text{fit}) \pm 0.0007(\text{PDF})^{+0.0011}_{-0.0012}(\mu)^{+0.0007}_{-0.0009}(m_t^{pole})$
ABMP16	$0.1169 \pm 0.0009(\text{fit}) \pm 0.0010(\text{PDF})^{+0.0008}_{-0.0007}(\mu)^{+0.0006}_{-0.0006}(m_t^{pole})$

Table 3: The m_t^{pole} values extracted at NLO using different PDFs, together with their fit, PDF, scale (μ), and α_S uncertainties. An additional theoretical uncertainty of the order of $+1$ GeV due to missing Coulomb and soft-gluon resummation near the $t\bar{t}$ production threshold is not shown.

PDF set	m_t^{pole} [GeV]
CT14	$171.1 \pm 0.7(\text{fit}) \pm 0.2(\text{PDF})^{+0.4}_{-0.4}(\mu)^{+0.1}_{-0.1}(\alpha_S)$
HERAPDF2.0	$170.8 \pm 0.6(\text{fit}) \pm 0.1(\text{PDF})^{+0.3}_{-0.3}(\mu)^{+0.1}_{-0.1}(\alpha_S)$
ABMP16	$170.9 \pm 0.7(\text{fit}) \pm 0.1(\text{PDF})^{+0.4}_{-0.3}(\mu)^{+0.2}_{-0.2}(\alpha_S)$

Attributing a $+1\%$ total cross section correction to our first $M(t\bar{t})$ interval and assuming it to be independent of $|y(t\bar{t})|$ and N_{jet} leads to an increase of the predicted cross section in each of the lowest $M(t\bar{t})$ bins by 5%. The effect of such a correction on the extraction of parameters has been tested for the simultaneous PDF, α_S, and m_t^{pole} fit described in Section 10. A shift of $+0.7$ GeV is observed for m_t^{pole} with respect to the nominal result listed in Eq. 8, while shifts of α_S and PDFs are small. No attempt was made to further quantify the effects on the separate α_S and m_t^{pole} extractions discussed in the present section. In the future, theoretical calculations should include gluon resummation effects to accurately extract m_t^{pole} from differential $t\bar{t}$ cross sections. For the time being one can assume an additional theoretical uncertainty in the performed m_t^{pole} extraction of the order of $+1$ GeV due to neglecting these effects.

Furthermore, the impact of the parton shower was discussed in Ref. [7], where the predictions for $t\bar{t} + 1$ jet production obtained at NLO and using POWHEG NLO calculations matched with the PYTHIA parton shower have been compared (as shown in Fig. 1 of Ref. [7]) and agreement between different approaches was found to be within 0.5 GeV for the extracted m_t^{pole}.

Moreover, electroweak corrections can be significant in some regions of phase space [100, 101], but for the analysis in this paper no electroweak corrections were applied. For inclusive $t\bar{t}$ production in the kinematic region of this analysis, electroweak corrections are calculated in [101] and found to be smaller than 2% for any region of the $M(t\bar{t})$ distribution and smaller than 1% for the $y(t\bar{t})$ distribution.

The α_S and m_t^{pole} extraction is validated by repeating the procedure:

1. *Using single-differential N_{jet}, $M(t\bar{t})$, $|y(t\bar{t})|$ cross sections.* The plots are available in Appendix B. The largest sensitivity to α_S is observed when using the $|y(t\bar{t})|$ cross sections; the value for α_S is, however, strongly dependent on the PDF set used. The N_{jet} distribution provides a smaller α_S sensitivity, but with little dependence on the PDFs. For m_t^{pole}, the largest sensitivity is observed when using the $M(t\bar{t})$ cross sections. In fact, almost no

sensitivity to m_t^{pole} is present in $|y(t\bar{t})|$ or N_{jet} single-differential cross sections. All determinations using the single-differential cross sections yielded $\alpha_S(m_Z)$ and m_t^{pole} values that are consistent with the nominal determination,

2. *Using triple-differential* $[N_{jet}^{0,1,2+}, M(t\bar{t}), y(t\bar{t})]$ *cross sections.* The distributions are available in Appendix B. The extracted $\alpha_S(m_Z)$ and m_t^{pole} values are consistent with the nominal ones obtained using two N_{jet} bins and have similar precision with a slightly different uncertainty composition: smaller data uncertainties but larger scale uncertainties are present when using three N_{jet} bins. The different uncertainties are expected since more N_{jet} bins provide more sensitivity to α_S, while the NLO theoretical prediction for the last N_{jet} bins (two or more extra jets) have larger scale uncertainties compared to the other bins (as shown in Fig. 13). This shows that NLO QCD predictions are able to describe $t\bar{t}$ data with up to two hard extra jets, however higher-order calculations are desirable to match the experimental precision in order to achieve a most accurate α_S and m_t^{pole} determination.

3. *Using triple-differential* $[p_T(t\bar{t}), M(t\bar{t}), y(t\bar{t})]$ *cross sections with two* $p_T(t\bar{t})$ *bins.* The NLO calculations for inclusive $t\bar{t}$ and $t\bar{t}+1$ jet production with an appropriate jet p_T threshold are used to describe the distribution in the two $p_T(t\bar{t})$ bins (see Appendix B.1 for further details). The extracted $\alpha_S(m_Z)$ and m_t^{pole} values (the plots are available in Appendix B.1) are consistent with the nominal ones but have slightly larger experimental, PDF, and scale uncertainties compared to the nominal results based on the $[N_{jet}^{0,1+}, M(t\bar{t}), y(t\bar{t})]$ cross sections. Nevertheless, these results are an important cross-check, because the $[p_T(t\bar{t}), M(t\bar{t}), y(t\bar{t})]$ cross sections are provided at parton level and do not require non-perturbative corrections, which have to be applied for distributions involving N_{jet}.

4. *Using unnormalised cross sections.* Consistent $\alpha_S(m_Z)$ and m_t^{pole} values are obtained, but with substantially larger experimental and scale uncertainties due to the increased scale dependence of the NLO predictions for the unnormalised cross sections and uncancelled normalisation uncertainties in the measured cross sections.

5. *Using NNLO/NLO factors as a function of* $M(t\bar{t})$. The ratios of NNLO over NLO calculations from Ref. [86] are used to multiply the NLO calculations. The NNLO/NLO corrections are obtained with the CT14, MMHT2014, and NNPDF3.0 PDF sets and $m_t^{pole} = 173.1$ GeV, and applied independently of $y(t\bar{t})$ or N_{jet} (note that NNLO/NLO corrections for the $y(t\bar{t})$ distribution are generally smaller than for $M(t\bar{t})$, and no NNLO corrections for the N_{jet} distribution are available). The NNLO/NLO corrections for the $M(t\bar{t})$ bins used in this analysis do not exceed 2%, and the impact on the extracted m_t^{pole} and α_S values is -0.2 GeV, -0.4 GeV, $+0.01$ GeV, and -0.0005, -0.0006, -0.0004 using the CT14, MMHT2014, NNPDF3.0 PDFs, respectively, which is compatible with the uncertainties assigned to the NLO results. Because of the several assumptions explained above, this study should not be interpreted as an extraction of m_t^{pole} and α_S at NNLO, but only as a test of the scale uncertainties assigned to the NLO results.

6. *Using a NLO calculation matched to parton showers.* The POWHEG + PYTHIA simulation with the NNPDF3.0 PDF set is used to determine the m_t^{pole} value. The extracted value is lower by 0.4 GeV than the nominal one determined using the NLO calculations, which is compatible with the uncertainties assigned to the NLO results.

10 Simultaneous PDF, α_S, and m_t^{pole} fit

The triple-differential normalised $[N_{jet}^{0,1+}, M(t\bar{t}), y(t\bar{t})]$ cross sections are used in a simultaneous PDF, α_S, and m_t^{pole} fit at NLO (also referred to as a QCD analysis, or PDF fit), together with the combined HERA inclusive deep inelastic scattering (DIS) data [89]. The XFITTER program (version 2.0.0) [102], an open-source QCD fit framework for PDF determination, is used. The precise HERA DIS data, obtained from the combination of individual H1 and ZEUS results, are directly sensitive to the valence and sea quark distributions and probe the gluon distribution through scaling violations. Therefore, these data form the core of all PDF fits. The measured $t\bar{t}$ cross sections are included in the fit to constrain α_S, m_t^{pole}, and the gluon distribution at high values of x, where x is the fraction of the proton momentum carried by a parton. The typical probed x values can be estimated using the LO kinematic relation

$$x = \frac{M(t\bar{t})}{\sqrt{s}} e^{\pm y(t\bar{t})}. \tag{6}$$

The present measurement is expected to be mostly sensitive to x values in the region $0.01 \lesssim x \lesssim 0.1$, as estimated using the highest or lowest $|y(t\bar{t})|$ or $M(t\bar{t})$ bins and taking the low or high bin edge where the cross section is largest.

10.1 Details of the QCD analysis

The scale evolution of partons is calculated through DGLAP equations [103–109] at NLO, as implemented in the QCDNUM program [110] (version 17.01.14). The Thorne–Roberts [111–113] variable-flavour number scheme at NLO is used for the treatment of the heavy-quark contributions. The number of flavours is set to 5, with c and b quark mass parameters $M_c = 1.47\,\text{GeV}$ and $M_b = 4.5\,\text{GeV}$ [89]. For the DIS data μ_r and μ_f are set to Q, which denotes the four-momentum transfer. The Q^2 range of the HERA data is restricted to $Q^2 > Q^2_{min} = 3.5\,\text{GeV}^2$ [89]. The theoretical predictions for the $t\bar{t}$ cross sections are calculated as described in Section 9 and are included in the fit using the MG5_aMC@NLO (version 2.6.0) [38] framework, interfaced with the AMCFAST (version 1.3.0) [114] and APPLGRID (version 1.4.70) [115] programs. The α_S and m_t^{pole} are left free in the fit. Technically, ApplGrid tables have been produced for fixed values of m_t^{pole}, while the theoretical predictions as a function of m_t^{pole} were obtained by linear interpolation between two predictions using different m_t^{pole} values. The results do not depend significantly on which particular m_t^{pole} values are used for linear interpolation. Consistent results were also obtained using a cubic spline interpolation.

The procedure for the determination of the PDFs follows the approach of HERAPDF2.0 [89]. The parametrised PDFs are the gluon distribution $xg(x)$, the valence quark distributions $xu_v(x)$ and $xd_v(x)$, and the u- and d-type antiquark distributions $x\overline{U}(x)$ and $x\overline{D}(x)$. At the initial QCD evolution scale $\mu_{f0}^2 = 1.9\,\text{GeV}^2$, the PDFs are parametrised as:

$$\begin{aligned}
xg(x) &= A_g x^{B_g} (1-x)^{C_g} (1 + E_g x^2) - A'_g x^{B'_g} (1-x)^{C'_g}, \\
xu_v(x) &= A_{u_v} x^{B_{u_v}} (1-x)^{C_{u_v}} (1 + D_{u_v} x), \\
xd_v(x) &= A_{d_v} x^{B_{d_v}} (1-x)^{C_{d_v}}, \\
x\overline{U}(x) &= A_{\overline{U}} x^{B_{\overline{U}}} (1-x)^{C_{\overline{U}}} (1 + D_{\overline{U}} x), \\
x\overline{D}(x) &= A_{\overline{D}} x^{B_{\overline{D}}} (1-x)^{C_{\overline{D}}},
\end{aligned} \tag{7}$$

assuming the relations $x\overline{\mathrm{U}}(x) = x\overline{\mathrm{u}}(x)$ and $x\overline{\mathrm{D}}(x) = x\overline{\mathrm{d}}(x) + x\overline{\mathrm{s}}(x)$. Here, $x\overline{\mathrm{u}}(x)$, $x\overline{\mathrm{d}}(x)$, and $x\overline{\mathrm{s}}(x)$ are the up, down, and strange antiquark distributions, respectively. The sea quark distribution is defined as $x\Sigma(x) = x\overline{\mathrm{u}}(x) + x\overline{\mathrm{d}}(x) + x\overline{\mathrm{s}}(x)$. The normalisation parameters $A_{\mathrm{u_v}}$, $A_{\mathrm{d_v}}$, and A_{g} are determined by the QCD sum rules. The B and B' parameters determine the PDFs at small x, and the C parameters describe the shape of the distributions as $x \to 1$. The parameter C'_{g} is fixed to 25 such that the term does not contribute at large x [89, 116]. Additional constraints $B_{\overline{\mathrm{U}}} = B_{\overline{\mathrm{D}}}$ and $A_{\overline{\mathrm{U}}} = A_{\overline{\mathrm{D}}}(1 - f_{\mathrm{s}})$ are imposed to ensure the same normalisation for the $x\overline{\mathrm{u}}$ and $x\overline{\mathrm{d}}$ distributions as $x \to 0$. The strangeness fraction $f_{\mathrm{s}} = x\overline{\mathrm{s}}/(x\overline{\mathrm{d}} + x\overline{\mathrm{s}})$ is fixed to $f_{\mathrm{s}} = 0.4$ as in the HERAPDF2.0 analysis [89]. This value is consistent with the determination of the strangeness fraction when using the CMS measurements of W+c production [117].

The D and E parameters are added for some distributions in order to provide a more flexible functional form. The parameters in Eq. (7) are selected by first fitting with all D and E parameters set to zero, and then including them independently one at a time in the fit. The improvement in the χ^2 of the fit is monitored and the procedure is stopped when no further improvement is observed. This leads to a 15-parameter fit. The χ^2 definition used for the HERA DIS data follows that of Eq. (32) in Ref. [89]. It includes an additional logarithmic term that is relevant when the estimated statistical and uncorrelated systematic uncertainties in the data are rescaled during the fit [118]. For the $\mathrm{t\bar{t}}$ data presented here, a χ^2 definition without such a logarithmic term is employed. The treatment of the experimental uncertainties in the $\mathrm{t\bar{t}}$ double-differential cross section measurements follows the prescription given in Section 8. The correlated systematic uncertainties are treated through nuisance parameters. For each nuisance parameter a Gaussian probability density function is assumed and a corresponding penalty term is added to the χ^2. The treatment of the experimental uncertainties for the HERA DIS data follows the prescription given in Ref. [89].

The uncertainties are estimated according to the general approach of HERAPDF2.0 [89] in which the fit, model, and parametrisation uncertainties are taken into account. Fit uncertainties are determined using the criterion of $\Delta\chi^2 = 1$. Model uncertainties arise from the variations in the values assumed for the c quark mass parameter of $1.41 \leq M_{\mathrm{c}} \leq 1.53\,\mathrm{GeV}$, the strangeness fraction $0.3 \leq f_{\mathrm{s}} \leq 0.5$, and the value of Q^2_{min} imposed on the HERA data. The latter is varied within $2.5 \leq Q^2_{\mathrm{min}} \leq 5.0\,\mathrm{GeV}^2$, following Ref. [89]. The parametrisation uncertainty is estimated by varying the functional form in Eq. (7) of all parton distributions, with D and E parameters added or removed one at a time. Additional parametrisation uncertainties are considered by using two other functional forms in Eq. (7): with $A'_{\mathrm{g}} = 0$ and $E_{\mathrm{g}} = 0$, since the χ^2 in these variants of the fit are only a few units worse than that with the nominal parametrisation. Furthermore, μ^2_{f0} is changed from 1.9 to 1.6 and $2.2\,\mathrm{GeV}^2$. The parametrisation uncertainty is constructed as an envelope, built from the maximal differences between the PDFs or QCD parameters resulting from the central fit and all parametrisation variations. For the PDFs, this uncertainty is valid in the x range covered by the PDF fit to the data. The total uncertainty is obtained by adding the fit, model, and parametrisation uncertainties in quadrature. For α_{S} and $m_{\mathrm{t}}^{\mathrm{pole}}$ extraction, the scale uncertainties in the theoretical predictions for $\mathrm{t\bar{t}}$ production are also considered.

A cross-check is performed using the MC method [119, 120]. It is based on analysing a large number of pseudo-data sets called replicas. For this cross-check, 1000 replicas are created by taking the data and fluctuating the values of the cross sections randomly within their statistical and systematic uncertainties taking correlations into account. All uncertainties are assumed to follow Gaussian distributions. The central values for the fitted parameters and their uncertainties are estimated using the mean and RMS values over the replicas. The obtained values

of the PDF parameters, $\alpha_S(m_Z)$, and m_t^{pole} and their fit uncertainties are in agreement with the nominal results.

10.2 Fit results

The resulting values of $\alpha_S(m_Z)$ and m_t^{pole} extracted using NLO calculations are:

$$\begin{aligned}\alpha_S(m_Z) &= 0.1135 \pm 0.0016(\text{fit})^{+0.0002}_{-0.0004}(\text{model})^{+0.0008}_{-0.0001}(\text{param})^{+0.0011}_{-0.0005}(\text{scale}) = 0.1135^{+0.0021}_{-0.0017}(\text{total}),\\ m_t^{pole} &= 170.5 \pm 0.7(\text{fit}) \pm 0.1(\text{model})^{+0.0}_{-0.1}(\text{param}) \pm 0.3(\text{scale})\,\text{GeV} = 170.5 \pm 0.8(\text{total})\,\text{GeV}.\end{aligned} \tag{8}$$

Here 'fit', 'model' and 'param' denote the fit, model and parameter uncertainties discussed above. The uncertainties arising from the scale variations are estimated by repeating the fit with altered values of the scales as described in Section 9 and taking the differences with respect to the nominal result. The individual contributions to the uncertainties are listed in Table 4. The extracted $\alpha_S(m_Z)$ and m_t^{pole} values have only weak positive correlation $\rho(\alpha_S(m_Z), m_t^{pole}) = 0.3$, where the correlation was obtained from the data uncertainties propagated to the fit. This shows that the two SM parameters can be simultaneously determined from these data to high precision with only weak correlation between them. As discussed in Section 9, one expects an additional theoretical uncertainty in the extracted m_t^{pole} value of the order of $+1\,\text{GeV}$ due to gluon resummation corrections that are missing in the NLO calculation.

The global and partial χ^2 values of the fit are listed in Table 5, illustrating the consistency of the input data with the fit model. In particular, the $t\bar{t}$ data are well described in the fit. The DIS data show χ^2/dof values slightly larger than unity, similar to what is observed and investigated in Ref. [89]. For the $t\bar{t}$ data, the full χ^2 (including uncorrelated and correlated data uncertainties) is 20 for 23 degrees of freedom. The $t\bar{t}$ cross sections are compared to the NLO predictions obtained after the fit in Fig. 19. Furthermore, in Fig. 20 the $[y(t), p_T(t)]$ cross sections (which were not used in the fit) are compared to NLO predictions obtained using the fitted PDFs, α_S and m_t^{pole}, as well as other global PDF sets. The data are in satisfactory agreement with the predictions obtained in this analysis. In particular, these predictions or predictions obtained using the ABMP16 PDF set describe the slope of $p_T(t)$ considerably better than the predictions obtained using the NNPDF3.1 PDF set, while the difference in the χ^2 values is less significant. Additionally, the predicted $p_T(t)$ slope is sensitive to the m_t^{pole} values used in the calculations.

Fits were performed for a series of $\alpha_S(m_Z)$ values ranging from $\alpha_S(m_Z) = 0.100$ to $\alpha_S(m_Z) = 0.130$ using only HERA DIS data, or HERA and $t\bar{t}$ data. The results are shown in Fig. 21. A shallow χ^2 dependence on $\alpha_S(m_Z)$ is present when using only the HERA DIS data, similar to the findings of the HERAPDF2.0 analysis [89]. Once the $t\bar{t}$ data are included in the fit, a distinctly sharper minimum in χ^2 is observed which coincides with the one found in the simultaneous PDF and $\alpha_S(m_Z)$ fit given in Eq. (8).

Both the $t\bar{t}$ and the HERA DIS data are sensitive to the $\alpha_S(m_Z)$ value in the fit: while the constraints from the $t\bar{t}$ data seem to be dominant, the residual dependence of $\alpha_S(m_Z)$ on the HERA DIS data may remain nonnegligible. There is no way to assess the latter quantitatively because the HERA DIS data cannot be removed from the PDF fit. However, as was investigated in the HERAPDF2.0 analysis [89], when using only HERA DIS the minima are strongly dependent on the Q^2_{min} threshold. As a cross-check, the extraction of $\alpha_S(m_Z)$ was repeated for a larger threshold variation $2.5 \leq Q^2_{min} \leq 30.0\,\text{GeV}^2$. In contrast to the results of Ref. [89] obtained using only HERA DIS data, when adding the $t\bar{t}$ data the extracted values of $\alpha_S(m_Z)$ show no systematic dependence on Q^2_{min} and are consistent with the nominal result of Eq. (8) within the

Table 4: The individual contributions to the uncertainties for the $\alpha_S(m_Z)$ and m_t^{pole} determination.

Parameter	Variation	$\alpha_S(m_Z)$	m_t^{pole} [GeV]
	Fit uncertainty		
Total	$\Delta\chi^2 = 1$	± 0.0016	± 0.7
	Model uncertainty		
f_s	$f_s = 0.5$	$+0.0001$	0.0
f_s	$f_s = 0.3$	0.0000	0.0
Q^2_{min}	$Q^2_{min} = 5.0\,\mathrm{GeV}^2$	$+0.0002$	$+0.1$
Q^2_{min}	$Q^2_{min} = 2.5\,\mathrm{GeV}^2$	-0.0004	-0.1
M_c	$M_c = 1.49\,\mathrm{GeV}$	$+0.0001$	0.0
M_c	$M_c = 1.37\,\mathrm{GeV}$	0.0000	0.0
Total		$^{+0.0002}_{-0.0004}$	$^{+0.1}_{-0.1}$
	PDF parametrisation uncertainty		
$\mu^2_{f,0}$	$\mu^2_{f,0} = 2.2\,\mathrm{GeV}^2$	-0.0001	0.0
$\mu^2_{f,0}$	$\mu^2_{f,0} = 1.6\,\mathrm{GeV}^2$	$+0.0002$	0.0
A'_g	set to 0	$+0.0002$	-0.1
E_g	set to 0	$+0.0008$	0.0
Total		$^{+0.0008}_{-0.0001}$	-0.1
	Scale uncertainty		
μ_r variation	$\mu_r = H'$	$+0.0004$	-0.2
μ_r variation	$\mu_r = H'/4$	$+0.0007$	$+0.1$
μ_f variation	$\mu_f = H'$	-0.0002	$+0.3$
μ_f variation	$\mu_f = H'/4$	$+0.0001$	-0.3
$\mu_{r,f}$ variation	$\mu_{r,f} = H'$	$+0.0004$	$+0.1$
$\mu_{r,f}$ variation	$\mu_{r,f} = H'/4$	$+0.0011$	-0.2
alternative $\mu_{r,f}$	$\mu_{r,f} = H/2$	-0.0005	$+0.1$
Total		$^{+0.0011}_{-0.0005}$	$^{+0.3}_{-0.3}$

Table 5: The global and partial χ^2/dof values for all variants of the QCD analysis. The variant of the fit that uses the HERA DIS only is denoted as 'Nominal fit'. For the HERA measurements, the energy of the proton beam, E_p, is listed for each data set, with the electron energy being $E_e = 27.5\,\text{GeV}$, CC and NC standing for charged and neutral current, respectively. The correlated χ^2 and the log-penalty χ^2 entries refer to the χ^2 contributions from the nuisance parameters and from the logarithmic term, respectively, as described in the text.

Data sets	χ^2/dof	
	Nominal fit	$+[N_{\text{jet}}^{0,1+}, M(\text{t}\bar{\text{t}}), y(\text{t}\bar{\text{t}})]$
CMS $\text{t}\bar{\text{t}}$		10/23
CMS $\text{t}\bar{\text{t}}$ Correlated χ^2		10
HERA CC e^-p, $E_p = 920\,\text{GeV}$	55/42	55/42
HERA CC e^+p, $E_p = 920\,\text{GeV}$	38/39	39/39
HERA NC e^-p, $E_p = 920\,\text{GeV}$	218/159	217/159
HERA NC e^+p, $E_p = 920\,\text{GeV}$	438/377	448/377
HERA NC e^+p, $E_p = 820\,\text{GeV}$	70/70	71/70
HERA NC e^+p, $E_p = 575\,\text{GeV}$	220/254	222/254
HERA NC e^+p, $E_p = 460\,\text{GeV}$	219/204	220/204
HERA Correlated χ^2	82	80
HERA Log-penalty χ^2	+2	−7
Total χ^2/dof	1341/1130	1364/1151

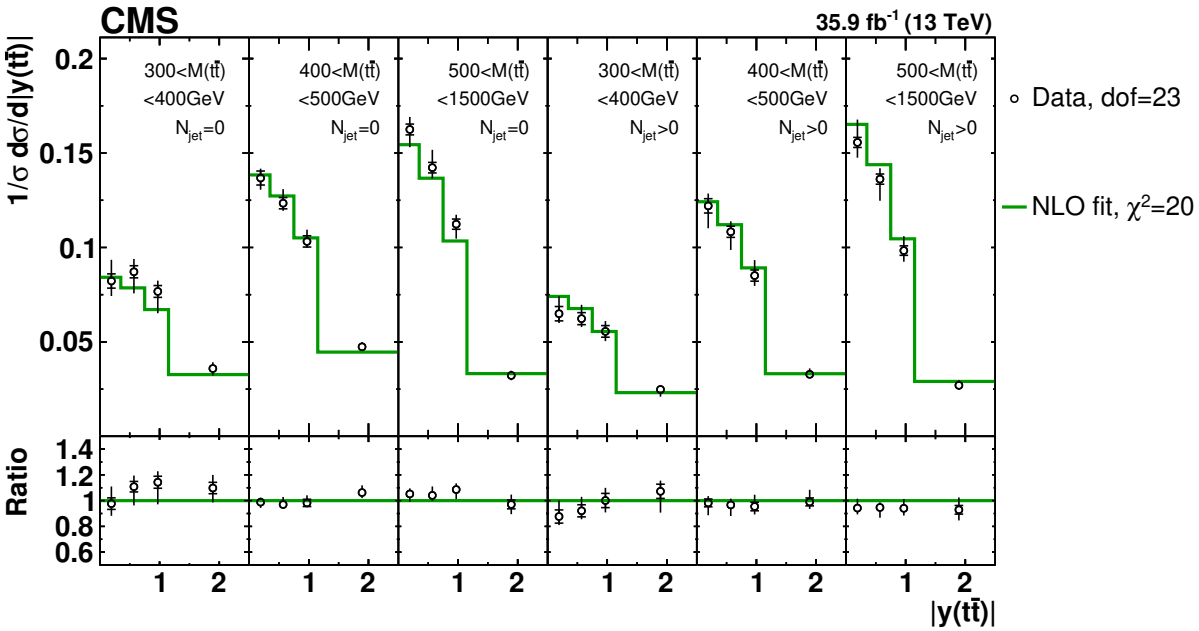

Figure 19: Comparison of the measured $[N_{\text{jet}}^{0,1+}, M(\text{t}\bar{\text{t}}), y(\text{t}\bar{\text{t}})]$ cross sections to the NLO predictions using the parameter values from the simultaneous PDF, α_S, and m_t^{pole} fit (further details can be found in Fig. 3). Values of χ^2 and dof are reported.

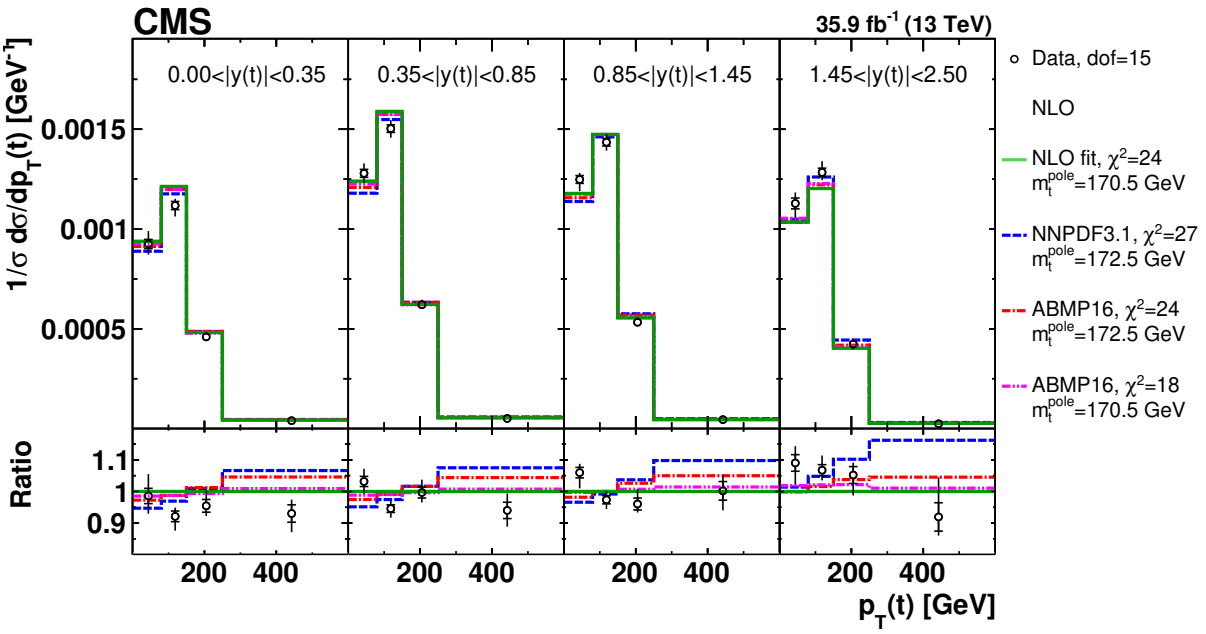

Figure 20: Comparison of the measured $[y(t), p_T(t)]$ cross sections to the NLO predictions using the parameter values from the simultaneous PDF, α_S and m_t^{pole} fit of the $[N_{jet}^{0,1+}, M(t\bar{t}), y(t\bar{t})]$ cross sections, as well as the predictions obtained using the NNPDF3.1 and ABMP16 PDF sets with different values of m_t^{pole} (see Fig. 3 for further details). In the lower panel, the ratios of the data and theoretical predictions to the predictions from the fit are shown. For each theoretical prediction, values of χ^2 and dof for the comparison to the data are reported.

total uncertainty.

To demonstrate the added value of the $t\bar{t}$ cross sections, the QCD analysis is first performed using only the HERA DIS data. In this fit, $\alpha_S(m_Z)$ is fixed to the value extracted from the fit using the $t\bar{t}$ data, $\alpha_S(m_Z) = 0.1135$, and the $\alpha_S(m_Z)$ uncertainty of ± 0.0016 is added to the fit uncertainties. Then the $[N_{jet}^{0,1+}, M(t\bar{t}), y(t\bar{t})]$ measurement is added to the fit. The global and partial χ^2 values for the two variants of the fit are listed in Table 5.

The corresponding PDFs are compared in Fig. 22. The largest impact of the $t\bar{t}$ data is observed at $x \gtrsim 0.1$. In this region the gluon distribution lacks direct constraints in the fit using the HERA DIS data only. The impact on the valence and sea quark PDFs is expected because of the correlations between the different distributions in the fit arising in the PDF evolution and from the momentum sum rule.

In Fig. 23 the total PDF uncertainties are shown for the two variants of the fits. A reduction of uncertainties is observed for the gluon distribution, especially at $x \sim 0.1$ where the included $t\bar{t}$ data are expected to provide constraints, while the improvement at $x \lesssim 0.1$ originates mainly from the reduced correlation between $\alpha_S(m_Z)$ and the gluon PDF. A smaller uncertainty reduction is observed for other PDFs as well (valence and sea quark distributions), because of the correlations between the PDF distributions in the fit, as explained above. In addition to the fit uncertainty reduction, the $t\bar{t}$ data constrain the large asymmetric model uncertainty of the gluon PDF at high x. This uncertainty originates from the variation of Q^2_{min} in the fit, using the HERA DIS data only, because of a lack of direct constraints from these data.

In Fig. 24 the extracted α_S, m_t^{pole}, and gluon PDF at the scale $\mu_f^2 = 30\,000\,\text{GeV}^2$ for several values of x are shown, together with their correlations. For this plot, the asymmetric α_S and

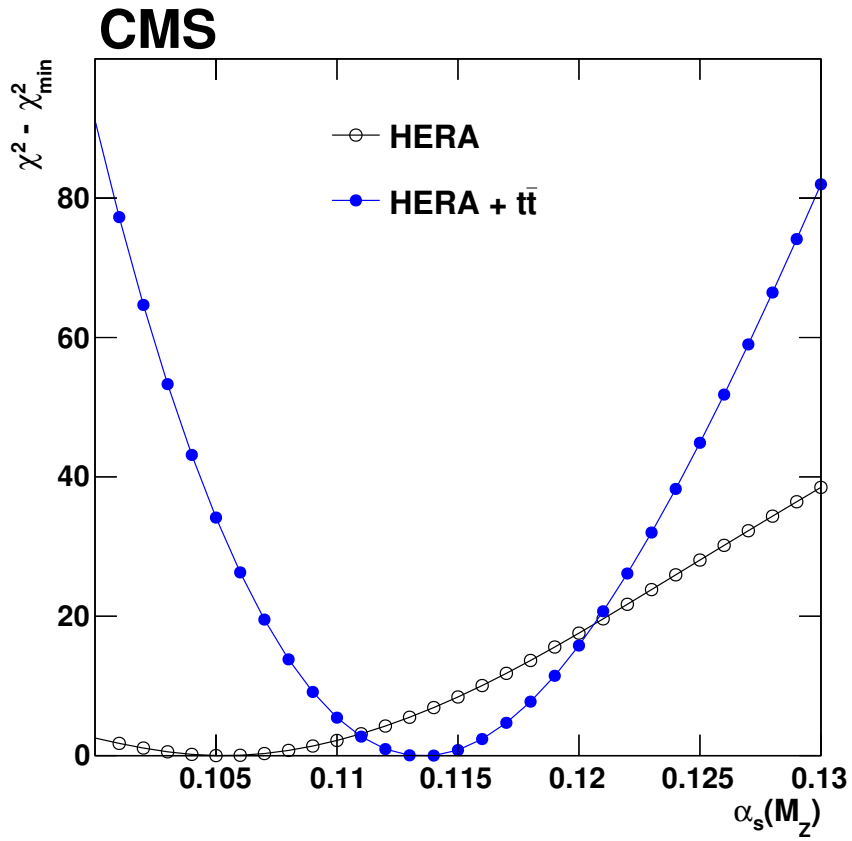

Figure 21: $\Delta\chi^2 = \chi^2 - \chi^2_{\text{min}}$ as a function of $\alpha_S(m_Z)$ in the QCD analysis using the HERA DIS data only, or HERA and $t\bar{t}$ data.

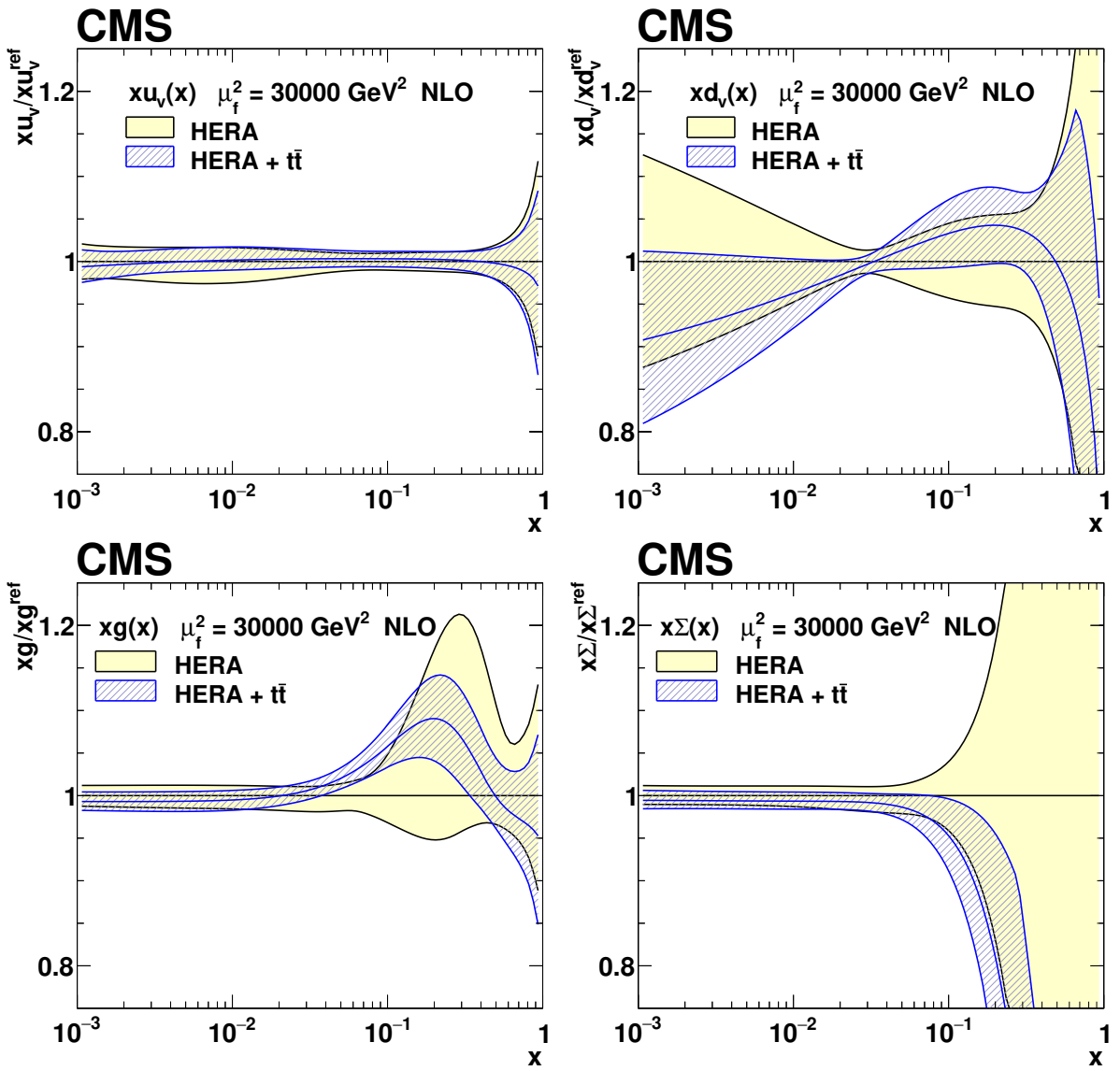

Figure 22: The PDFs with their total uncertainties in the fit using the HERA DIS data only, and the HERA DIS and $t\bar{t}$ data. The results are normalised to the PDFs obtained using the HERA DIS data only.

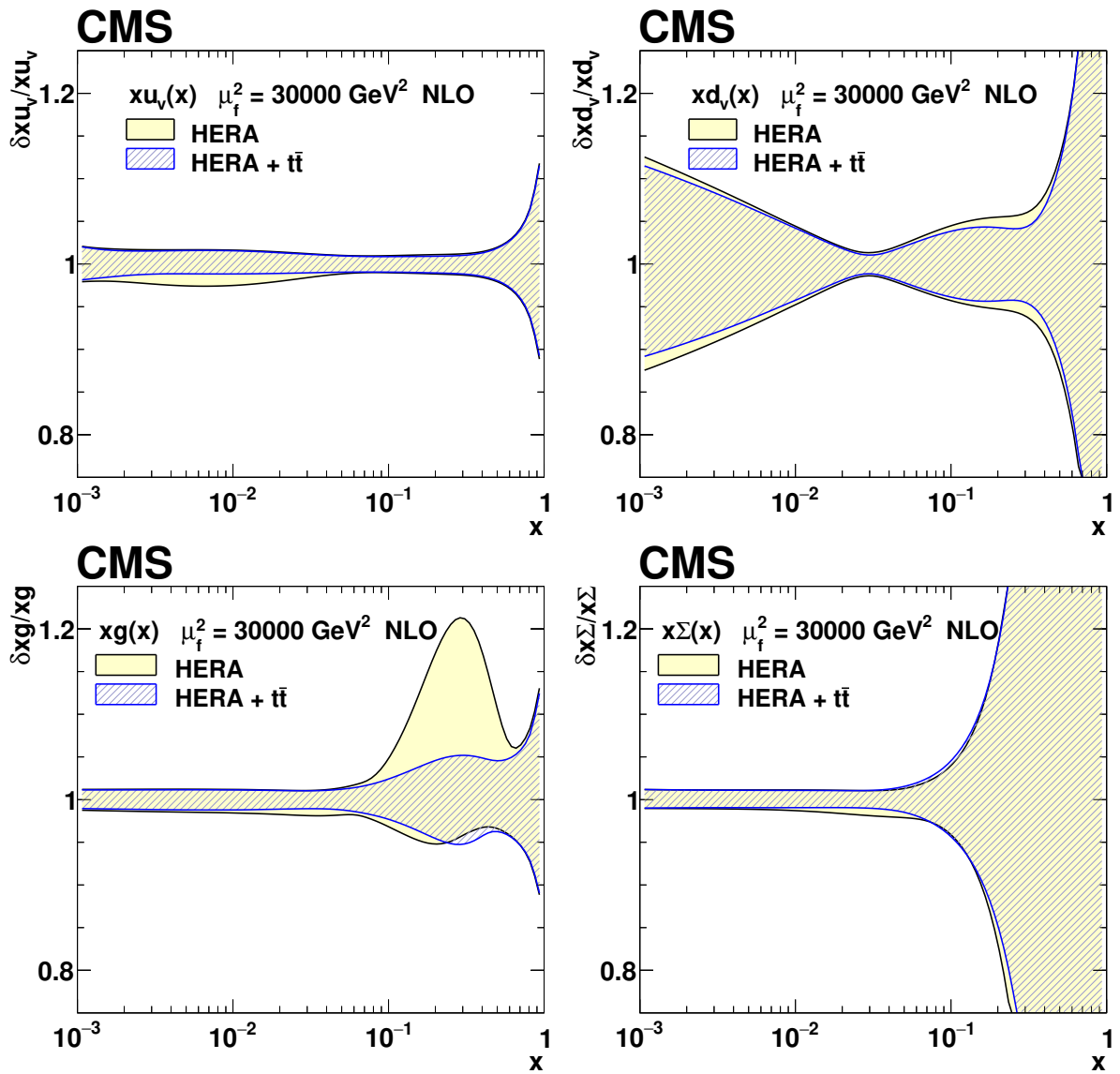

Figure 23: The relative total PDF uncertainties in the fit using the HERA DIS data only, and the HERA DIS and $t\bar{t}$ data.

m_t^{pole} uncertainties are symmetrised by taking the largest deviation, and the correlation of the fit uncertainties is assumed for the total uncertainties as well. The evolution of PDFs involves $\alpha_S(m_Z)$, therefore PDFs always depend on the $\alpha_S(m_Z)$ assumed during their extraction. When using only the HERA DIS data, the largest dependence on $\alpha_S(m_Z)$ is observed for the gluon distribution. The $t\bar{t}$ data reduce this dependence, because they provide constraints on both the gluon distribution and α_S, reducing their correlation. In addition, the multi-differential $[N_{jet}^{0,1+}, M(t\bar{t}), y(t\bar{t})]$ cross sections provide constraints on m_t^{pole}. As a result, the gluon PDF, $\alpha_S(m_Z)$, and m_t^{pole} can be determined simultaneously and their fitted values depend only weakly on each other. This makes future PDF fits at NNLO, once corresponding theoretical predictions for inclusive $t\bar{t}$ production with additional jets become available, very interesting.

11 Summary

A measurement was presented of normalised multi-differential $t\bar{t}$ production cross sections in pp collisions at $\sqrt{s} = 13\,\text{TeV}$, performed using events containing two oppositely charged leptons (electron or muon). The analysed data were recorded in 2016 with the CMS detector at the LHC, and correspond to an integrated luminosity of $35.9\,\text{fb}^{-1}$. The normalised $t\bar{t}$ cross section is measured in the full phase space as a function of different pairs of kinematic variables that describe either the top quark or the $t\bar{t}$ system. None of the central predictions of the tested Monte Carlo models is able to correctly describe all the distributions. The data exhibit softer transverse momentum $p_T(t)$ distributions than given by the theoretical predictions, as was reported in previous single-differential and double-differential $t\bar{t}$ cross section measurements. The effect of the softer $p_T(t)$ spectra in the data relative to the predictions is enhanced at larger values of the invariant mass of the $t\bar{t}$ system. The predicted $p_T(t)$ slopes are strongly sensitive to the parton distribution functions (PDFs) and the top quark pole mass m_t^{pole} value used in the calculations, and the description of the data can be improved by changing these parameters.

The measured $t\bar{t}$ cross sections as a function of the invariant mass and rapidity of the $t\bar{t}$ system, and the multiplicity of additional jets, have been incorporated into two specific fits of QCD parameters at next-to-leading order, after applying corrections for nonperturbative effects, together with the inclusive deep inelastic scattering data from HERA. When fitting only $\alpha_S(m_Z)$ and m_t^{pole} to the data, using external PDFs, the two parameters are determined with high accuracy and rather weak correlation between them, however, the extracted $\alpha_S(m_Z)$ values depend on the PDF set. In a simultaneous fit of α_S, m_t^{pole}, and PDFs, the inclusion of the new multi-differential $t\bar{t}$ measurements has a significant impact on the extracted gluon PDF at large values of x, where x is the fraction of the proton momentum carried by a parton, and at the same time allows an accurate determination of α_S and m_t^{pole}. The values $\alpha_S(m_Z) = 0.1135^{+0.0021}_{-0.0017}$ and $m_t^{pole} = 170.5 \pm 0.8\,\text{GeV}$ are obtained, which account for experimental and theoretical uncertainties.

The extraction of m_t^{pole} performed in this paper exploits the sensitivity of the $t\bar{t}$ invariant mass distribution to the value of m_t^{pole}. The highest sensitivity comes from the region of low $t\bar{t}$ masses. Threshold corrections from Coulomb and soft-gluon resummation are expected to affect this region. In Ref. [98] an estimate of these effects is provided, showing an expected increase of the total inclusive $t\bar{t}$ production cross section by about 1%. A more recent study for the total cross section shows that these corrections are presently known only with a large relative uncertainty [99]. Threshold corrections are neglected in the m_t^{pole} extraction performed

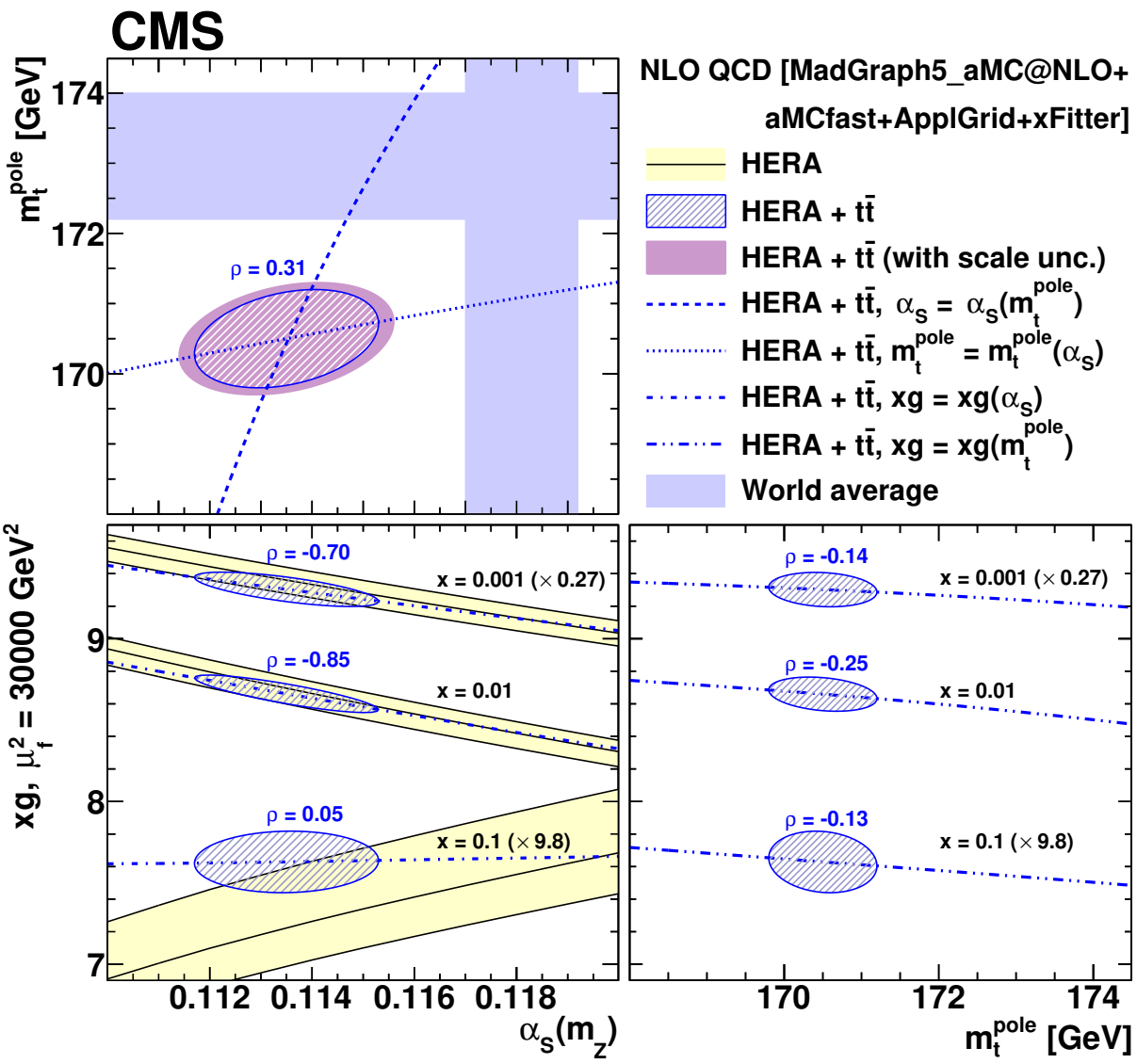

Figure 24: The extracted values and their correlations for α_S and m_t^{pole} (upper left), α_S and gluon PDF (lower left), and m_t^{pole} and gluon PDF (lower, right). The gluon PDF is shown at the scale $\mu_f^2 = 30\,000\,\text{GeV}^2$ for several values of x. For the extracted values of α_S and m_t^{pole}, the additional uncertainties arising from the dependence on scale are shown (see Eq. (8) and Table 4). The correlation coefficients ρ are also displayed. Furthermore, values of α_S (m_t^{pole}, gluon PDF) extracted using fixed values of m_t^{pole} (α_S) are displayed as dashed, dotted, or dash-dotted lines. The world average values $\alpha_S(m_Z) = 0.1181 \pm 0.0011$ and $m_t^{pole} = 173.1 \pm 0.9\,\text{GeV}$ from Ref. [97] are shown for reference.

in the present analysis. A rough estimate shows that the inclusion of these corrections according to the size estimated in Ref. [98] could lead to an increase of the extracted $m_{\mathrm{t}}^{\mathrm{pole}}$ value by up to $+0.7$ GeV. In the future, once precise calculations including threshold corrections are available for differential $\mathrm{t\bar{t}}$ cross sections, such corrections should be included for an improved $m_{\mathrm{t}}^{\mathrm{pole}}$ extraction. For the time being one can assume an additional theoretical uncertainty in the extracted $m_{\mathrm{t}}^{\mathrm{pole}}$ value of the order of $+1$ GeV due to neglected gluon resummation effects.

Acknowledgments

We congratulate our colleagues in the CERN accelerator departments for the excellent performance of the LHC and thank the technical and administrative staffs at CERN and at other CMS institutes for their contributions to the success of the CMS effort. In addition, we gratefully acknowledge the computing centres and personnel of the Worldwide LHC Computing Grid for delivering so effectively the computing infrastructure essential to our analyses. Finally, we acknowledge the enduring support for the construction and operation of the LHC and the CMS detector provided by the following funding agencies: the Austrian Federal Ministry of Education, Science and Research and the Austrian Science Fund; the Belgian Fonds de la Recherche Scientifique, and Fonds voor Wetenschappelijk Onderzoek; the Brazilian Funding Agencies (CNPq, CAPES, FAPERJ, FAPERGS, and FAPESP); the Bulgarian Ministry of Education and Science; CERN; the Chinese Academy of Sciences, Ministry of Science and Technology, and National Natural Science Foundation of China; the Colombian Funding Agency (COLCIENCIAS); the Croatian Ministry of Science, Education and Sport, and the Croatian Science Foundation; the Research Promotion Foundation, Cyprus; the Secretariat for Higher Education, Science, Technology and Innovation, Ecuador; the Ministry of Education and Research, Estonian Research Council via IUT23-4, IUT23-6 and PRG445 and European Regional Development Fund, Estonia; the Academy of Finland, Finnish Ministry of Education and Culture, and Helsinki Institute of Physics; the Institut National de Physique Nucléaire et de Physique des Particules / CNRS, and Commissariat à l'Énergie Atomique et aux Énergies Alternatives / CEA, France; the Bundesministerium für Bildung und Forschung, Deutsche Forschungsgemeinschaft, and Helmholtz-Gemeinschaft Deutscher Forschungszentren, Germany; the General Secretariat for Research and Technology, Greece; the National Research, Development and Innovation Fund, Hungary; the Department of Atomic Energy and the Department of Science and Technology, India; the Institute for Studies in Theoretical Physics and Mathematics, Iran; the Science Foundation, Ireland; the Istituto Nazionale di Fisica Nucleare, Italy; the Ministry of Science, ICT and Future Planning, and National Research Foundation (NRF), Republic of Korea; the Ministry of Education and Science of the Republic of Latvia; the Lithuanian Academy of Sciences; the Ministry of Education, and University of Malaya (Malaysia); the Ministry of Science of Montenegro; the Mexican Funding Agencies (BUAP, CINVESTAV, CONACYT, LNS, SEP, and UASLP-FAI); the Ministry of Business, Innovation and Employment, New Zealand; the Pakistan Atomic Energy Commission; the Ministry of Science and Higher Education and the National Science Centre, Poland; the Fundação para a Ciência e a Tecnologia, Portugal; JINR, Dubna; the Ministry of Education and Science of the Russian Federation, the Federal Agency of Atomic Energy of the Russian Federation, Russian Academy of Sciences, the Russian Foundation for Basic Research, and the National Research Center "Kurchatov Institute"; the Ministry of Education, Science and Technological Development of Serbia; the Secretaría de Estado de Investigación, Desarrollo e Innovación, Programa Consolider-Ingenio 2010, Plan Estatal de Investigación Científica y Técnica y de Innovación 2013–2016, Plan de Ciencia, Tecnología e Innovación 2013–2017 del Principado de Asturias,

and Fondo Europeo de Desarrollo Regional, Spain; the Ministry of Science, Technology and Research, Sri Lanka; the Swiss Funding Agencies (ETH Board, ETH Zurich, PSI, SNF, UniZH, Canton Zurich, and SER); the Ministry of Science and Technology, Taipei; the Thailand Center of Excellence in Physics, the Institute for the Promotion of Teaching Science and Technology of Thailand, Special Task Force for Activating Research and the National Science and Technology Development Agency of Thailand; the Scientific and Technical Research Council of Turkey, and Turkish Atomic Energy Authority; the National Academy of Sciences of Ukraine, and State Fund for Fundamental Researches, Ukraine; the Science and Technology Facilities Council, UK; the US Department of Energy, and the US National Science Foundation.

Individuals have received support from the Marie-Curie programme and the European Research Council and Horizon 2020 Grant, contract Nos. 675440 and 765710 (European Union); the Leventis Foundation; the A.P. Sloan Foundation; the Alexander von Humboldt Foundation; the Belgian Federal Science Policy Office; the Fonds pour la Formation à la Recherche dans l'Industrie et dans l'Agriculture (FRIA-Belgium); the Agentschap voor Innovatie door Wetenschap en Technologie (IWT-Belgium); the F.R.S.-FNRS and FWO (Belgium) under the "Excellence of Science – EOS" – be.h project n. 30820817; the Beijing Municipal Science & Technology Commission, No. Z181100004218003; the Ministry of Education, Youth and Sports (MEYS) of the Czech Republic; the Lendület ("Momentum") Programme and the János Bolyai Research Scholarship of the Hungarian Academy of Sciences, the New National Excellence Program ÚNKP, the NKFIA research grants 123842, 123959, 124845, 124850, 125105, 128713, 128786, and 129058 (Hungary); the Council of Scientific and Industrial Research, India; the HOMING PLUS programme of the Foundation for Polish Science, cofinanced from European Union, Regional Development Fund, the Mobility Plus programme of the Ministry of Science and Higher Education, the National Science Center (Poland), contracts Harmonia 2014/14/M/ST2/00428, Opus 2014/13/B/ST2/02543, 2014/15/B/ST2/03998, and 2015/19/B/ST2/02861, Sonata-bis 2012/07/E/ST2/01406; the National Priorities Research Program by Qatar National Research Fund; the Programa de Excelencia María de Maeztu, and the Programa Severo Ochoa del Principado de Asturias; the Thalis and Aristeia programmes cofinanced by EU-ESF, and the Greek NSRF; the Rachadapisek Sompot Fund for Postdoctoral Fellowship, Chulalongkorn University, and the Chulalongkorn Academic into Its 2nd Century Project Advancement Project (Thailand); the Welch Foundation, contract C-1845; and the Weston Havens Foundation (USA).

References

[1] M. Czakon, M. L. Mangano, A. Mitov, and J. Rojo, "Constraints on the gluon PDF from top quark pair production at hadron colliders", *JHEP* **07** (2013) 167, doi:10.1007/JHEP07(2013)167, arXiv:1303.7215.

[2] M. Guzzi, K. Lipka, and S. Moch, "Top-quark pair production at hadron colliders: differential cross section and phenomenological applications with DiffTop", *JHEP* **01** (2015) 082, doi:10.1007/JHEP01(2015)082, arXiv:1406.0386.

[3] M. Czakon et al., "Pinning down the large-x gluon with NNLO top-quark pair differential distributions", *JHEP* **04** (2017) 044, doi:10.1007/JHEP04(2017)044, arXiv:1611.08609.

[4] V. A. Novikov et al., "Charmonium and Gluons: Basic Experimental Facts and Theoretical Introduction", *Phys. Rept.* **41** (1978) 1, doi:10.1016/0370-1573(78)90120-5.

[5] R. Tarrach, "The Pole Mass in Perturbative QCD", *Nucl. Phys. B* **183** (1981) 384, doi:10.1016/0550-3213(81)90140-1.

[6] M. C. Smith and S. S. Willenbrock, "Top quark pole mass", *Phys. Rev. Lett.* **79** (1997) 3825, doi:10.1103/PhysRevLett.79.3825, arXiv:hep-ph/9612329.

[7] S. Alioli et al., "A new observable to measure the top-quark mass at hadron colliders", *Eur. Phys. J. C* **73** (2013) 2438, doi:10.1140/epjc/s10052-013-2438-2, arXiv:1303.6415.

[8] CDF Collaboration, "First measurement of the $t\bar{t}$ differential cross section $d\sigma/dM_{t\bar{t}}$ in $p\bar{p}$ collisions at $\sqrt{s} = 1.96$ TeV", *Phys. Rev. Lett.* **102** (2009) 222003, doi:10.1103/PhysRevLett.102.222003, arXiv:0903.2850.

[9] D0 Collaboration, "Measurement of differential $t\bar{t}$ production cross sections in $p\bar{p}$ collisions", *Phys. Rev. D* **90** (2014) 092006, doi:10.1103/PhysRevD.90.092006, arXiv:1401.5785.

[10] ATLAS Collaboration, "Measurements of top quark pair relative differential cross-sections with ATLAS in pp collisions at $\sqrt{s} = 7$ TeV", *Eur. Phys. J. C* **73** (2013) 2261, doi:10.1140/epjc/s10052-012-2261-1, arXiv:1207.5644.

[11] CMS Collaboration, "Measurement of differential top-quark pair production cross sections in pp collisions at $\sqrt{s} = 7$ TeV", *Eur. Phys. J. C* **73** (2013) 2339, doi:10.1140/epjc/s10052-013-2339-4, arXiv:1211.2220.

[12] ATLAS Collaboration, "Measurements of normalized differential cross-sections for $t\bar{t}$ production in pp collisions at $\sqrt{s} = 7$ TeV using the ATLAS detector", *Phys. Rev. D* **90** (2014) 072004, doi:10.1103/PhysRevD.90.072004, arXiv:1407.0371.

[13] ATLAS Collaboration, "Differential top-antitop cross-section measurements as a function of observables constructed from final-state particles using pp collisions at $\sqrt{s} = 7$ TeV in the ATLAS detector", *JHEP* **06** (2015) 100, doi:10.1007/JHEP06(2015)100, arXiv:1502.05923.

[14] ATLAS Collaboration, "Measurement of top quark pair differential cross-sections in the dilepton channel in pp collisions at $\sqrt{s} = 7$ and 8 TeV with ATLAS", *Phys. Rev. D* **94** (2016) 092003, doi:10.1103/PhysRevD.94.092003, arXiv:1607.07281.

[15] CMS Collaboration, "Measurement of the differential cross section for top quark pair production in pp collisions at $\sqrt{s} = 8$ TeV", *Eur. Phys. J. C* **75** (2015) 542, doi:10.1140/epjc/s10052-015-3709-x, arXiv:1505.04480.

[16] ATLAS Collaboration, "Measurements of top-quark pair differential cross-sections in the lepton+jets channel in pp collisions at $\sqrt{s} = 8$ TeV using the ATLAS detector", *Eur. Phys. J. C* **76** (2016) 538, doi:10.1140/epjc/s10052-016-4366-4, arXiv:1511.04716.

[17] ATLAS Collaboration, "Measurement of the differential cross-section of highly boosted top quarks as a function of their transverse momentum in $\sqrt{s} = 8$ TeV proton-proton collisions using the ATLAS detector", *Phys. Rev. D* **93** (2016) 032009, doi:10.1103/PhysRevD.93.032009, arXiv:1510.03818.

[18] CMS Collaboration, "Measurement of the $\mathrm{t\bar{t}}$ production cross section in the all-jets final state in pp collisions at $\sqrt{s} = 8$ TeV", *Eur. Phys. J. C* **76** (2016) 128, doi:10.1140/epjc/s10052-016-3956-5, arXiv:1509.06076.

[19] CMS Collaboration, "Measurement of the integrated and differential $\mathrm{t\bar{t}}$ production cross sections for high-p_{T} top quarks in pp collisions at $\sqrt{s} = 8$ TeV", *Phys. Rev. D* **94** (2016) 072002, doi:10.1103/PhysRevD.94.072002, arXiv:1605.00116.

[20] CMS Collaboration, "Measurement of double-differential cross sections for top quark pair production in pp collisions at $\sqrt{s} = 8$ TeV and impact on parton distribution functions", *Eur. Phys. J. C* **77** (2017) 459, doi:10.1140/epjc/s10052-017-4984-5, arXiv:1703.01630.

[21] ATLAS Collaboration, "Measurement of the top-quark mass in $t\bar{t} + 1$-jet events collected with the ATLAS detector in pp collisions at $\sqrt{s} = 8$ TeV", (2019). arXiv:1905.02302.

[22] CMS Collaboration, "Measurement of differential cross sections for top quark pair production using the lepton+jets final state in proton-proton collisions at 13 TeV", *Phys. Rev. D* **95** (2017) 092001, doi:10.1103/PhysRevD.95.092001, arXiv:1610.04191.

[23] CMS Collaboration, "Measurement of differential cross sections for the production of top quark pairs and of additional jets in lepton+jets events from pp collisions at $\sqrt{s} =$ 13 TeV", *Phys. Rev. D* **97** (2018) 112003, doi:10.1103/PhysRevD.97.112003, arXiv:1803.08856.

[24] ATLAS Collaboration, "Measurement of jet activity produced in top-quark events with an electron, a muon and two b-tagged jets in the final state in pp collisions at $\sqrt{s} = 13$ TeV with the ATLAS detector", *Eur. Phys. J. C* **77** (2017) 220, doi:10.1140/epjc/s10052-017-4766-0, arXiv:1610.09978.

[25] ATLAS Collaboration, "Measurements of top-quark pair differential cross-sections in the eμ channel in pp collisions at $\sqrt{s} = 13$ TeV using the ATLAS detector", *Eur. Phys. J. C* **77** (2017) 292, doi:10.1140/epjc/s10052-017-4821-x, arXiv:1612.05220.

[26] CMS Collaboration, "Measurement of normalized differential $\mathrm{t\bar{t}}$ cross sections in the dilepton channel from pp collisions at $\sqrt{s} = 13$ TeV", *JHEP* **04** (2018) 060, doi:10.1007/JHEP04(2018)060, arXiv:1708.07638.

[27] CMS Collaboration, "Measurements of $\mathrm{t\bar{t}}$ differential cross sections in proton-proton collisions at $\sqrt{s} = 13$ TeV using events containing two leptons", *JHEP* **02** (2019) 149, doi:10.1007/JHEP02(2019)149, arXiv:1811.06625.

[28] CMS Collaboration, "Measurement of $\mathrm{t\bar{t}}$ production with additional jet activity, including b quark jets, in the dilepton decay channel using pp collisions at $\sqrt{s} = 8$ TeV", *Eur. Phys. J. C* **76** (2016) 379, doi:10.1140/epjc/s10052-016-4105-x, arXiv:1510.03072.

[29] ATLAS Collaboration, "Measurement of jet activity in top quark events using the eμ final state with two b-tagged jets in pp collisions at $\sqrt{s} = 8$ TeV with the ATLAS detector", *JHEP* **09** (2016) 074, doi:10.1007/JHEP09(2016)074, arXiv:1606.09490.

[30] D0 Collaboration, "Determination of the pole and $\overline{MS}$ masses of the top quark from the $t\bar{t}$ cross section", *Phys. Lett. B* **703** (2011) 422, doi:10.1016/j.physletb.2011.08.015, arXiv:1104.2887.

[31] CMS Collaboration, "Determination of the top-quark pole mass and strong coupling constant from the $t\bar{t}$ production cross section in pp collisions at $\sqrt{s}$ = 7 TeV", *Phys. Lett. B* **728** (2014) 496, doi:10.1016/j.physletb.2013.12.009, arXiv:1307.1907. [Erratum: doi:10.1016/j.physletb.2014.08.040].

[32] ATLAS Collaboration, "Measurement of the $t\bar{t}$ production cross-section using eμ events with b-tagged jets in pp collisions at $\sqrt{s}$ = 7 and 8 TeV with the ATLAS detector", *Eur. Phys. J. C* **74** (2014) 3109, doi:10.1140/epjc/s10052-016-4501-2, arXiv:1406.5375. [Addendum: *Eur. Phys. J. C* **76** (2016) 642].

[33] D0 Collaboration, "Measurement of the inclusive $t\bar{t}$ production cross section in $p\bar{p}$ collisions at $\sqrt{s} = 1.96$ TeV and determination of the top quark pole mass", *Phys. Rev. D* **94** (2016) 092004, doi:10.1103/PhysRevD.94.092004, arXiv:1605.06168.

[34] CMS Collaboration, "Measurement of the $t\bar{t}$ production cross section in the eμ channel in proton-proton collisions at $\sqrt{s}$ = 7 and 8 TeV", *JHEP* **08** (2016) 029, doi:10.1007/JHEP08(2016)029, arXiv:1603.02303.

[35] CMS Collaboration, "Measurement of the $t\bar{t}$ production cross section, the top quark mass, and the strong coupling constant using dilepton events in pp collisions at $\sqrt{s} = 13$ TeV", *Eur. Phys. J. C* **79** (2019), no. 5, 368, doi:10.1140/epjc/s10052-019-6863-8, arXiv:1812.10505.

[36] S. Frixione, P. Nason, and C. Oleari, "Matching NLO QCD computations with parton shower simulations: the POWHEG method", *JHEP* **11** (2007) 070, doi:10.1088/1126-6708/2007/11/070, arXiv:0709.2092.

[37] E. Re, "Single-top Wt-channel production matched with parton showers using the POWHEG method", *Eur. Phys. J. C* **71** (2011) 1547, doi:10.1140/epjc/s10052-011-1547-z, arXiv:1009.2450.

[38] J. Alwall et al., "The automated computation of tree-level and next-to-leading order differential cross sections, and their matching to parton shower simulations", *JHEP* **07** (2014) 079, doi:10.1007/JHEP07(2014)079, arXiv:1405.0301.

[39] T. Sjöstrand, S. Mrenna, and P. Z. Skands, "PYTHIA 6.4 physics and manual", *JHEP* **05** (2006) 026, doi:10.1088/1126-6708/2006/05/026, arXiv:hep-ph/0603175.

[40] T. Sjöstrand et al., "An introduction to PYTHIA 8.2", *Comput. Phys. Commun.* **191** (2015) 159, doi:10.1016/j.cpc.2015.01.024, arXiv:1410.3012.

[41] CMS Collaboration, "The CMS trigger system", *JINST* **12** (2017) P01020, doi:10.1088/1748-0221/12/01/P01020, arXiv:1609.02366.

[42] CMS Collaboration, "The CMS experiment at the CERN LHC", *JINST* **3** (2008) S08004, doi:10.1088/1748-0221/3/08/S08004.

[43] NNPDF Collaboration, "Unbiased global determination of parton distributions and their uncertainties at NNLO and LO", *Nucl. Phys. B* **855** (2012) 153, doi:10.1016/j.nuclphysb.2011.09.024, arXiv:1107.2652.

[44] Particle Data Group, C. Patrignani et al., "Review of particle physics", *Chin. Phys. C* **40** (2016) 100001, doi:10.1088/1674-1137/40/10/100001.

[45] S. Frixione, P. Nason, and G. Ridolfi, "A positive-weight next-to-leading-order Monte Carlo for heavy flavour hadroproduction", *JHEP* **09** (2007) 126, doi:10.1088/1126-6708/2007/09/126, arXiv:0707.3088.

[46] S. Alioli, P. Nason, C. Oleari, and E. Re, "A general framework for implementing NLO calculations in shower Monte Carlo programs: the POWHEG BOX", *JHEP* **06** (2010) 043, doi:10.1007/JHEP06(2010)043, arXiv:1002.2581.

[47] CMS Collaboration, "Investigations of the impact of the parton shower tuning in PYTHIA in the modelling of $\mathrm{t\bar{t}}$ at $\sqrt{s} = 8$ and 13 TeV", CMS Physics Analysis Summary CMS-PAS-TOP-16-021, 2016.

[48] CMS Collaboration, "Event generator tunes obtained from underlying event and multiparton scattering measurements", *Eur. Phys. J. C* **76** (2016) 155, doi:10.1140/epjc/s10052-016-3988-x, arXiv:1512.00815.

[49] P. Skands, S. Carrazza, and J. Rojo, "Tuning PYTHIA 8.1: the Monash 2013 Tune", *Eur. Phys. J. C* **74** (2014) 3024, doi:10.1140/epjc/s10052-014-3024-y, arXiv:1404.5630.

[50] P. Artoisenet, R. Frederix, O. Mattelaer, and R. Rietkerk, "Automatic spin-entangled decays of heavy resonances in Monte Carlo simulations", *JHEP* **03** (2013) 015, doi:10.1007/JHEP03(2013)015, arXiv:1212.3460.

[51] R. Frederix and S. Frixione, "Merging meets matching in MC@NLO", *JHEP* **12** (2012) 061, doi:10.1007/JHEP12(2012)061, arXiv:1209.6215.

[52] M. Bähr et al., "Herwig++ physics and manual", *Eur. Phys. J. C* **58** (2008) 639, doi:10.1140/epjc/s10052-008-0798-9, arXiv:0803.0883.

[53] M. H. Seymour and A. Siodmok, "Constraining MPI models using σ_{eff} and recent Tevatron and LHC underlying event data", *JHEP* **10** (2013) 113, doi:10.1007/JHEP10(2013)113, arXiv:1307.5015.

[54] S. Alioli, P. Nason, C. Oleari, and E. Re, "NLO single-top production matched with shower in POWHEG: s- and t-channel contributions", *JHEP* **09** (2009) 111, doi:10.1088/1126-6708/2009/09/111, arXiv:0907.4076. [Erratum: doi:10.1007/JHEP02(2010)011].

[55] J. Alwall et al., "Comparative study of various algorithms for the merging of parton showers and matrix elements in hadronic collisions", *Eur. Phys. J. C* **53** (2008) 473, doi:10.1140/epjc/s10052-007-0490-5, arXiv:0706.2569.

[56] N. Kidonakis, "Two-loop soft anomalous dimensions for single top quark associated production with $\mathrm{W^-}$ or $\mathrm{H^-}$", *Phys. Rev. D* **82** (2010) 054018, doi:10.1103/PhysRevD.82.054018, arXiv:hep-ph/1005.4451.

[57] Y. Li and F. Petriello, "Combining QCD and electroweak corrections to dilepton production in FEWZ", *Phys. Rev. D* **86** (2012) 094034, doi:10.1103/PhysRevD.86.094034, arXiv:1208.5967.

[58] J. M. Campbell, R. K. Ellis, and C. Williams, "Vector boson pair production at the LHC", *JHEP* **07** (2011) 018, doi:10.1007/JHEP07(2011)018, arXiv:1105.0020.

[59] M. Czakon and A. Mitov, "Top++: a program for the calculation of the top-pair cross-section at hadron colliders", *Comput. Phys. Commun.* **185** (2014) 2930, doi:10.1016/j.cpc.2014.06.021, arXiv:1112.5675.

[60] S. Dulat et al., "New parton distribution functions from a global analysis of quantum chromodynamics", *Phys. Rev. D* **93** (2016) 033006, doi:10.1103/PhysRevD.93.033006, arXiv:1506.07443.

[61] ATLAS Collaboration, "Measurement of the inelastic proton-proton cross section at $\sqrt{s} = 13$ TeV with the ATLAS detector at the LHC", *Phys. Rev. Lett.* **117** (2016) 182002, doi:10.1103/PhysRevLett.117.182002, arXiv:1606.02625.

[62] GEANT4 Collaboration, "GEANT4—a simulation toolkit", *Nucl. Instrum. Meth. A* **506** (2003) 250, doi:10.1016/S0168-9002(03)01368-8.

[63] CMS Collaboration, "Particle-flow reconstruction and global event description with the CMS detector", *JINST* **12** (2017) P10003, doi:10.1088/1748-0221/12/10/P10003, arXiv:1706.04965.

[64] M. Cacciari, G. P. Salam, and G. Soyez, "The catchment area of jets", *JHEP* **04** (2008) 005, doi:10.1088/1126-6708/2008/04/005, arXiv:0802.1188.

[65] CMS Collaboration, "Performance of electron reconstruction and selection with the CMS detector in proton-proton collisions at $\sqrt{s} = 8$ TeV", *JINST* **10** (2015) P06005, doi:10.1088/1748-0221/10/06/P06005, arXiv:1502.02701.

[66] M. Cacciari, G. P. Salam, and G. Soyez, "The anti-k_{T} jet clustering algorithm", *JHEP* **04** (2008) 063, doi:10.1088/1126-6708/2008/04/063, arXiv:0802.1189.

[67] M. Cacciari, G. P. Salam, and G. Soyez, "FastJet user manual", *Eur. Phys. J. C* **72** (2012) 1896, doi:10.1140/epjc/s10052-012-1896-2, arXiv:1111.6097.

[68] CMS Collaboration, "Jet energy scale and resolution in the CMS experiment in pp collisions at 8 TeV", *JINST* **12** (2017) P02014, doi:10.1088/1748-0221/12/02/P02014, arXiv:1607.03663.

[69] CMS Collaboration, "Identification of heavy-flavour jets with the CMS detector in pp collisions at 13 TeV", *JINST* **13** (2018) P05011, doi:10.1088/1748-0221/13/05/P05011, arXiv:1712.07158.

[70] S. Schmitt, "TUnfold: an algorithm for correcting migration effects in high energy physics", *JINST* **7** (2012) T10003, doi:10.1088/1748-0221/7/10/T10003, arXiv:1205.6201.

[71] A. N. Tikhonov, "Solution of incorrectly formulated problems and the regularization method", *Sov. Math. Dokl.* **4** (1963) 1035.

[72] S. Schmitt, "Data unfolding methods in high energy physics", *Eur. Phys. J. Web Conf.* **137** (2017) 11008, doi:10.1051/epjconf/201713711008, arXiv:1611.01927.

[73] CMS Collaboration, "Measurement of the Drell-Yan cross section in pp collisions at $\sqrt{s} = 7$ TeV", *JHEP* **10** (2011) 007, doi:10.1007/JHEP10(2011)007, arXiv:1108.0566.

[74] CMS Collaboration, "Measurement of the top quark pair production cross section in proton-proton collisions at $\sqrt{s} = 13$ TeV", *Phys. Rev. Lett.* **116** (2016) 052002, doi:10.1103/PhysRevLett.116.052002, arXiv:1510.05302.

[75] CMS Collaboration, "CMS luminosity measurements for the 2016 data taking period", CMS Physics Analysis Summary CMS-PAS-LUM-17-001, 2017.

[76] S. Argyropoulos and T. Sjöstrand, "Effects of color reconnection on $t\bar{t}$ final states at the LHC", *JHEP* **11** (2014) 043, doi:10.1007/JHEP11(2014)043, arXiv:1407.6653.

[77] J. R. Christiansen and P. Z. Skands, "String formation beyond leading colour", *JHEP* **08** (2015) 003, doi:10.1007/JHEP08(2015)003, arXiv:1505.01681.

[78] M. G. Bowler, "e^+e^- Production of heavy quarks in the string model", *Z. Phys. C* **11** (1981) 169, doi:10.1007/BF01574001.

[79] C. Peterson, D. Schlatter, I. Schmitt, and P. M. Zerwas, "Scaling violations in inclusive e^+e^- annihilation spectra", *Phys. Rev. D* **27** (1983) 105, doi:10.1103/PhysRevD.27.105.

[80] M. L. Mangano, P. Nason, and G. Ridolfi, "Heavy quark correlations in hadron collisions at next-to-leading order", *Nucl. Phys. B* **373** (1992) 295, doi:10.1016/0550-3213(92)90435-E.

[81] S. Dittmaier, P. Uwer, and S. Weinzierl, "NLO QCD corrections to $t\bar{t}$+jet production at hadron colliders", *Phys. Rev. Lett.* **98** (2007) 262002, doi:10.1103/PhysRevLett.98.262002, arXiv:hep-ph/0703120.

[82] G. Bevilacqua, M. Czakon, C. G. Papadopoulos, and M. Worek, "Dominant QCD Backgrounds in Higgs Boson Analyses at the LHC: A Study of $pp \to t\bar{t} + 2$ jets at Next-To-Leading Order", *Phys. Rev. Lett.* **104** (2010) 162002, doi:10.1103/PhysRevLett.104.162002, arXiv:1002.4009.

[83] G. Bevilacqua, M. Czakon, C. G. Papadopoulos, and M. Worek, "Hadronic top-quark pair production in association with two jets at Next-to-Leading Order QCD", *Phys. Rev. D* **84** (2011) 114017, doi:10.1103/PhysRevD.84.114017, arXiv:1108.2851.

[84] S. Höche et al., "Next-to-leading order QCD predictions for top-quark pair production with up to three jets", *Eur. Phys. J. C* **77** (2017) 145, doi:10.1140/epjc/s10052-017-4715-y, arXiv:1607.06934.

[85] M. Czakon, D. Heymes, and A. Mitov, "High-precision differential predictions for top-quark pairs at the LHC", *Phys. Rev. Lett.* **116** (2016) 082003, doi:10.1103/PhysRevLett.116.082003, arXiv:1511.00549.

[86] M. Czakon, D. Heymes, and A. Mitov, "Dynamical scales for multi-TeV top-pair production at the LHC", *JHEP* **04** (2017) 071, doi:10.1007/JHEP04(2017)071, arXiv:1606.03350.

[87] S. Alekhin, J. Blümlein, and S. Moch, "NLO PDFs from the ABMP16 fit", *Eur. Phys. J. C* **78** (2018) 477, doi:10.1140/epjc/s10052-018-5947-1, arXiv:1803.07537.

[88] A. Accardi et al., "Constraints on large-x parton distributions from new weak boson production and deep-inelastic scattering data", *Phys. Rev. D* **93** (2016) 114017, doi:10.1103/PhysRevD.93.114017, arXiv:1602.03154.

[89] H1, ZEUS Collaboration, "Combination of measurements of inclusive deep inelastic $e^{\pm}p$ scattering cross sections and QCD analysis of HERA data", *Eur. Phys. J. C* **75** (2015) 580, doi:10.1140/epjc/s10052-015-3710-4, arXiv:1506.06042.

[90] P. Jimenez-Delgado and E. Reya, "Delineating parton distributions and the strong coupling", *Phys. Rev. D* **89** (2014) 074049, doi:10.1103/PhysRevD.89.074049, arXiv:1403.1852.

[91] L. A. Harland-Lang, A. D. Martin, P. Motylinski, and R. S. Thorne, "Parton distributions in the LHC era: MMHT 2014 PDFs", *Eur. Phys. J. C* **75** (2015) 204, doi:10.1140/epjc/s10052-015-3397-6, arXiv:1412.3989.

[92] NNPDF Collaboration, "Parton distributions from high-precision collider data", *Eur. Phys. J. C* **77** (2017) 663, doi:10.1140/epjc/s10052-017-5199-5, arXiv:1706.00428.

[93] A. Buckley et al., "LHAPDF6: parton density access in the LHC precision era", *Eur. Phys. J. C* **75** (2015) 132, doi:10.1140/epjc/s10052-015-3318-8, arXiv:1412.7420.

[94] M. Cacciari et al., "Updated predictions for the total production cross sections of top and of heavier quark pairs at the Tevatron and at the LHC", *JHEP* **09** (2008) 127, doi:10.1088/1126-6708/2008/09/127, arXiv:0804.2800.

[95] J. Butterworth et al., "PDF4LHC recommendations for LHC Run II", *J. Phys. G* **43** (2016) 023001, doi:10.1088/0954-3899/43/2/023001, arXiv:1510.03865.

[96] A. Accardi et al., "A critical appraisal and evaluation of modern PDFs", *Eur. Phys. J. C* **76** (2016), no. 8, 471, doi:10.1140/epjc/s10052-016-4285-4, arXiv:1603.08906.

[97] Particle Data Group, M. Tanabashi et al., "Review of particle physics", *Phys. Rev. D* **98** (2018) 030001, doi:10.1103/PhysRevD.98.030001.

[98] Y. Kiyo et al., "Top-quark pair production near threshold at LHC", *Eur. Phys. J. C* **60** (2009) 375, doi:10.1140/epjc/s10052-009-0892-7, arXiv:0812.0919.

[99] J. Piclum and C. Schwinn, "Soft-gluon and Coulomb corrections to hadronic top-quark pair production beyond NNLO", *JHEP* **03** (2018) 164, doi:10.1007/JHEP03(2018)164, arXiv:1801.05788.

[100] J. H. Kühn, A. Scharf, and P. Uwer, "Weak Interactions in Top-Quark Pair Production at Hadron Colliders: An Update", *Phys. Rev. D* **91** (2015) 014020, doi:10.1103/PhysRevD.91.014020, arXiv:1305.5773.

[101] M. Czakon et al., "Top-pair production at the LHC through NNLO QCD and NLO EW", *JHEP* **10** (2017) 186, doi:10.1007/JHEP10(2017)186, arXiv:1705.04105.

[102] S. Alekhin et al., "HERAFitter", *Eur. Phys. J. C* **75** (2015) 304, doi:10.1140/epjc/s10052-015-3480-z, arXiv:1410.4412. xFITTER web site, https://www.xfitter.org.

[103] Y. L. Dokshitzer, "Calculation of the structure functions for deep inelastic scattering and e^+e^- annihilation by perturbation theory in quantum chromodynamics", *Sov. Phys. JETP* **46** (1977) 641.

[104] V. N. Gribov and L. N. Lipatov, "Deep inelastic ep scattering in perturbation theory", *Sov. J. Nucl. Phys.* **15** (1972) 438.

[105] G. Altarelli and G. Parisi, "Asymptotic freedom in parton language", *Nucl. Phys. B* **126** (1977) 298, doi:10.1016/0550-3213(77)90384-4.

[106] G. Curci, W. Furmanski, and R. Petronzio, "Evolution of parton densities beyond leading order: the nonsinglet case", *Nucl. Phys. B* **175** (1980) 27, doi:10.1016/0550-3213(80)90003-6.

[107] W. Furmanski and R. Petronzio, "Singlet parton densities beyond leading order", *Phys. Lett. B* **97** (1980) 437, doi:10.1016/0370-2693(80)90636-X.

[108] S. Moch, J. A. M. Vermaseren, and A. Vogt, "The three-loop splitting functions in QCD: the nonsinglet case", *Nucl. Phys. B* **688** (2004) 101, doi:10.1016/j.nuclphysb.2004.03.030, arXiv:hep-ph/0403192.

[109] A. Vogt, S. Moch, and J. A. M. Vermaseren, "The three-loop splitting functions in QCD: the singlet case", *Nucl. Phys. B* **691** (2004) 129, doi:10.1016/j.nuclphysb.2004.04.024, arXiv:hep-ph/0404111.

[110] M. Botje, "QCDNUM: Fast QCD evolution and convolution", *Comput. Phys. Commun.* **182** (2011) 490, doi:10.1016/j.cpc.2010.10.020, arXiv:1005.1481.

[111] R. S. Thorne and R. G. Roberts, "An ordered analysis of heavy flavor production in deep inelastic scattering", *Phys. Rev. D* **57** (1998) 6871, doi:10.1103/PhysRevD.57.6871, arXiv:hep-ph/9709442.

[112] R. S. Thorne, "A variable-flavor number scheme for NNLO", *Phys. Rev. D* **73** (2006) 054019, doi:10.1103/PhysRevD.73.054019, arXiv:hep-ph/0601245.

[113] R. S. Thorne, "Effect of changes of variable flavor number scheme on parton distribution functions and predicted cross sections", *Phys. Rev. D* **86** (2012) 074017, doi:10.1103/PhysRevD.86.074017, arXiv:1201.6180.

[114] V. Bertone et al., "aMCfast: automation of fast NLO computations for PDF fits", *JHEP* **08** (2014) 166, doi:10.1007/JHEP08(2014)166, arXiv:1406.7693.

[115] T. Carli et al., "A posteriori inclusion of parton density functions in NLO QCD final-state calculations at hadron colliders: The APPLGRID project", *Eur. Phys. J. C* **66** (2010) 503, doi:10.1140/epjc/s10052-010-1255-0, arXiv:0911.2985.

[116] A. D. Martin, W. J. Stirling, R. S. Thorne, and G. Watt, "Parton distributions for the LHC", *Eur. Phys. J. C* **63** (2009) 189, doi:10.1140/epjc/s10052-009-1072-5, arXiv:0901.0002.

[117] CMS Collaboration, "Measurement of the muon charge asymmetry in inclusive $pp \to W + X$ production at $\sqrt{s} = 7$ TeV and an improved determination of light parton distribution functions", *Phys. Rev. D* **90** (2014) 032004, doi:10.1103/PhysRevD.90.032004, arXiv:1312.6283.

[118] H1 Collaboration, "Inclusive deep inelastic scattering at high Q^2 with longitudinally polarised lepton beams at HERA", *JHEP* **09** (2012) 061, doi:10.1007/JHEP09(2012)061, arXiv:1206.7007.

[119] W. T. Giele and S. Keller, "Implications of hadron collider observables on parton distribution function uncertainties", *Phys. Rev. D* **58** (1998) 094023, doi:10.1103/PhysRevD.58.094023, arXiv:hep-ph/9803393.

[120] W. T. Giele, S. A. Keller, and D. A. Kosower, "Parton distribution function uncertainties", (2001). arXiv:hep-ph/0104052.

A Measured cross sections

Tables A.1 to A.47 provide the measured cross sections, including their correlation matrices of statistical uncertainties and detailed breakdown of systematic uncertainties. The description of JES uncertainty sources can be found in Ref. [68].

Table A.1: The measured $[y(\mathrm{t}), p_{\mathrm{T}}(\mathrm{t})]$ cross sections, along with their relative statistical and systematic uncertainties.

$\lvert y(\mathrm{t})\rvert$	$p_{\mathrm{t}}(\mathrm{t})$ [GeV]	$\frac{1}{\sigma(\mathrm{t\bar{t}})}\frac{\mathrm{d}\sigma}{\mathrm{d}p_{\mathrm{t}}(\mathrm{t})}$[GeV^{-1}]	stat. [%]	syst. [%]	bin
0.00–0.35	0–80	9.251×10^{-4}	2.5	$^{+6.6}_{-5.2}$	1
0.00–0.35	80–150	1.118×10^{-3}	1.8	$^{+2.4}_{-4.6}$	2
0.00–0.35	150–250	4.596×10^{-4}	2.1	$^{+4.6}_{-2.7}$	3
0.00–0.35	250–600	3.993×10^{-5}	2.9	$^{+3.7}_{-5.6}$	4
0.35–0.85	0–80	1.279×10^{-3}	1.6	$^{+3.6}_{-3.4}$	5
0.35–0.85	80–150	1.503×10^{-3}	1.3	$^{+2.5}_{-2.8}$	6
0.35–0.85	150–250	6.206×10^{-4}	1.7	$^{+3.7}_{-2.6}$	7
0.35–0.85	250–600	5.097×10^{-5}	2.8	$^{+4.9}_{-4.7}$	8
0.85–1.45	0–80	1.248×10^{-3}	1.6	$^{+2.1}_{-4.4}$	9
0.85–1.45	80–150	1.435×10^{-3}	1.3	$^{+2.6}_{-2.7}$	10
0.85–1.45	150–250	5.328×10^{-4}	2.0	$^{+4.6}_{-2.0}$	11
0.85–1.45	250–600	4.516×10^{-5}	2.9	$^{+4.0}_{-5.4}$	12
1.45–2.50	0–80	1.128×10^{-3}	2.4	$^{+4.2}_{-5.8}$	13
1.45–2.50	80–150	1.284×10^{-3}	1.6	$^{+4.0}_{-2.5}$	14
1.45–2.50	150–250	4.238×10^{-4}	2.5	$^{+2.7}_{-5.6}$	15
1.45–2.50	250–600	2.430×10^{-5}	4.9	$^{+12.7}_{-4.2}$	16

Table A.2: The correlation matrix of statistical uncertainties for the measured $[y(\mathrm{t}), p_{\mathrm{T}}(\mathrm{t})]$ cross sections. The values are expressed as percentages. For bin indices see Table A.1.

bin	2	3	4	5	6	7	8	9	10	11	12	13	14	15	16
1	−22	−11	+3	−29	−31	+5	−2	−43	−4	+5	−3	+5	+4	−5	0
2		−20	+1	−28	−3	−17	+5	−4	−12	+3	0	+1	−3	0	0
3			−37	+10	−16	−21	+3	+7	+4	−2	+3	−9	−2	+1	0
4				−2	+7	+4	−22	−3	+1	+2	+3	−3	−2	0	0
5					+4	−12	+4	+36	−17	−3	+2	−43	−10	+9	−2
6						+2	−5	−19	+23	−18	+5	−15	−15	+3	+1
7							−31	−5	−17	−7	−2	0	−1	−3	+2
8								+1	+5	−1	−17	−6	−2	+2	+2
9									−9	−13	+3	−18	−32	+5	−1
10										−3	−4	−34	+2	−12	+5
11											−33	−2	−17	−12	+1
12												−4	+3	+1	−14
13													−14	−28	+6
14														−12	−7
15															−41

Table A.3: Sources and values of the relative systematic uncertainties in percent of the measured $[y(t), p_T(t)]$ cross sections. For bin indices see Table A.1.

source / bin	1	2	3	4	5	6	7	8	9	10	11	12	13	14	15	16
JER	+0.4	−0.9	−0.3	0.0	+0.1	+0.2	+0.2	−0.5	−0.7	−0.1	+0.4	−0.7	+0.7	+0.4	−0.2	−0.3
	+0.7	−0.3	−0.2	+0.8	+0.2	+0.1	+0.3	−0.2	−0.6	−0.1	+0.7	−0.1	−0.9	+0.3	−0.3	+1.0
JESAbsoluteMPFBias	+0.6	−0.3	+0.2	+0.2	+0.3	0.0	0.0	−0.3	0.0	+0.1	+0.1	0.0	−1.2	+0.3	+0.1	+0.8
	+1.0	−0.5	+0.1	−0.1	+0.7	−0.4	+0.3	0.0	−0.6	+0.1	+0.4	−0.4	−0.9	+0.3	−0.1	+0.2
JESAbsoluteScale	−0.5	−0.5	+0.4	0.0	+0.7	−0.1	+0.1	−0.1	+0.4	−0.5	+0.1	−0.5	+0.2	+0.1	−0.9	+2.1
	0.0	−0.2	+0.2	−0.3	+0.2	−0.2	+0.4	−0.2	−0.4	−0.1	+0.4	+0.2	+0.3	0.0	−0.5	+1.7
JESAbsoluteStat	+1.2	−0.1	−0.8	−0.2	+0.1	0.0	+0.1	−0.8	+0.3	0.0	−0.3	−0.1	+0.1	−0.3	−0.8	−0.5
	−2.1	+0.5	+0.1	+0.6	−0.4	+0.2	+0.8	+0.4	−0.2	−0.2	+0.4	+0.1	+0.6	+0.2	−0.3	+1.5
JESFlavourQCD	+0.4	−0.2	+0.3	+0.7	+0.5	−0.3	−0.1	+0.6	−0.3	−0.2	+0.5	+0.8	−1.1	+0.3	+0.2	+0.7
	+0.4	+0.2	+0.3	−1.5	−0.3	+0.3	+0.3	−0.8	−0.6	+0.2	0.0	−1.5	−0.1	+0.3	+0.1	−0.8
JESFragmentation	−0.4	−0.4	+0.6	0.0	0.0	+0.2	+0.6	−0.8	−0.2	+0.2	−0.3	+0.7	+0.2	−0.1	−0.5	+1.0
	−0.3	−0.3	+0.4	0.0	+0.5	−0.3	+0.2	−0.5	+0.1	−0.2	+0.4	−0.4	+0.1	+0.4	−0.9	+0.7
JESPileUpDataMC	−0.5	+0.4	+0.3	+0.4	−1.0	−0.2	−0.1	0.0	−0.1	−0.1	+0.2	+0.1	+0.8	+0.4	−0.3	+2.5
	+0.8	−0.3	+0.4	−0.4	−0.4	+0.2	+0.4	−0.6	−0.1	−0.1	+0.3	−1.0	+0.3	−0.4	−0.5	+0.9
JESPileUpPtBB	+0.5	−0.6	+0.2	+0.1	+0.4	−0.4	0.0	+0.3	−0.1	−0.3	+0.6	0.0	+0.3	−0.3	−0.3	+1.2
	+1.0	−0.5	+0.1	−0.3	+0.1	−0.2	−0.1	−0.6	−0.1	−0.1	+0.3	−0.2	+0.8	−0.7	−0.4	+0.4
JESPileUpPtEC1	+0.8	+0.1	+0.5	0.0	+0.4	+0.4	+0.9	+0.3	−0.4	+0.2	−0.1	+0.7	−1.7	−0.6	−0.3	+1.2
	−0.1	−0.9	−0.2	−0.6	+0.1	0.0	−0.3	−0.5	+0.3	+0.2	−0.1	−0.1	+0.9	−0.2	+0.4	−0.8
JESPileUpPtEC2	0.0	0.0	0.0	0.0	0.0	0.0	0.0	0.0	0.0	0.0	0.0	0.0	0.0	0.0	0.0	0.0
	0.0	0.0	0.0	0.0	0.0	0.0	0.0	0.0	0.0	0.0	0.0	0.0	0.0	0.0	0.0	0.0
JESPileUpPtHF	0.0	0.0	0.0	0.0	0.0	0.0	0.0	0.0	0.0	0.0	0.0	0.0	0.0	0.0	0.0	0.0
	0.0	0.0	0.0	0.0	0.0	0.0	0.0	0.0	0.0	0.0	0.0	0.0	0.0	0.0	0.0	0.0
JESPileUpPtRef	+0.6	−0.8	+0.3	+0.2	+0.4	−0.2	+0.8	0.0	+0.1	−0.5	+1.4	−0.2	−1.0	−0.1	0.0	+1.4
	−0.3	+0.3	−0.7	+0.4	+0.2	+0.1	0.0	−1.1	0.0	−0.4	+0.8	−0.9	+0.4	+0.1	−0.6	+0.4
JESRelativeBal	+0.1	−0.7	−0.1	+0.9	+1.1	+0.1	+0.2	+0.1	−0.2	0.0	+0.4	−0.2	+0.1	−0.4	−1.7	+1.9
	−0.5	−0.6	+0.1	−0.5	+0.1	0.0	0.0	−0.5	−0.3	+0.2	+0.4	−1.0	+0.1	+0.7	0.0	+1.7
JESRelativeFSR	−1.1	−0.3	+0.5	0.0	+0.4	+0.1	0.0	−0.4	−0.3	+0.2	+0.2	−0.4	−0.1	+0.7	−0.5	+1.1
	+1.4	−0.9	+0.3	−0.3	+0.2	−0.2	−0.1	+0.6	−0.5	−0.1	+1.0	−0.6	+0.2	−0.3	−1.0	+2.6
JESRelativeJEREC1	−0.6	−0.1	+0.1	−0.2	+0.2	+0.3	0.0	0.0	0.0	−0.3	−0.1	0.0	0.0	+0.4	−0.1	+0.4
	−0.2	−0.2	+0.2	−0.3	+0.3	+0.3	−0.1	−0.1	+0.2	+0.1	0.0	+0.2	−0.1	−0.5	−0.3	+1.0
JESRelativeJEREC2	0.0	0.0	0.0	0.0	0.0	0.0	0.0	0.0	0.0	0.0	0.0	0.0	0.0	0.0	0.0	0.0
	0.0	0.0	0.0	0.0	0.0	0.0	0.0	0.0	0.0	0.0	0.0	0.0	0.0	0.0	0.0	0.0
JESRelativeJERHF	0.0	0.0	0.0	0.0	0.0	0.0	0.0	0.0	0.0	0.0	0.0	0.0	0.0	0.0	0.0	0.0
	0.0	0.0	0.0	0.0	0.0	0.0	0.0	0.0	0.0	0.0	0.0	0.0	0.0	0.0	0.0	0.0
JESRelativePtBB	+1.2	−0.4	+0.2	−0.2	−0.2	−0.7	+0.1	−0.2	−0.3	−0.3	+1.2	−0.3	+0.3	0.0	−0.4	+0.7
	−0.6	+0.1	+0.5	0.0	+0.2	+0.2	−0.2	−0.1	+0.2	0.0	+0.1	−0.2	−0.4	+0.1	−0.6	+2.2
JESRelativePtEC1	−0.1	−0.1	+0.4	−0.1	+0.4	+0.3	+0.7	−0.1	+0.3	−0.4	+0.1	+0.2	−0.2	−0.5	−1.2	0.0
	−0.2	−0.2	−0.3	−0.5	+0.3	0.0	−0.1	−0.1	−0.3	+0.3	0.0	+0.1	−0.3	+0.3	+0.5	+0.7
JESRelativePtEC2	0.0	0.0	0.0	0.0	0.0	0.0	0.0	0.0	0.0	0.0	0.0	0.0	0.0	0.0	0.0	0.0
	0.0	0.0	0.0	0.0	0.0	0.0	0.0	0.0	0.0	0.0	0.0	0.0	0.0	0.0	0.0	0.0
JESRelativePtHF	0.0	0.0	0.0	0.0	0.0	0.0	0.0	0.0	0.0	0.0	0.0	0.0	0.0	0.0	0.0	0.0
	0.0	0.0	0.0	0.0	0.0	0.0	0.0	0.0	0.0	0.0	0.0	0.0	0.0	0.0	0.0	0.0
JESRelativeStatEC	−0.3	+0.2	0.0	−0.4	+0.4	0.0	+0.5	−0.2	−0.1	−0.5	−0.1	+0.2	−0.1	+0.4	−0.4	−0.1
	−0.7	−0.4	+0.2	−0.4	+0.5	+0.1	+0.1	0.0	+0.4	+0.1	+0.2	−0.2	−0.5	−0.1	+0.2	+0.4
JESRelativeStatFSR	−1.1	+0.1	+0.1	+0.2	0.0	−0.1	+0.1	−0.4	+0.1	−0.1	+0.5	−0.4	+0.4	+0.3	−0.5	+0.8
	+0.6	−0.8	+0.5	+0.2	+0.5	−0.3	−0.3	−0.2	−0.5	+0.2	+0.3	−0.1	−0.1	+0.6	−1.1	+1.5
JESRelativeStatHF	0.0	0.0	0.0	0.0	0.0	0.0	0.0	0.0	0.0	0.0	0.0	0.0	0.0	0.0	0.0	0.0
	0.0	0.0	0.0	0.0	0.0	0.0	0.0	0.0	0.0	0.0	0.0	0.0	0.0	0.0	0.0	0.0
JESSinglePionECAL	+0.1	−0.2	−0.1	−0.5	+0.4	0.0	0.0	−0.3	−0.1	−0.1	−0.1	−0.5	+0.2	+0.2	−0.2	+0.5
	−1.6	0.0	0.0	+0.4	+0.6	+0.6	−0.1	+0.4	+0.2	+0.3	+0.4	−0.1	−0.9	−0.2	+0.1	+0.6

Table A.4: Table A.3 continued.

source / bin	1	2	3	4	5	6	7	8	9	10	11	12	13	14	15	16
JESSinglePionHCAL	−0.1	−0.3	−0.2	0.0	+0.2	+0.3	+0.2	−0.6	+0.2	−0.1	0.0	0.0	−0.1	−0.1	0.0	+0.1
	+0.2	+0.1	−0.3	+0.4	−0.1	−0.5	+0.6	−0.4	+0.1	−0.2	+0.2	+0.6	−0.1	+0.3	−0.3	+0.9
JESTimePtEta	+0.8	−0.7	+0.6	+0.1	−0.6	−0.3	−0.4	−0.2	−0.7	+0.2	+0.3	0.0	+0.5	+0.8	−0.5	+1.5
	−0.1	+0.2	+0.1	+0.1	+0.3	−0.4	+0.1	+0.1	−0.2	−0.5	+0.6	−0.4	+0.7	0.0	−1.2	+1.6
$\vec{p}_{\mathrm{T}}^{\,\mathrm{miss}}$	+0.7	−0.6	+0.6	−0.1	+0.2	−0.1	+0.1	−0.6	+0.3	+0.1	−0.3	−0.1	−0.6	−0.1	−0.3	+0.5
	−0.2	+0.1	0.0	+0.5	−0.2	+0.4	−0.1	+0.1	−0.2	−0.2	+0.4	+0.2	+0.2	−0.2	0.0	+0.4
lepton ID/ISO	−0.2	+0.1	0.0	−0.4	0.0	+0.2	0.0	−0.2	−0.1	+0.2	−0.1	−0.3	−0.1	+0.3	0.0	−0.6
	+0.2	−0.1	0.0	+0.4	0.0	−0.2	0.0	+0.2	+0.1	−0.2	+0.1	+0.3	+0.1	−0.3	0.0	+0.6
pileup	−0.1	+0.3	0.0	−0.2	+0.1	+0.2	+0.1	0.0	−0.1	−0.1	0.0	−0.2	−0.1	−0.2	−0.1	−0.2
	0.0	−0.3	0.0	+0.3	−0.1	−0.2	−0.1	0.0	+0.1	+0.1	0.0	+0.1	+0.1	+0.1	+0.1	+0.2
trigger	0.0	+0.1	0.0	0.0	+0.1	+0.2	+0.1	+0.2	0.0	+0.1	+0.1	+0.1	−0.4	−0.2	−0.2	−0.2
	0.0	−0.1	0.0	0.0	−0.1	−0.2	−0.1	−0.2	0.0	−0.1	−0.1	−0.1	+0.4	+0.2	+0.2	+0.2
trigger (η)	−0.2	−0.2	−0.2	−0.2	−0.1	−0.1	−0.1	−0.1	0.0	0.0	0.0	0.0	+0.4	+0.3	+0.2	+0.2
	+0.2	+0.2	+0.2	+0.2	+0.1	+0.1	+0.1	+0.1	0.0	0.0	0.0	0.0	−0.4	−0.3	−0.2	−0.2
non-$\mathrm{t\bar{t}}$ background	−0.9	+0.6	+0.9	+1.0	−0.8	+0.6	+0.8	+1.0	−0.7	+0.6	+0.6	+1.1	−2.0	+0.1	+1.1	+0.2
	+0.9	−0.6	−0.9	−0.9	+0.7	−0.5	−0.8	−0.9	+0.7	−0.5	−0.6	−1.0	+1.9	−0.1	−1.0	−0.2
b-tagging	−0.1	+0.1	0.0	0.0	−0.1	0.0	0.0	+0.1	−0.1	0.0	0.0	+0.1	0.0	+0.1	+0.1	+0.1
	+0.1	−0.1	0.0	0.0	+0.1	0.0	0.0	0.0	+0.1	0.0	0.0	−0.1	0.0	−0.1	−0.1	−0.1
b-tagging (light jets)	−0.2	+0.2	+0.3	+0.3	−0.2	+0.2	+0.3	+0.2	−0.3	+0.1	+0.2	+0.2	−0.6	0.0	+0.2	+0.1
	+0.2	−0.2	−0.3	−0.3	+0.2	−0.2	−0.3	−0.2	+0.3	−0.1	−0.2	−0.2	+0.6	0.0	−0.2	−0.1
luminosity	0.0	0.0	0.0	0.0	0.0	0.0	0.0	0.0	0.0	0.0	0.0	0.0	0.0	0.0	0.0	0.0
	0.0	0.0	0.0	0.0	0.0	0.0	0.0	0.0	0.0	0.0	0.0	0.0	0.0	0.0	0.0	0.0
branching ratio $\mathrm{t\bar{t}} \to \ell\ell$	0.0	0.0	0.0	0.0	0.0	0.0	0.0	0.0	0.0	0.0	0.0	0.0	0.0	0.0	0.0	0.0
	0.0	0.0	0.0	0.0	0.0	0.0	0.0	0.0	0.0	0.0	0.0	0.0	0.0	0.0	0.0	0.0
PDF eigenvector 1	0.0	0.0	0.0	0.0	0.0	0.0	0.0	0.0	0.0	0.0	0.0	0.0	0.0	0.0	0.0	0.0
	0.0	0.0	0.0	0.0	0.0	0.0	0.0	0.0	0.0	0.0	0.0	0.0	0.0	0.0	0.0	+0.1
PDF eigenvector 2	−0.2	−0.1	0.0	+0.1	−0.1	0.0	0.0	+0.1	0.0	0.0	+0.1	0.0	+0.1	+0.1	0.0	−0.2
	+0.1	0.0	0.0	−0.1	0.0	−0.1	0.0	−0.1	0.0	0.0	0.0	−0.1	0.0	0.0	+0.1	−0.1
PDF eigenvector 3	+0.1	+0.1	0.0	0.0	0.0	0.0	0.0	0.0	0.0	0.0	0.0	0.0	−0.1	−0.1	−0.1	+0.1
	0.0	0.0	0.0	0.0	0.0	0.0	0.0	0.0	0.0	0.0	0.0	0.0	0.0	+0.1	+0.1	0.0
PDF eigenvector 4	−0.2	0.0	0.0	+0.1	−0.1	0.0	0.0	+0.1	0.0	0.0	0.0	+0.1	+0.1	+0.1	+0.1	0.0
	+0.1	0.0	0.0	−0.1	0.0	0.0	0.0	−0.1	0.0	0.0	0.0	−0.1	0.0	0.0	0.0	0.0
PDF eigenvector 5	0.0	−0.1	0.0	−0.2	0.0	−0.1	0.0	−0.2	0.0	0.0	0.0	−0.1	0.0	+0.1	+0.1	−0.2
	+0.1	+0.1	+0.1	+0.1	+0.1	+0.1	+0.1	+0.1	0.0	0.0	−0.1	0.0	−0.1	−0.2	−0.3	+0.2
PDF eigenvector 6	−0.1	0.0	0.0	+0.1	0.0	+0.1	0.0	+0.1	0.0	0.0	0.0	+0.1	0.0	0.0	0.0	+0.1
	+0.1	0.0	0.0	−0.1	0.0	0.0	0.0	−0.1	0.0	0.0	0.0	−0.1	0.0	0.0	0.0	−0.1
PDF eigenvector 7	0.0	−0.1	−0.1	−0.3	0.0	−0.1	−0.1	−0.3	0.0	0.0	+0.1	−0.2	+0.1	+0.2	+0.2	−0.4
	0.0	+0.1	0.0	+0.2	0.0	+0.1	0.0	+0.1	0.0	0.0	−0.1	+0.1	−0.1	−0.1	−0.1	+0.2
PDF eigenvector 8	0.0	0.0	0.0	0.0	0.0	0.0	0.0	0.0	0.0	0.0	0.0	0.0	0.0	+0.1	0.0	0.0
	0.0	0.0	0.0	0.0	0.0	0.0	0.0	0.0	0.0	0.0	0.0	0.0	0.0	−0.1	0.0	0.0
PDF eigenvector 9	0.0	0.0	0.0	0.0	0.0	−0.1	0.0	0.0	0.0	0.0	0.0	0.0	+0.1	0.0	0.0	−0.1
	0.0	0.0	0.0	0.0	0.0	+0.1	0.0	0.0	0.0	0.0	0.0	0.0	−0.1	0.0	−0.1	+0.1
PDF eigenvector 10	0.0	+0.1	0.0	+0.1	0.0	+0.1	0.0	+0.1	0.0	0.0	−0.1	+0.1	0.0	−0.1	−0.1	+0.2
	0.0	−0.1	0.0	−0.2	0.0	−0.1	0.0	−0.1	0.0	0.0	+0.1	−0.1	0.0	+0.1	+0.1	−0.2
PDF eigenvector 11	0.0	0.0	0.0	0.0	0.0	0.0	0.0	0.0	0.0	0.0	0.0	0.0	0.0	0.0	0.0	0.0
	0.0	0.0	0.0	−0.1	0.0	0.0	0.0	−0.1	0.0	0.0	0.0	0.0	0.0	0.0	+0.1	−0.1
PDF eigenvector 12	0.0	0.0	0.0	−0.1	0.0	0.0	0.0	−0.1	0.0	0.0	0.0	−0.1	0.0	+0.1	0.0	−0.1
	0.0	0.0	0.0	+0.1	0.0	0.0	0.0	+0.1	0.0	0.0	0.0	+0.1	0.0	−0.1	0.0	+0.1
PDF eigenvector 13	+0.1	0.0	0.0	0.0	0.0	0.0	0.0	0.0	0.0	0.0	−0.1	0.0	−0.1	0.0	−0.1	+0.1
	−0.1	0.0	0.0	0.0	0.0	0.0	0.0	0.0	0.0	0.0	+0.1	0.0	+0.1	0.0	+0.1	−0.1
PDF eigenvector 14	0.0	0.0	0.0	0.0	0.0	0.0	0.0	0.0	0.0	0.0	0.0	0.0	0.0	0.0	0.0	−0.1
	0.0	0.0	0.0	0.0	0.0	0.0	0.0	+0.1	0.0	0.0	0.0	+0.1	0.0	0.0	0.0	+0.1

Table A.5: Table A.3 continued.

source / bin	1	2	3	4	5	6	7	8	9	10	11	12	13	14	15	16
PDF eigenvector 15	+0.1	0.0	0.0	−0.1	0.0	0.0	0.0	−0.1	0.0	0.0	0.0	−0.1	0.0	0.0	0.0	−0.1
	0.0	0.0	0.0	0.0	0.0	0.0	0.0	0.0	0.0	0.0	0.0	0.0	0.0	0.0	0.0	0.0
PDF eigenvector 16	0.0	0.0	0.0	0.0	0.0	0.0	0.0	0.0	0.0	0.0	0.0	0.0	0.0	0.0	0.0	0.0
	0.0	0.0	0.0	0.0	0.0	0.0	0.0	0.0	0.0	0.0	0.0	0.0	0.0	0.0	0.0	−0.1
PDF eigenvector 17	0.0	0.0	0.0	0.0	0.0	0.0	0.0	0.0	0.0	0.0	0.0	0.0	0.0	0.0	0.0	−0.1
	0.0	0.0	0.0	+0.1	0.0	0.0	0.0	+0.1	0.0	0.0	0.0	+0.1	0.0	0.0	0.0	+0.1
PDF eigenvector 18	−0.1	0.0	0.0	+0.1	−0.1	0.0	0.0	+0.1	0.0	0.0	0.0	+0.1	+0.1	0.0	+0.2	+0.1
	+0.1	0.0	0.0	−0.1	+0.1	0.0	0.0	−0.1	0.0	0.0	0.0	−0.1	−0.1	0.0	−0.2	−0.1
PDF eigenvector 19	0.0	0.0	0.0	+0.1	0.0	0.0	0.0	+0.1	0.0	0.0	0.0	+0.1	0.0	0.0	0.0	+0.1
	+0.1	0.0	0.0	−0.2	0.0	0.0	0.0	−0.2	0.0	0.0	0.0	−0.1	0.0	+0.1	0.0	−0.2
PDF eigenvector 20	0.0	0.0	0.0	0.0	0.0	0.0	0.0	0.0	0.0	0.0	0.0	+0.1	+0.1	0.0	+0.1	+0.2
	0.0	0.0	0.0	−0.1	0.0	0.0	0.0	0.0	0.0	0.0	0.0	0.0	0.0	0.0	0.0	−0.1
PDF eigenvector 21	−0.1	0.0	0.0	0.0	0.0	0.0	0.0	0.0	0.0	0.0	0.0	+0.1	+0.1	+0.1	+0.1	0.0
	+0.1	+0.1	0.0	0.0	0.0	0.0	0.0	0.0	0.0	0.0	0.0	0.0	−0.1	−0.1	−0.1	+0.1
PDF eigenvector 22	−0.2	−0.1	−0.1	+0.1	−0.1	−0.1	0.0	+0.1	0.0	0.0	+0.1	+0.1	+0.2	+0.2	+0.4	−0.1
	+0.2	+0.1	0.0	0.0	+0.1	+0.1	0.0	0.0	0.0	0.0	−0.1	−0.1	−0.2	−0.1	−0.3	+0.2
PDF eigenvector 23	+0.2	0.0	0.0	−0.1	+0.1	0.0	0.0	−0.1	0.0	0.0	0.0	−0.2	−0.2	−0.1	−0.3	−0.1
	0.0	0.0	0.0	0.0	0.0	0.0	0.0	0.0	0.0	0.0	0.0	0.0	+0.1	0.0	+0.1	0.0
PDF eigenvector 24	+0.1	0.0	0.0	−0.1	0.0	0.0	0.0	−0.1	0.0	0.0	0.0	0.0	0.0	0.0	+0.1	0.0
	−0.1	−0.1	0.0	−0.1	0.0	0.0	0.0	−0.1	+0.1	0.0	+0.1	−0.1	0.0	0.0	−0.1	−0.3
PDF eigenvector 25	0.0	0.0	0.0	−0.1	0.0	0.0	0.0	−0.1	+0.1	0.0	+0.1	−0.1	0.0	0.0	−0.1	−0.2
	+0.1	−0.1	−0.1	−0.2	0.0	−0.1	0.0	−0.1	0.0	0.0	0.0	−0.1	0.0	+0.1	+0.2	−0.1
PDF eigenvector 26	0.0	0.0	0.0	0.0	0.0	0.0	0.0	0.0	0.0	0.0	0.0	0.0	0.0	0.0	0.0	0.0
	0.0	0.0	0.0	0.0	0.0	0.0	0.0	0.0	0.0	0.0	0.0	0.0	0.0	0.0	0.0	0.0
PDF eigenvector 27	0.0	0.0	+0.1	+0.1	0.0	−0.1	0.0	+0.1	+0.1	0.0	0.0	0.0	+0.1	−0.1	0.0	−0.1
	−0.1	0.0	0.0	0.0	0.0	0.0	0.0	0.0	0.0	0.0	0.0	0.0	0.0	0.0	0.0	0.0
PDF eigenvector 28	0.0	0.0	0.0	0.0	0.0	0.0	0.0	0.0	0.0	0.0	0.0	0.0	0.0	0.0	0.0	0.0
	−0.1	0.0	0.0	0.0	0.0	0.0	0.0	0.0	0.0	0.0	0.0	+0.1	0.0	+0.1	0.0	0.0
α_S	+0.1	0.0	+0.1	0.0	0.0	0.0	0.0	0.0	0.0	0.0	0.0	0.0	0.0	−0.1	0.0	0.0
	−0.1	0.0	−0.1	0.0	0.0	0.0	−0.1	0.0	0.0	0.0	0.0	0.0	0.0	+0.1	0.0	0.0
m_t^{MC}	+0.4	−0.8	+0.6	+0.9	+0.4	−0.6	+0.4	+1.8	+0.2	−0.6	+0.4	+1.6	−0.8	−0.2	+0.6	+2.4
	−0.1	+0.9	−0.4	−2.1	−0.4	+0.6	−0.1	−1.2	−0.2	+0.7	−0.5	−1.7	0.0	+0.3	−0.3	−2.2
$\mu_{r,f}$	+0.3	−0.2	+0.2	−0.5	−0.1	−0.6	+0.1	−0.2	+0.4	−0.2	+0.3	0.0	+0.6	−0.4	+0.3	0.0
	−0.3	+0.2	−0.1	+0.5	+0.1	+0.6	−0.1	+0.4	−0.4	+0.2	−0.2	+0.2	−0.6	+0.3	−0.5	+0.1
h_{damp}	+1.2	−0.9	+0.5	−0.8	+0.4	−0.5	+0.9	−0.3	−0.4	−0.6	+0.6	+0.1	−0.7	+0.6	−0.1	+1.8
	+0.1	0.0	−0.2	−1.0	−1.4	+0.6	−0.2	+0.6	−0.9	+1.0	−0.5	−1.0	+0.2	+0.9	+0.2	+2.2
PS ISR	+0.2	−1.1	+1.7	−1.0	+0.4	−0.1	−0.1	+0.1	−1.0	−0.3	+0.4	0.0	0.0	+1.0	−0.3	+2.0
	+1.1	+0.4	−0.2	+0.3	+0.3	−0.3	−0.4	+0.8	−1.0	−0.6	+0.9	−0.5	−0.3	+0.6	+0.2	−0.1
PS FSR	0.0	+0.7	−0.4	−1.2	0.0	+0.4	−0.9	−0.3	0.0	+0.8	−0.5	−1.2	−0.4	+0.5	−0.7	−0.7
	−0.2	−0.1	+0.1	+0.7	+0.3	−0.3	+0.2	+1.0	−0.2	−0.1	+0.5	+0.6	−0.6	+0.4	−0.8	+2.9
UE tune	+0.5	+0.1	−0.7	−0.8	+0.4	+0.3	0.0	+0.2	−1.2	+0.1	−0.3	0.0	−0.5	+0.6	+0.6	+0.9
	+2.2	+0.2	+0.2	0.0	−1.2	+0.2	+0.2	−1.5	−1.6	−0.1	+0.5	+0.3	0.0	+0.8	0.0	+0.6
colour reconnection	+0.3	−0.2	+1.4	+0.2	+0.3	−0.3	−0.9	+1.5	−0.2	−0.2	−0.2	+0.7	−0.7	+0.2	+0.2	+2.8
	+0.5	+0.1	0.0	−0.8	0.0	−0.2	−0.2	+0.6	+0.1	0.0	−0.4	+0.4	−0.4	+0.2	+0.5	−0.7
	+0.7	−0.2	+0.1	−0.6	−0.1	−0.4	+0.6	+0.5	−1.0	+0.2	+0.7	−0.4	−0.6	+1.0	−0.6	+0.9
fragmentation b → B	+0.7	−0.2	−0.2	+0.3	+0.4	−0.3	−0.2	+0.6	+0.6	−0.2	−0.2	+0.5	0.0	−0.6	−0.4	+0.7
	−0.4	+0.1	+0.1	−0.1	−0.2	+0.1	+0.2	−0.2	−0.2	+0.1	+0.1	−0.1	0.0	+0.2	+0.3	−0.2
	+0.1	0.0	0.0	+0.1	+0.1	−0.1	0.0	+0.1	+0.1	0.0	0.0	+0.1	0.0	−0.1	−0.1	+0.1
	+0.7	−0.3	−0.1	+0.4	+0.4	−0.4	−0.2	+0.3	+0.5	−0.3	−0.1	+0.5	+0.2	−0.5	−0.2	+0.4
branching ratio $B \to \mu$	−0.1	0.0	+0.1	−0.1	0.0	0.0	0.0	0.0	−0.1	0.0	+0.1	−0.1	0.0	0.0	0.0	0.0
	+0.1	−0.1	−0.1	+0.1	+0.1	−0.1	−0.1	+0.1	+0.1	−0.1	0.0	+0.1	0.0	−0.1	0.0	+0.2

Table A.6: The measured $[M(\mathrm{t\bar{t}}), y(\mathrm{t})]$ cross sections, along with their relative statistical and systematic uncertainties.

$M(\mathrm{t\bar{t}})$ [GeV]	$\lvert y(\mathrm{t})\rvert$	$\frac{1}{\sigma(\mathrm{t\bar{t}})}\frac{\mathrm{d}\sigma}{\mathrm{d}\lvert y(\mathrm{t})\rvert}$	stat. [%]	syst. [%]	bin
300–400	0.00–0.35	1.506×10^{-1}	3.1	$^{+6.6}_{-5.4}$	1
300–400	0.35–0.85	1.511×10^{-1}	2.2	$^{+3.5}_{-8.1}$	2
300–400	0.85–1.45	1.161×10^{-1}	2.2	$^{+4.2}_{-6.2}$	3
300–400	1.45–2.50	4.794×10^{-2}	4.6	$^{+19.5}_{-10.1}$	4
400–500	0.00–0.35	2.317×10^{-1}	1.9	$^{+3.9}_{-3.1}$	5
400–500	0.35–0.85	2.181×10^{-1}	1.3	$^{+2.2}_{-2.4}$	6
400–500	0.85–1.45	1.605×10^{-1}	1.5	$^{+4.2}_{-3.0}$	7
400–500	1.45–2.50	7.230×10^{-2}	2.1	$^{+6.8}_{-2.2}$	8
500–650	0.00–0.35	1.538×10^{-1}	2.2	$^{+5.9}_{-2.2}$	9
500–650	0.35–0.85	1.438×10^{-1}	1.8	$^{+1.7}_{-6.8}$	10
500–650	0.85–1.45	1.062×10^{-1}	1.9	$^{+3.7}_{-2.5}$	11
500–650	1.45–2.50	5.345×10^{-2}	2.5	$^{+3.2}_{-7.4}$	12
650–1500	0.00–0.35	6.963×10^{-2}	2.8	$^{+4.3}_{-8.6}$	13
650–1500	0.35–0.85	7.045×10^{-2}	2.3	$^{+6.2}_{-4.6}$	14
650–1500	0.85–1.45	6.765×10^{-2}	2.0	$^{+3.1}_{-5.5}$	15
650–1500	1.45–2.50	4.155×10^{-2}	2.2	$^{+4.8}_{-3.2}$	16

Table A.7: The correlation matrix of statistical uncertainties for the measured $[M(\mathrm{t\bar{t}}), y(\mathrm{t})]$ cross sections. The values are expressed as percentages. For bin indices see Table A.6.

bin	2	3	4	5	6	7	8	9	10	11	12	13	14	15	16
1	−34	−23	+8	−28	−29	0	+3	−8	+6	+4	−6	+2	−1	−3	−2
2		+18	−32	−19	−1	−23	−7	+10	−12	−3	+9	−1	+3	+5	−2
3			−21	+3	−21	−13	−32	+3	−1	−11	+2	−2	+1	+3	+2
4				−5	−9	−24	−14	−11	−4	−1	−32	−4	−8	−9	0
5					−5	−11	−2	−19	−22	+1	+3	−2	+7	+2	−2
6						+19	−15	−17	+4	−22	−1	+8	−9	+4	+2
7							+1	+4	−14	−2	−21	0	+4	−7	+5
8								−2	−1	−15	−5	−3	−3	+3	−17
9									−17	−3	+2	−38	−4	+4	−1
10										−2	−5	+2	−28	−12	+2
11											−8	+2	−1	−27	−9
12												−1	+3	+5	−34
13													−24	+2	−1
14														−19	+2
15															−23

Table A.8: Sources and values of the relative systematic uncertainties in percent of the measured $[M(\mathrm{t\bar{t}}), y(\mathrm{t})]$ cross sections. For bin indices see Table A.6.

source / bin	1	2	3	4	5	6	7	8	9	10	11	12	13	14	15	16
JER	−0.6	+0.3	−0.3	+2.4	+0.3	0.0	−0.2	−0.2	+0.4	−0.6	+0.6	−0.8	−1.1	−0.4	−0.2	−0.1
	−0.2	−1.1	−0.7	+3.9	+0.7	−0.2	−0.3	+0.8	0.0	−0.7	−0.1	−1.6	−0.2	+0.3	−0.2	+0.7
JESAbsoluteMPFBias	−0.9	+0.1	−0.7	+0.1	+0.9	0.0	−0.4	+1.4	+0.3	−1.1	−0.3	0.0	+0.1	+0.2	+0.2	+0.3
	−1.3	−0.5	−0.8	+1.7	+0.7	+0.5	+0.2	+0.6	+0.1	−0.7	+0.2	−1.0	−0.4	−0.2	−0.1	+0.2
JESAbsoluteScale	−0.2	−0.8	+0.7	+2.1	+0.7	−0.2	−0.3	−0.4	+0.3	−0.4	0.0	−1.2	0.0	−0.6	0.0	+0.9
	−0.5	−1.0	−0.4	+3.8	+0.4	−0.3	+0.1	+0.2	+0.4	−0.3	−0.2	−1.0	−0.9	0.0	−0.1	+0.1
JESAbsoluteStat	+0.3	+0.1	0.0	+1.8	−0.4	−0.4	−0.3	+0.5	+0.5	−0.6	+0.4	−0.7	−0.4	−0.1	+0.1	−0.2
	+1.2	−1.8	−0.3	+0.1	+0.1	0.0	+0.1	+1.3	+0.2	−0.8	+0.1	−0.3	+0.1	+0.5	0.0	+0.3
JESFlavourQCD	+1.5	−0.1	0.0	+2.5	−0.6	−0.8	−0.5	0.0	+0.2	−0.6	+0.1	−0.7	+0.3	+0.7	+0.5	+0.3
	−0.5	−1.9	−0.2	+1.7	+1.0	+0.3	+0.6	+0.8	+0.7	−0.4	−0.3	−0.7	−1.8	−0.4	−0.9	−0.1
JESFragmentation	−0.3	−0.7	0.0	+0.7	+0.2	−0.3	−0.3	+0.7	+0.6	+0.1	+0.3	−0.7	−0.1	−0.4	+0.3	+0.3
	+0.5	−0.6	−0.6	+3.0	0.0	0.0	−0.2	0.0	+0.5	−0.8	+0.3	−0.4	−0.6	−0.2	−0.1	−0.2
JESPileUpDataMC	+0.5	−1.4	+0.4	+0.3	+0.1	−0.5	+0.4	+0.3	+0.8	−0.8	0.0	−0.4	+0.2	0.0	+0.4	+0.4
	+0.8	−0.9	−0.3	+3.7	−0.2	+0.2	−0.3	+0.6	+0.8	−0.9	−0.3	−1.1	−1.0	−0.3	−0.6	0.0
JESPileUpPtBB	−0.7	−0.2	0.0	+1.6	+0.2	−0.2	−0.4	+0.4	+0.9	−0.6	−0.1	−0.6	−0.3	−0.3	+0.3	+0.4
	−0.4	+0.3	0.0	+1.8	0.0	−0.1	+0.1	+0.5	+0.7	−1.1	0.0	−1.3	−1.0	0.0	−0.1	+0.2
JESPileUpPtEC1	−0.1	+0.7	0.0	−1.5	+0.8	+0.2	−0.5	−0.5	+0.3	−0.1	0.0	0.0	−0.1	+0.2	+0.4	−0.3
	−0.2	−0.9	−0.3	+3.7	−0.6	−0.4	0.0	+1.0	−0.1	−0.6	0.0	−0.1	−0.7	−0.1	−0.2	+0.2
JESPileUpPtEC2	0.0	0.0	0.0	0.0	0.0	0.0	0.0	0.0	0.0	0.0	0.0	0.0	0.0	0.0	0.0	0.0
	0.0	0.0	0.0	0.0	0.0	0.0	0.0	0.0	0.0	0.0	0.0	0.0	0.0	0.0	0.0	0.0
JESPileUpPtHF	0.0	0.0	0.0	0.0	0.0	0.0	0.0	0.0	0.0	0.0	0.0	0.0	0.0	0.0	0.0	0.0
	0.0	0.0	0.0	0.0	0.0	0.0	0.0	0.0	0.0	0.0	0.0	0.0	0.0	0.0	0.0	0.0
JESPileUpPtRef	+0.3	+0.5	+0.4	+0.1	−0.9	0.0	−0.3	+0.1	+0.5	−0.4	+0.1	−0.4	+0.2	+0.1	0.0	+0.2
	+0.1	−0.6	+0.2	+2.1	0.0	−0.1	−0.1	+0.8	−0.3	−0.2	+0.5	−1.2	−0.2	−1.0	−0.6	+0.2
JESRelativeBal	+0.9	+0.3	+0.8	+1.4	−0.4	−0.2	−0.2	−0.1	+0.3	−0.8	−0.5	−1.6	+0.1	+0.4	+0.2	+0.4
	−1.7	−0.7	−0.7	+1.3	+0.4	+0.1	+1.0	+1.0	+0.7	−1.9	+0.3	−0.3	−1.0	+0.4	−0.4	+0.6
JESRelativeFSR	+0.1	−0.4	−0.2	+2.3	−0.3	−0.2	−0.1	+0.6	+1.2	−1.0	+1.3	−1.4	−0.8	−0.4	−0.8	+0.3
	+0.2	−0.6	+0.5	+3.2	+0.3	−0.6	−0.6	−0.2	+0.4	−0.7	+0.1	−0.5	−0.7	+0.5	0.0	+0.2
JESRelativeJEREC1	−0.5	−0.6	+0.1	+3.1	+0.3	−0.2	−0.6	+1.0	−0.1	−0.5	0.0	−0.8	−0.3	−0.1	−0.1	+0.1
	−0.6	−0.3	−0.3	+1.3	0.0	−0.1	−0.1	+0.5	0.0	−0.3	+0.6	−0.2	0.0	−0.3	+0.2	−0.2
JESRelativeJEREC2	0.0	0.0	0.0	0.0	0.0	0.0	0.0	0.0	0.0	0.0	0.0	0.0	0.0	0.0	0.0	0.0
	0.0	0.0	0.0	0.0	0.0	0.0	0.0	0.0	0.0	0.0	0.0	0.0	0.0	0.0	0.0	0.0
JESRelativeJERHF	0.0	0.0	0.0	0.0	0.0	0.0	0.0	0.0	0.0	0.0	0.0	0.0	0.0	0.0	0.0	0.0
	0.0	0.0	0.0	0.0	0.0	0.0	0.0	0.0	0.0	0.0	0.0	0.0	0.0	0.0	0.0	0.0
JESRelativePtBB	+0.7	−2.1	−0.6	+3.0	+0.4	0.0	+0.3	+1.0	0.0	−0.7	−0.2	−1.0	−0.2	+0.1	−0.1	+0.1
	+0.9	−1.3	+0.3	+1.3	+0.4	0.0	+0.3	+0.1	+0.5	−0.9	−0.1	−0.9	−0.3	+0.1	−0.3	+0.3
JESRelativePtEC1	+0.6	0.0	−0.2	+1.5	+0.1	0.0	−0.3	+0.4	+0.2	−0.3	+0.1	−1.5	−0.3	0.0	+0.3	−0.3
	−0.7	−0.5	−0.5	+2.0	−0.4	−0.1	−0.2	+1.2	+0.1	−0.6	+0.4	+0.4	−0.7	0.0	−0.2	+0.1
JESRelativePtEC2	0.0	0.0	0.0	0.0	0.0	0.0	0.0	0.0	0.0	0.0	0.0	0.0	0.0	0.0	0.0	0.0
	0.0	0.0	0.0	0.0	0.0	0.0	0.0	0.0	0.0	0.0	0.0	0.0	0.0	0.0	0.0	0.0
JESRelativePtHF	0.0	0.0	0.0	0.0	0.0	0.0	0.0	0.0	0.0	0.0	0.0	0.0	0.0	0.0	0.0	0.0
	0.0	0.0	0.0	0.0	0.0	0.0	0.0	0.0	0.0	0.0	0.0	0.0	0.0	0.0	0.0	0.0
JESRelativeStatEC	−0.1	−0.2	+0.1	+1.1	+0.6	−0.3	−0.8	+1.2	+0.2	−0.2	−0.2	−0.4	−0.5	+0.1	+0.1	−0.3
	−0.8	+0.3	+1.3	−0.8	−0.3	0.0	−0.1	+0.3	+0.2	−0.5	0.0	+0.1	−0.3	+0.4	+0.1	−0.1
JESRelativeStatFSR	−0.4	−0.8	−0.1	+2.7	+0.4	−0.1	+0.4	+0.3	+0.2	−1.5	0.0	−1.0	+0.1	−0.2	+0.1	+0.3
	−1.0	+0.5	+0.5	+1.5	−0.2	0.0	−0.3	+0.6	+1.0	−1.1	−0.3	−0.7	−0.7	−0.4	+0.1	+0.2
JESRelativeStatHF	0.0	0.0	0.0	0.0	0.0	0.0	0.0	0.0	0.0	0.0	0.0	0.0	0.0	0.0	0.0	0.0
	0.0	0.0	0.0	0.0	0.0	0.0	0.0	0.0	0.0	0.0	0.0	0.0	0.0	0.0	0.0	0.0
JESSinglePionECAL	+0.4	−0.8	−0.4	+3.4	−0.2	+0.2	−0.4	+1.1	+0.1	−0.7	−0.3	−0.8	−0.8	−0.1	−0.3	−0.2
	−0.5	−0.4	−0.3	+2.7	0.0	0.0	−0.1	+0.3	+0.5	−0.9	+0.4	−1.2	−0.4	+0.3	0.0	+0.3

Table A.9: Table A.8 continued.

source / bin	1	2	3	4	5	6	7	8	9	10	11	12	13	14	15	16
JESSinglePionHCAL	0.0	−0.7	−0.1	+2.4	0.0	+0.2	−0.4	+0.5	+0.5	−0.6	0.0	−0.5	−0.8	−0.4	0.0	−0.1
	+0.2	−0.1	−0.5	+2.4	−0.2	−0.1	−0.7	+0.4	+0.3	−0.5	+0.1	−0.8	0.0	−0.3	+0.3	+0.3
JESTimePtEta	+1.4	−1.2	+0.7	+2.3	−0.5	−0.2	−0.5	+0.7	+0.8	−0.8	+0.4	−1.2	−0.4	−0.7	0.0	+0.4
	−0.5	−0.4	+0.2	+0.7	+0.6	−0.2	−0.1	+1.2	+0.2	−0.8	−0.1	−1.2	0.0	+0.3	0.0	+0.3
$\vec{p}_{\mathrm{T}}^{\,\mathrm{miss}}$	+0.7	−0.2	−0.5	−2.2	−0.1	+0.3	+0.5	+1.0	−0.2	−0.1	+0.2	−0.1	0.0	−0.2	−0.2	0.0
	−0.4	−1.0	−0.8	+3.4	+0.8	+0.1	+0.3	+0.1	−0.1	−1.0	−0.2	−0.8	−0.2	+0.2	+0.1	−0.1
lepton ID/ISO	−0.2	−0.6	−0.6	−0.2	+0.4	+0.4	+0.6	+0.5	−0.2	−0.3	−0.1	−0.4	−0.2	+0.1	−0.2	+0.1
	+0.2	0.0	+0.1	+0.4	−0.1	−0.2	−0.1	−0.2	0.0	0.0	+0.1	0.0	+0.3	+0.1	+0.1	0.0
pileup	+0.3	+0.1	0.0	−0.5	0.0	+0.2	−0.2	−0.4	0.0	+0.1	0.0	+0.1	−0.1	+0.1	0.0	+0.2
	−0.2	−0.7	−0.5	+0.7	+0.3	0.0	+0.6	+0.6	−0.2	−0.5	0.0	−0.5	+0.1	0.0	−0.1	−0.1
trigger	+0.2	−0.1	−0.2	−0.4	+0.2	+0.2	+0.3	−0.1	−0.1	−0.1	+0.1	−0.5	0.0	+0.2	0.0	−0.2
	−0.1	−0.1	0.0	+0.5	−0.1	−0.1	−0.1	+0.2	0.0	−0.1	−0.1	+0.3	0.0	−0.1	−0.1	+0.2
trigger (η)	−0.3	−0.2	0.0	+1.1	−0.2	−0.1	0.0	+0.3	−0.2	−0.1	−0.1	0.0	−0.2	−0.1	+0.1	+0.1
	+0.3	+0.2	0.0	−1.1	+0.2	+0.1	0.0	−0.3	+0.2	+0.1	+0.1	0.0	+0.2	+0.1	−0.1	−0.1
non-$\mathrm{t\bar{t}}$ background	−0.9	−0.6	−1.0	−4.7	+0.2	+0.5	+0.4	−0.3	+0.8	+0.7	+0.5	+0.5	+1.3	+1.1	+1.1	+1.1
	+1.0	+0.2	+0.5	+4.6	+0.1	−0.4	−0.1	+0.5	−0.8	−0.9	−0.4	−0.8	−1.2	−0.9	−1.1	−1.0
b-tagging	−0.1	−0.1	−0.1	−0.1	0.0	0.0	0.0	+0.1	+0.1	0.0	0.0	0.0	0.0	+0.1	+0.1	+0.1
	+0.1	+0.1	+0.1	+0.1	0.0	0.0	0.0	−0.1	−0.1	0.0	0.0	0.0	0.0	−0.1	−0.1	−0.1
b-tagging (light jets)	−0.2	−0.1	−0.2	−1.2	+0.1	+0.2	+0.1	−0.2	+0.2	+0.2	+0.1	+0.1	+0.3	+0.2	+0.2	+0.1
	+0.2	−0.5	−0.3	+1.4	+0.2	0.0	+0.4	+0.4	−0.4	−0.6	0.0	−0.5	−0.3	−0.1	−0.3	0.0
luminosity	0.0	0.0	0.0	0.0	0.0	0.0	0.0	0.0	0.0	0.0	0.0	0.0	0.0	0.0	0.0	0.0
	0.0	0.0	0.0	0.0	0.0	0.0	0.0	0.0	0.0	0.0	0.0	0.0	0.0	0.0	0.0	0.0
branching ratio $\mathrm{t\bar{t}} \to \ell\ell$	0.0	0.0	0.0	0.0	0.0	0.0	0.0	0.0	0.0	0.0	0.0	0.0	0.0	0.0	0.0	0.0
	0.0	0.0	0.0	0.0	0.0	0.0	0.0	0.0	0.0	0.0	0.0	0.0	0.0	0.0	0.0	0.0
PDF eigenvector 1	0.0	0.0	0.0	0.0	0.0	0.0	0.0	0.0	0.0	0.0	0.0	0.0	0.0	0.0	0.0	0.0
	0.0	0.0	0.0	0.0	0.0	0.0	0.0	−0.1	0.0	0.0	0.0	0.0	0.0	0.0	0.0	0.0
PDF eigenvector 2	−0.3	0.0	+0.1	+0.2	0.0	0.0	0.0	0.0	0.0	0.0	0.0	−0.1	+0.2	+0.2	+0.1	0.0
	+0.2	0.0	−0.1	−0.2	0.0	−0.1	0.0	+0.1	0.0	+0.1	+0.1	+0.1	0.0	0.0	0.0	−0.1
PDF eigenvector 3	+0.1	0.0	0.0	−0.1	+0.1	+0.1	0.0	−0.1	0.0	0.0	−0.1	0.0	−0.1	−0.1	0.0	+0.1
	−0.1	0.0	0.0	+0.1	0.0	0.0	0.0	+0.1	0.0	0.0	0.0	0.0	0.0	0.0	0.0	−0.1
PDF eigenvector 4	−0.3	0.0	+0.1	+0.3	0.0	0.0	0.0	+0.1	0.0	−0.1	0.0	0.0	+0.1	+0.1	+0.1	0.0
	+0.2	−0.1	−0.2	−0.1	+0.1	0.0	+0.1	+0.1	0.0	0.0	+0.1	−0.1	0.0	0.0	−0.1	0.0
PDF eigenvector 5	+0.1	−0.2	−0.2	0.0	0.0	−0.1	+0.1	+0.3	−0.1	−0.1	+0.2	0.0	0.0	+0.1	0.0	−0.1
	+0.1	−0.1	−0.1	−0.1	+0.2	+0.2	+0.2	−0.2	+0.1	0.0	−0.2	−0.2	−0.1	0.0	−0.1	+0.2
PDF eigenvector 6	−0.2	0.0	0.0	+0.1	0.0	+0.1	0.0	0.0	0.0	−0.1	−0.1	0.0	+0.1	+0.1	+0.1	+0.1
	+0.1	0.0	0.0	−0.1	0.0	0.0	0.0	0.0	0.0	0.0	+0.1	0.0	0.0	0.0	0.0	0.0
PDF eigenvector 7	+0.1	0.0	−0.1	−0.2	−0.2	−0.2	0.0	+0.3	0.0	+0.1	+0.4	+0.1	0.0	0.0	0.0	−0.3
	0.0	0.0	0.0	+0.1	+0.1	+0.1	0.0	−0.2	0.0	0.0	−0.2	−0.1	0.0	0.0	0.0	+0.2
PDF eigenvector 8	−0.1	0.0	0.0	0.0	0.0	0.0	0.0	+0.1	0.0	0.0	0.0	0.0	0.0	0.0	0.0	0.0
	0.0	0.0	0.0	0.0	0.0	0.0	0.0	−0.1	0.0	0.0	0.0	0.0	0.0	0.0	0.0	0.0
PDF eigenvector 9	+0.1	−0.1	−0.1	+0.1	+0.1	0.0	+0.1	0.0	0.0	−0.1	0.0	−0.1	−0.1	0.0	0.0	0.0
	−0.1	−0.2	−0.2	0.0	+0.1	+0.1	+0.2	+0.1	−0.1	−0.1	0.0	−0.1	+0.1	+0.1	0.0	+0.1
PDF eigenvector 10	−0.1	−0.1	−0.1	+0.2	+0.2	+0.1	+0.1	−0.1	−0.1	−0.2	−0.2	−0.1	−0.1	0.0	0.0	+0.2
	+0.1	0.0	−0.1	−0.2	−0.1	−0.1	0.0	+0.1	0.0	+0.1	+0.2	0.0	+0.1	0.0	0.0	−0.1
PDF eigenvector 11	0.0	0.0	0.0	0.0	0.0	0.0	0.0	0.0	0.0	0.0	−0.1	0.0	0.0	0.0	0.0	0.0
	+0.1	−0.2	−0.2	0.0	0.0	0.0	+0.1	+0.1	0.0	−0.1	+0.1	−0.1	+0.1	+0.1	0.0	0.0
PDF eigenvector 12	+0.1	−0.2	−0.2	−0.1	0.0	0.0	+0.2	+0.2	0.0	−0.1	+0.1	−0.1	+0.1	+0.1	0.0	0.0
	0.0	0.0	0.0	+0.1	0.0	0.0	0.0	−0.1	0.0	0.0	−0.1	0.0	−0.1	0.0	0.0	+0.1
PDF eigenvector 13	+0.1	0.0	0.0	0.0	0.0	+0.1	0.0	0.0	0.0	0.0	−0.1	0.0	−0.1	−0.1	−0.1	0.0
	−0.1	0.0	0.0	0.0	0.0	−0.1	0.0	0.0	0.0	0.0	+0.1	0.0	+0.1	+0.1	+0.1	0.0
PDF eigenvector 14	0.0	0.0	0.0	−0.1	0.0	0.0	0.0	0.0	0.0	0.0	0.0	0.0	0.0	0.0	0.0	0.0
	0.0	−0.1	−0.1	+0.2	+0.1	+0.1	+0.1	0.0	−0.1	−0.1	0.0	−0.1	0.0	0.0	0.0	+0.1

Table A.10: Table A.8 continued.

source / bin	1	2	3	4	5	6	7	8	9	10	11	12	13	14	15	16
PDF eigenvector 15	+0.1	0.0	0.0	−0.1	0.0	0.0	0.0	0.0	0.0	+0.1	+0.1	0.0	0.0	0.0	0.0	0.0
	0.0	0.0	0.0	0.0	0.0	0.0	0.0	0.0	0.0	0.0	0.0	0.0	0.0	0.0	0.0	0.0
PDF eigenvector 16	0.0	0.0	0.0	0.0	0.0	0.0	0.0	0.0	0.0	0.0	0.0	0.0	0.0	0.0	0.0	0.0
	0.0	−0.1	−0.1	0.0	+0.1	0.0	+0.1	+0.1	0.0	−0.1	+0.1	−0.1	0.0	+0.1	0.0	0.0
PDF eigenvector 17	+0.1	−0.1	−0.1	0.0	+0.1	0.0	+0.1	+0.1	0.0	−0.1	+0.1	−0.1	0.0	+0.1	0.0	0.0
	−0.1	0.0	0.0	+0.1	0.0	+0.1	0.0	0.0	0.0	−0.1	−0.1	0.0	−0.1	0.0	0.0	+0.1
PDF eigenvector 18	−0.1	−0.2	−0.1	+0.3	+0.1	0.0	+0.1	+0.1	−0.1	−0.2	0.0	−0.1	0.0	+0.1	+0.1	+0.1
	+0.1	0.0	0.0	−0.2	0.0	0.0	0.0	0.0	0.0	+0.1	0.0	0.0	0.0	−0.1	−0.1	0.0
PDF eigenvector 19	−0.1	0.0	+0.1	+0.2	0.0	0.0	0.0	−0.1	0.0	−0.1	−0.1	0.0	0.0	0.0	0.0	+0.1
	+0.1	0.0	−0.1	−0.3	−0.1	−0.1	0.0	+0.1	0.0	+0.1	+0.2	0.0	+0.1	0.0	−0.1	−0.1
PDF eigenvector 20	0.0	−0.1	−0.1	+0.2	+0.1	+0.1	+0.1	0.0	−0.1	−0.1	0.0	0.0	0.0	0.0	0.0	+0.1
	+0.1	−0.2	−0.2	−0.1	+0.1	0.0	+0.2	+0.1	0.0	−0.1	+0.1	−0.1	0.0	+0.1	−0.1	0.0
PDF eigenvector 21	−0.1	0.0	0.0	+0.1	0.0	0.0	0.0	+0.1	0.0	0.0	0.0	0.0	+0.1	+0.1	+0.1	0.0
	+0.1	0.0	0.0	−0.1	+0.1	+0.1	0.0	−0.1	0.0	0.0	−0.1	0.0	−0.1	−0.1	−0.1	+0.1
PDF eigenvector 22	−0.3	−0.1	0.0	+0.4	−0.1	−0.1	−0.1	+0.2	−0.1	−0.1	+0.1	+0.1	+0.1	+0.2	+0.2	−0.1
	+0.3	0.0	0.0	−0.2	+0.1	+0.1	0.0	−0.2	+0.1	+0.1	−0.1	0.0	−0.2	−0.2	−0.1	+0.1
PDF eigenvector 23	+0.3	+0.1	−0.1	−0.5	0.0	0.0	+0.1	−0.1	+0.1	+0.2	+0.1	−0.1	0.0	−0.1	−0.2	0.0
	0.0	−0.2	−0.1	+0.2	+0.1	0.0	+0.1	+0.2	−0.1	−0.2	0.0	0.0	0.0	+0.1	0.0	0.0
PDF eigenvector 24	+0.1	−0.2	−0.2	0.0	0.0	0.0	+0.1	+0.2	−0.1	−0.1	+0.1	0.0	0.0	0.0	0.0	0.0
	0.0	−0.1	−0.1	−0.2	0.0	0.0	+0.2	+0.1	0.0	0.0	+0.1	−0.3	+0.2	+0.2	0.0	−0.1
PDF eigenvector 25	0.0	0.0	0.0	−0.3	0.0	−0.1	+0.1	0.0	+0.1	+0.2	+0.1	−0.1	+0.2	+0.1	0.0	−0.1
	+0.1	0.0	−0.1	−0.1	−0.1	−0.1	0.0	+0.2	0.0	0.0	+0.2	+0.2	0.0	0.0	0.0	−0.1
PDF eigenvector 26	0.0	0.0	0.0	0.0	0.0	0.0	0.0	0.0	0.0	0.0	0.0	0.0	0.0	0.0	0.0	0.0
	0.0	0.0	0.0	0.0	0.0	0.0	0.0	0.0	0.0	0.0	0.0	0.0	0.0	0.0	0.0	0.0
PDF eigenvector 27	−0.1	+0.1	+0.2	+0.2	0.0	−0.1	−0.1	−0.2	+0.1	0.0	0.0	0.0	−0.1	0.0	0.0	0.0
	−0.1	0.0	0.0	0.0	0.0	0.0	0.0	0.0	0.0	0.0	0.0	0.0	0.0	0.0	0.0	0.0
PDF eigenvector 28	+0.1	0.0	0.0	−0.1	0.0	0.0	0.0	−0.1	0.0	0.0	0.0	+0.1	0.0	0.0	0.0	0.0
	−0.1	0.0	0.0	+0.1	0.0	0.0	0.0	+0.1	−0.1	−0.1	0.0	0.0	0.0	0.0	0.0	0.0
α_S	+0.1	+0.1	+0.1	0.0	0.0	0.0	−0.1	−0.2	+0.1	+0.1	0.0	0.0	−0.1	−0.1	0.0	0.0
	−0.1	−0.1	−0.1	0.0	0.0	0.0	+0.1	+0.2	−0.1	−0.1	0.0	0.0	+0.1	+0.1	0.0	0.0
m_t^{MC}	−1.2	−1.9	−2.1	−2.5	−0.2	+0.1	+0.3	+0.2	+1.0	+0.8	+0.8	+0.1	+1.6	+2.4	+1.5	+1.8
	+1.5	+1.5	+1.4	+0.8	+0.5	+0.2	+0.5	+0.5	−1.0	−0.9	−0.8	−0.4	−2.8	−1.9	−2.0	−1.6
$\mu_{r,f}$	+0.7	+0.4	+0.7	+0.6	−0.1	−0.4	−0.3	−0.7	+0.4	+0.2	+0.1	0.0	−1.4	−0.8	−0.1	0.0
	−0.8	−0.5	−0.8	−0.8	+0.1	+0.4	+0.3	+0.7	−0.4	−0.2	0.0	−0.2	+1.8	+1.1	+0.1	0.0
h_{damp}	+0.8	−0.6	−0.3	0.0	0.0	+0.1	−0.2	0.0	+0.3	+0.3	+0.1	−0.3	−0.7	+0.4	−0.5	+0.7
	+0.1	−1.9	−1.3	−0.8	−0.6	+0.3	+1.9	+1.1	+1.1	−0.8	+0.3	−0.3	−1.7	+1.4	−1.6	+1.5
PS ISR	−0.5	+0.4	−0.9	−0.7	−0.2	0.0	−0.4	+0.5	+1.6	−0.6	+0.4	+1.3	−1.2	+0.6	−0.1	−0.7
	+1.6	0.0	−1.6	−1.0	−0.8	−0.2	+0.3	+0.8	+1.2	−0.4	+0.5	+0.4	−0.5	+0.6	−0.7	−0.1
PS FSR	−0.6	+0.3	0.0	−1.0	+0.8	+0.4	+0.7	+0.6	+0.2	−0.8	+0.7	−0.3	−1.8	−0.5	−1.7	−0.3
	+0.2	+0.3	−0.7	−1.2	−0.7	−0.1	+0.3	0.0	+0.5	−0.6	+0.6	0.0	+0.8	+1.5	−0.1	+0.7
UE tune	−0.7	0.0	0.0	−2.3	+0.6	+0.6	+0.4	+0.8	−0.1	−0.7	−1.0	+1.1	−1.5	+1.0	−0.6	+0.2
	+0.8	−0.6	−1.3	−1.1	+0.3	+0.7	0.0	+0.1	+1.1	−0.5	+0.8	0.0	−0.4	−1.0	−0.6	+0.5
colour reconnection	−0.6	−0.2	−0.8	−1.1	+0.3	−0.1	+0.5	+0.3	+1.2	−0.7	−0.2	+1.0	+0.3	+1.1	−0.5	0.0
	+0.3	−0.1	0.0	−0.5	0.0	+0.2	0.0	−0.5	+0.2	−0.5	−0.1	+0.5	−0.9	+0.6	+0.4	+0.4
	+0.6	−0.4	−0.9	−0.6	−0.6	−0.1	+0.6	+0.2	+0.1	−0.1	+0.4	+0.2	−0.2	+1.3	−0.5	+0.3
fragmentation b → B	+1.1	+0.4	+0.5	+0.2	+0.3	−0.2	+0.2	−0.4	−0.3	−0.4	+0.2	−0.6	−0.9	−0.4	−0.3	−0.2
	−0.5	−0.4	−0.4	0.0	−0.1	+0.1	+0.1	+0.2	+0.1	+0.1	−0.1	+0.2	+0.5	+0.3	+0.2	+0.2
	+0.2	+0.1	+0.1	0.0	0.0	0.0	0.0	−0.1	0.0	0.0	0.0	−0.1	−0.1	−0.1	0.0	−0.1
	+1.3	+1.0	+0.9	+0.5	−0.2	−0.3	−0.3	−0.5	−0.3	−0.3	−0.1	−0.4	−0.7	−0.7	−0.2	−0.4
branching ratio $B \to \mu$	−0.1	−0.1	−0.1	−0.2	+0.1	+0.1	+0.1	0.0	+0.1	0.0	+0.1	0.0	−0.1	0.0	−0.1	0.0
	+0.2	+0.1	+0.1	+0.2	−0.1	−0.1	−0.1	−0.1	−0.1	0.0	−0.1	−0.1	+0.1	0.0	+0.1	+0.1

Table A.11: The measured $[M(\mathrm{t\bar{t}}), y(\mathrm{t\bar{t}})]$ cross sections, along with their relative statistical and systematic uncertainties.

$M(\mathrm{t\bar{t}})$ [GeV]	$\lvert y(\mathrm{t\bar{t}})\rvert$	$\frac{1}{\sigma(\mathrm{t\bar{t}})}\frac{\mathrm{d}\sigma}{\mathrm{d}\lvert y(\mathrm{t\bar{t}})\rvert}$	stat. [%]	syst. [%]	bin
300–400	0.00–0.35	1.554×10^{-1}	2.5	$^{+6.7}_{-4.5}$	1
300–400	0.35–0.75	1.485×10^{-1}	2.3	$^{+3.9}_{-9.6}$	2
300–400	0.75–1.15	1.320×10^{-1}	2.4	$^{+6.3}_{-5.6}$	3
300–400	1.15–2.50	5.856×10^{-2}	2.4	$^{+10.9}_{-6.9}$	4
400–500	0.00–0.35	2.506×10^{-1}	1.4	$^{+3.4}_{-1.8}$	5
400–500	0.35–0.75	2.296×10^{-1}	1.3	$^{+1.4}_{-3.9}$	6
400–500	0.75–1.15	1.889×10^{-1}	1.5	$^{+3.9}_{-2.3}$	7
400–500	1.15–2.50	8.038×10^{-2}	1.2	$^{+3.7}_{-3.9}$	8
500–650	0.00–0.35	1.833×10^{-1}	1.7	$^{+3.0}_{-2.2}$	9
500–650	0.35–0.75	1.714×10^{-1}	1.6	$^{+2.0}_{-5.2}$	10
500–650	0.75–1.15	1.340×10^{-1}	2.0	$^{+6.7}_{-2.1}$	11
500–650	1.15–2.50	4.390×10^{-2}	2.3	$^{+2.7}_{-7.7}$	12
650–1500	0.00–0.35	1.331×10^{-1}	1.6	$^{+3.0}_{-4.5}$	13
650–1500	0.35–0.75	1.079×10^{-1}	2.0	$^{+5.2}_{-4.2}$	14
650–1500	0.75–1.15	8.007×10^{-2}	2.6	$^{+5.1}_{-7.9}$	15
650–1500	1.15–2.50	1.731×10^{-2}	4.7	$^{+11.3}_{-6.3}$	16

Table A.12: The correlation matrix of statistical uncertainties for the measured $[M(t\bar{t}), y(t\bar{t})]$ cross sections. The values are expressed as percentages. For bin indices see Table A.11.

bin	2	3	4	5	6	7	8	9	10	11	12	13	14	15	16
1	−23	−20	+2	−33	−24	+3	0	−15	+4	+4	−5	+5	−1	−4	−2
2		+13	−27	−20	−6	−25	−5	+5	−15	−3	+7	0	+4	+3	−4
3			−9	+3	−25	−14	−30	+3	−4	−15	−7	−3	+2	+4	+3
4				−4	−7	−25	−16	−9	0	−6	−43	−6	−8	−2	+6
5					+2	−7	−6	−11	−18	+1	−1	−6	+4	+1	−3
6						+20	−15	−18	+11	−16	−6	+6	−10	+1	+1
7							+3	+1	−15	+5	−15	+2	+2	−10	−1
8								−2	−8	−18	+27	−6	−2	0	−33
9									−11	−4	0	−31	−5	+4	−2
10										+4	−11	−4	−20	−12	+3
11											−5	+5	−9	−23	−11
12												−3	+2	−7	−32
13													−26	+1	−1
14														−16	−3
15															−16

Table A.13: Sources and values of the relative systematic uncertainties in percent of the measured $[M(t\bar{t}), y(t\bar{t})]$ cross sections. For bin indices see Table A.11.

source / bin	1	2	3	4	5	6	7	8	9	10	11	12	13	14	15	16
JER	+0.5	−1.4	+1.0	+1.4	+0.2	−0.1	+0.3	−0.5	0.0	−0.4	+0.6	−0.7	−0.1	0.0	−1.3	+0.2
	−0.3	−1.1	+0.1	+1.1	+0.2	−0.2	+0.1	+0.1	0.0	−0.8	+0.1	−0.5	−0.1	+0.6	+0.2	+1.0
JESAbsoluteMPFBias	−0.2	−0.8	0.0	+0.5	+0.6	−0.1	+0.4	−0.2	+0.1	−1.0	+0.2	−0.8	−0.1	+0.9	−0.1	+1.2
	−0.4	−1.1	−0.1	+1.0	+0.4	0.0	+0.9	−0.3	+0.2	−0.6	+0.5	−1.0	−0.6	+0.9	−1.0	+0.7
JESAbsoluteScale	+0.6	−1.0	−0.3	+1.4	+0.2	0.0	+0.3	−0.2	0.0	−0.4	−0.6	−1.0	−0.4	+0.1	+0.3	+1.6
	−0.7	−1.7	0.0	+1.5	+0.5	+0.1	+0.7	−0.3	0.0	−0.3	+0.5	−1.0	−0.3	0.0	−0.7	+1.1
JESAbsoluteStat	+0.6	−1.0	+0.4	+1.4	−0.1	+0.2	+0.2	−0.5	−0.1	0.0	+0.3	−1.4	−0.2	+0.5	−0.5	+0.2
	−0.4	−0.4	+0.5	+0.6	+0.1	−0.6	+0.2	+0.4	−0.2	−0.6	+0.7	−0.7	+0.1	+0.4	−0.1	−0.2
JESFlavourQCD	+1.3	−0.6	+0.5	+1.9	−0.4	−1.2	−0.8	−0.2	+0.2	−0.8	+0.3	−0.5	+0.2	+0.9	+0.3	+0.5
	−0.4	−1.9	+0.1	+1.8	+0.8	+0.4	+0.6	0.0	+0.3	−0.2	0.0	−1.4	−0.9	0.0	−1.5	+0.6
JESFragmentation	+0.7	−0.5	+0.4	+0.2	0.0	−0.6	+0.3	−0.3	+0.5	−0.6	+0.3	−0.5	−0.3	+1.0	−1.0	+1.5
	+0.3	−1.5	+0.5	+1.8	+0.4	+0.1	+0.5	−0.7	+0.3	−0.8	+0.2	−1.3	−0.3	+0.1	−0.5	+1.1
JESPileUpDataMC	+1.4	−1.4	0.0	+0.5	0.0	−0.1	0.0	−0.1	−0.3	−0.3	+0.1	−0.8	+0.1	+0.8	−0.3	+1.8
	−0.2	0.0	+0.3	+0.9	+0.3	0.0	+0.3	−0.3	+0.1	−0.7	+0.4	−0.9	−0.4	0.0	−0.9	+1.1
JESPileUpPtBB	−0.4	−0.7	−0.8	+0.7	−0.2	+0.1	+0.2	+0.7	0.0	−0.1	+0.3	−0.6	+0.3	−0.2	−0.3	+0.5
	−0.1	−1.4	+0.8	+0.9	+0.2	+0.3	+0.5	0.0	−0.2	−0.4	+0.1	−1.0	−0.4	+0.2	−1.0	+1.0
JESPileUpPtEC1	+0.5	+0.6	+0.2	−0.6	+0.2	−0.1	+0.1	−0.7	+0.4	−0.3	0.0	−0.2	−0.3	+0.4	+0.1	+1.3
	−1.1	−0.3	−0.2	+2.0	−0.5	−0.6	+0.4	+0.4	+0.1	−0.4	+0.2	−0.1	0.0	0.0	−0.3	−0.7
JESPileUpPtEC2	0.0	+0.1	+0.2	+0.1	0.0	−0.1	−0.1	−0.1	0.0	+0.1	+0.1	−0.1	0.0	−0.1	0.0	0.0
	0.0	+0.1	+0.2	+0.1	0.0	−0.1	−0.1	−0.1	0.0	+0.1	+0.1	−0.1	0.0	−0.1	0.0	0.0
JESPileUpPtHF	0.0	+0.1	+0.2	+0.1	0.0	−0.1	−0.1	−0.1	0.0	+0.1	+0.1	−0.1	0.0	−0.1	0.0	0.0
	0.0	+0.1	+0.2	+0.1	0.0	−0.1	−0.1	−0.1	0.0	+0.1	+0.1	−0.1	0.0	−0.1	0.0	0.0
JESPileUpPtRef	−0.7	+0.7	−0.3	−0.2	−0.2	+0.1	+0.3	−0.3	−0.2	0.0	+0.2	−0.2	+0.4	+0.2	0.0	+1.1
	+0.2	−1.9	+0.3	+1.6	+0.4	−0.5	+0.7	+0.1	+0.4	−0.6	+0.4	−0.6	−0.6	+0.3	−1.3	−0.1
JESRelativeBal	+0.4	−0.5	+1.3	+0.7	+0.1	−0.4	+0.2	−0.7	−0.1	−0.1	−0.6	−0.5	−0.1	+1.2	−0.8	+1.5
	−0.3	−1.5	−0.3	+1.1	+0.1	−0.1	+0.5	+0.8	−0.5	−0.7	+0.3	−0.5	0.0	+0.4	−1.1	+0.7
JESRelativeFSR	+0.3	−1.3	−0.6	+1.4	+0.1	−0.1	+0.5	0.0	+0.4	−0.3	+0.1	−0.7	−0.4	+0.3	−0.9	+0.5
	+0.4	+0.3	+0.7	+0.6	0.0	−0.4	+0.2	−0.4	+0.2	−0.8	0.0	−0.5	−0.3	+0.8	−0.5	+0.6
JESRelativeJEREC1	−0.1	−1.0	−0.7	+1.8	−0.1	+0.2	+0.3	−0.2	+0.3	−0.6	+0.1	−0.9	−0.2	+0.3	0.0	+0.5
	−0.7	−0.4	+0.7	+1.1	+0.1	−0.4	+0.2	−0.2	+0.2	−0.3	−0.2	−0.2	−0.2	+0.3	−0.1	+0.7
JESRelativeJEREC2	0.0	+0.1	+0.2	+0.1	0.0	−0.1	−0.1	−0.1	0.0	+0.1	+0.1	−0.1	0.0	−0.1	0.0	0.0
	0.0	+0.1	+0.2	+0.1	0.0	−0.1	−0.1	−0.1	0.0	+0.1	+0.1	−0.1	0.0	−0.1	0.0	0.0
JESRelativeJERHF	0.0	+0.1	+0.2	+0.1	0.0	−0.1	−0.1	−0.1	0.0	+0.1	+0.1	−0.1	0.0	−0.1	0.0	0.0
	0.0	+0.1	+0.2	+0.1	0.0	−0.1	−0.1	−0.1	0.0	+0.1	+0.1	−0.1	0.0	−0.1	0.0	0.0
JESRelativePtBB	+0.4	−0.7	+0.8	+0.4	+0.1	−0.4	−0.1	+0.3	−0.7	−0.5	+0.4	+0.4	+0.1	+0.1	−0.5	−0.8
	0.0	−1.5	+0.4	+0.8	+0.6	+0.1	+0.1	−0.3	+0.1	−0.8	+0.4	−0.3	−0.4	+0.4	−0.6	+1.1
JESRelativePtEC1	−0.3	+0.5	+0.3	+1.2	+0.5	−0.1	−0.4	−0.4	+0.2	−0.4	0.0	−1.0	−0.2	+0.2	−0.4	+0.4
	−0.1	−1.0	−0.5	+1.2	−0.4	−0.7	+0.4	+0.7	0.0	−0.7	+0.2	+0.7	−0.2	+0.2	−0.6	+0.2
JESRelativePtEC2	0.0	+0.1	+0.2	+0.1	0.0	−0.1	−0.1	−0.1	0.0	+0.1	+0.1	−0.1	0.0	−0.1	0.0	0.0
	0.0	+0.1	+0.2	+0.1	0.0	−0.1	−0.1	−0.1	0.0	+0.1	+0.1	−0.1	0.0	−0.1	0.0	0.0
JESRelativePtHF	0.0	0.0	0.0	0.0	0.0	0.0	0.0	0.0	0.0	0.0	0.0	0.0	0.0	0.0	0.0	0.0
	0.0	+0.1	+0.1	+0.1	0.0	−0.1	−0.1	−0.1	0.0	+0.1	+0.1	−0.1	0.0	−0.1	0.0	0.0
JESRelativeStatEC	+0.4	−0.8	+0.1	+1.3	−0.2	0.0	+0.5	−0.3	0.0	−0.3	+0.5	−0.9	−0.2	+0.1	−1.3	+0.7
	+0.2	−0.5	+0.1	+1.4	−0.2	−0.5	+0.3	−0.1	+0.1	−0.8	+0.3	−0.9	−0.1	+0.5	−0.2	+0.8
JESRelativeStatFSR	−0.4	−1.7	+0.8	+1.2	+0.3	+0.1	+0.5	−0.5	+0.1	−0.4	+0.1	−1.1	+0.1	+0.5	−0.9	+1.6
	−0.7	−1.5	+0.7	+1.3	+0.4	−0.1	+0.5	+0.1	+0.1	−0.4	+0.1	−0.9	−0.2	+0.3	−0.9	+0.3
JESRelativeStatHF	0.0	+0.1	+0.2	+0.1	0.0	−0.1	−0.1	−0.1	0.0	+0.1	+0.1	−0.1	0.0	−0.1	0.0	0.0
	0.0	+0.1	+0.2	+0.1	0.0	−0.1	−0.1	−0.1	0.0	+0.1	+0.1	−0.1	0.0	−0.1	0.0	0.0
JESSinglePionECAL	+0.4	−2.0	+0.3	+1.7	+0.5	−0.1	+0.7	+0.1	−0.5	−0.8	−0.4	−0.7	−0.2	+0.2	−0.9	+0.9
	−0.5	−0.3	+0.2	+1.0	+0.1	−0.2	−0.3	−0.1	+0.3	−0.5	+0.6	−0.3	−0.1	+0.3	−0.3	+0.3

Table A.14: Table A.13 continued.

source / bin	1	2	3	4	5	6	7	8	9	10	11	12	13	14	15	16
JESSinglePionHCAL	−0.3	−1.3	+0.1	+1.4	+0.5	−0.1	+0.6	−0.1	−0.2	−0.3	+0.5	−1.1	−0.2	+0.2	−1.2	+0.8
	−0.4	−0.9	−0.5	+1.5	+0.3	−0.3	+0.1	+0.1	+0.1	−0.4	+0.3	−1.3	+0.1	+0.3	−0.3	+2.2
JESTimePtEta	+1.4	−1.0	−0.1	+1.4	−0.2	−0.6	+0.1	0.0	−0.1	−0.5	+0.7	−1.2	−0.2	+0.5	−0.8	+1.2
	−0.3	+0.2	+1.4	+0.3	−0.1	−0.5	+0.4	−0.2	+0.2	−0.9	0.0	−0.6	0.0	+0.5	+0.1	+1.0
$\vec{p}_{\mathrm{T}}^{\,\mathrm{miss}}$	+1.7	−0.3	−0.4	0.0	−0.3	+0.4	−0.1	0.0	−0.1	−0.3	−0.1	−0.2	+0.1	−0.1	−0.1	−0.4
	−1.0	0.0	0.0	+1.1	+0.1	−0.1	+0.4	0.0	−0.3	−0.4	−0.2	−0.3	0.0	+0.2	0.0	+0.5
lepton ID/ISO	−0.2	0.0	−0.3	−0.3	+0.1	+0.2	0.0	+0.4	−0.1	+0.1	0.0	−0.2	0.0	−0.1	−0.1	−0.5
	+0.2	0.0	+0.3	+0.2	−0.1	−0.2	−0.1	−0.4	+0.1	−0.1	0.0	+0.2	0.0	+0.1	+0.1	+0.5
pileup	+0.2	0.0	−0.3	−0.5	+0.1	+0.2	+0.1	−0.2	+0.1	+0.2	+0.1	0.0	+0.1	+0.1	−0.1	−0.1
	−0.1	−0.1	+0.2	+0.5	−0.1	−0.2	−0.1	+0.2	0.0	−0.2	−0.1	0.0	−0.1	−0.1	+0.1	+0.1
trigger	+0.1	+0.2	+0.1	−0.3	+0.2	+0.1	0.0	−0.1	+0.1	+0.1	−0.1	−0.2	+0.1	0.0	−0.1	−0.1
	−0.1	−0.1	+0.1	+0.4	−0.2	−0.3	−0.1	0.0	−0.1	0.0	+0.2	+0.2	−0.1	−0.1	+0.1	+0.2
trigger (η)	−0.3	−0.2	−0.1	+0.6	−0.2	−0.1	−0.2	+0.4	−0.2	−0.2	−0.2	+0.3	+0.1	−0.1	−0.2	+0.1
	+0.3	+0.2	+0.1	−0.6	+0.2	+0.1	+0.1	−0.4	+0.2	+0.2	+0.2	−0.3	−0.1	+0.1	+0.2	−0.1
non-$\mathrm{t\bar{t}}$ background	−0.7	−0.1	−0.5	−3.1	+0.2	−0.2	0.0	−0.2	+0.5	+1.1	+1.2	+0.3	+1.1	+0.8	+1.3	+0.8
	+0.9	+0.4	+1.2	+3.1	−0.3	−0.4	−0.3	0.0	−0.5	−0.7	−0.7	−0.5	−1.0	−1.0	−1.2	−0.7
b-tagging	−0.1	−0.1	−0.2	−0.1	0.0	0.0	0.0	+0.1	0.0	0.0	0.0	0.0	+0.1	+0.1	+0.1	+0.1
	+0.1	+0.1	+0.3	+0.2	0.0	−0.2	−0.1	−0.2	0.0	+0.1	+0.1	−0.1	0.0	−0.2	−0.1	−0.1
b-tagging (light jets)	−0.1	0.0	−0.2	−0.8	+0.1	+0.1	+0.1	−0.1	+0.2	+0.2	+0.2	+0.1	+0.2	+0.2	+0.2	+0.1
	+0.2	0.0	+0.2	+0.9	−0.1	−0.1	−0.1	+0.1	−0.2	−0.2	−0.2	−0.1	−0.2	−0.2	−0.2	−0.1
luminosity	0.0	0.0	0.0	0.0	0.0	0.0	0.0	0.0	0.0	0.0	0.0	0.0	0.0	0.0	0.0	0.0
	0.0	0.0	0.0	0.0	0.0	0.0	0.0	0.0	0.0	0.0	0.0	0.0	0.0	0.0	0.0	0.0
branching ratio $\mathrm{t\bar{t}} \to \ell\ell$	0.0	0.0	0.0	0.0	0.0	0.0	0.0	0.0	0.0	0.0	0.0	0.0	0.0	0.0	0.0	0.0
	0.0	0.0	0.0	0.0	0.0	0.0	0.0	0.0	0.0	0.0	0.0	0.0	0.0	0.0	0.0	0.0
PDF eigenvector 1	0.0	0.0	0.0	0.0	0.0	0.0	0.0	0.0	0.0	0.0	0.0	0.0	0.0	0.0	0.0	0.0
	0.0	0.0	0.0	0.0	0.0	0.0	0.0	0.0	0.0	0.0	0.0	−0.1	0.0	0.0	0.0	0.0
PDF eigenvector 2	−0.1	−0.1	+0.1	+0.1	0.0	0.0	0.0	0.0	−0.1	0.0	+0.1	0.0	+0.1	0.0	−0.1	−0.3
	0.0	0.0	+0.1	0.0	−0.1	−0.1	0.0	+0.1	0.0	0.0	0.0	+0.1	−0.1	−0.1	−0.1	+0.1
PDF eigenvector 3	+0.1	+0.1	+0.1	0.0	+0.1	0.0	0.0	−0.2	+0.1	+0.1	0.0	−0.2	+0.1	0.0	+0.1	−0.1
	0.0	0.0	+0.1	0.0	0.0	−0.1	−0.1	0.0	0.0	0.0	+0.1	+0.1	0.0	−0.1	0.0	+0.2
PDF eigenvector 4	−0.1	−0.1	0.0	+0.1	0.0	0.0	0.0	0.0	−0.1	0.0	0.0	+0.1	+0.1	0.0	0.0	−0.1
	+0.1	+0.1	+0.1	0.0	0.0	−0.1	−0.1	0.0	+0.1	+0.1	+0.1	−0.1	0.0	−0.1	0.0	0.0
PDF eigenvector 5	0.0	0.0	+0.1	+0.1	−0.1	−0.2	−0.1	+0.2	0.0	0.0	+0.1	+0.3	−0.2	−0.2	−0.1	+0.4
	+0.1	+0.1	0.0	−0.1	+0.1	+0.1	+0.1	−0.2	+0.1	+0.1	0.0	−0.5	+0.1	+0.1	+0.1	−0.3
PDF eigenvector 6	−0.1	0.0	0.0	0.0	0.0	0.0	0.0	0.0	−0.1	0.0	0.0	−0.1	+0.1	0.0	+0.1	+0.1
	+0.1	0.0	+0.1	0.0	0.0	−0.1	0.0	0.0	0.0	0.0	0.0	0.0	−0.1	−0.1	−0.1	0.0
PDF eigenvector 7	0.0	0.0	+0.1	+0.1	−0.2	−0.2	−0.1	+0.3	0.0	0.0	0.0	+0.5	−0.3	−0.3	−0.2	+0.5
	0.0	0.0	0.0	−0.1	+0.1	+0.1	+0.1	−0.2	0.0	0.0	0.0	−0.3	+0.2	+0.2	+0.2	−0.2
PDF eigenvector 8	−0.1	0.0	0.0	0.0	0.0	0.0	−0.1	+0.1	0.0	0.0	0.0	0.0	0.0	−0.1	0.0	+0.2
	+0.1	0.0	+0.1	+0.1	0.0	−0.1	−0.1	−0.1	0.0	+0.1	+0.1	0.0	0.0	0.0	0.0	0.0
PDF eigenvector 9	+0.1	+0.1	+0.2	+0.1	0.0	−0.1	−0.1	−0.1	0.0	+0.1	+0.1	−0.1	0.0	−0.1	−0.1	−0.2
	0.0	0.0	0.0	−0.1	0.0	0.0	−0.1	0.0	0.0	0.0	0.0	0.0	0.0	0.0	+0.1	+0.3
PDF eigenvector 10	0.0	0.0	−0.1	0.0	+0.1	+0.1	+0.1	−0.2	0.0	0.0	0.0	−0.2	+0.1	+0.1	+0.1	−0.2
	0.0	0.0	+0.1	0.0	−0.1	−0.1	−0.1	+0.2	0.0	0.0	0.0	+0.2	−0.1	−0.2	−0.1	+0.2
PDF eigenvector 11	0.0	+0.1	+0.1	0.0	0.0	0.0	0.0	−0.1	0.0	+0.1	+0.1	−0.1	0.0	0.0	0.0	−0.1
	0.0	0.0	0.0	0.0	−0.1	−0.1	0.0	+0.1	0.0	0.0	0.0	+0.1	−0.1	−0.1	−0.1	+0.1
PDF eigenvector 12	0.0	0.0	0.0	0.0	−0.1	−0.1	0.0	+0.1	0.0	0.0	0.0	+0.1	−0.1	−0.1	−0.1	+0.1
	0.0	+0.1	+0.1	0.0	+0.1	0.0	0.0	−0.2	0.0	+0.1	+0.1	−0.1	+0.1	0.0	+0.1	−0.1
PDF eigenvector 13	0.0	0.0	−0.1	−0.1	0.0	+0.1	0.0	0.0	0.0	0.0	−0.1	−0.1	0.0	0.0	+0.1	+0.1
	0.0	0.0	+0.1	+0.1	0.0	−0.1	0.0	0.0	0.0	0.0	+0.1	+0.1	0.0	0.0	−0.1	−0.1
PDF eigenvector 14	0.0	0.0	+0.1	0.0	0.0	−0.1	−0.1	0.0	0.0	+0.1	+0.1	0.0	0.0	−0.1	0.0	+0.1
	0.0	0.0	0.0	0.0	0.0	0.0	0.0	−0.1	0.0	0.0	0.0	0.0	0.0	0.0	0.0	−0.1

Table A.15: Table A.13 continued.

source / bin	1	2	3	4	5	6	7	8	9	10	11	12	13	14	15	16
PDF eigenvector 15	0.0	0.0	0.0	0.0	0.0	0.0	0.0	+0.1	0.0	0.0	0.0	0.0	−0.1	0.0	0.0	0.0
	0.0	0.0	0.0	0.0	0.0	0.0	0.0	0.0	0.0	0.0	0.0	0.0	0.0	0.0	0.0	0.0
PDF eigenvector 16	0.0	0.0	+0.1	0.0	0.0	−0.1	−0.1	0.0	0.0	0.0	+0.1	0.0	0.0	0.0	0.0	0.0
	0.0	0.0	0.0	0.0	0.0	0.0	0.0	0.0	0.0	0.0	0.0	0.0	0.0	0.0	0.0	0.0
PDF eigenvector 17	0.0	0.0	0.0	0.0	0.0	0.0	0.0	0.0	0.0	0.0	0.0	0.0	0.0	0.0	0.0	0.0
	0.0	0.0	−0.1	−0.1	+0.1	+0.1	0.0	−0.1	0.0	0.0	−0.1	−0.1	0.0	+0.1	+0.1	0.0
PDF eigenvector 18	0.0	0.0	0.0	+0.1	0.0	0.0	0.0	−0.1	−0.1	0.0	+0.1	+0.1	+0.1	+0.1	0.0	0.0
	0.0	0.0	0.0	−0.1	0.0	0.0	0.0	+0.1	+0.1	0.0	−0.1	−0.1	−0.1	−0.1	0.0	0.0
PDF eigenvector 19	0.0	+0.1	+0.1	0.0	+0.1	0.0	0.0	−0.2	0.0	0.0	+0.1	−0.1	+0.1	+0.1	+0.1	−0.2
	0.0	0.0	0.0	0.0	−0.1	−0.1	−0.1	+0.2	0.0	0.0	0.0	+0.2	−0.2	−0.2	−0.1	+0.3
PDF eigenvector 20	0.0	0.0	0.0	0.0	0.0	0.0	0.0	−0.1	0.0	0.0	0.0	0.0	0.0	0.0	0.0	0.0
	0.0	0.0	0.0	0.0	0.0	0.0	0.0	+0.1	0.0	0.0	0.0	0.0	0.0	0.0	0.0	+0.1
PDF eigenvector 21	−0.1	−0.1	0.0	0.0	0.0	0.0	0.0	+0.1	−0.1	0.0	0.0	+0.2	0.0	0.0	0.0	+0.1
	+0.1	+0.1	+0.1	0.0	0.0	0.0	0.0	−0.1	+0.1	+0.1	0.0	−0.2	0.0	0.0	0.0	−0.1
PDF eigenvector 22	−0.1	−0.1	0.0	+0.1	−0.1	−0.1	0.0	+0.1	−0.2	−0.1	+0.1	+0.4	0.0	0.0	0.0	+0.1
	+0.1	+0.2	+0.1	−0.1	+0.1	0.0	0.0	−0.1	+0.1	+0.1	0.0	−0.3	0.0	0.0	+0.1	0.0
PDF eigenvector 23	+0.1	+0.1	+0.1	−0.1	0.0	0.0	0.0	+0.1	+0.2	+0.1	0.0	−0.3	−0.1	−0.1	−0.1	−0.1
	0.0	0.0	0.0	0.0	0.0	0.0	0.0	0.0	0.0	0.0	0.0	+0.2	0.0	0.0	0.0	+0.2
PDF eigenvector 24	0.0	0.0	0.0	0.0	−0.1	−0.1	0.0	+0.1	0.0	0.0	0.0	+0.2	−0.1	−0.1	0.0	+0.2
	0.0	0.0	+0.2	+0.1	−0.1	−0.1	−0.1	+0.1	0.0	+0.1	+0.2	−0.1	0.0	−0.1	−0.1	−0.2
PDF eigenvector 25	0.0	0.0	+0.1	+0.1	−0.1	−0.1	0.0	+0.1	+0.1	0.0	+0.1	−0.1	0.0	−0.1	−0.1	−0.2
	0.0	0.0	0.0	0.0	−0.1	−0.1	−0.1	+0.2	0.0	0.0	0.0	+0.3	−0.2	−0.2	−0.1	+0.4
PDF eigenvector 26	0.0	0.0	0.0	0.0	0.0	0.0	0.0	0.0	0.0	0.0	0.0	0.0	0.0	0.0	0.0	0.0
	0.0	0.0	0.0	0.0	0.0	0.0	0.0	0.0	0.0	0.0	0.0	+0.1	0.0	0.0	0.0	+0.1
PDF eigenvector 27	+0.1	+0.1	+0.3	+0.2	0.0	−0.1	0.0	−0.3	+0.1	+0.1	+0.2	−0.1	+0.1	0.0	0.0	−0.4
	0.0	0.0	0.0	0.0	0.0	0.0	−0.1	0.0	0.0	0.0	0.0	0.0	0.0	0.0	0.0	+0.1
PDF eigenvector 28	+0.1	+0.1	+0.1	0.0	0.0	−0.1	−0.1	−0.1	+0.1	+0.1	+0.1	0.0	0.0	−0.1	0.0	0.0
	−0.1	0.0	−0.1	0.0	0.0	0.0	0.0	+0.1	−0.1	0.0	0.0	0.0	0.0	0.0	0.0	+0.1
α_S	+0.1	0.0	+0.2	+0.1	0.0	−0.1	0.0	−0.2	+0.1	+0.1	+0.1	0.0	0.0	0.0	0.0	−0.2
	−0.1	0.0	−0.2	−0.1	0.0	+0.1	0.0	+0.2	−0.1	−0.1	−0.1	+0.1	0.0	0.0	0.0	+0.3
m_t^{MC}	−1.4	−1.6	−1.5	−2.4	−0.2	−0.3	−0.3	+0.4	+0.7	+0.6	+1.0	+0.9	+1.5	+1.6	+2.1	+2.7
	+1.4	+1.6	+1.4	+1.7	+0.6	+0.5	+0.4	−0.3	−0.4	−0.7	−0.5	−1.4	−1.7	−2.1	−1.9	−2.5
$\mu_{r,f}$	+1.0	+0.4	+1.5	+1.0	−0.1	−0.5	+0.2	−1.4	+0.6	+0.3	+0.7	−0.5	0.0	−0.3	−1.1	−2.8
	−1.1	−0.3	−1.3	−1.1	0.0	+0.3	−0.5	+1.3	−0.6	−0.2	−0.6	+0.6	0.0	+0.2	+1.5	+3.9
h_{damp}	+1.0	+0.3	+0.1	−0.5	−0.5	+0.1	0.0	−0.5	+0.1	+0.2	+1.0	−0.6	0.0	+0.2	−1.2	+1.9
	+0.9	−1.3	−2.0	−0.4	−0.4	0.0	+0.8	+1.1	+0.1	0.0	+1.6	−1.0	+0.2	−0.5	+0.3	−0.5
PS ISR	+0.5	−0.6	0.0	−0.4	0.0	−0.6	0.0	+0.1	+0.3	0.0	+1.9	−0.4	−0.1	−0.4	0.0	+0.1
	+1.0	+0.7	−1.1	−0.7	−0.2	−0.9	+0.1	+0.5	+0.7	−0.6	+1.6	−0.5	−0.6	+0.5	−0.5	+0.7
PS FSR	+0.5	−0.9	+0.9	−0.1	+0.8	0.0	+0.8	0.0	+0.1	−0.3	+1.9	−1.6	−1.2	−0.8	−1.5	0.0
	+0.2	+0.6	+0.2	−1.0	−0.2	−0.6	−0.7	+0.2	+0.2	0.0	+1.4	−0.8	+0.3	+0.6	+1.7	0.0
UE tune	+0.5	−0.2	0.0	−1.0	+1.0	−0.1	+0.3	+0.3	−0.4	−0.6	+1.5	−1.1	−0.1	+0.1	−0.7	+0.1
	+1.1	−0.6	−1.5	−0.3	+0.6	0.0	−0.1	+0.3	+0.3	0.0	+1.2	−0.6	−0.7	−0.8	+0.9	−0.2
colour reconnection	+0.1	−0.7	−0.3	−1.1	+0.5	−0.4	−0.1	+0.4	+1.0	−1.0	+0.8	+0.4	−0.5	+1.1	+0.1	+0.3
	−0.2	+0.2	0.0	−0.1	+0.6	−0.5	0.0	−0.2	−0.1	−0.5	+1.1	−0.8	+0.3	+0.3	−0.5	+1.8
	+0.2	+0.7	−0.6	−0.5	−0.2	−0.7	−0.6	+0.5	+0.2	+0.1	+1.4	−0.6	−0.1	+0.8	−0.2	+0.4
fragmentation b → B	+1.2	+0.7	+1.3	+0.4	+0.1	−0.2	0.0	−0.8	+0.2	0.0	0.0	−0.8	0.0	−0.7	−0.8	−1.1
	−0.6	−0.4	−0.6	−0.3	0.0	0.0	−0.1	+0.3	0.0	0.0	+0.1	+0.4	0.0	+0.4	+0.5	+0.6
	+0.2	+0.1	+0.2	+0.1	0.0	0.0	0.0	−0.2	0.0	0.0	0.0	−0.1	0.0	−0.1	−0.1	−0.2
	+1.4	+0.8	+1.3	+0.7	−0.1	−0.2	−0.1	−0.6	0.0	−0.2	−0.3	−0.8	−0.2	−0.5	−0.8	−1.0
branching ratio $B \to \mu$	0.0	0.0	0.0	0.0	+0.1	−0.1	0.0	0.0	+0.1	+0.1	+0.2	0.0	0.0	−0.1	−0.1	−0.1
	+0.1	+0.2	+0.2	+0.1	−0.1	−0.1	−0.1	0.0	−0.1	−0.1	−0.1	−0.1	+0.1	+0.1	+0.1	+0.2

Table A.16: The measured $[M(t\bar{t}), \Delta\eta(t,\bar{t})]$ cross sections, along with their relative statistical and systematic uncertainties.

$M(t\bar{t})$ [GeV]	$\Delta\eta(t,\bar{t})$	$\frac{1}{\sigma(t\bar{t})}\frac{d\sigma}{d\Delta\eta(t,\bar{t})}$	stat. [%]	syst. [%]	bin
300–400	0.0–0.4	1.874×10^{-1}	4.4	$^{+5.0}_{-14.4}$	1
300–400	0.4–1.2	1.260×10^{-1}	1.5	$^{+3.4}_{-6.0}$	2
300–400	1.2–6.0	1.444×10^{-2}	4.4	$^{+17.7}_{-7.2}$	3
400–500	0.0–0.4	1.633×10^{-1}	2.7	$^{+7.3}_{-6.1}$	4
400–500	0.4–1.2	1.587×10^{-1}	1.4	$^{+5.2}_{-3.1}$	5
400–500	1.2–6.0	3.510×10^{-2}	1.1	$^{+3.1}_{-3.4}$	6
500–650	0.0–0.4	5.389×10^{-2}	4.2	$^{+5.8}_{-7.4}$	7
500–650	0.4–1.2	6.632×10^{-2}	2.6	$^{+6.4}_{-4.3}$	8
500–650	1.2–6.0	3.601×10^{-2}	1.0	$^{+1.4}_{-2.9}$	9
650–1500	0.0–0.4	1.803×10^{-2}	4.8	$^{+8.5}_{-5.4}$	10
650–1500	0.4–1.2	1.991×10^{-2}	3.3	$^{+6.0}_{-7.0}$	11
650–1500	1.2–6.0	2.575×10^{-2}	1.0	$^{+3.9}_{-3.5}$	12

Table A.17: The correlation matrix of statistical uncertainties for the measured $[M(t\bar{t}), \Delta\eta(t,\bar{t})]$ cross sections. The values are expressed as percentages. For bin indices see Table A.16.

bin	2	3	4	5	6	7	8	9	10	11	12
1	+11	−77	−3	−37	−22	−8	−2	+16	+1	−1	−13
2		−8	−44	+13	−35	+11	−8	−18	−4	−1	−1
3			+2	−2	−7	+5	+6	−29	−2	−1	+11
4				−19	−17	−21	−25	+2	+4	+10	+1
5					+10	−14	+6	−30	+7	−6	+3
6						+10	−15	+1	−3	+6	−21
7							−34	+1	−44	+6	+3
8								−12	+10	−36	−5
9									0	+1	−42
10										−28	+1
11											−10

Table A.18: Sources and values of the relative systematic uncertainties in percent of the measured $[M(t\bar{t}), \Delta\eta(t, \bar{t})]$ cross sections. For bin indices see Table A.16.

source / bin	1	2	3	4	5	6	7	8	9	10	11	12
JER	−1.7	−0.1	+2.3	+0.8	+0.4	−0.2	−0.2	+0.4	−0.6	−0.5	−1.0	0.0
	−0.2	−1.3	+0.4	+1.6	−0.2	+0.1	−0.6	+0.3	−0.4	+1.1	+0.1	+0.6
JESAbsoluteMPFBias	−1.1	−0.5	+1.2	+0.8	−0.1	+0.2	−0.2	−0.3	−0.4	+0.4	+0.2	+0.5
	−1.5	−0.4	+1.0	+0.2	+0.7	0.0	+0.1	0.0	−0.3	+0.7	+0.1	+0.1
JESAbsoluteScale	−0.3	−0.5	+2.2	+0.4	−0.2	−0.3	−0.5	+0.5	−0.4	+0.6	+0.2	+0.1
	−0.6	−0.5	+0.6	+1.3	−0.4	−0.1	0.0	0.0	+0.3	0.0	+0.2	0.0
JESAbsoluteStat	−2.1	+0.1	+2.8	+0.2	+0.3	−0.4	−0.7	+0.7	−0.5	+1.0	−0.2	+0.2
	−1.1	−1.1	+0.9	+0.7	−0.1	+0.5	−0.6	+0.4	−0.3	+0.3	+0.1	+0.5
JESFlavourQCD	−1.1	+0.1	+3.7	+0.8	−0.3	−1.2	+0.6	−0.2	−0.5	+1.0	+1.4	+0.5
	−0.7	−1.5	+0.6	+2.7	−0.1	+0.7	−1.3	−0.7	0.0	−0.5	−1.1	−0.4
JESFragmentation	−2.4	+0.2	+2.4	+0.1	+0.3	−0.2	+0.2	+0.2	−0.3	0.0	+0.1	+0.3
	−3.1	−0.3	+3.0	−0.2	+0.5	+0.2	+1.5	−0.7	−0.2	−0.1	−0.2	+0.1
JESPileUpDataMC	−2.6	+0.5	+0.4	+0.2	+0.7	0.0	−1.0	+0.2	−0.3	+1.2	+0.9	+0.4
	+0.2	−0.4	+1.1	+0.8	−0.2	+0.2	0.0	−0.6	−0.4	0.0	−1.1	+0.1
JESPileUpPtBB	−1.7	−0.7	+2.4	+1.2	−0.1	−0.3	+0.2	+0.2	−0.2	+1.1	−0.2	+0.2
	−1.2	−0.5	+1.9	+0.8	0.0	+0.1	−0.7	+0.1	−0.3	0.0	0.0	−0.1
JESPileUpPtEC1	+0.3	−0.6	+1.1	−0.1	+0.4	−0.6	+0.3	+0.7	−0.3	0.0	+0.4	+0.1
	−0.3	0.0	+0.3	0.0	−0.1	−0.2	+0.2	−0.1	0.0	−0.6	−1.0	+0.5
JESPileUpPtEC2	0.0	0.0	0.0	0.0	0.0	0.0	0.0	0.0	0.0	0.0	0.0	0.0
	0.0	0.0	0.0	0.0	0.0	0.0	0.0	0.0	0.0	0.0	0.0	0.0
JESPileUpPtHF	0.0	0.0	0.0	0.0	0.0	0.0	0.0	0.0	0.0	0.0	0.0	0.0
	0.0	0.0	0.0	0.0	0.0	0.0	0.0	0.0	0.0	0.0	0.0	0.0
JESPileUpPtRef	−0.5	+0.3	+0.2	+1.1	−0.1	−0.4	0.0	−0.1	−0.3	+1.0	+0.3	+0.4
	−0.7	−0.2	+1.2	+1.1	−0.2	−0.1	−0.5	−0.4	+0.1	+0.5	−0.9	−0.1
JESRelativeBal	−2.5	+0.1	+2.9	−0.2	+0.5	−0.1	−0.5	+0.1	−0.6	+1.3	+1.2	+0.2
	−3.1	−0.7	+1.2	+1.0	+0.8	+0.6	+0.6	−0.4	−0.5	−0.2	−0.5	+0.4
JESRelativeFSR	−1.0	−1.0	+1.2	+1.9	−0.2	−0.1	−0.3	0.0	0.0	+0.3	−0.6	+0.1
	−1.3	−0.6	+3.2	0.0	−0.4	−0.4	+0.2	0.0	−0.1	+0.3	+0.4	+0.4
JESRelativeJEREC1	+1.2	−0.3	−0.3	+0.1	+0.2	−0.3	+0.4	−0.3	−0.2	0.0	0.0	+0.2
	−1.5	0.0	+2.1	0.0	+0.1	−0.3	+0.3	0.0	−0.1	+0.3	−0.3	+0.1
JESRelativeJEREC2	0.0	0.0	0.0	0.0	0.0	0.0	0.0	0.0	0.0	0.0	0.0	0.0
	0.0	0.0	0.0	0.0	0.0	0.0	0.0	0.0	0.0	0.0	0.0	0.0
JESRelativeJERHF	0.0	0.0	0.0	0.0	0.0	0.0	0.0	0.0	0.0	0.0	0.0	0.0
	0.0	0.0	0.0	0.0	0.0	0.0	0.0	0.0	0.0	0.0	0.0	0.0
JESRelativePtBB	−2.0	0.0	+2.3	+0.5	0.0	0.0	+0.4	−0.2	−0.4	+0.6	0.0	+0.2
	−4.2	−0.7	+3.5	+0.6	+0.5	+0.4	+1.3	−0.1	−0.4	−0.4	−0.1	+0.2
JESRelativePtEC1	−1.0	+0.2	+1.8	+0.1	+0.3	−0.4	+0.4	−0.2	−0.2	−0.2	+0.4	−0.1
	−1.1	−0.2	−0.1	+0.5	+0.5	0.0	+0.1	−0.5	+0.1	−0.2	−0.5	+0.4
JESRelativePtEC2	0.0	0.0	0.0	0.0	0.0	0.0	0.0	0.0	0.0	0.0	0.0	0.0
	0.0	0.0	0.0	0.0	0.0	0.0	0.0	0.0	0.0	0.0	0.0	0.0
JESRelativePtHF	0.0	0.0	0.0	0.0	0.0	0.0	0.0	0.0	0.0	0.0	0.0	0.0
	0.0	0.0	0.0	0.0	0.0	0.0	0.0	0.0	0.0	0.0	0.0	0.0
JESRelativeStatEC	−0.8	−0.1	+1.9	+0.5	0.0	−0.4	+0.6	0.0	−0.3	−0.4	−0.1	+0.1
	−1.5	−0.2	+1.7	−0.3	+0.6	−0.1	+0.1	+0.1	−0.5	0.0	−0.4	+0.5
JESRelativeStatFSR	−0.7	+0.1	+0.7	+0.5	+0.3	−0.2	−0.7	−0.1	−0.3	+0.3	−0.1	+0.3
	−1.6	−0.8	+1.7	+1.0	+0.3	0.0	−0.7	+0.1	−0.3	+0.9	−0.3	+0.2
JESRelativeStatHF	0.0	0.0	0.0	0.0	0.0	0.0	0.0	0.0	0.0	0.0	0.0	0.0
	0.0	0.0	0.0	0.0	0.0	0.0	0.0	0.0	0.0	0.0	0.0	0.0
JESSinglePionECAL	−2.4	−0.3	+2.3	+1.5	+0.4	−0.1	−0.5	−0.8	−0.3	+0.5	+0.2	+0.2
	−1.9	−0.8	+2.8	+0.7	+0.4	−0.4	+0.7	+0.8	−0.6	−0.6	+0.1	+0.4

Table A.19: Table A.18 continued.

source / bin	1	2	3	4	5	6	7	8	9	10	11	12
JESSinglePionHCAL	−1.2	−0.6	+2.2	+0.4	+0.1	+0.1	+0.9	−0.1	−0.4	−0.6	+0.1	+0.1
	−0.3	−0.5	+1.2	+0.8	−0.3	−0.2	−0.2	−0.1	−0.2	+0.6	+0.7	+0.3
JESTimePtEta	−1.2	−0.2	+2.4	+0.8	0.0	−0.3	+0.1	+0.1	−0.6	0.0	−0.1	+0.3
	−1.3	−0.8	+2.2	+0.4	+0.1	+0.3	+0.9	−0.5	−0.7	+0.1	+0.7	+0.4
$\vec{p}_{\mathrm{T}}^{\,\mathrm{miss}}$	−0.4	0.0	−0.3	+0.7	−0.1	+0.2	−0.1	−0.2	0.0	+0.4	−0.3	0.0
	−1.0	+0.7	+0.3	−0.1	+0.1	−0.1	+0.4	0.0	−0.2	+0.5	0.0	+0.1
lepton ID/ISO	−0.2	+0.2	−0.6	−0.1	+0.3	+0.1	0.0	−0.3	+0.2	−0.3	−0.4	−0.1
	+0.2	−0.2	+0.6	+0.1	−0.3	−0.1	0.0	+0.4	−0.2	+0.4	+0.4	+0.1
pileup	+0.3	+0.2	−0.7	−0.5	+0.2	0.0	+0.2	+0.1	0.0	−0.3	−0.2	+0.1
	−0.4	−0.2	+0.7	+0.5	−0.1	0.0	−0.3	−0.1	0.0	+0.4	+0.2	−0.1
trigger	−0.1	0.0	+0.1	0.0	+0.1	0.0	+0.1	0.0	0.0	+0.1	+0.1	−0.1
	+0.1	0.0	−0.1	0.0	−0.1	0.0	−0.1	0.0	0.0	−0.1	−0.1	+0.1
trigger (η)	+0.3	+0.1	−0.2	+0.2	0.0	−0.1	+0.1	−0.1	−0.1	0.0	−0.1	0.0
	−0.3	−0.1	+0.2	−0.2	0.0	+0.1	−0.1	+0.1	+0.1	0.0	+0.1	0.0
non-$\mathrm{t\bar{t}}$ background	−0.6	−0.3	−3.6	0.0	+1.0	−0.3	+0.3	+1.1	+0.3	+0.8	+1.1	+0.9
	+0.5	+0.3	+3.5	+0.1	−1.0	+0.3	−0.2	−1.1	−0.3	−0.8	−1.0	−0.9
b-tagging	−0.2	0.0	−0.1	0.0	+0.1	0.0	+0.1	−0.1	0.0	+0.1	0.0	+0.1
	+0.2	0.0	+0.1	0.0	−0.1	0.0	−0.1	+0.1	0.0	−0.1	0.0	−0.1
b-tagging (light jets)	−0.1	−0.1	−0.9	+0.1	+0.3	−0.1	+0.2	+0.4	0.0	+0.3	+0.2	+0.1
	+0.1	+0.1	+0.9	−0.1	−0.3	+0.1	−0.2	−0.4	0.0	−0.3	−0.2	−0.1
luminosity	0.0	0.0	0.0	0.0	0.0	0.0	0.0	0.0	0.0	0.0	0.0	0.0
	0.0	0.0	0.0	0.0	0.0	0.0	0.0	0.0	0.0	0.0	0.0	0.0
branching ratio $\mathrm{t\bar{t}} \to \ell\ell$	0.0	0.0	0.0	0.0	0.0	0.0	0.0	0.0	0.0	0.0	0.0	0.0
	0.0	0.0	0.0	0.0	0.0	0.0	0.0	0.0	0.0	0.0	0.0	0.0
PDF eigenvector 1	0.0	0.0	0.0	0.0	0.0	0.0	0.0	0.0	0.0	0.0	0.0	0.0
	0.0	0.0	0.0	0.0	0.0	0.0	0.0	0.0	0.0	0.0	0.0	0.0
PDF eigenvector 2	+0.2	−0.1	−0.4	0.0	0.0	0.0	−0.1	+0.1	0.0	0.0	0.0	+0.2
	−0.2	−0.1	+0.3	0.0	0.0	0.0	0.0	0.0	+0.1	−0.1	−0.1	0.0
PDF eigenvector 3	0.0	0.0	+0.1	0.0	0.0	0.0	0.0	0.0	0.0	0.0	+0.1	−0.1
	0.0	0.0	−0.1	0.0	0.0	0.0	0.0	0.0	0.0	0.0	0.0	+0.1
PDF eigenvector 4	+0.2	0.0	−0.4	0.0	0.0	0.0	0.0	0.0	−0.1	+0.1	+0.1	+0.1
	−0.1	−0.1	+0.3	0.0	0.0	0.0	0.0	0.0	0.0	0.0	−0.1	−0.1
PDF eigenvector 5	−0.2	−0.1	+0.2	−0.1	0.0	0.0	0.0	0.0	+0.1	−0.1	−0.2	0.0
	0.0	0.0	+0.1	0.0	0.0	+0.1	+0.1	−0.1	0.0	+0.1	+0.1	−0.1
PDF eigenvector 6	+0.1	+0.1	−0.3	0.0	+0.1	0.0	0.0	0.0	−0.1	+0.1	+0.2	+0.1
	0.0	−0.1	+0.2	0.0	−0.1	0.0	0.0	0.0	0.0	−0.1	−0.1	0.0
PDF eigenvector 7	−0.3	−0.1	+0.4	−0.1	0.0	−0.1	0.0	0.0	+0.2	−0.2	−0.4	0.0
	+0.2	+0.1	−0.2	+0.1	0.0	0.0	0.0	0.0	−0.1	+0.2	+0.2	0.0
PDF eigenvector 8	−0.1	+0.1	−0.1	−0.1	+0.1	0.0	0.0	−0.1	0.0	−0.1	0.0	0.0
	+0.1	−0.1	+0.1	0.0	−0.1	0.0	0.0	+0.1	0.0	+0.1	0.0	0.0
PDF eigenvector 9	+0.1	0.0	+0.1	0.0	−0.1	0.0	0.0	+0.1	0.0	−0.1	−0.1	0.0
	−0.1	+0.1	−0.1	0.0	+0.1	0.0	0.0	−0.1	0.0	+0.1	+0.1	0.0
PDF eigenvector 10	+0.2	+0.1	−0.3	+0.1	0.0	0.0	0.0	0.0	−0.1	+0.1	+0.2	0.0
	−0.2	−0.1	+0.3	−0.1	0.0	0.0	0.0	0.0	+0.1	−0.2	−0.2	0.0
PDF eigenvector 11	+0.1	0.0	−0.1	0.0	0.0	0.0	0.0	0.0	0.0	0.0	+0.1	0.0
	−0.1	−0.1	+0.1	0.0	0.0	0.0	0.0	0.0	+0.1	−0.1	−0.1	0.0
PDF eigenvector 12	−0.2	0.0	+0.1	−0.1	0.0	0.0	0.0	0.0	+0.1	−0.1	−0.1	0.0
	+0.2	0.0	−0.1	+0.1	0.0	0.0	0.0	0.0	−0.1	+0.1	+0.1	0.0
PDF eigenvector 13	−0.1	+0.1	+0.1	0.0	+0.1	0.0	0.0	−0.1	0.0	0.0	+0.1	−0.1
	+0.1	−0.1	−0.1	0.0	−0.1	0.0	0.0	+0.1	0.0	0.0	−0.1	+0.1
PDF eigenvector 14	−0.1	0.0	+0.1	0.0	0.0	0.0	0.0	0.0	0.0	0.0	−0.1	0.0
	+0.1	0.0	−0.1	0.0	0.0	0.0	0.0	0.0	−0.1	0.0	+0.1	0.0

Table A.20: Table A.18 continued.

source / bin	1	2	3	4	5	6	7	8	9	10	11	12
PDF eigenvector 15	−0.1	0.0	+0.2	0.0	0.0	0.0	0.0	0.0	+0.1	0.0	−0.1	0.0
	0.0	0.0	−0.1	0.0	0.0	0.0	0.0	0.0	0.0	0.0	0.0	0.0
PDF eigenvector 16	0.0	0.0	−0.1	0.0	0.0	0.0	0.0	0.0	0.0	0.0	0.0	0.0
	0.0	0.0	+0.1	0.0	0.0	0.0	0.0	0.0	0.0	0.0	−0.1	0.0
PDF eigenvector 17	−0.1	0.0	+0.1	0.0	0.0	0.0	0.0	0.0	0.0	0.0	−0.1	0.0
	+0.1	+0.1	−0.2	0.0	+0.1	0.0	0.0	0.0	−0.1	+0.1	+0.1	0.0
PDF eigenvector 18	+0.3	0.0	−0.2	+0.1	−0.1	0.0	0.0	+0.1	−0.1	0.0	+0.1	+0.1
	−0.3	0.0	+0.2	−0.1	0.0	0.0	0.0	−0.1	+0.1	0.0	−0.1	−0.1
PDF eigenvector 19	+0.2	0.0	−0.2	+0.1	0.0	0.0	0.0	0.0	−0.1	+0.1	+0.2	0.0
	−0.3	−0.1	+0.3	−0.1	0.0	0.0	0.0	0.0	+0.1	−0.2	−0.2	0.0
PDF eigenvector 20	+0.1	0.0	−0.1	0.0	0.0	0.0	0.0	0.0	0.0	+0.1	+0.2	0.0
	−0.1	0.0	+0.1	0.0	0.0	0.0	0.0	0.0	0.0	−0.1	−0.1	0.0
PDF eigenvector 21	0.0	0.0	−0.2	0.0	0.0	0.0	0.0	0.0	0.0	0.0	0.0	+0.1
	0.0	0.0	+0.1	0.0	0.0	0.0	0.0	0.0	0.0	0.0	0.0	−0.1
PDF eigenvector 22	+0.3	0.0	−0.5	0.0	0.0	−0.1	−0.1	+0.2	−0.1	0.0	0.0	+0.2
	−0.2	+0.1	+0.3	0.0	0.0	+0.1	+0.1	−0.1	0.0	0.0	+0.1	−0.2
PDF eigenvector 23	−0.4	0.0	+0.5	−0.1	0.0	+0.1	0.0	−0.2	+0.1	−0.1	−0.2	−0.2
	+0.1	0.0	−0.1	0.0	0.0	0.0	0.0	+0.1	0.0	0.0	0.0	0.0
PDF eigenvector 24	−0.1	0.0	+0.2	0.0	0.0	0.0	0.0	+0.1	0.0	0.0	0.0	0.0
	−0.2	−0.1	+0.1	−0.1	−0.1	0.0	0.0	0.0	+0.1	−0.1	−0.2	+0.1
PDF eigenvector 25	−0.2	−0.1	+0.2	−0.1	−0.1	0.0	0.0	0.0	+0.1	−0.1	−0.2	0.0
	−0.2	−0.1	+0.3	0.0	0.0	0.0	0.0	+0.1	+0.1	−0.2	−0.2	0.0
PDF eigenvector 26	0.0	0.0	0.0	0.0	0.0	0.0	0.0	0.0	0.0	0.0	0.0	0.0
	0.0	0.0	0.0	0.0	0.0	0.0	0.0	0.0	0.0	0.0	0.0	0.0
PDF eigenvector 27	+0.4	−0.1	0.0	+0.1	−0.2	0.0	−0.1	+0.2	0.0	0.0	0.0	0.0
	0.0	0.0	−0.2	0.0	+0.1	0.0	0.0	0.0	0.0	0.0	0.0	0.0
PDF eigenvector 28	0.0	0.0	+0.1	0.0	0.0	0.0	0.0	0.0	0.0	0.0	0.0	0.0
	0.0	+0.1	−0.2	0.0	+0.1	0.0	0.0	0.0	0.0	0.0	+0.1	0.0
α_S	+0.2	−0.1	+0.1	+0.1	−0.2	0.0	0.0	+0.1	0.0	0.0	0.0	0.0
	−0.2	+0.1	−0.1	−0.1	+0.2	0.0	0.0	−0.1	0.0	0.0	0.0	0.0
m_t^{MC}	−2.1	−1.8	−1.0	−0.1	+0.8	−1.0	+2.7	+2.3	+0.3	+2.5	+2.3	+1.7
	+1.0	+1.8	+1.3	−1.1	−0.1	+1.3	−2.3	−1.8	−0.3	−2.5	−2.9	−1.8
$\mu_{r,f}$	+1.7	−0.9	+1.1	+0.3	−1.1	0.0	−0.6	+0.8	+0.1	−0.1	−1.0	−0.2
	−1.9	+0.9	−1.2	−0.2	+1.1	0.0	+1.0	−0.9	−0.1	+0.1	+1.4	+0.2
h_{damp}	−2.0	−0.2	+2.3	−1.4	+0.6	−0.3	−1.9	+1.4	+0.3	+2.6	−0.8	−0.1
	−1.4	−0.9	−1.0	−0.9	+1.5	+0.4	−2.5	+1.5	+0.3	−0.1	−0.3	0.0
PS ISR	+2.1	−0.4	−1.7	−1.9	+0.5	−0.3	+0.3	+2.3	+0.1	−0.9	−0.9	−0.1
	−1.1	+0.5	+0.1	−1.9	+0.8	−0.4	+0.1	+1.3	+0.2	+0.9	−1.2	+0.1
PS FSR	−1.9	−0.2	+1.1	−0.1	+0.9	+0.8	−1.8	−0.3	+0.2	−1.0	−2.1	−0.8
	+0.9	+0.4	−0.5	−1.8	0.0	−0.7	+0.9	+0.8	+0.2	+1.6	+1.2	+0.4
UE tune	−1.6	−0.5	+1.3	−1.3	+0.8	+0.4	−2.5	−0.3	+0.4	+1.1	0.0	−0.2
	−0.7	−0.9	−0.1	−0.6	+0.9	+0.3	−0.4	+1.1	+0.3	−0.1	−0.1	−0.5
colour reconnection	−1.4	−0.4	+0.5	−0.5	+0.4	0.0	−0.1	+1.0	+0.3	+0.7	+0.5	0.0
	−1.9	+0.1	+1.3	−2.0	+1.2	0.0	+0.3	+0.6	−0.3	−1.2	+0.8	+0.4
	−0.7	+0.1	0.0	−0.3	+0.5	−0.5	0.0	+0.1	+0.2	−0.5	−0.1	+0.5
fragmentation b → B	0.0	−0.3	+2.5	0.0	−0.9	+0.4	+0.1	−0.6	0.0	+1.6	+0.5	−0.7
	+0.1	+0.1	−1.3	0.0	+0.4	−0.2	0.0	+0.3	0.0	−0.6	−0.1	+0.4
	0.0	−0.1	+0.5	0.0	−0.2	+0.1	0.0	−0.1	0.0	+0.3	+0.1	−0.1
	+0.6	+0.2	+2.2	−0.2	−0.7	+0.1	0.0	−0.5	−0.2	+1.5	+0.4	−0.7
branching ratio $B \to \mu$	0.0	−0.1	−0.2	+0.1	+0.1	+0.1	+0.1	0.0	0.0	0.0	−0.2	0.0
	+0.1	+0.2	+0.3	−0.2	−0.1	−0.1	0.0	−0.1	−0.1	+0.2	+0.2	0.0

Table A.21: The measured $[M(t\bar{t}), \Delta\phi(t,\bar{t})]$ cross sections, along with their relative statistical and systematic uncertainties.

$M(t\bar{t})$ [GeV]	$\Delta\phi(t,\bar{t})$ [rad]	$\frac{1}{\sigma(t\bar{t})}\frac{d\sigma}{d\Delta\phi(t,\bar{t})}[\text{rad}^{-1}]$	stat. [%]	syst. [%]	bin
300–400	0.00–2.20	3.535×10^{-2}	3.0	$^{+6.3}_{-16.2}$	1
300–400	2.20–2.95	1.249×10^{-1}	1.9	$^{+9.7}_{-5.6}$	2
300–400	2.95–3.14	4.024×10^{-1}	3.2	$^{+20.3}_{-15.5}$	3
400–500	0.00–2.20	2.617×10^{-2}	3.0	$^{+13.6}_{-10.7}$	4
400–500	2.20–2.95	1.957×10^{-1}	1.2	$^{+5.7}_{-6.3}$	5
400–500	2.95–3.14	8.082×10^{-1}	1.3	$^{+6.7}_{-5.6}$	6
500–650	0.00–2.20	1.439×10^{-2}	4.0	$^{+4.9}_{-14.4}$	7
500–650	2.20–2.95	1.250×10^{-1}	1.8	$^{+6.9}_{-6.9}$	8
500–650	2.95–3.14	6.251×10^{-1}	1.4	$^{+5.9}_{-6.2}$	9
650–1500	0.00–2.20	7.308×10^{-3}	4.8	$^{+12.2}_{-7.6}$	10
650–1500	2.20–2.95	7.475×10^{-2}	2.1	$^{+6.9}_{-6.1}$	11
650–1500	2.95–3.14	3.923×10^{-1}	1.5	$^{+5.4}_{-6.2}$	12

Table A.22: The correlation matrix of statistical uncertainties for the measured $[M(t\bar{t}), \Delta\phi(t,\bar{t})]$ cross sections. The values are expressed as percentages. For bin indices see Table A.21.

bin	2	3	4	5	6	7	8	9	10	11	12
1	+4	−50	−39	−26	+1	−11	−5	+9	+6	+2	−5
2		−23	−26	+16	−50	+6	−13	+1	−2	−2	0
3			+18	−37	−12	+4	+4	−19	−6	−3	−1
4				+1	−10	−30	−18	0	−1	+2	+1
5					−7	−12	+19	−35	+5	−15	+10
6						+5	−30	−1	−3	+8	−11
7							−9	−4	−43	−8	+4
8								−24	+1	−25	−6
9									+2	+1	−32
10										−23	+1
11											−34

Table A.23: Sources and values of the relative systematic uncertainties in percent of the measured $[M(t\bar{t}), \Delta\phi(t,\bar{t})]$ cross sections. For bin indices see Table A.21.

source / bin	1	2	3	4	5	6	7	8	9	10	11	12
JER	−1.8	−0.1	+2.7	+0.7	−0.4	+0.3	−2.1	+0.1	+0.1	−0.1	+0.2	−0.6
	−0.8	−0.1	−1.1	+0.5	+0.8	+0.1	−2.4	+0.7	−0.6	+1.9	+0.4	+0.3
JESAbsoluteMPFBias	−3.0	+1.1	+1.1	+0.9	+0.7	−0.1	−2.9	0.0	−0.5	+1.7	0.0	+0.3
	−3.6	+0.1	+2.1	+2.0	+0.2	+0.1	+0.1	+0.2	−0.6	−0.3	+0.2	−0.1
JESAbsoluteScale	−1.0	+0.3	+0.9	0.0	+0.3	0.0	−2.1	+0.7	−0.8	0.0	+0.6	0.0
	−1.8	+0.4	+0.5	−0.9	+0.7	0.0	−0.4	+0.8	−0.4	+0.4	+0.2	−0.2
JESAbsoluteStat	−4.8	+0.7	+6.8	−4.1	−1.8	+2.6	−1.9	−2.2	+1.8	−1.7	−2.8	+1.7
	+2.3	+0.9	−5.4	+3.6	+1.6	−2.5	+0.9	+2.8	−2.6	+2.3	+3.2	−1.3
JESFlavourQCD	−0.9	+1.6	+1.4	−1.8	−0.1	−0.7	−2.4	+0.4	−0.2	+0.1	+0.8	+0.7
	−2.8	0.0	+0.9	+1.4	+0.9	+0.4	+0.8	−0.1	−0.6	−0.2	+0.2	−1.0
JESFragmentation	−0.7	+0.8	+0.2	−2.5	+0.4	0.0	+0.1	+0.4	−0.2	+0.5	+0.4	0.0
	−1.7	+0.9	+1.7	+0.3	+0.2	−0.5	−2.0	+1.0	−0.5	+1.2	+0.1	−0.4
JESPileUpDataMC	−0.7	+0.6	+0.1	−0.4	+0.3	−0.4	−1.2	+1.0	−0.6	−0.6	+1.0	+0.2
	−1.3	+1.4	0.0	+0.2	+0.2	+0.1	−0.8	+0.4	−0.7	−0.7	+0.3	−0.3
JESPileUpPtBB	−0.9	+0.5	0.0	+0.1	+0.1	−0.1	−1.6	+0.4	−0.1	+1.1	+0.4	0.0
	−1.6	+0.8	+0.5	+0.2	+0.3	+0.2	−0.5	−0.4	−0.2	−0.4	+0.3	−0.1
JESPileUpPtEC1	−0.7	+0.9	+0.2	−1.1	0.0	+0.1	−0.3	+0.2	−0.1	−0.8	−0.1	+0.2
	−0.7	+0.7	−0.3	−0.3	−0.2	+0.2	+1.2	0.0	−0.2	+1.4	+0.1	−0.2
JESPileUpPtEC2	0.0	0.0	0.0	0.0	0.0	0.0	0.0	0.0	0.0	0.0	0.0	0.0
	0.0	0.0	0.0	0.0	0.0	0.0	0.0	0.0	0.0	0.0	0.0	0.0
JESPileUpPtHF	0.0	0.0	0.0	0.0	0.0	0.0	0.0	0.0	0.0	0.0	0.0	0.0
	0.0	0.0	0.0	0.0	0.0	0.0	0.0	0.0	0.0	0.0	0.0	0.0
JESPileUpPtRef	−1.6	+0.4	+1.1	+0.4	+0.1	−0.5	−1.2	+0.5	−0.2	−0.4	+0.7	+0.3
	−1.8	+0.9	+1.3	+0.4	0.0	−0.3	+0.1	+0.6	−0.4	+0.5	0.0	−0.5
JESRelativeBal	+0.1	+1.7	−0.2	−1.5	−0.1	0.0	−1.2	−0.2	−0.3	−0.4	+0.7	+0.3
	−2.6	−0.8	+1.1	+2.5	+0.4	+0.4	−1.1	−0.1	−0.6	+2.0	+0.9	−0.4
JESRelativeFSR	−0.1	+0.3	+0.4	−0.9	−0.2	+0.4	−0.8	+0.4	−0.4	+0.9	+0.3	−0.4
	−0.7	+0.7	+0.9	−1.8	+0.4	−0.5	−1.4	+0.9	−0.5	+1.1	+0.2	+0.1
JESRelativeJEREC1	−1.4	+0.5	+0.9	+0.4	+0.1	−0.4	−0.2	+0.3	−0.3	+0.9	0.0	+0.2
	−0.8	+1.1	−0.6	−1.7	+0.3	+0.4	+0.3	0.0	−0.2	+0.3	+0.3	−0.1
JESRelativeJEREC2	0.0	0.0	0.0	0.0	0.0	0.0	0.0	0.0	0.0	0.0	0.0	0.0
	0.0	0.0	0.0	0.0	0.0	0.0	0.0	0.0	0.0	0.0	0.0	0.0
JESRelativeJERHF	0.0	0.0	0.0	0.0	0.0	0.0	0.0	0.0	0.0	0.0	0.0	0.0
	0.0	0.0	0.0	0.0	0.0	0.0	0.0	0.0	0.0	0.0	0.0	0.0
JESRelativePtBB	−2.0	+1.1	+0.6	+1.0	+0.1	−0.1	−0.4	−0.2	−0.5	−0.5	+0.7	0.0
	−0.8	−0.2	+0.2	+1.5	+0.4	0.0	−2.0	+0.1	−0.2	+0.5	+0.5	−0.3
JESRelativePtEC1	−0.7	+0.8	+0.7	−0.7	+0.1	+0.3	−0.7	+0.1	−0.5	−0.7	−0.1	+0.1
	−0.4	−0.4	−0.4	+0.2	+0.1	+0.4	−0.3	+0.3	0.0	+0.8	+0.1	−0.1
JESRelativePtEC2	0.0	0.0	0.0	0.0	0.0	0.0	0.0	0.0	0.0	0.0	0.0	0.0
	0.0	0.0	0.0	0.0	0.0	0.0	0.0	0.0	0.0	0.0	0.0	0.0
JESRelativePtHF	0.0	0.0	0.0	0.0	0.0	0.0	0.0	0.0	0.0	0.0	0.0	0.0
	0.0	0.0	0.0	0.0	0.0	0.0	0.0	0.0	0.0	0.0	0.0	0.0
JESRelativeStatEC	−1.1	+0.1	+1.0	−0.9	0.0	+0.3	+0.5	+0.5	−0.4	−0.2	0.0	0.0
	−0.3	0.0	+0.5	+0.1	+0.1	+0.1	−2.3	+0.2	−0.3	+1.8	+0.3	0.0
JESRelativeStatFSR	−1.1	+0.9	+0.4	−0.2	+0.4	−0.4	−1.6	+0.2	−0.3	+1.3	+0.6	0.0
	−1.5	+1.2	+0.7	+0.2	+0.1	0.0	−1.1	−0.2	−0.3	−0.2	+0.5	−0.1
JESRelativeStatHF	0.0	0.0	0.0	0.0	0.0	0.0	0.0	0.0	0.0	0.0	0.0	0.0
	0.0	0.0	0.0	0.0	0.0	0.0	0.0	0.0	0.0	0.0	0.0	0.0
JESSinglePionECAL	−1.1	+0.1	+1.4	+0.3	−0.2	+0.5	−2.0	0.0	−0.5	+0.8	+0.5	−0.3
	−1.1	+0.4	+1.1	−1.7	+0.3	+0.2	−1.0	+0.4	−0.3	+0.3	+0.5	0.0

Table A.24: Table A.23 continued.

source / bin	1	2	3	4	5	6	7	8	9	10	11	12
JESSinglePionHCAL	−1.6	+1.0	+0.8	−0.2	+0.3	+0.1	0.0	−0.5	−0.2	+0.5	+0.2	−0.2
	−1.3	+1.3	+0.9	−0.2	−0.3	−0.3	−1.7	−0.1	+0.2	−0.1	+0.7	+0.2
JESTimePtEta	−1.1	+0.4	+0.7	+0.3	+0.2	+0.1	−1.7	+0.1	−0.2	+1.3	+0.3	−0.2
	−1.8	+0.2	+1.8	+0.2	−0.2	+0.3	−1.7	−0.1	−0.3	+1.0	+0.6	+0.1
$\vec{p}_{\mathrm{T}}^{\,\mathrm{miss}}$	−5.6	−2.7	+10.1	+0.3	−3.4	+3.3	+0.1	−3.8	+2.4	−0.3	−1.5	+0.5
	+1.6	+4.1	−6.2	−1.0	+2.3	−2.1	−1.3	+2.2	−1.7	−0.2	+1.4	−0.4
lepton ID/ISO	−0.1	0.0	−0.4	−0.2	+0.4	+0.1	+0.2	0.0	−0.1	0.0	0.0	−0.2
	+0.1	0.0	+0.4	+0.2	−0.4	−0.1	−0.1	0.0	+0.1	0.0	0.0	+0.2
pileup	−1.6	−0.7	+2.8	−0.7	−0.9	+1.0	−0.1	−1.0	+0.8	−0.1	−0.6	+0.3
	+1.5	+0.7	−2.8	+0.7	+0.9	−1.0	0.0	+1.0	−0.8	+0.1	+0.6	−0.3
trigger	0.0	0.0	−0.1	−0.1	+0.1	0.0	0.0	0.0	0.0	−0.2	−0.1	0.0
	0.0	0.0	+0.1	+0.1	−0.1	0.0	0.0	0.0	0.0	+0.2	+0.1	0.0
trigger (η)	0.0	0.0	0.0	−0.1	0.0	0.0	−0.1	−0.1	0.0	+0.2	+0.1	0.0
	0.0	0.0	0.0	+0.1	0.0	0.0	+0.1	+0.1	0.0	−0.2	−0.1	0.0
non-$\mathrm{t\bar{t}}$ background	−1.8	−1.4	−1.5	−0.5	+0.5	+0.3	+0.8	+0.5	+0.6	+0.7	+1.1	+1.1
	+0.9	+1.6	+0.9	+1.1	+0.1	−0.4	−1.4	−0.5	−0.7	−0.1	−1.2	−0.9
b-tagging	+0.1	−0.1	−0.3	+0.1	+0.1	0.0	+0.1	0.0	0.0	+0.2	+0.1	+0.1
	−0.1	+0.1	+0.3	−0.1	−0.1	0.0	−0.1	0.0	0.0	−0.2	−0.1	−0.1
b-tagging (light jets)	−0.7	−0.3	0.0	−0.4	+0.1	+0.2	−0.1	+0.1	+0.3	−0.4	+0.2	+0.2
	+0.7	+0.3	0.0	+0.4	−0.1	−0.2	+0.1	−0.1	−0.3	+0.4	−0.2	−0.2
luminosity	0.0	0.0	0.0	0.0	0.0	0.0	0.0	0.0	0.0	0.0	0.0	0.0
	0.0	0.0	0.0	0.0	0.0	0.0	0.0	0.0	0.0	0.0	0.0	0.0
branching ratio $\mathrm{t\bar{t}} \to \ell\ell$	0.0	0.0	0.0	0.0	0.0	0.0	0.0	0.0	0.0	0.0	0.0	0.0
	0.0	0.0	0.0	0.0	0.0	0.0	0.0	0.0	0.0	0.0	0.0	0.0
PDF eigenvector 1	0.0	0.0	0.0	0.0	0.0	0.0	0.0	0.0	0.0	+0.1	0.0	0.0
	0.0	0.0	0.0	0.0	0.0	0.0	0.0	0.0	0.0	0.0	0.0	0.0
PDF eigenvector 2	−0.1	−0.1	−0.1	+0.1	−0.1	0.0	+0.1	0.0	0.0	+0.3	+0.2	+0.1
	0.0	0.0	+0.2	−0.1	0.0	0.0	0.0	+0.1	0.0	−0.2	−0.1	−0.1
PDF eigenvector 3	+0.1	0.0	0.0	+0.1	0.0	0.0	+0.1	0.0	0.0	0.0	0.0	0.0
	0.0	0.0	0.0	0.0	0.0	0.0	0.0	0.0	0.0	0.0	0.0	0.0
PDF eigenvector 4	0.0	0.0	−0.1	0.0	0.0	0.0	0.0	−0.1	0.0	+0.2	+0.1	+0.1
	0.0	0.0	+0.1	0.0	0.0	0.0	0.0	0.0	0.0	−0.1	−0.1	−0.1
PDF eigenvector 5	−0.1	0.0	+0.1	−0.2	0.0	0.0	−0.1	+0.1	+0.1	−0.1	−0.1	0.0
	+0.1	0.0	−0.1	+0.1	0.0	0.0	+0.1	−0.1	−0.1	0.0	0.0	0.0
PDF eigenvector 6	0.0	0.0	−0.2	0.0	+0.1	0.0	0.0	−0.1	0.0	+0.2	0.0	+0.1
	0.0	0.0	+0.1	0.0	−0.1	0.0	0.0	+0.1	0.0	−0.1	0.0	−0.1
PDF eigenvector 7	−0.1	0.0	+0.2	−0.3	0.0	0.0	−0.2	+0.2	+0.1	−0.2	−0.1	−0.1
	+0.1	0.0	−0.1	+0.1	0.0	0.0	+0.1	−0.1	−0.1	+0.1	0.0	+0.1
PDF eigenvector 8	0.0	0.0	−0.1	−0.1	+0.1	0.0	0.0	0.0	0.0	0.0	0.0	0.0
	0.0	0.0	+0.1	0.0	−0.1	0.0	0.0	0.0	0.0	0.0	0.0	0.0
PDF eigenvector 9	+0.1	0.0	+0.1	0.0	−0.1	0.0	0.0	+0.1	0.0	−0.1	0.0	−0.1
	−0.1	0.0	−0.1	0.0	+0.1	0.0	0.0	−0.1	0.0	+0.1	0.0	+0.1
PDF eigenvector 10	+0.1	0.0	−0.1	+0.1	0.0	0.0	0.0	−0.1	−0.1	+0.1	0.0	+0.1
	−0.1	0.0	+0.1	−0.1	0.0	0.0	−0.1	+0.1	+0.1	−0.1	0.0	−0.1
PDF eigenvector 11	0.0	0.0	0.0	0.0	0.0	0.0	0.0	0.0	0.0	0.0	0.0	0.0
	0.0	0.0	+0.1	0.0	0.0	0.0	0.0	+0.1	0.0	0.0	0.0	0.0
PDF eigenvector 12	0.0	0.0	0.0	−0.1	0.0	0.0	0.0	+0.1	0.0	0.0	0.0	0.0
	+0.1	0.0	0.0	0.0	0.0	0.0	0.0	−0.1	0.0	0.0	0.0	0.0
PDF eigenvector 13	0.0	+0.1	0.0	0.0	+0.1	0.0	0.0	0.0	0.0	−0.1	−0.1	0.0
	0.0	−0.1	0.0	0.0	−0.1	0.0	0.0	0.0	0.0	+0.1	+0.1	0.0
PDF eigenvector 14	0.0	0.0	0.0	0.0	0.0	0.0	0.0	0.0	0.0	0.0	0.0	0.0
	0.0	0.0	0.0	0.0	0.0	0.0	0.0	0.0	0.0	0.0	0.0	0.0

Table A.25: Table A.23 continued.

source / bin	1	2	3	4	5	6	7	8	9	10	11	12
PDF eigenvector 15	0.0	0.0	0.0	0.0	0.0	0.0	0.0	0.0	0.0	−0.1	0.0	0.0
	0.0	0.0	0.0	0.0	0.0	0.0	0.0	0.0	0.0	0.0	0.0	0.0
PDF eigenvector 16	0.0	0.0	0.0	0.0	0.0	0.0	0.0	0.0	0.0	0.0	0.0	0.0
	0.0	0.0	0.0	0.0	0.0	0.0	0.0	0.0	0.0	0.0	0.0	0.0
PDF eigenvector 17	0.0	0.0	0.0	0.0	0.0	0.0	0.0	0.0	0.0	0.0	0.0	0.0
	0.0	0.0	−0.1	0.0	+0.1	0.0	0.0	−0.1	0.0	+0.1	0.0	0.0
PDF eigenvector 18	0.0	−0.1	0.0	+0.1	−0.1	0.0	0.0	0.0	0.0	+0.1	+0.1	+0.1
	0.0	+0.1	0.0	−0.1	+0.1	0.0	0.0	0.0	0.0	−0.1	−0.1	−0.1
PDF eigenvector 19	+0.1	0.0	0.0	+0.1	0.0	0.0	0.0	−0.1	0.0	0.0	0.0	0.0
	−0.1	0.0	+0.1	−0.1	0.0	0.0	0.0	+0.1	+0.1	−0.1	−0.1	−0.1
PDF eigenvector 20	0.0	0.0	+0.1	−0.1	0.0	0.0	0.0	0.0	0.0	−0.4	0.0	+0.1
	0.0	0.0	0.0	0.0	0.0	0.0	0.0	0.0	0.0	0.0	0.0	0.0
PDF eigenvector 21	0.0	0.0	0.0	0.0	0.0	0.0	0.0	0.0	0.0	+0.1	+0.1	+0.1
	+0.1	0.0	0.0	0.0	0.0	0.0	0.0	0.0	0.0	−0.1	−0.1	−0.1
PDF eigenvector 22	−0.1	−0.1	−0.1	0.0	−0.1	0.0	−0.1	0.0	0.0	+0.2	+0.2	+0.2
	+0.1	+0.1	0.0	0.0	+0.1	0.0	0.0	0.0	0.0	−0.2	−0.2	−0.1
PDF eigenvector 23	0.0	0.0	+0.1	−0.1	0.0	0.0	0.0	+0.1	0.0	−0.3	−0.2	−0.2
	0.0	0.0	0.0	0.0	0.0	0.0	−0.1	0.0	0.0	0.0	0.0	0.0
PDF eigenvector 24	0.0	0.0	+0.1	−0.1	0.0	0.0	−0.1	0.0	0.0	−0.2	−0.1	0.0
	−0.1	−0.1	+0.1	0.0	−0.1	0.0	+0.1	+0.1	0.0	+0.1	+0.1	0.0
PDF eigenvector 25	−0.1	0.0	+0.1	0.0	−0.1	0.0	0.0	+0.1	0.0	0.0	0.0	0.0
	−0.1	0.0	+0.2	−0.1	0.0	0.0	−0.1	+0.1	+0.1	−0.2	−0.1	0.0
PDF eigenvector 26	0.0	0.0	0.0	0.0	0.0	0.0	0.0	0.0	0.0	−0.1	0.0	0.0
	0.0	0.0	0.0	0.0	0.0	0.0	0.0	0.0	0.0	0.0	0.0	0.0
PDF eigenvector 27	+0.1	0.0	+0.2	+0.1	−0.2	0.0	0.0	0.0	0.0	0.0	0.0	0.0
	0.0	0.0	−0.1	0.0	+0.1	0.0	0.0	0.0	0.0	+0.1	0.0	+0.1
PDF eigenvector 28	0.0	0.0	+0.1	0.0	0.0	0.0	0.0	0.0	0.0	−0.1	0.0	0.0
	0.0	0.0	−0.1	0.0	+0.1	0.0	0.0	0.0	0.0	+0.1	0.0	0.0
α_S	0.0	−0.1	+0.2	+0.1	−0.2	0.0	+0.1	0.0	0.0	+0.1	0.0	−0.1
	0.0	+0.1	−0.2	−0.1	+0.2	0.0	−0.1	0.0	0.0	−0.1	0.0	+0.1
m_t^{MC}	−0.5	−1.7	−2.6	+0.4	+0.1	−0.5	−0.7	+0.8	+1.2	+0.8	+1.4	+2.1
	+0.2	+1.6	+2.3	+1.0	0.0	+0.5	−0.5	−0.6	−1.1	−0.7	−1.2	−2.6
$\mu_{r,f}$	+0.5	−0.4	+1.4	+2.1	−1.4	−0.3	+2.8	−0.2	−0.3	+2.9	+0.4	−1.1
	−0.8	+0.3	−1.3	−2.7	+1.5	+0.5	−3.9	+0.3	+0.6	−3.9	−0.7	+1.4
h_{damp}	−1.3	+0.5	+2.2	−0.2	−0.6	+0.1	−1.2	−0.3	+0.9	−1.5	−1.1	+0.2
	−0.1	−1.3	−3.0	+6.2	−0.1	−0.7	−0.8	+0.9	−0.4	+3.7	+1.2	−0.3
PS ISR	+0.3	+0.1	+0.1	−1.3	−0.5	+0.2	−2.0	+0.8	+1.1	−1.8	−0.2	−0.3
	+1.9	+0.2	−2.9	+2.5	−0.4	−0.7	−0.2	+1.1	−0.1	+2.6	−0.4	−0.3
PS FSR	+1.3	−0.1	−2.5	+3.0	+1.0	−0.6	+0.1	+1.2	−1.2	+2.0	+0.5	−2.1
	−1.0	+0.9	−0.2	−1.0	+0.2	−0.3	−1.5	+0.1	+0.5	+0.9	−1.1	+1.5
UE tune	−0.6	+0.1	+0.2	+0.7	+0.4	−0.1	−0.1	0.0	−0.3	+0.8	−0.6	−0.1
	−1.8	−0.1	+0.5	+1.8	0.0	+0.4	−2.1	0.0	+0.6	+1.0	−0.3	−0.8
colour reconnection	+0.1	−0.3	−0.7	+0.1	−0.3	0.0	−0.7	+0.6	+0.4	+1.1	−0.5	+0.4
	−0.5	0.0	+0.9	−0.8	−0.9	+1.0	−2.5	−1.1	+1.3	−0.5	−0.2	+0.4
	+0.7	+1.0	−2.3	−1.6	−0.1	+0.2	−0.6	+0.6	+0.3	+2.3	−0.7	+0.4
fragmentation b → B	+0.7	+0.4	+1.2	+0.2	−0.3	−0.3	+0.4	+0.1	−0.6	−0.1	−0.3	−0.5
	−0.3	−0.2	−0.6	−0.1	+0.1	+0.1	0.0	0.0	+0.3	+0.1	+0.2	+0.3
	+0.1	+0.1	+0.2	+0.1	−0.1	−0.1	+0.1	0.0	−0.1	0.0	0.0	−0.1
	+1.0	+0.8	+1.3	−0.4	−0.2	−0.4	−0.2	−0.1	−0.5	−0.7	−0.5	−0.5
branching ratio $B \to \mu$	−0.1	−0.1	−0.1	0.0	0.0	+0.1	0.0	+0.1	0.0	−0.1	0.0	−0.1
	+0.3	+0.2	0.0	−0.1	−0.1	−0.1	0.0	−0.1	−0.1	+0.1	0.0	+0.1

Table A.26: The measured $[M(t\bar{t}), p_T(t\bar{t})]$ cross sections, along with their relative statistical and systematic uncertainties.

$M(t\bar{t})$ [GeV]	$p_t(t\bar{t})$ [GeV]	$\frac{1}{\sigma(t\bar{t})}\frac{d\sigma}{dp_t(t\bar{t})}$ [GeV^{-1}]	stat. [%]	syst. [%]	bin
300–400	0–30	3.671×10^{-3}	1.8	$^{+12.4}_{-9.3}$	1
300–400	30–75	1.660×10^{-3}	2.1	$^{+10.6}_{-14.1}$	2
300–400	75–150	5.749×10^{-4}	3.3	$^{+9.7}_{-8.4}$	3
300–400	150–500	5.519×10^{-5}	5.1	$^{+8.1}_{-9.7}$	4
400–500	0–30	4.915×10^{-3}	1.1	$^{+9.8}_{-8.0}$	5
400–500	30–75	2.609×10^{-3}	1.2	$^{+7.8}_{-7.8}$	6
400–500	75–150	8.995×10^{-4}	1.9	$^{+7.1}_{-8.0}$	7
400–500	150–500	8.845×10^{-5}	3.8	$^{+6.4}_{-10.8}$	8
500–650	0–30	3.107×10^{-3}	1.6	$^{+12.1}_{-11.3}$	9
500–650	30–75	1.733×10^{-3}	1.7	$^{+10.1}_{-11.2}$	10
500–650	75–150	6.394×10^{-4}	2.5	$^{+6.8}_{-8.0}$	11
500–650	150–500	7.086×10^{-5}	3.6	$^{+5.8}_{-5.2}$	12
650–1500	0–30	1.705×10^{-3}	2.6	$^{+13.7}_{-12.3}$	13
650–1500	30–75	9.328×10^{-4}	3.3	$^{+13.2}_{-15.5}$	14
650–1500	75–150	4.219×10^{-4}	2.9	$^{+7.0}_{-6.2}$	15
650–1500	150–500	5.924×10^{-5}	2.7	$^{+6.1}_{-5.1}$	16

Table A.27: The correlation matrix of statistical uncertainties for the measured $[M(t\bar{t}), p_T(t\bar{t})]$ cross sections. The values are expressed as percentages. For bin indices see Table A.26.

bin	2	3	4	5	6	7	8	9	10	11	12	13	14	15	16
1	−28	−27	+2	−19	−35	+5	−1	−27	+1	+9	−5	0	0	−8	−2
2		+12	−9	−37	+2	−29	+4	0	−13	−5	+1	+2	−2	+3	−3
3			−9	0	−33	−30	−7	+11	−9	−18	+7	−5	+3	+6	−3
4				0	+4	−10	−63	−4	+2	+6	+10	0	−1	−2	−1
5					−3	−14	−1	+13	−34	−4	+1	−17	+6	+3	−4
6						+21	−7	−34	+25	−20	+3	+7	−11	+2	+1
7							+3	−7	−18	−7	−10	+4	+1	−8	+5
8								+1	+1	−9	−46	−1	0	+3	+8
9									−21	−16	+2	−16	−13	+12	−3
10										+5	−5	−16	+2	−17	+6
11											−8	+9	−13	−27	+1
12												−2	+3	−2	−45
13													−57	+3	+1
14														−30	0
15															−21

Table A.28: Sources and values of the relative systematic uncertainties in percent of the measured $[M(t\bar{t}), p_T(t\bar{t})]$ cross sections. For bin indices see Table A.26.

source / bin	1	2	3	4	5	6	7	8	9	10	11	12	13	14	15	16
JER	+0.4	−0.8	−0.1	+0.5	+0.7	0.0	−0.4	−1.8	+0.9	−0.2	−0.8	+0.4	+0.2	−1.2	−0.1	+0.1
	−0.3	−0.8	+0.2	+0.1	−0.1	+0.7	+0.1	−0.6	−0.9	+0.7	0.0	+0.1	−0.3	+0.3	+1.5	+0.3
JESAbsoluteMPFBias	−0.1	−0.1	−0.2	−0.1	+0.4	+0.5	−0.5	−0.9	−0.5	0.0	−0.5	0.0	+0.1	+0.4	+0.5	−0.4
	+0.3	−0.5	−0.5	−3.0	+0.2	+0.2	−0.2	+1.6	0.0	+0.2	−0.4	−0.1	−0.2	−0.1	+0.7	0.0
JESAbsoluteScale	+0.7	−0.3	−0.2	−0.4	+0.1	+0.1	0.0	−0.4	−0.5	+0.2	−0.8	−0.4	−0.1	+0.4	+0.4	−0.1
	+0.1	−0.1	−0.8	−1.9	+0.2	+0.3	+0.1	+0.5	0.0	−0.1	−0.1	+0.3	−0.6	+0.2	+0.2	0.0
JESAbsoluteStat	+4.4	−3.4	−3.0	−2.9	+3.7	−1.9	−4.2	−2.6	+4.0	−2.2	−3.5	−1.9	+4.8	−2.6	−2.7	−2.3
	−3.5	+2.8	+3.8	+1.1	−3.6	+2.1	+3.3	+1.5	−5.0	+2.2	+3.8	+2.6	−4.1	+2.2	+3.3	+3.0
JESFlavourQCD	+1.2	−0.3	0.0	+2.6	−0.4	−0.2	−1.3	−2.6	−0.3	+0.9	−0.3	−1.2	+0.2	+1.2	+0.6	+0.5
	0.0	−1.0	−0.3	0.0	+0.4	+0.5	+0.7	+0.1	−0.1	+0.1	+0.3	−0.1	−0.8	−1.1	−0.2	−0.1
JESFragmentation	−0.1	−0.2	+0.4	+1.5	+0.1	+0.5	−1.2	−2.4	−0.2	+0.7	+0.2	+0.6	−0.3	+0.1	+0.6	0.0
	+0.3	−0.6	+0.5	+0.4	+0.3	−0.1	−0.3	−0.8	0.0	+0.1	−0.2	+0.5	−0.6	−0.2	+0.5	−0.1
JESPileUpDataMC	+0.5	−0.5	−0.9	−0.4	−0.1	+0.2	−0.1	−0.7	−0.1	+0.1	−0.3	−0.2	−0.1	+0.6	+0.7	+0.4
	+0.1	0.0	+0.2	−0.6	+0.4	+0.5	−0.2	−0.4	−0.5	−0.1	−0.2	+0.4	−0.4	−0.2	−0.4	+0.3
JESPileUpPtBB	−0.3	−0.6	0.0	+0.3	+0.1	+0.6	−0.6	−0.5	−0.3	+0.5	−0.1	+0.5	+0.3	−0.2	+0.5	0.0
	+0.4	+0.3	−0.3	0.0	+0.1	+0.3	0.0	−0.7	−0.2	−0.1	−0.9	+0.1	−0.3	−0.1	+0.2	−0.2
JESPileUpPtEC1	+0.9	−0.2	−0.6	+1.0	−0.1	+0.2	−0.7	−1.9	−0.7	+0.5	+0.3	+1.0	+0.1	+0.2	−0.2	0.0
	+0.3	−0.1	+0.1	+0.5	0.0	−0.2	−0.1	−0.5	−0.3	−0.1	+0.8	+0.1	−0.1	+0.2	−0.3	+0.2
JESPileUpPtEC2	0.0	0.0	0.0	0.0	0.0	0.0	0.0	0.0	0.0	0.0	0.0	0.0	0.0	0.0	0.0	0.0
	0.0	0.0	0.0	0.0	0.0	0.0	0.0	0.0	0.0	0.0	0.0	0.0	0.0	0.0	0.0	0.0
JESPileUpPtHF	0.0	0.0	0.0	0.0	0.0	0.0	0.0	0.0	0.0	0.0	0.0	0.0	0.0	0.0	0.0	0.0
	0.0	0.0	0.0	0.0	0.0	0.0	0.0	0.0	0.0	0.0	0.0	0.0	0.0	0.0	0.0	0.0
JESPileUpPtRef	+0.2	−0.1	−0.5	+0.6	0.0	+0.1	−0.5	−1.4	−0.3	+0.3	+0.2	+0.9	+0.2	+0.4	+0.4	+0.1
	+0.7	+0.2	−0.5	−1.6	+0.3	+0.3	−0.3	−0.3	−0.8	+0.2	+0.3	+0.7	−0.4	−0.2	−0.5	−0.5
JESRelativeBal	+0.8	+0.1	+1.2	+1.1	−0.4	+0.3	−0.7	−1.7	−0.7	+0.3	−0.7	−0.6	+0.4	+0.1	+0.7	+0.3
	−0.5	−1.6	−0.6	−1.4	+0.6	+0.9	+0.8	+0.7	−0.4	0.0	−0.4	−0.2	0.0	−0.5	+0.7	+0.6
JESRelativeFSR	+0.2	−0.7	+0.4	+1.4	+0.1	+0.3	−0.6	−1.5	−0.3	+0.6	+0.1	+1.0	0.0	−0.5	+0.2	+0.1
	+0.5	−0.4	+0.1	+2.3	0.0	+0.2	−0.5	−2.7	−0.2	+0.2	−0.5	+0.9	−0.4	+0.5	+0.8	0.0
JESRelativeJEREC1	0.0	−0.2	−0.3	−0.1	+0.3	+0.3	−0.6	−0.4	−0.2	+0.1	+0.2	−0.1	−0.1	+0.3	+0.2	+0.1
	−0.1	0.0	−0.1	+0.3	+0.2	+0.3	−0.7	−0.5	−0.4	+0.4	+0.1	0.0	−0.1	−0.2	+0.3	−0.1
JESRelativeJEREC2	0.0	0.0	0.0	0.0	0.0	0.0	0.0	0.0	0.0	0.0	0.0	0.0	0.0	0.0	0.0	0.0
	0.0	0.0	0.0	0.0	0.0	0.0	0.0	0.0	0.0	0.0	0.0	0.0	0.0	0.0	0.0	0.0
JESRelativeJERHF	0.0	0.0	0.0	0.0	0.0	0.0	0.0	0.0	0.0	0.0	0.0	0.0	0.0	0.0	0.0	0.0
	0.0	0.0	0.0	0.0	0.0	0.0	0.0	0.0	0.0	0.0	0.0	0.0	0.0	0.0	0.0	0.0
JESRelativePtBB	0.0	−0.2	−0.7	+0.5	+0.3	+0.2	−0.3	−0.4	+0.2	−0.3	−0.4	+0.1	+0.2	−0.3	+1.0	−0.3
	−0.1	+0.2	+0.1	−1.2	+0.2	+0.3	−0.4	+0.5	−0.2	−0.1	−0.6	+0.1	−0.3	−0.2	+0.6	+0.3
JESRelativePtEC1	+0.5	−0.2	+0.1	+1.2	+0.2	+0.2	−0.7	−0.8	−0.6	+0.2	+0.2	+0.3	−0.5	+0.4	+0.1	−0.6
	−0.3	−0.5	−0.6	+0.3	+0.1	+0.6	−0.5	−0.7	−0.1	+0.4	+0.7	+0.2	−0.1	0.0	+0.3	+0.1
JESRelativePtEC2	0.0	0.0	0.0	0.0	0.0	0.0	0.0	0.0	0.0	0.0	0.0	0.0	0.0	0.0	0.0	0.0
	0.0	0.0	0.0	0.0	0.0	0.0	0.0	0.0	0.0	0.0	0.0	0.0	0.0	0.0	0.0	0.0
JESRelativePtHF	0.0	0.0	0.0	0.0	0.0	0.0	0.0	0.0	0.0	0.0	0.0	0.0	0.0	0.0	0.0	0.0
	0.0	0.0	0.0	0.0	0.0	0.0	0.0	0.0	0.0	0.0	0.0	0.0	0.0	0.0	0.0	0.0
JESRelativeStatEC	+0.9	+0.6	−1.5	+1.3	−0.4	+0.2	−0.5	−1.0	−0.4	+0.1	+0.4	+0.6	−0.2	+0.2	−0.3	−0.2
	+0.7	−0.4	−0.6	−0.4	0.0	+0.1	−0.1	+0.4	−0.6	+0.5	−0.1	−0.8	−0.3	+0.4	+0.1	+0.6
JESRelativeStatFSR	+0.5	−0.6	−0.6	+0.6	0.0	+0.4	−0.1	−0.3	−0.3	0.0	−0.1	−0.6	0.0	+0.5	+0.2	+0.4
	0.0	−0.1	0.0	+0.1	+0.3	+0.6	−1.2	+0.3	−0.5	+0.4	+0.1	−0.9	−0.1	−0.5	+0.3	+0.4
JESRelativeStatHF	0.0	0.0	0.0	0.0	0.0	0.0	0.0	0.0	0.0	0.0	0.0	0.0	0.0	0.0	0.0	0.0
	0.0	0.0	0.0	0.0	0.0	0.0	0.0	0.0	0.0	0.0	0.0	0.0	0.0	0.0	0.0	0.0
JESSinglePionECAL	−0.1	−0.3	+1.1	0.0	+0.4	+0.4	−0.3	−0.9	−0.4	0.0	−0.7	−0.1	−0.4	0.0	+0.3	0.0
	+0.4	−0.6	+0.1	+0.5	+0.1	+0.1	−0.6	−1.5	+0.1	+0.5	−0.6	+0.9	+0.2	+0.2	+0.2	−0.1

Table A.29: Table A.28 continued.

source / bin	1	2	3	4	5	6	7	8	9	10	11	12	13	14	15	16
JESSinglePionHCAL	+0.5	−0.4	−1.2	−1.0	+0.3	+0.2	−0.1	+0.7	−0.3	+0.4	−0.2	−0.9	−0.3	−0.3	+0.5	+0.1
	+0.5	+0.4	−1.0	+0.2	0.0	+0.1	−0.7	−0.4	−0.1	+0.1	−0.5	−0.6	+0.6	−0.4	+0.7	+0.5
JESTimePtEta	+0.2	+0.4	−0.1	−0.4	+0.2	+0.4	−0.8	−0.4	−0.5	+0.2	−0.2	−0.7	+0.1	−0.3	+0.2	+0.5
	−0.1	−0.1	−0.6	−0.2	+0.4	+0.6	−0.5	−0.7	−0.3	−0.1	−0.9	+0.8	0.0	+0.2	+0.9	+0.2
$\vec{p}_{\mathrm{T}}^{\,\mathrm{miss}}$	+6.5	−7.8	−3.1	−0.8	+5.2	−4.8	−1.4	−0.2	+6.7	−7.2	−1.9	−0.5	+7.5	−9.9	+0.2	−0.6
	−4.0	+5.6	+1.0	+0.4	−3.6	+4.2	+0.3	+0.1	−5.0	+5.7	−0.4	−0.3	−4.8	+6.7	−0.2	+0.5
lepton ID/ISO	−0.2	−0.3	−0.1	0.0	+0.2	+0.3	+0.1	0.0	−0.1	0.0	0.0	0.0	−0.1	−0.1	−0.1	−0.2
	+0.1	+0.4	0.0	0.0	−0.2	−0.2	−0.2	0.0	+0.1	+0.1	0.0	+0.1	0.0	+0.3	0.0	+0.2
pileup	+1.7	−2.0	−1.1	−0.1	+1.6	−1.4	−1.1	−0.1	+2.0	−1.9	−0.8	0.0	+2.1	−2.2	−0.3	−0.5
	−1.9	+2.1	+1.0	+0.2	−1.7	+1.5	+1.0	+0.2	−2.1	+2.0	+0.7	0.0	−2.1	+2.2	+0.3	+0.6
trigger	0.0	0.0	0.0	+0.1	0.0	+0.1	0.0	0.0	0.0	0.0	0.0	0.0	0.0	0.0	0.0	0.0
	0.0	0.0	0.0	−0.1	0.0	−0.1	0.0	0.0	0.0	0.0	0.0	0.0	0.0	0.0	0.0	0.0
trigger (η)	0.0	0.0	0.0	+0.1	0.0	0.0	0.0	0.0	−0.1	0.0	−0.1	−0.1	0.0	+0.1	0.0	0.0
	−0.1	0.0	−0.1	−0.1	0.0	0.0	0.0	0.0	0.0	+0.1	0.0	+0.1	−0.1	0.0	−0.1	0.0
non-$t\bar{t}$ background	−1.3	−2.1	−1.0	+0.3	+0.4	0.0	+0.4	+0.1	+0.5	+0.2	+0.7	+0.5	+0.8	+0.9	+1.3	+0.9
	+0.9	+2.4	+0.7	−0.3	−0.4	+0.3	−0.5	0.0	−0.6	0.0	−0.8	−0.4	−0.9	−0.6	−1.4	−0.8
b-tagging	−0.2	−0.2	+0.2	−0.2	0.0	0.0	+0.2	+0.1	0.0	−0.1	+0.1	+0.1	+0.1	0.0	+0.2	+0.2
	+0.1	+0.2	−0.3	+0.2	0.0	+0.1	−0.2	−0.1	0.0	+0.1	−0.1	−0.1	−0.1	0.0	−0.2	−0.1
b-tagging (light jets)	−0.1	−0.5	−0.7	+0.1	+0.2	+0.1	−0.2	−0.1	+0.2	+0.1	0.0	0.0	+0.2	+0.2	+0.1	0.0
	0.0	+0.6	+0.6	−0.1	−0.2	0.0	+0.2	+0.1	−0.3	−0.1	0.0	0.0	−0.2	−0.2	−0.1	0.0
luminosity	0.0	0.0	0.0	0.0	0.0	0.0	0.0	0.0	0.0	0.0	0.0	0.0	0.0	0.0	0.0	0.0
	0.0	0.0	0.0	0.0	0.0	0.0	0.0	0.0	0.0	0.0	0.0	0.0	0.0	0.0	0.0	0.0
branching ratio $t\bar{t} \to \ell\ell$	0.0	0.0	0.0	0.0	0.0	0.0	0.0	0.0	0.0	0.0	0.0	0.0	0.0	0.0	0.0	0.0
	0.0	0.0	0.0	0.0	0.0	0.0	0.0	0.0	0.0	0.0	0.0	0.0	0.0	0.0	0.0	0.0
PDF eigenvector 1	0.0	0.0	0.0	0.0	0.0	0.0	0.0	0.0	0.0	0.0	0.0	0.0	0.0	0.0	0.0	0.0
	0.0	0.0	0.0	0.0	0.0	0.0	0.0	0.0	0.0	0.0	0.0	0.0	0.0	0.0	0.0	0.0
PDF eigenvector 2	−0.1	−0.1	−0.1	0.0	0.0	0.0	0.0	0.0	0.0	0.0	0.0	0.0	+0.2	+0.2	+0.2	+0.1
	+0.1	0.0	0.0	−0.1	0.0	0.0	0.0	−0.1	+0.1	0.0	0.0	0.0	−0.1	−0.1	−0.1	−0.1
PDF eigenvector 3	0.0	0.0	0.0	+0.1	0.0	0.0	0.0	+0.1	0.0	0.0	0.0	0.0	−0.1	0.0	0.0	0.0
	0.0	0.0	0.0	0.0	0.0	0.0	0.0	0.0	0.0	0.0	0.0	0.0	0.0	+0.1	0.0	0.0
PDF eigenvector 4	−0.1	0.0	−0.1	0.0	0.0	0.0	0.0	+0.1	0.0	0.0	−0.1	0.0	+0.1	+0.2	+0.1	+0.1
	+0.1	0.0	0.0	0.0	0.0	0.0	0.0	−0.1	0.0	0.0	0.0	0.0	−0.1	−0.1	−0.1	−0.1
PDF eigenvector 5	0.0	0.0	−0.1	−0.1	0.0	0.0	−0.1	−0.2	+0.1	+0.1	+0.1	0.0	0.0	0.0	−0.1	−0.1
	0.0	0.0	0.0	+0.1	0.0	0.0	0.0	+0.1	−0.1	−0.1	0.0	0.0	−0.1	0.0	0.0	0.0
PDF eigenvector 6	−0.1	0.0	−0.1	+0.1	0.0	+0.1	0.0	+0.1	−0.1	0.0	−0.1	0.0	+0.1	+0.1	+0.1	+0.1
	+0.1	+0.1	0.0	0.0	0.0	0.0	0.0	−0.1	0.0	0.0	0.0	0.0	−0.1	0.0	0.0	−0.1
PDF eigenvector 7	0.0	0.0	−0.1	−0.2	0.0	0.0	−0.1	−0.3	+0.1	+0.2	+0.1	−0.1	0.0	−0.1	−0.1	−0.2
	0.0	0.0	0.0	+0.1	0.0	0.0	0.0	+0.2	−0.1	−0.1	−0.1	0.0	0.0	0.0	+0.1	+0.1
PDF eigenvector 8	−0.1	0.0	−0.1	0.0	0.0	+0.1	0.0	0.0	−0.1	0.0	−0.1	0.0	0.0	+0.1	0.0	0.0
	0.0	0.0	0.0	0.0	0.0	−0.1	0.0	0.0	0.0	0.0	0.0	0.0	0.0	0.0	0.0	0.0
PDF eigenvector 9	+0.1	+0.1	+0.1	0.0	0.0	−0.1	0.0	0.0	0.0	0.0	0.0	0.0	−0.1	0.0	0.0	0.0
	−0.1	0.0	−0.1	0.0	0.0	+0.1	0.0	+0.1	0.0	0.0	−0.1	0.0	+0.1	0.0	0.0	0.0
PDF eigenvector 10	−0.1	0.0	0.0	+0.1	0.0	+0.1	0.0	+0.2	−0.1	−0.1	−0.1	0.0	0.0	+0.1	+0.1	+0.2
	0.0	0.0	−0.1	−0.1	0.0	0.0	−0.1	−0.2	+0.1	+0.1	+0.1	0.0	0.0	0.0	−0.1	−0.2
PDF eigenvector 11	0.0	0.0	0.0	0.0	0.0	0.0	0.0	0.0	0.0	0.0	0.0	0.0	0.0	0.0	0.0	0.0
	0.0	0.0	0.0	−0.1	0.0	0.0	0.0	−0.1	0.0	0.0	0.0	0.0	0.0	0.0	0.0	−0.1
PDF eigenvector 12	0.0	0.0	−0.1	−0.1	0.0	0.0	0.0	−0.1	0.0	+0.1	0.0	0.0	0.0	0.0	0.0	−0.1
	0.0	0.0	0.0	+0.1	0.0	0.0	0.0	+0.1	0.0	0.0	0.0	0.0	0.0	0.0	0.0	+0.1
PDF eigenvector 13	0.0	0.0	0.0	0.0	0.0	+0.1	0.0	0.0	−0.1	0.0	0.0	0.0	−0.1	−0.1	−0.1	0.0
	0.0	0.0	−0.1	0.0	0.0	0.0	0.0	0.0	0.0	0.0	0.0	0.0	0.0	+0.1	+0.1	0.0
PDF eigenvector 14	0.0	0.0	0.0	0.0	0.0	0.0	0.0	0.0	0.0	0.0	0.0	0.0	0.0	0.0	0.0	0.0
	0.0	0.0	0.0	0.0	0.0	0.0	0.0	0.0	0.0	0.0	0.0	0.0	0.0	0.0	0.0	+0.1

Table A.30: Table A.28 continued.

source / bin	1	2	3	4	5	6	7	8	9	10	11	12	13	14	15	16
PDF eigenvector 15	0.0	0.0	0.0	0.0	0.0	0.0	0.0	−0.1	0.0	0.0	0.0	0.0	0.0	0.0	−0.1	−0.1
	0.0	0.0	0.0	0.0	0.0	0.0	0.0	0.0	0.0	0.0	0.0	0.0	0.0	0.0	0.0	0.0
PDF eigenvector 16	0.0	0.0	0.0	0.0	0.0	0.0	0.0	0.0	0.0	0.0	0.0	0.0	0.0	0.0	0.0	0.0
	0.0	0.0	0.0	0.0	0.0	0.0	0.0	0.0	0.0	0.0	0.0	0.0	0.0	0.0	0.0	0.0
PDF eigenvector 17	0.0	0.0	0.0	0.0	0.0	0.0	0.0	0.0	0.0	0.0	0.0	0.0	0.0	0.0	0.0	0.0
	−0.1	0.0	0.0	+0.1	0.0	+0.1	0.0	+0.1	−0.1	0.0	−0.1	0.0	0.0	0.0	0.0	+0.1
PDF eigenvector 18	0.0	0.0	0.0	0.0	0.0	0.0	0.0	+0.1	0.0	0.0	0.0	0.0	0.0	+0.1	+0.1	+0.1
	0.0	0.0	0.0	0.0	0.0	+0.1	0.0	−0.1	0.0	0.0	0.0	0.0	−0.1	−0.1	−0.1	−0.1
PDF eigenvector 19	0.0	0.0	0.0	+0.1	0.0	0.0	0.0	+0.1	−0.1	−0.1	0.0	0.0	0.0	+0.1	+0.1	+0.1
	0.0	0.0	−0.1	−0.1	0.0	0.0	−0.1	−0.2	+0.1	+0.1	0.0	0.0	0.0	0.0	−0.1	−0.2
PDF eigenvector 20	0.0	0.0	0.0	+0.1	0.0	0.0	0.0	−0.1	0.0	0.0	0.0	+0.1	0.0	0.0	0.0	−0.1
	0.0	0.0	0.0	0.0	0.0	0.0	0.0	−0.1	0.0	0.0	0.0	0.0	0.0	0.0	0.0	0.0
PDF eigenvector 21	0.0	0.0	−0.1	0.0	0.0	0.0	0.0	0.0	0.0	0.0	0.0	0.0	+0.1	+0.1	+0.1	+0.1
	0.0	+0.1	+0.1	+0.1	0.0	0.0	0.0	0.0	0.0	0.0	0.0	0.0	−0.1	−0.1	−0.1	0.0
PDF eigenvector 22	−0.1	0.0	−0.1	−0.1	0.0	0.0	−0.1	0.0	0.0	0.0	0.0	0.0	+0.2	+0.2	+0.2	+0.1
	0.0	+0.1	+0.1	+0.1	0.0	+0.1	0.0	+0.1	−0.1	0.0	0.0	+0.1	−0.2	−0.2	−0.2	−0.1
PDF eigenvector 23	+0.1	0.0	0.0	0.0	0.0	0.0	0.0	−0.1	+0.1	+0.1	+0.1	0.0	−0.2	−0.2	−0.2	−0.2
	0.0	0.0	0.0	0.0	0.0	0.0	0.0	0.0	0.0	0.0	0.0	0.0	0.0	0.0	0.0	0.0
PDF eigenvector 24	0.0	0.0	0.0	0.0	0.0	0.0	0.0	−0.1	+0.1	0.0	0.0	0.0	0.0	0.0	−0.1	−0.1
	0.0	0.0	−0.1	−0.1	0.0	0.0	−0.1	−0.1	+0.1	0.0	0.0	0.0	+0.1	0.0	0.0	−0.1
PDF eigenvector 25	+0.1	−0.1	−0.1	−0.1	0.0	−0.1	0.0	−0.1	+0.1	0.0	+0.1	0.0	0.0	0.0	0.0	−0.1
	0.0	0.0	0.0	−0.1	0.0	0.0	−0.1	−0.2	+0.1	+0.1	+0.1	0.0	0.0	0.0	−0.1	−0.2
PDF eigenvector 26	0.0	0.0	0.0	0.0	0.0	0.0	0.0	0.0	0.0	0.0	0.0	0.0	0.0	0.0	0.0	0.0
	0.0	0.0	0.0	0.0	0.0	0.0	0.0	0.0	0.0	0.0	0.0	0.0	0.0	0.0	0.0	0.0
PDF eigenvector 27	+0.1	+0.1	+0.1	+0.1	−0.1	−0.2	0.0	0.0	0.0	0.0	+0.1	0.0	−0.1	0.0	0.0	+0.1
	−0.1	0.0	0.0	0.0	0.0	+0.1	0.0	0.0	0.0	0.0	0.0	0.0	+0.1	0.0	0.0	0.0
PDF eigenvector 28	0.0	0.0	0.0	−0.1	0.0	0.0	0.0	0.0	0.0	0.0	0.0	0.0	0.0	0.0	0.0	−0.1
	−0.1	0.0	0.0	0.0	0.0	+0.1	0.0	0.0	−0.1	0.0	−0.1	0.0	0.0	+0.1	0.0	+0.1
α_S	+0.1	+0.1	+0.1	+0.1	−0.1	−0.1	0.0	0.0	+0.1	0.0	0.0	+0.1	−0.1	0.0	−0.1	0.0
	−0.1	0.0	−0.1	−0.1	0.0	+0.2	0.0	0.0	−0.1	0.0	−0.1	−0.1	+0.1	+0.1	0.0	0.0
m_t^{MC}	−1.4	−2.0	−1.8	−0.9	−0.2	+0.1	−0.1	−0.9	+0.8	+1.1	+0.6	+0.3	+2.0	+2.3	+1.3	+0.9
	+1.1	+1.6	+2.1	+1.1	+0.2	+0.2	+0.6	+1.1	−0.7	−1.0	−0.9	−0.2	−2.3	−2.3	−1.5	−1.2
$\mu_{r,f}$	+1.1	+0.8	+0.5	+1.2	−0.3	−0.8	−0.5	+1.1	+0.3	−0.2	−0.5	+0.6	−1.2	−0.5	−0.9	+0.8
	−1.3	−1.0	−0.7	−1.8	+0.3	+0.8	+0.6	−1.4	−0.1	+0.3	+0.7	−1.2	+1.4	+0.9	+1.2	−1.0
h_{damp}	−0.2	−0.3	+1.0	−2.7	−0.2	−0.2	+0.4	−0.8	+0.9	0.0	−0.1	+0.2	−0.9	+2.2	−0.7	−0.6
	−0.9	−0.8	+1.6	−2.9	−0.4	+0.3	+1.4	+2.2	0.0	+0.7	−0.6	−0.6	−1.1	+1.2	0.0	−0.1
PS ISR	−0.4	−0.7	+0.3	+0.5	−0.4	+0.4	+0.2	−0.8	+0.8	+1.0	−0.7	+0.1	−1.2	+1.6	−0.7	−0.9
	−1.3	−0.2	+3.3	−0.1	−1.3	+0.3	+1.3	+0.7	−1.1	+1.5	+0.8	+0.6	−0.3	−0.4	−0.1	+1.5
PS FSR	−1.2	+0.2	+2.0	+1.0	−0.8	+0.6	+2.4	+2.1	−1.1	+0.1	+1.1	+1.0	−3.4	+0.7	−1.0	+0.6
	+0.3	−0.1	−0.1	−2.1	−0.6	+0.1	−0.5	−1.1	−0.1	+0.9	+0.5	−0.6	+0.2	+2.3	−0.3	−0.5
UE tune	+0.2	−1.0	+0.5	−0.9	−0.2	+0.3	+1.0	+1.1	+0.2	−0.3	−0.8	+0.3	−0.8	+1.7	−1.5	−0.3
	−0.6	−0.6	−1.0	+1.3	−0.1	+0.6	+1.1	−0.8	−0.1	+1.0	+0.6	+0.2	−1.8	+0.8	+0.2	−0.7
colour reconnection	−0.2	−1.4	+0.8	+0.8	+0.1	−0.3	+0.2	−1.0	+0.1	+0.3	+1.4	−0.7	0.0	+0.8	−0.8	+1.1
	+0.7	−1.5	−0.2	−0.2	+1.2	−0.6	−0.6	−1.3	+1.8	−0.5	−2.2	−1.2	+0.1	+1.9	−0.9	−0.9
	−0.5	−0.6	+0.6	−0.1	−0.2	+0.3	+0.4	−2.2	+0.4	+0.3	0.0	+1.1	+0.4	+0.3	0.0	+0.1
fragmentation b → B	+0.5	+0.7	+1.2	+0.6	−0.3	−0.2	0.0	+0.2	−0.5	−0.1	+0.1	+0.3	−1.2	−0.3	−0.3	+0.2
	−0.3	−0.3	−0.6	−0.3	+0.1	+0.1	0.0	−0.1	+0.2	+0.1	−0.1	−0.1	+0.6	+0.3	+0.2	0.0
	+0.1	+0.1	+0.2	+0.1	−0.1	0.0	0.0	+0.1	−0.1	0.0	0.0	+0.1	−0.2	0.0	0.0	+0.1
	+0.7	+1.0	+1.2	+1.4	−0.4	−0.2	0.0	−0.2	−0.5	−0.2	0.0	−0.1	−1.0	−0.6	−0.2	0.0
branching ratio $B \to \mu$	−0.1	−0.1	−0.1	−0.2	+0.1	+0.1	0.0	+0.1	0.0	+0.1	+0.1	0.0	−0.1	−0.1	−0.1	0.0
	+0.1	+0.2	+0.1	+0.2	−0.1	−0.1	−0.1	0.0	−0.1	−0.1	−0.1	0.0	+0.1	+0.1	+0.1	+0.1

Table A.31: The measured $[M(t\bar{t}), p_T(t)]$ cross sections, along with their relative statistical and systematic uncertainties.

$M(t\bar{t})$ [GeV]	$p_t(t)$ [GeV]	$\frac{1}{\sigma(t\bar{t})}\frac{d\sigma}{dp_t(t)}$[GeV^{-1}]	stat. [%]	syst. [%]	bin
300–450	0–100	3.173×10^{-3}	0.6	$^{+2.7}_{-2.5}$	1
300–450	100–180	1.440×10^{-3}	1.2	$^{+5.5}_{-5.7}$	2
300–450	180–600	1.956×10^{-5}	6.5	$^{+27.8}_{-28.8}$	3
450–600	0–100	1.199×10^{-3}	1.2	$^{+4.9}_{-4.6}$	4
450–600	100–180	2.104×10^{-3}	0.7	$^{+4.4}_{-4.6}$	5
450–600	180–600	1.424×10^{-4}	1.9	$^{+2.6}_{-3.4}$	6
600–1500	0–100	5.409×10^{-4}	2.5	$^{+5.4}_{-5.1}$	7
600–1500	100–180	8.166×10^{-4}	1.9	$^{+5.4}_{-4.6}$	8
600–1500	180–600	2.187×10^{-4}	1.0	$^{+4.4}_{-4.4}$	9

Table A.32: The correlation matrix of statistical uncertainties for the measured $[M(t\bar{t}), p_T(t)]$ cross sections. The values are expressed as percentages. For bin indices see Table A.31.

bin	2	3	4	5	6	7	8	9
1	−19	−12	−8	−51	−9	−36	−7	−2
2		−7	−41	0	−26	+3	−16	+1
3			+2	−3	−22	−1	+3	+1
4				+2	−16	−17	−27	−1
5					−5	−15	+5	−16
6						+7	−2	−30
7							−27	−7
8								−22

Table A.33: Sources and values of the relative systematic uncertainties in percent of the measured $[M(t\bar{t}), p_T(t)]$ cross sections. For bin indices see Table A.31.

source / bin	1	2	3	4	5	6	7	8	9
JER	+0.3	+0.1	−3.7	−0.3	0.0	+0.2	+0.5	−0.7	−0.2
	−0.2	0.0	−0.9	−0.1	+0.1	+0.1	+0.8	0.0	+0.3
JESAbsoluteMPFBias	0.0	+0.3	−1.7	−0.1	−0.2	0.0	+0.3	−0.2	+0.3
	−0.2	+0.6	−0.4	0.0	−0.1	0.0	−0.1	0.0	+0.1
JESAbsoluteScale	+0.2	−0.2	−0.1	0.0	−0.2	+0.1	+0.1	0.0	+0.1
	+0.1	−0.3	−1.0	+0.5	−0.2	+0.2	−0.4	−0.3	+0.1
JESAbsoluteStat	+0.6	−0.8	−8.2	−0.3	+0.4	−0.5	0.0	−0.4	+0.1
	−0.4	+0.5	+6.6	+0.2	−0.6	+0.4	+1.5	−0.4	+0.2
JESFlavourQCD	+0.3	−0.7	−0.9	−0.9	+0.1	+0.3	−0.2	+0.5	+0.6
	−0.4	+1.0	−1.2	+1.0	−0.2	+0.1	+0.5	−0.3	−0.8
JESFragmentation	+0.1	−0.3	+0.2	−0.2	−0.1	+0.3	+0.5	−0.2	+0.2
	+0.1	0.0	−1.3	+0.2	−0.3	+0.1	+0.5	−0.2	−0.1
JESPileUpDataMC	−0.1	+0.1	−1.8	−0.4	0.0	−0.2	+0.6	+0.1	+0.3
	+0.2	+0.4	−2.9	+0.2	−0.3	+0.4	−0.9	−0.1	−0.3
JESPileUpPtBB	−0.1	−0.2	−2.5	−0.1	0.0	+0.5	+0.7	−0.1	+0.1
	+0.1	+0.2	+0.1	+0.1	−0.2	+0.2	+0.3	−0.4	−0.2
JESPileUpPtEC1	+0.1	+0.2	−3.5	−0.3	+0.2	+0.3	−1.3	−0.1	+0.4
	−0.2	+0.1	+0.4	+0.2	−0.3	−0.1	+1.8	+0.1	−0.3
JESPileUpPtEC2	0.0	0.0	0.0	0.0	0.0	0.0	0.0	0.0	0.0
	0.0	0.0	0.0	0.0	0.0	0.0	0.0	0.0	0.0
JESPileUpPtHF	0.0	0.0	0.0	0.0	0.0	0.0	0.0	0.0	0.0
	0.0	0.0	0.0	0.0	0.0	0.0	0.0	0.0	0.0
JESPileUpPtRef	0.0	−0.3	+0.6	−0.3	−0.1	+0.7	−0.3	+0.4	+0.4
	+0.1	+0.1	−1.2	+0.1	+0.1	−0.4	+0.2	0.0	−0.4
JESRelativeBal	+0.3	+0.3	−2.0	−0.6	−0.1	−0.3	−0.4	−0.5	+0.6
	−0.4	+0.8	+1.6	+0.2	−0.3	−0.2	+1.0	0.0	−0.1
JESRelativeFSR	0.0	−0.1	−0.4	+0.1	+0.1	−0.1	+0.4	−0.2	−0.2
	+0.1	−0.1	−0.8	−0.3	−0.2	+0.1	−0.1	+0.3	+0.2
JESRelativeJEREC1	0.0	+0.1	+0.1	−0.1	−0.1	−0.1	+0.2	0.0	+0.1
	0.0	−0.3	+1.3	+0.2	−0.1	−0.2	0.0	+0.1	+0.1
JESRelativeJEREC2	0.0	0.0	0.0	0.0	0.0	0.0	0.0	0.0	0.0
	0.0	0.0	0.0	0.0	0.0	0.0	0.0	0.0	0.0
JESRelativeJERHF	0.0	0.0	0.0	0.0	0.0	0.0	0.0	0.0	0.0
	0.0	0.0	0.0	0.0	0.0	0.0	0.0	0.0	0.0
JESRelativePtBB	0.0	−0.2	−0.7	+0.4	−0.2	0.0	+0.5	−0.4	+0.2
	0.0	+0.3	−1.0	−0.1	0.0	0.0	+0.2	−0.3	−0.1
JESRelativePtEC1	+0.3	0.0	−2.4	−0.5	−0.2	+0.6	−0.7	−0.2	+0.1
	−0.2	−0.1	+0.5	+0.1	−0.1	0.0	+1.2	+0.2	−0.2
JESRelativePtEC2	0.0	0.0	0.0	0.0	0.0	0.0	0.0	0.0	0.0
	0.0	0.0	0.0	0.0	0.0	0.0	0.0	0.0	0.0
JESRelativePtHF	0.0	0.0	0.0	0.0	0.0	0.0	0.0	0.0	0.0
	0.0	0.0	0.0	0.0	0.0	0.0	0.0	0.0	0.0
JESRelativeStatEC	+0.2	0.0	−2.2	−0.2	0.0	+0.4	−0.5	−0.3	+0.1
	0.0	−0.2	−0.8	+0.1	−0.1	+0.2	+0.3	+0.1	0.0
JESRelativeStatFSR	0.0	0.0	−0.1	0.0	−0.1	−0.4	+0.3	−0.1	+0.2
	+0.1	0.0	+0.5	0.0	0.0	−0.2	−0.4	+0.2	−0.1
JESRelativeStatHF	0.0	0.0	0.0	0.0	0.0	0.0	0.0	0.0	0.0
	0.0	0.0	0.0	0.0	0.0	0.0	0.0	0.0	0.0
JESSinglePionECAL	0.0	+0.1	−0.8	+0.2	−0.3	+0.1	+0.4	0.0	−0.2
	0.0	0.0	−2.4	−0.5	0.0	+0.4	+0.3	0.0	+0.2

Table A.34: Table A.33 continued.

source / bin	1	2	3	4	5	6	7	8	9
JESSinglePionHCAL	−0.1	+0.3	−0.2	+0.4	−0.1	−0.2	+0.7	−0.5	−0.1
	+0.1	−0.3	−0.1	−0.2	−0.2	−0.3	+0.3	+0.1	+0.4
JESTimePtEta	0.0	+0.1	−1.6	−0.1	0.0	0.0	+0.2	−0.2	+0.2
	+0.1	−0.1	−1.4	+0.1	−0.3	+0.4	0.0	0.0	+0.2
$\vec{p}_{\mathrm{T}}^{\,\mathrm{miss}}$	+0.2	−0.6	−1.3	+0.2	+0.1	−0.6	−0.1	−0.2	0.0
	0.0	+0.4	+0.7	−0.3	−0.2	+0.1	−0.2	+0.4	+0.1
lepton ID/ISO	+0.2	−0.7	+0.5	−0.7	+0.6	−0.3	+0.7	0.0	−0.3
	−0.2	+0.7	−0.5	+0.7	−0.7	+0.3	−0.7	+0.1	+0.3
pileup	0.0	−0.2	−0.7	−0.1	+0.1	−0.1	0.0	+0.2	0.0
	0.0	+0.2	+0.7	+0.1	−0.1	+0.1	−0.1	−0.2	0.0
trigger	+0.1	−0.1	+0.2	−0.2	+0.1	0.0	−0.1	−0.2	0.0
	0.0	+0.1	−0.2	+0.2	−0.2	0.0	+0.1	+0.2	0.0
trigger (η)	0.0	0.0	+0.1	−0.2	0.0	0.0	+0.3	0.0	−0.1
	0.0	0.0	−0.1	+0.2	0.0	0.0	−0.3	0.0	+0.1
non-$\mathrm{t\bar{t}}$ background	−1.0	−0.4	+0.9	−0.8	+1.2	+0.5	+0.9	+1.2	+1.1
	+1.1	+0.2	−0.8	+0.7	−1.2	−0.4	−0.9	−1.1	−1.1
b-tagging	0.0	−0.1	+0.2	−0.1	+0.1	0.0	+0.2	+0.1	0.0
	0.0	+0.1	−0.2	+0.1	−0.1	0.0	−0.2	0.0	0.0
b-tagging (light jets)	−0.2	0.0	−0.2	−0.3	+0.3	+0.3	−0.2	+0.2	+0.3
	+0.2	0.0	+0.2	+0.3	−0.3	−0.3	+0.2	−0.2	−0.3
luminosity	0.0	0.0	0.0	0.0	0.0	0.0	0.0	0.0	0.0
	0.0	0.0	0.0	0.0	0.0	0.0	0.0	0.0	0.0
branching ratio $\mathrm{t\bar{t}} \to \ell\ell$	0.0	0.0	0.0	0.0	0.0	0.0	0.0	0.0	0.0
	0.0	0.0	0.0	0.0	0.0	0.0	0.0	0.0	0.0
PDF eigenvector 1	0.0	0.0	+0.1	0.0	0.0	0.0	0.0	0.0	0.0
	0.0	0.0	+0.2	0.0	0.0	0.0	0.0	0.0	0.0
PDF eigenvector 2	−0.1	0.0	+0.2	0.0	−0.1	0.0	+0.3	+0.4	+0.1
	0.0	+0.1	−0.4	+0.2	−0.1	0.0	−0.1	0.0	−0.1
PDF eigenvector 3	0.0	0.0	+0.3	0.0	0.0	0.0	−0.1	−0.1	0.0
	0.0	0.0	−0.1	0.0	0.0	0.0	+0.1	+0.1	0.0
PDF eigenvector 4	0.0	−0.1	+0.3	−0.2	0.0	0.0	+0.1	+0.1	+0.1
	0.0	+0.1	−0.2	+0.2	−0.1	0.0	−0.1	0.0	−0.1
PDF eigenvector 5	0.0	0.0	−0.7	+0.1	0.0	0.0	+0.1	0.0	−0.1
	0.0	0.0	+0.5	0.0	0.0	0.0	−0.1	−0.1	0.0
PDF eigenvector 6	0.0	−0.1	+0.4	−0.2	+0.1	0.0	0.0	−0.1	+0.1
	0.0	+0.1	−0.2	+0.1	−0.1	0.0	0.0	+0.1	−0.1
PDF eigenvector 7	−0.1	0.0	−1.2	+0.2	+0.1	−0.1	+0.2	+0.1	−0.1
	+0.1	0.0	+0.6	−0.1	0.0	+0.1	−0.1	−0.1	+0.1
PDF eigenvector 8	+0.1	−0.2	+0.2	−0.2	+0.2	−0.1	+0.1	−0.1	0.0
	0.0	+0.1	−0.1	+0.1	−0.2	+0.1	−0.1	+0.1	0.0
PDF eigenvector 9	0.0	+0.1	0.0	+0.1	−0.2	0.0	0.0	+0.2	0.0
	0.0	−0.1	+0.1	−0.2	+0.2	0.0	+0.1	−0.2	0.0
PDF eigenvector 10	+0.1	0.0	+0.6	−0.2	0.0	+0.1	−0.1	−0.1	+0.1
	−0.1	0.0	−0.7	+0.2	0.0	0.0	+0.1	+0.1	−0.1
PDF eigenvector 11	0.0	0.0	+0.2	−0.1	0.0	0.0	0.0	0.0	0.0
	0.0	0.0	−0.3	+0.1	0.0	0.0	+0.1	+0.1	0.0
PDF eigenvector 12	0.0	0.0	−0.2	+0.1	0.0	−0.1	+0.1	+0.1	0.0
	0.0	0.0	+0.3	−0.1	0.0	+0.1	−0.1	0.0	0.0
PDF eigenvector 13	+0.1	−0.1	0.0	−0.1	+0.1	0.0	−0.1	−0.3	0.0
	−0.1	+0.1	0.0	+0.1	−0.2	0.0	+0.1	+0.3	0.0
PDF eigenvector 14	0.0	0.0	−0.1	0.0	0.0	0.0	0.0	0.0	0.0
	0.0	0.0	+0.2	0.0	0.0	0.0	−0.1	0.0	0.0

Table A.35: Table A.33 continued.

source / bin	1	2	3	4	5	6	7	8	9
PDF eigenvector 15	0.0	0.0	−0.2	0.0	0.0	0.0	0.0	0.0	0.0
	0.0	0.0	+0.1	0.0	0.0	0.0	0.0	0.0	0.0
PDF eigenvector 16	0.0	0.0	+0.1	−0.1	0.0	0.0	0.0	0.0	0.0
	0.0	0.0	−0.1	+0.1	0.0	0.0	0.0	0.0	0.0
PDF eigenvector 17	0.0	0.0	−0.1	+0.1	−0.1	0.0	0.0	+0.1	0.0
	+0.1	−0.1	+0.3	−0.2	+0.1	0.0	−0.1	−0.2	0.0
PDF eigenvector 18	0.0	+0.1	+0.3	0.0	−0.1	0.0	0.0	+0.2	+0.1
	0.0	−0.1	−0.2	0.0	+0.1	0.0	0.0	−0.2	−0.1
PDF eigenvector 19	0.0	0.0	+0.3	−0.1	0.0	+0.1	−0.1	0.0	+0.1
	0.0	−0.1	−0.5	+0.1	+0.1	−0.1	+0.1	0.0	−0.1
PDF eigenvector 20	0.0	0.0	−0.4	0.0	0.0	+0.1	−0.1	0.0	0.0
	0.0	−0.1	−0.1	0.0	0.0	0.0	+0.1	0.0	0.0
PDF eigenvector 21	0.0	0.0	0.0	0.0	0.0	0.0	+0.1	+0.2	0.0
	0.0	0.0	+0.1	0.0	0.0	0.0	−0.1	−0.2	0.0
PDF eigenvector 22	−0.1	0.0	0.0	−0.1	0.0	0.0	+0.1	+0.3	+0.1
	+0.1	0.0	+0.1	0.0	+0.1	0.0	−0.2	−0.3	−0.1
PDF eigenvector 23	0.0	0.0	−0.5	+0.2	0.0	−0.1	0.0	−0.1	−0.2
	0.0	0.0	−0.1	0.0	0.0	0.0	−0.1	0.0	0.0
PDF eigenvector 24	0.0	0.0	−0.4	+0.1	0.0	0.0	−0.1	0.0	0.0
	−0.1	0.0	−0.3	+0.2	−0.1	−0.1	+0.3	+0.3	−0.1
PDF eigenvector 25	−0.1	0.0	−0.4	+0.2	−0.1	−0.1	+0.2	+0.3	−0.1
	0.0	0.0	−0.7	+0.1	0.0	0.0	0.0	0.0	0.0
PDF eigenvector 26	0.0	0.0	−0.1	0.0	0.0	0.0	0.0	0.0	0.0
	0.0	0.0	−0.2	0.0	0.0	0.0	0.0	0.0	0.0
PDF eigenvector 27	−0.1	+0.3	0.0	+0.2	−0.3	+0.1	−0.2	+0.2	0.0
	0.0	−0.1	+0.1	−0.1	+0.1	0.0	+0.1	−0.1	0.0
PDF eigenvector 28	0.0	+0.1	−0.3	+0.1	−0.1	+0.1	−0.1	0.0	0.0
	0.0	−0.1	+0.3	−0.2	+0.1	0.0	+0.1	−0.1	0.0
α_S	−0.1	+0.3	+0.2	+0.3	−0.2	+0.1	−0.2	+0.1	0.0
	+0.1	−0.3	−0.2	−0.2	+0.2	−0.1	+0.2	−0.1	0.0
m_t^{MC}	−0.5	−2.7	−1.7	+0.5	+0.9	−0.2	+0.4	+1.4	+2.1
	+0.5	+2.5	+3.6	−0.2	−0.8	+0.1	−1.1	−1.2	−2.1
$\mu_{r,f}$	−0.7	+1.7	+10.2	+2.1	−2.2	0.0	−0.4	+1.8	−0.3
	+0.9	−1.8	−14.6	−2.2	+2.3	+0.2	+0.1	−2.0	+0.5
h_{damp}	+0.2	−0.4	−6.7	−0.1	0.0	+0.7	−0.4	+0.7	+0.1
	−0.5	−0.1	+11.3	+0.3	+0.4	−0.8	−0.6	+1.1	−0.3
PS ISR	−0.1	−0.6	+1.1	+0.1	+0.5	+0.1	−0.7	+0.1	+0.1
	0.0	−0.6	+3.8	+0.2	+0.3	−0.5	−1.4	+1.2	−0.1
PS FSR	−0.4	+1.3	+7.4	+1.4	−0.4	−0.8	0.0	0.0	−1.4
	+0.2	−1.2	−0.7	−0.5	+0.5	−0.4	−0.6	+0.3	+1.0
UE tune	+0.1	−0.1	+4.3	+0.4	+0.2	−1.4	−1.8	+0.7	0.0
	−0.2	0.0	+2.7	+0.2	+0.3	−0.1	−0.5	+0.3	−0.2
colour reconnection	−0.2	−0.4	+1.1	+0.2	+0.3	−0.2	+0.9	−0.9	+0.6
	+0.1	−0.3	−0.3	−0.3	+0.2	−0.7	+0.2	+0.6	+0.1
	−0.1	−0.2	−1.4	−0.6	+0.3	−0.1	−0.1	+1.4	0.0
fragmentation b → B	−0.1	+0.7	−0.6	+0.9	−0.7	−0.3	−0.2	−0.1	+0.2
	0.0	−0.3	+0.3	−0.4	+0.3	+0.2	0.0	+0.1	0.0
	0.0	+0.1	−0.1	+0.2	−0.2	0.0	−0.1	0.0	0.0
	+0.2	+0.5	−1.3	+0.3	−0.6	−0.2	−0.5	−0.3	+0.2
branching ratio $B \to \mu$	0.0	0.0	−0.2	+0.1	0.0	+0.1	−0.1	0.0	−0.1
	+0.1	−0.1	+0.2	−0.1	−0.1	−0.1	0.0	0.0	+0.1

Table A.36: The measured $[N_{\text{jet}}^{0,1+}, M(\text{t}\bar{\text{t}}), y(\text{t}\bar{\text{t}})]$ cross sections, along with their relative statistical and systematic uncertainties, and NP corrections (see Section 9).

N_{jet}	$M(\text{t}\bar{\text{t}})$ [GeV]	$\lvert y(\text{t}\bar{\text{t}})\rvert$	$\frac{1}{\sigma(\text{t}\bar{\text{t}})}\frac{\text{d}\sigma}{\text{d}\lvert y(\text{t}\bar{\text{t}})\rvert}$	stat. [%]	syst. [%]	$\mathcal{C}_{\text{NP}}$	bin
0	300–400	0.00–0.35	8.224×10^{-2}	4.6	$^{+12.9}_{-8.5}$	0.973	1
0	300–400	0.35–0.75	8.712×10^{-2}	3.7	$^{+6.9}_{-12.6}$	0.974	2
0	300–400	0.75–1.15	7.671×10^{-2}	4.1	$^{+6.3}_{-14.5}$	0.973	3
0	300–400	1.15–2.50	3.590×10^{-2}	4.0	$^{+8.4}_{-9.4}$	0.975	4
0	400–500	0.00–0.35	1.368×10^{-1}	2.7	$^{+2.4}_{-3.6}$	0.971	5
0	400–500	0.35–0.75	1.234×10^{-1}	2.4	$^{+5.5}_{-2.2}$	0.971	6
0	400–500	0.75–1.15	1.032×10^{-1}	2.9	$^{+5.3}_{-1.4}$	0.972	7
0	400–500	1.15–2.50	4.739×10^{-2}	2.3	$^{+4.8}_{-3.3}$	0.974	8
0	500–1500	0.00–0.35	1.625×10^{-1}	1.8	$^{+3.7}_{-5.5}$	0.976	9
0	500–1500	0.35–0.75	1.422×10^{-1}	2.0	$^{+6.3}_{-3.5}$	0.978	10
0	500–1500	0.75–1.15	1.123×10^{-1}	2.4	$^{+3.7}_{-6.4}$	0.977	11
0	500–1500	1.15–2.50	3.223×10^{-2}	3.5	$^{+7.0}_{-7.0}$	0.982	12
≥ 1	300–400	0.00–0.35	6.493×10^{-2}	5.9	$^{+12.9}_{-4.8}$	1.033	13
≥ 1	300–400	0.35–0.75	6.231×10^{-2}	5.1	$^{+10.6}_{-5.0}$	1.031	14
≥ 1	300–400	0.75–1.15	5.557×10^{-2}	5.5	$^{+8.1}_{-7.4}$	1.035	15
≥ 1	300–400	1.15–2.50	2.482×10^{-2}	5.2	$^{+5.8}_{-14.6}$	1.037	16
≥ 1	400–500	0.00–0.35	1.220×10^{-1}	3.1	$^{+4.4}_{-9.2}$	1.036	17
≥ 1	400–500	0.35–0.75	1.083×10^{-1}	2.7	$^{+4.3}_{-8.5}$	1.034	18
≥ 1	400–500	0.75–1.15	8.512×10^{-2}	3.5	$^{+9.0}_{-5.4}$	1.036	19
≥ 1	400–500	1.15–2.50	3.283×10^{-2}	3.1	$^{+9.0}_{-4.6}$	1.037	20
≥ 1	500–1500	0.00–0.35	1.556×10^{-1}	1.7	$^{+7.6}_{-4.9}$	1.024	21
≥ 1	500–1500	0.35–0.75	1.362×10^{-1}	2.0	$^{+3.7}_{-8.2}$	1.024	22
≥ 1	500–1500	0.75–1.15	9.834×10^{-2}	2.5	$^{+7.3}_{-5.4}$	1.025	23
≥ 1	500–1500	1.15–2.50	2.700×10^{-2}	3.6	$^{+9.7}_{-8.1}$	1.022	24

Table A.37: The correlation matrix of statistical uncertainties for the measured $[N_{\text{jet}}^{0,1+}, M(\text{t}\bar{\text{t}}), y(\text{t}\bar{\text{t}})]$ cross sections. The values are expressed as percentages. For bin indices see Table A.36.

bin	2	3	4	5	6	7	8	9	10	11	12	13	14	15	16	17	18	19	20	21	22	23	24
1	−17	−17	+2	−40	−23	+9	+3	−6	+7	0	−5	−20	−4	+4	−2	+4	+7	+1	−4	+3	−3	−4	0
2		+16	−23	−20	−10	−31	−4	+9	−12	+3	+5	−3	−12	−10	+5	+7	−2	+3	+4	−2	+3	+3	−5
3			−2	+8	−31	−20	−29	+1	+2	−9	+1	+4	−10	−12	−6	+1	+2	0	+3	−3	+2	+3	+1
4				−1	−2	−24	+1	−9	−1	0	−31	−3	+3	−5	−25	−6	0	+2	−13	−5	−9	−4	+10
5					+3	−9	−5	−21	−10	+3	−1	−2	+4	+2	−3	−12	−4	+1	+1	+2	+4	0	−1
6						+22	−13	−10	−6	−15	−1	+5	−5	0	+3	−4	−7	−6	0	+5	−1	+3	0
7							+11	+4	−13	−10	−12	+3	+1	−4	0	+1	−5	−7	−4	+1	+4	0	+1
8								−4	−3	−15	−2	−5	+4	+1	−20	−2	−3	−3	−8	−5	−4	0	−8
9									−25	−4	0	+6	−1	−3	0	−4	+2	+2	0	−22	+2	+4	−2
10										−10	−11	−1	+4	+4	−5	+2	−5	+1	+1	+3	−17	−6	+4
11											−13	−3	+3	+4	+1	+1	0	−4	0	+4	−4	−17	−3
12												0	−4	+2	+9	−2	−1	0	−12	−5	+2	0	−29
13													−16	−13	+3	−50	−26	+12	+4	−3	+9	+1	−4
14														+11	−16	−24	−17	−36	+6	+10	−11	+5	+6
15															−1	+10	−37	−28	−28	+1	+5	−7	+8
16																+3	+5	−26	−23	−4	+3	+7	−29
17																	+6	−8	−2	−22	−10	+4	+1
18																		+23	−7	−12	−8	−16	+2
19																			+14	+5	−14	−12	−10
20																				+2	+2	−13	−13
21																					−31	−1	+3
22																						−16	−6
23																							−21

Table A.38: Sources and values of the relative systematic uncertainties in percent of the measured $[N_{\text{jet}}^{0,1+}, M(\text{t}\bar{\text{t}}), y(\text{t}\bar{\text{t}})]$ cross sections. For bin indices see Table A.36.

source / bin	1	2	3	4	5	6	7	8	9	10	11	12	13	14	15	16	17	18	19	20	21	22	23	24
JER	+0.2	+0.6	+0.4	+0.8	+0.1	+0.7	+0.5	+0.8	+0.1	+0.5	+0.2	+0.9	−0.6	−0.1	+0.1	−0.8	−0.5	−0.6	+0.3	−1.0	−0.6	−0.6	−0.5	−1.8
	−0.4	−1.0	−2.1	−0.8	−0.7	+0.2	−0.2	+0.1	−0.3	−0.4	+0.2	−0.1	+2.1	0.0	+0.7	−0.4	+0.4	−0.2	+0.5	+1.2	+0.6	+0.6	+0.1	+0.4
JESAbsoluteMPFBias	+0.8	+0.4	−0.1	+0.7	−0.1	+0.4	+0.4	+0.4	+0.3	0.0	+0.2	−0.5	+1.2	+0.7	+0.3	−0.2	−0.4	−0.6	−0.6	−0.2	−0.5	−0.4	−0.3	−1.0
	−0.8	−0.9	−1.5	−0.3	−0.1	+0.1	+0.1	+0.1	−0.1	+0.2	0.0	0.0	−0.3	−0.8	+0.2	−0.8	+0.5	+0.3	+0.5	+0.4	+0.5	+0.2	+0.4	+0.7
JESAbsoluteScale	+0.6	0.0	0.0	+0.6	−0.1	+0.4	+0.3	+0.3	+0.1	−0.1	+0.2	0.0	+0.5	+0.7	0.0	+0.1	−0.2	−0.4	−0.5	+0.2	−0.3	−0.4	−0.3	−1.3
	−0.7	−0.7	−1.1	−0.4	−0.1	0.0	+0.3	+0.2	−0.1	+0.1	+0.2	+0.1	−0.3	−0.4	+0.2	0.0	+0.4	+0.3	−0.1	+0.2	+0.3	+0.3	0.0	+0.3
JESAbsoluteStat	+0.4	+1.0	−1.1	−0.3	−0.4	0.0	−0.2	+0.5	+0.2	+0.2	+0.7	+0.5	+0.6	+1.0	+0.1	+0.6	−0.7	−0.6	−0.7	−0.6	+0.1	+0.3	0.0	−1.4
	−1.2	−0.4	−0.3	−0.3	+0.4	+0.1	+0.4	+0.3	−0.4	−0.3	−0.5	+0.6	+0.5	−0.6	−0.1	+1.4	0.0	+0.3	+0.3	+0.3	−0.2	+0.2	−0.2	−0.7
JESFlavourQCD	+3.0	+2.9	+1.4	+2.0	0.0	+0.9	+0.3	+1.1	+1.2	+1.3	+1.1	+1.0	+1.9	0.0	−0.8	−2.5	−2.7	−2.4	−1.3	−1.3	−1.6	−1.4	−1.6	−2.3
	−3.3	−3.7	−3.4	−2.1	−0.2	−0.4	−0.1	−0.6	−1.4	−0.8	−0.9	−0.6	−0.2	+0.8	+0.5	+0.5	+1.9	+1.9	+2.4	+2.7	+1.8	+1.4	+1.4	+1.5
JESFragmentation	+0.2	−0.2	−0.1	+0.4	+0.2	+0.5	+0.6	+0.5	+0.3	+0.3	−0.2	−0.4	+0.4	+0.4	+0.1	−0.7	−0.5	−0.6	−0.6	−0.2	−0.2	−0.1	+0.2	−0.7
	−0.4	−0.6	−1.2	−0.1	−0.1	0.0	0.0	+0.2	−0.2	−0.2	−0.2	−0.2	+0.2	+0.2	+0.7	+0.1	+0.4	+0.3	−0.1	+0.8	+0.2	+0.1	0.0	+0.2
JESPileUpDataMC	+0.6	+0.1	−0.5	0.0	0.0	+0.5	+0.5	+0.8	+0.3	+0.4	+0.3	+0.6	0.0	−0.2	−0.1	−0.4	−0.5	−0.6	−0.3	−0.6	−0.2	−0.3	+0.1	−1.2
	−0.6	−1.0	−1.1	−0.5	0.0	+0.1	+0.2	−0.1	−0.3	−0.4	−0.2	−0.5	+0.4	+0.7	+0.9	0.0	+0.6	+0.4	0.0	+0.8	+0.2	+0.4	0.0	+0.4
JESPileUpPtBB	+0.1	−0.3	−0.5	+0.2	−0.2	+0.5	+0.6	+0.4	+0.5	+0.2	+0.5	+0.4	−0.7	−0.7	−0.2	−1.0	−0.2	−0.4	−0.5	0.0	−0.1	0.0	−0.2	0.0
	−0.2	−0.5	−0.5	−0.2	0.0	−0.1	−0.3	0.0	−0.4	−0.2	−0.2	−0.1	+0.5	+1.7	+1.9	0.0	+0.2	+0.2	−0.1	+0.3	0.0	0.0	−0.2	0.0
JESPileUpPtEC1	+1.1	+1.5	−0.1	+0.2	+0.2	+0.5	+0.4	+0.4	+0.6	+0.9	+0.7	+0.4	+0.4	+0.5	−0.2	−2.4	−0.4	−0.8	−0.8	−1.0	−0.5	−0.5	−0.3	−1.3
	−0.9	−1.2	−1.3	−0.2	−0.7	−0.4	−0.1	+0.3	−0.6	−0.7	−0.7	−0.4	−0.1	−0.3	+0.9	+1.8	+0.4	+0.3	+0.9	+1.3	+0.5	+0.5	+0.5	+0.5
JESPileUpPtEC2	0.0	0.0	0.0	0.0	0.0	0.0	0.0	0.0	0.0	0.0	0.0	0.0	0.0	0.0	0.0	0.0	0.0	0.0	0.0	0.0	0.0	0.0	0.0	0.0
	0.0	0.0	0.0	0.0	0.0	0.0	0.0	0.0	0.0	0.0	0.0	0.0	0.0	0.0	0.0	0.0	0.0	0.0	0.0	0.0	0.0	0.0	0.0	0.0
JESPileUpPtHF	0.0	0.0	0.0	0.0	0.0	0.0	0.0	0.0	0.0	0.0	0.0	0.0	0.0	0.0	0.0	0.0	0.0	0.0	0.0	0.0	0.0	0.0	0.0	0.0
	0.0	0.0	0.0	0.0	0.0	0.0	0.0	0.0	0.0	0.0	0.0	0.0	0.0	0.0	0.0	0.0	0.0	0.0	0.0	0.0	0.0	0.0	0.0	0.0
JESPileUpPtRef	+0.2	0.0	−0.4	+0.4	+0.3	+0.7	+0.2	+0.6	+0.6	+0.7	+0.1	+0.2	−0.2	−0.7	−0.8	−1.0	−0.7	−0.5	−0.1	−0.6	−0.1	−0.2	+0.1	−0.8
	−0.2	−1.0	−1.1	0.0	−0.3	+0.2	0.0	−0.3	−0.6	−0.5	−1.0	−0.4	+0.6	+0.8	+0.9	+1.6	+0.7	+0.4	+0.3	+0.5	+0.3	+0.1	+0.3	0.0
JESRelativeBal	+2.0	+2.4	+1.7	+2.0	0.0	+0.5	−0.1	+0.2	+0.6	+0.6	+0.4	−1.0	+1.5	+0.5	+0.6	−2.2	−1.0	−1.3	−0.8	−0.8	−0.9	−1.0	−1.2	−1.1
	−2.8	−2.9	−2.9	−1.8	−0.2	−0.3	+0.1	+0.7	−0.8	−0.6	−0.2	+1.2	−0.2	+0.4	0.0	−0.3	+0.5	+0.5	+1.2	+1.5	+1.1	+1.0	+1.4	+1.3
JESRelativeFSR	−0.6	−0.9	−0.8	−0.3	+0.2	+0.1	+0.2	+0.1	−0.2	−0.2	−0.2	0.0	−0.2	−0.5	−0.1	+0.3	+0.4	+0.4	+0.2	+0.3	+0.3	+0.3	+0.2	0.0
	+0.2	+0.6	+0.3	+0.1	+0.1	+0.3	+0.2	+0.3	0.0	0.0	+0.4	+0.2	+0.6	+0.8	0.0	+0.3	−0.7	−0.6	−0.6	+0.1	−0.2	−0.3	−0.5	−1.2
JESRelativeJEREC1	0.0	0.0	−0.2	+0.2	+0.1	0.0	+0.1	+0.2	0.0	0.0	+0.4	−0.2	+0.1	0.0	+0.3	−0.4	−0.1	0.0	−0.2	0.0	0.0	0.0	−0.4	+0.2
	0.0	0.0	−0.7	+0.2	0.0	0.0	0.0	+0.4	0.0	−0.2	−0.2	−0.3	+0.1	0.0	+0.3	−0.6	−0.1	0.0	−0.2	+0.1	0.0	+0.1	−0.1	+0.8
JESRelativeJEREC2	0.0	0.0	0.0	0.0	0.0	0.0	0.0	0.0	0.0	0.0	0.0	0.0	0.0	0.0	0.0	0.0	0.0	0.0	0.0	0.0	0.0	0.0	0.0	0.0
	0.0	0.0	0.0	0.0	0.0	0.0	0.0	0.0	0.0	0.0	0.0	0.0	0.0	0.0	0.0	0.0	0.0	0.0	0.0	0.0	0.0	0.0	0.0	0.0
JESRelativeJERHF	0.0	0.0	0.0	0.0	0.0	0.0	0.0	0.0	0.0	0.0	0.0	0.0	0.0	0.0	0.0	0.0	0.0	0.0	0.0	0.0	0.0	0.0	0.0	0.0
	0.0	0.0	0.0	0.0	0.0	0.0	0.0	0.0	0.0	0.0	0.0	0.0	0.0	0.0	0.0	0.0	0.0	0.0	0.0	0.0	0.0	0.0	0.0	0.0
JESRelativePtBB	+0.3	+0.3	+0.1	+0.2	−0.2	−0.1	+0.3	+0.2	+0.1	+0.1	+0.1	0.0	+0.5	+0.1	+0.3	−0.3	−0.5	−0.2	−0.5	−0.1	−0.2	−0.2	−0.3	+0.1
	−0.4	−1.6	−0.8	+0.3	+0.3	+0.5	+0.5	−0.1	−0.1	−0.1	0.0	0.0	−0.5	+0.8	+0.3	−0.9	+0.5	0.0	−0.1	+0.1	+0.2	+0.1	+0.1	+0.1
JESRelativePtEC1	0.0	+1.2	+0.3	+0.5	+0.3	+0.4	+0.1	+0.2	+0.3	+0.3	+0.2	0.0	+0.3	+0.5	+0.2	−1.0	+0.2	−0.4	−0.4	−0.5	−0.4	−0.2	−0.3	−2.0
	−0.6	−0.8	−1.1	−0.5	−0.4	−0.5	+0.1	+0.7	−0.3	−0.4	−0.1	+0.7	+0.1	−0.7	−0.8	+0.5	−0.1	+0.2	+0.5	+0.7	+0.3	+0.5	+0.4	+0.6
JESRelativePtEC2	0.0	0.0	0.0	0.0	0.0	0.0	0.0	0.0	0.0	0.0	0.0	0.0	0.0	0.0	0.0	0.0	0.0	0.0	0.0	0.0	0.0	0.0	0.0	0.0
	0.0	0.0	0.0	0.0	0.0	0.0	0.0	0.0	0.0	0.0	0.0	0.0	0.0	0.0	0.0	0.0	0.0	0.0	0.0	0.0	0.0	0.0	0.0	0.0
JESRelativePtHF	0.0	0.0	0.0	0.0	0.0	0.0	0.0	0.0	0.0	0.0	0.0	0.0	0.0	0.0	0.0	0.0	0.0	0.0	0.0	0.0	0.0	0.0	0.0	0.0
	0.0	0.0	0.0	0.0	0.0	0.0	0.0	0.0	0.0	0.0	0.0	0.0	0.0	0.0	0.0	0.0	0.0	0.0	0.0	0.0	0.0	0.0	0.0	0.0
JESRelativeStatEC	0.0	+0.3	0.0	+0.2	+0.1	+0.3	+0.4	+0.3	+0.2	−0.1	+0.3	−0.4	0.0	+0.2	+0.3	+0.3	0.0	−0.1	−0.6	−0.5	−0.1	0.0	−0.2	−1.0
	−0.2	−0.4	−1.0	+0.1	0.0	−0.1	+0.1	+0.4	−0.1	−0.1	+0.1	+0.2	+0.2	+0.1	+0.3	−0.8	−0.2	0.0	−0.1	+0.5	0.0	+0.1	0.0	+0.3
JESRelativeStatFSR	0.0	+0.1	−0.3	+0.1	−0.2	+0.1	+0.3	+0.3	+0.2	−0.1	+0.3	−0.1	+0.1	−0.2	+0.2	−0.2	+0.2	0.0	−0.3	0.0	−0.3	+0.1	−0.4	+0.1
	0.0	0.0	−0.8	0.0	−0.2	+0.1	0.0	+0.3	0.0	0.0	+0.1	+0.2	−0.2	−0.2	+0.1	−0.4	+0.2	0.0	−0.1	0.0	0.0	+0.1	−0.3	+0.4
JESRelativeStatHF	0.0	0.0	0.0	0.0	0.0	0.0	0.0	0.0	0.0	0.0	0.0	0.0	0.0	0.0	0.0	0.0	0.0	0.0	0.0	0.0	0.0	0.0	0.0	0.0
	0.0	0.0	0.0	0.0	0.0	0.0	0.0	0.0	0.0	0.0	0.0	0.0	0.0	0.0	0.0	0.0	0.0	0.0	0.0	0.0	0.0	0.0	0.0	0.0
JESSinglePionECAL	−0.7	−1.1	−0.8	0.0	+0.1	+0.2	0.0	0.0	−0.2	−0.4	−0.3	−0.2	+0.5	+0.3	+0.7	+0.2	+0.3	+0.3	+0.4	+0.2	+0.1	+0.4	+0.2	+0.3
	+0.3	0.0	−0.1	+0.3	0.0	+0.6	+0.5	+0.7	+0.6	+0.2	−0.2	−0.2	+0.3	+0.3	−0.4	−0.8	−0.5	−0.7	−0.6	+0.1	−0.4	−0.3	+0.1	−0.8

Table A.39: Table A.38 continued.

source / bin	1	2	3	4	5	6	7	8	9	10	11	12	13	14	15	16	17	18	19	20	21	22	23	24
JESSinglePionHCAL	−0.3	−0.9	−0.6	−0.1	−0.4	+0.1	+0.2	−0.1	−0.3	−0.2	−0.6	+0.2	+0.2	−0.3	+0.1	+0.2	+0.6	+0.5	+0.5	+0.2	+0.2	+0.2	+0.2	0.0
	+0.3	−0.1	−0.5	+0.5	+0.2	+0.6	+0.5	+0.6	+0.5	+0.1	−0.1	−0.3	+0.3	+0.7	+0.2	−0.7	−0.6	−0.6	−0.6	−0.1	−0.3	−0.1	+0.1	−0.8
JESTimePtEta	−0.1	−0.1	−0.4	−0.1	−0.2	−0.1	+0.3	0.0	+0.3	−0.1	+0.1	0.0	0.0	−0.1	0.0	+0.3	+0.2	+0.1	−0.4	0.0	−0.3	0.0	−0.1	+0.3
	−0.2	+0.2	0.0	+0.1	0.0	+0.3	0.0	−0.1	+0.1	−0.2	+0.1	+0.4	+0.4	+0.1	+0.1	+0.2	0.0	−0.1	0.0	0.0	−0.1	+0.1	−0.1	−1.6
$\vec{p}_{\mathrm{T}}^{\,\mathrm{miss}}$	−2.4	−0.3	−1.1	−0.2	+0.3	+0.3	−0.3	−0.2	+0.1	+0.1	+0.6	+0.3	+1.2	+0.3	+0.2	+0.5	−0.4	0.0	+0.1	0.0	+0.3	+0.1	+0.2	−0.1
	−0.1	−0.2	+0.8	+0.4	−0.1	−0.3	+0.2	+0.8	−0.1	+0.1	−0.5	−0.6	−0.4	+0.5	−0.4	+0.8	−0.1	+0.1	0.0	−0.2	−0.2	−0.3	−0.2	+0.1
lepton ID/ISO	−0.3	0.0	−0.5	−0.3	+0.1	+0.2	+0.1	+0.6	−0.1	−0.1	−0.1	−0.7	0.0	+0.1	0.0	+0.1	+0.3	+0.4	+0.3	+0.6	−0.1	−0.1	−0.2	−0.7
	+0.3	0.0	+0.5	+0.3	−0.1	−0.2	−0.1	−0.6	+0.1	+0.1	+0.1	+0.7	0.0	−0.1	0.0	−0.1	−0.3	−0.4	−0.3	−0.6	+0.2	+0.1	+0.2	+0.7
pileup	+0.6	−0.4	−0.5	−0.5	0.0	+0.2	+0.4	+0.2	+0.3	+0.4	+0.2	+0.2	−0.4	+0.6	−0.1	−1.0	+0.4	−0.3	−0.5	0.0	0.0	−0.4	+0.1	−0.3
	−0.7	+0.3	+0.6	+0.5	0.0	−0.2	−0.4	−0.3	−0.3	−0.3	−0.2	−0.2	+0.4	−0.5	+0.2	+1.1	−0.5	+0.2	+0.4	0.0	0.0	+0.3	−0.1	+0.3
trigger	+0.1	+0.2	+0.1	−0.4	+0.2	+0.1	0.0	−0.1	+0.1	0.0	−0.1	−0.3	+0.1	+0.2	+0.2	−0.3	+0.2	+0.2	+0.1	−0.2	+0.1	0.0	−0.1	−0.2
	−0.1	−0.2	−0.1	+0.4	−0.2	−0.1	0.0	+0.1	−0.1	0.0	+0.1	+0.3	−0.1	−0.2	−0.2	+0.3	−0.2	−0.2	−0.1	+0.2	−0.1	0.0	+0.1	+0.2
trigger (η)	−0.3	−0.2	−0.3	+0.7	−0.3	−0.2	−0.2	+0.4	0.0	−0.1	−0.2	+0.3	−0.2	−0.1	−0.3	+0.8	−0.3	−0.2	−0.2	+0.5	0.0	−0.1	−0.3	+0.2
	+0.3	+0.2	+0.3	−0.7	+0.3	+0.2	+0.2	−0.4	0.0	+0.1	+0.2	−0.3	+0.2	+0.1	+0.3	−0.8	+0.3	+0.2	+0.2	−0.5	0.0	+0.1	+0.3	−0.2
non-$t\bar{t}$ background	−1.0	−1.0	−2.0	−4.3	−0.3	−0.1	+0.3	−0.3	+0.5	+0.4	+0.5	−0.2	+1.6	+1.8	+1.7	−1.2	+0.4	+0.6	+0.5	+0.8	+1.0	+0.8	+0.8	−0.1
	+1.5	−0.1	+2.0	+4.1	+0.2	+0.6	+0.2	−0.2	−0.5	−0.1	−1.0	+0.7	−1.0	−1.2	−1.3	+1.1	−0.9	−0.8	−0.6	−0.5	−0.8	−0.7	−0.8	0.0
b-tagging	0.0	0.0	−0.1	−0.1	−0.1	−0.1	−0.1	0.0	−0.1	−0.1	−0.1	−0.1	−0.5	−0.5	−0.6	−0.2	+0.2	+0.2	+0.2	+0.2	+0.3	+0.2	+0.3	+0.3
	0.0	0.0	+0.1	+0.1	+0.1	+0.1	+0.1	0.0	+0.1	+0.1	+0.1	+0.1	+0.5	+0.5	+0.6	+0.2	−0.2	−0.2	−0.2	−0.2	−0.3	−0.2	−0.3	−0.3
b-tagging (light jets)	−0.3	−0.3	−0.6	−1.0	+0.1	+0.2	+0.4	+0.2	+0.2	+0.2	+0.2	+0.1	+0.5	+0.6	+0.3	−1.0	+0.1	+0.1	+0.2	+0.1	0.0	0.0	−0.1	−0.2
	+0.3	+0.3	+0.6	+1.0	−0.1	−0.2	−0.4	−0.2	−0.2	−0.2	−0.2	−0.1	−0.5	−0.5	−0.2	+1.0	−0.1	−0.1	−0.2	−0.1	0.0	0.0	+0.1	+0.2
luminosity	0.0	0.0	0.0	0.0	0.0	0.0	0.0	0.0	0.0	0.0	0.0	0.0	0.0	0.0	0.0	0.0	0.0	0.0	0.0	0.0	0.0	0.0	0.0	0.0
	0.0	0.0	0.0	0.0	0.0	0.0	0.0	0.0	0.0	0.0	0.0	0.0	0.0	0.0	0.0	0.0	0.0	0.0	0.0	0.0	0.0	0.0	0.0	0.0
branching ratio $t\bar{t} \to \ell\ell$	0.0	0.0	0.0	0.0	0.0	0.0	0.0	0.0	0.0	0.0	0.0	0.0	0.0	0.0	0.0	0.0	0.0	0.0	0.0	0.0	0.0	0.0	0.0	0.0
	0.0	0.0	0.0	0.0	0.0	0.0	0.0	0.0	0.0	0.0	0.0	0.0	0.0	0.0	0.0	0.0	0.0	0.0	0.0	0.0	0.0	0.0	0.0	0.0
PDF eigenvector 1	0.0	0.0	0.0	0.0	0.0	0.0	0.0	0.0	0.0	0.0	0.0	0.0	0.0	0.0	0.0	0.0	0.0	0.0	0.0	0.0	0.0	0.0	0.0	0.0
	0.0	0.0	0.0	0.0	0.0	0.0	0.0	−0.1	0.0	0.0	0.0	0.0	0.0	+0.1	0.0	0.0	0.0	0.0	−0.1	−0.1	0.0	0.0	+0.1	0.0
PDF eigenvector 2	0.0	−0.1	+0.1	+0.1	−0.3	−0.1	0.0	0.0	+0.2	+0.1	0.0	−0.1	+0.1	0.0	+0.1	+0.1	−0.4	−0.2	+0.1	0.0	+0.3	+0.1	0.0	−0.1
	0.0	0.0	0.0	0.0	+0.1	0.0	+0.1	+0.1	−0.1	−0.1	0.0	+0.1	−0.1	−0.1	0.0	0.0	+0.2	+0.1	+0.1	+0.1	−0.2	−0.1	−0.1	0.0
PDF eigenvector 3	+0.1	+0.1	0.0	−0.1	+0.1	0.0	−0.1	−0.2	0.0	0.0	+0.1	−0.2	+0.1	+0.1	+0.1	−0.1	+0.1	0.0	−0.1	−0.2	+0.1	+0.1	+0.1	+0.1
	0.0	0.0	0.0	0.0	0.0	0.0	0.0	+0.1	0.0	0.0	0.0	+0.2	0.0	−0.1	0.0	0.0	0.0	0.0	+0.1	+0.1	0.0	0.0	−0.1	0.0
PDF eigenvector 4	0.0	0.0	0.0	+0.1	−0.2	−0.1	0.0	0.0	+0.1	+0.1	0.0	0.0	+0.1	0.0	0.0	+0.1	−0.3	−0.1	0.0	+0.1	+0.2	+0.1	0.0	−0.1
	0.0	0.0	0.0	0.0	+0.1	0.0	0.0	0.0	0.0	0.0	0.0	0.0	0.0	0.0	0.0	0.0	+0.1	0.0	0.0	0.0	−0.1	−0.1	0.0	0.0
PDF eigenvector 5	−0.1	−0.3	−0.1	+0.1	+0.1	+0.1	+0.2	+0.2	−0.2	−0.1	−0.3	+0.5	−0.1	−0.2	−0.1	+0.1	+0.1	+0.1	+0.3	+0.4	−0.3	−0.2	−0.3	−0.1
	+0.1	+0.2	+0.1	−0.1	+0.1	+0.1	−0.1	−0.3	+0.1	+0.1	+0.1	−0.4	+0.1	+0.3	+0.1	−0.1	+0.1	0.0	−0.3	−0.5	+0.2	+0.2	+0.2	+0.1
PDF eigenvector 6	0.0	0.0	0.0	0.0	−0.1	0.0	−0.1	0.0	0.0	+0.1	+0.1	0.0	+0.1	+0.1	0.0	0.0	−0.2	−0.1	−0.1	0.0	+0.1	+0.1	+0.1	0.0
	0.0	0.0	0.0	0.0	0.0	0.0	0.0	0.0	0.0	−0.1	0.0	0.0	0.0	−0.1	0.0	0.0	+0.1	0.0	+0.1	0.0	−0.1	−0.1	0.0	0.0
PDF eigenvector 7	−0.2	−0.2	0.0	+0.1	+0.1	+0.1	+0.3	+0.5	−0.3	−0.3	−0.2	+0.5	−0.3	−0.4	−0.1	+0.2	+0.3	+0.3	+0.5	+0.5	−0.5	−0.4	−0.5	−0.2
	+0.1	+0.1	0.0	−0.1	0.0	0.0	−0.2	−0.3	+0.1	+0.2	+0.1	−0.3	+0.2	+0.3	+0.1	−0.1	−0.1	−0.1	−0.3	−0.3	+0.3	+0.2	+0.3	+0.1
PDF eigenvector 8	−0.1	0.0	−0.1	0.0	0.0	+0.1	0.0	+0.1	−0.1	0.0	−0.1	+0.1	0.0	0.0	0.0	0.0	0.0	+0.1	0.0	+0.1	−0.1	0.0	−0.1	0.0
	+0.1	0.0	+0.1	0.0	0.0	−0.1	0.0	−0.1	+0.1	0.0	+0.1	0.0	0.0	0.0	0.0	0.0	0.0	−0.1	0.0	−0.1	+0.1	0.0	0.0	0.0
PDF eigenvector 9	0.0	0.0	+0.1	+0.1	0.0	0.0	0.0	0.0	0.0	0.0	0.0	−0.2	+0.1	0.0	0.0	+0.1	0.0	0.0	+0.1	0.0	0.0	0.0	0.0	−0.1
	0.0	0.0	−0.1	−0.1	0.0	0.0	0.0	0.0	0.0	0.0	0.0	+0.2	−0.1	0.0	0.0	−0.1	0.0	0.0	−0.1	0.0	0.0	0.0	0.0	+0.1
PDF eigenvector 10	+0.1	+0.1	0.0	−0.1	−0.1	0.0	−0.1	−0.2	+0.1	+0.1	+0.1	−0.2	+0.2	+0.2	0.0	−0.1	−0.2	−0.1	−0.3	−0.3	+0.2	+0.2	+0.2	+0.1
	−0.1	−0.1	0.0	+0.1	+0.1	0.0	+0.1	+0.3	−0.1	−0.1	−0.1	+0.2	−0.2	−0.2	0.0	+0.1	+0.2	+0.1	+0.3	+0.3	−0.2	−0.2	−0.3	−0.1
PDF eigenvector 11	0.0	0.0	0.0	0.0	0.0	0.0	0.0	−0.1	0.0	0.0	0.0	−0.1	0.0	+0.1	0.0	0.0	0.0	0.0	−0.1	−0.1	0.0	+0.1	+0.1	0.0
	0.0	−0.1	0.0	0.0	0.0	0.0	0.0	+0.1	−0.1	−0.1	0.0	+0.2	−0.1	−0.1	0.0	0.0	+0.1	0.0	+0.1	+0.1	−0.1	−0.1	−0.1	0.0
PDF eigenvector 12	−0.1	−0.1	0.0	0.0	0.0	0.0	+0.1	+0.2	−0.1	−0.1	−0.1	+0.1	−0.1	−0.1	0.0	0.0	+0.1	+0.1	+0.1	+0.2	−0.1	−0.1	−0.1	0.0
	+0.1	+0.1	0.0	0.0	0.0	0.0	−0.1	−0.1	+0.1	+0.1	+0.1	−0.1	+0.1	+0.1	0.0	0.0	−0.1	−0.1	−0.1	−0.2	+0.1	+0.1	+0.1	0.0
PDF eigenvector 13	0.0	+0.1	0.0	−0.1	+0.1	+0.1	0.0	0.0	−0.1	0.0	0.0	0.0	0.0	0.0	0.0	−0.1	+0.2	+0.1	0.0	−0.1	−0.1	−0.1	0.0	0.0
	0.0	0.0	0.0	+0.1	−0.1	−0.1	0.0	0.0	+0.1	0.0	0.0	0.0	0.0	0.0	0.0	+0.1	−0.2	−0.1	0.0	+0.1	+0.1	0.0	0.0	0.0
PDF eigenvector 14	0.0	0.0	0.0	0.0	0.0	0.0	0.0	+0.1	0.0	0.0	0.0	0.0	−0.1	0.0	0.0	0.0	+0.1	+0.1	+0.1	+0.1	−0.1	−0.1	−0.1	0.0
	0.0	0.0	0.0	0.0	0.0	0.0	0.0	−0.1	0.0	0.0	0.0	−0.1	+0.1	+0.1	0.0	0.0	−0.1	−0.1	−0.1	−0.1	+0.1	+0.1	+0.1	0.0

Table A.40: Table A.38 continued.

source / bin	1	2	3	4	5	6	7	8	9	10	11	12	13	14	15	16	17	18	19	20	21	22	23	24
PDF eigenvector 15	0.0	0.0	0.0	0.0	+0.1	+0.1	0.0	+0.1	0.0	0.0	0.0	0.0	−0.1	−0.1	0.0	0.0	+0.1	+0.1	+0.1	+0.1	−0.1	−0.1	−0.1	0.0
	0.0	0.0	0.0	0.0	0.0	0.0	0.0	0.0	0.0	0.0	0.0	0.0	0.0	0.0	0.0	0.0	0.0	0.0	0.0	0.0	0.0	0.0	0.0	0.0
PDF eigenvector 16	0.0	0.0	0.0	0.0	0.0	0.0	0.0	0.0	0.0	0.0	0.0	0.0	0.0	0.0	0.0	0.0	0.0	0.0	0.0	0.0	0.0	0.0	0.0	0.0
	+0.1	−0.2	0.0	+0.1	0.0	+0.1	+0.1	0.0	0.0	0.0	−0.1	+0.1	+0.1	0.0	0.0	0.0	−0.1	0.0	0.0	+0.1	0.0	0.0	0.0	0.0
PDF eigenvector 17	0.0	0.0	0.0	0.0	0.0	0.0	0.0	0.0	0.0	0.0	0.0	0.0	0.0	−0.1	0.0	0.0	0.0	0.0	+0.1	0.0	0.0	0.0	0.0	0.0
	0.0	0.0	0.0	−0.1	0.0	0.0	−0.1	−0.1	0.0	0.0	0.0	0.0	+0.1	+0.1	0.0	−0.1	0.0	0.0	−0.1	−0.1	0.0	+0.1	+0.1	+0.1
PDF eigenvector 18	+0.1	0.0	0.0	0.0	−0.2	−0.1	−0.1	−0.1	+0.1	+0.1	+0.1	0.0	+0.1	+0.1	0.0	+0.1	−0.3	−0.2	−0.1	0.0	+0.2	+0.2	+0.2	0.0
	−0.1	0.0	0.0	0.0	+0.2	+0.1	+0.1	+0.1	−0.1	−0.1	−0.1	0.0	−0.1	0.0	0.0	−0.1	+0.3	+0.2	+0.1	0.0	−0.2	−0.1	−0.2	0.0
PDF eigenvector 19	+0.1	+0.1	0.0	0.0	−0.1	−0.1	−0.1	−0.2	+0.1	+0.1	+0.1	−0.2	+0.1	+0.1	0.0	0.0	−0.1	−0.1	−0.2	−0.2	+0.2	+0.2	+0.2	0.0
	−0.1	−0.1	0.0	0.0	+0.1	+0.1	+0.1	+0.3	−0.2	−0.2	−0.1	+0.3	−0.2	−0.2	0.0	0.0	+0.2	+0.2	+0.3	+0.3	−0.3	−0.3	−0.3	−0.1
PDF eigenvector 20	0.0	0.0	0.0	0.0	0.0	0.0	0.0	−0.1	0.0	0.0	+0.1	0.0	0.0	0.0	−0.1	0.0	0.0	0.0	0.0	0.0	+0.1	0.0	+0.1	−0.2
	0.0	0.0	0.0	0.0	0.0	0.0	0.0	+0.1	0.0	−0.1	−0.1	0.0	−0.1	0.0	0.0	0.0	+0.1	+0.1	+0.1	+0.1	−0.1	−0.1	−0.1	0.0
PDF eigenvector 21	0.0	−0.1	0.0	0.0	−0.1	−0.1	0.0	+0.1	0.0	0.0	0.0	+0.2	0.0	−0.1	0.0	+0.1	−0.2	−0.1	0.0	+0.1	+0.1	0.0	0.0	0.0
	0.0	+0.1	0.0	−0.1	+0.1	+0.1	0.0	−0.1	0.0	0.0	0.0	−0.1	0.0	+0.1	0.0	−0.1	+0.2	+0.1	−0.1	−0.2	0.0	0.0	0.0	0.0
PDF eigenvector 22	0.0	−0.1	−0.1	+0.1	−0.3	−0.2	0.0	+0.2	0.0	0.0	0.0	+0.3	+0.1	−0.1	−0.1	+0.2	−0.4	−0.3	+0.1	+0.3	+0.1	+0.1	0.0	−0.1
	0.0	+0.1	0.0	−0.1	+0.3	+0.2	0.0	−0.2	0.0	0.0	0.0	−0.2	0.0	+0.1	0.0	−0.1	+0.3	+0.2	−0.1	−0.3	−0.1	0.0	+0.1	+0.1
PDF eigenvector 23	−0.1	0.0	+0.1	−0.1	+0.3	+0.2	+0.1	0.0	−0.1	−0.1	−0.1	−0.2	−0.2	−0.1	+0.1	−0.1	+0.5	+0.3	+0.2	−0.1	−0.2	−0.2	−0.2	−0.1
	0.0	0.0	0.0	0.0	0.0	0.0	0.0	0.0	0.0	0.0	0.0	+0.2	0.0	0.0	−0.1	0.0	0.0	−0.1	0.0	+0.1	0.0	0.0	0.0	0.0
PDF eigenvector 24	0.0	0.0	0.0	0.0	+0.1	0.0	0.0	+0.1	−0.1	−0.1	0.0	+0.2	−0.1	−0.1	−0.1	0.0	+0.1	0.0	+0.1	+0.1	−0.2	−0.1	−0.1	0.0
	−0.1	−0.1	+0.1	+0.1	−0.1	0.0	+0.1	+0.1	+0.1	0.0	−0.1	−0.1	−0.1	−0.2	+0.1	+0.1	0.0	+0.1	+0.2	+0.1	0.0	−0.1	−0.2	−0.2
PDF eigenvector 25	−0.1	−0.1	+0.1	+0.1	0.0	0.0	+0.1	+0.1	0.0	0.0	−0.1	−0.1	−0.2	−0.2	+0.1	0.0	+0.1	+0.1	+0.2	0.0	0.0	−0.1	−0.2	−0.1
	−0.1	−0.1	−0.1	0.0	+0.1	0.0	+0.1	+0.2	−0.2	−0.2	−0.1	+0.4	−0.2	−0.2	−0.1	+0.1	+0.2	+0.1	+0.2	+0.3	−0.3	−0.2	−0.2	0.0
PDF eigenvector 26	0.0	0.0	0.0	0.0	0.0	0.0	0.0	0.0	0.0	0.0	0.0	0.0	0.0	0.0	0.0	0.0	+0.1	0.0	0.0	0.0	0.0	0.0	0.0	0.0
	0.0	0.0	0.0	0.0	0.0	0.0	0.0	0.0	0.0	0.0	0.0	+0.1	0.0	0.0	0.0	0.0	0.0	0.0	0.0	0.0	0.0	0.0	0.0	0.0
PDF eigenvector 27	+0.1	0.0	+0.2	+0.1	−0.1	−0.1	+0.1	−0.2	+0.1	+0.1	0.0	−0.3	+0.1	0.0	+0.1	+0.1	−0.1	−0.1	0.0	−0.2	+0.2	+0.1	+0.1	−0.1
	0.0	0.0	0.0	0.0	0.0	0.0	0.0	0.0	0.0	0.0	0.0	+0.1	0.0	0.0	0.0	0.0	0.0	0.0	0.0	0.0	0.0	0.0	0.0	0.0
PDF eigenvector 28	0.0	0.0	0.0	0.0	0.0	0.0	0.0	0.0	0.0	0.0	0.0	0.0	0.0	0.0	0.0	0.0	+0.1	0.0	0.0	0.0	0.0	0.0	0.0	0.0
	0.0	0.0	−0.1	0.0	0.0	0.0	0.0	+0.1	0.0	0.0	0.0	+0.1	0.0	0.0	0.0	0.0	−0.1	0.0	0.0	+0.1	0.0	0.0	0.0	0.0
α_S	+0.1	0.0	+0.1	0.0	0.0	0.0	0.0	−0.2	0.0	0.0	0.0	−0.1	0.0	0.0	+0.1	0.0	0.0	0.0	0.0	−0.2	+0.1	0.0	+0.1	0.0
	−0.1	0.0	−0.1	0.0	0.0	0.0	0.0	+0.2	0.0	0.0	0.0	+0.2	0.0	0.0	−0.1	0.0	0.0	0.0	0.0	+0.2	−0.1	0.0	−0.1	0.0
m_t^{MC}	+1.8	−0.1	+0.6	−0.7	−0.8	−0.1	−0.4	−0.6	+0.2	+0.5	0.0	+0.1	+1.0	+0.2	−1.2	−1.1	−0.6	+0.3	+0.5	+0.3	+0.6	−0.1	0.0	+0.3
	+0.5	−1.9	−1.1	+0.8	+0.5	+1.0	+0.7	−0.4	−0.6	+0.1	−0.8	−0.3	−0.2	+1.2	−0.6	+0.1	−0.1	−0.1	+0.4	+0.8	+0.3	−0.7	+0.1	+0.4
$\mu_{r,f}$	+0.6	+0.2	+1.1	+0.5	−0.4	−0.5	0.0	−1.3	−0.1	−0.5	−0.6	−2.2	+0.9	+0.2	+1.0	+0.8	−0.4	−0.4	−0.1	−0.8	+1.6	+1.1	+1.2	+0.2
	−0.7	−0.2	−1.2	−0.6	+0.5	+0.6	+0.1	+1.4	+0.3	+0.7	+1.2	+3.5	−1.0	−0.2	−1.1	−1.0	+0.4	+0.3	−0.1	+0.5	−2.1	−1.5	−1.7	−0.5
h_{damp}	+1.3	+0.6	−1.4	−0.5	−0.9	+0.4	−0.1	−0.4	+0.1	+1.8	−0.4	+1.8	+3.8	+3.5	+0.7	−2.1	−2.6	−1.1	+0.7	−0.4	+0.7	−2.3	−1.6	+2.1
	+2.5	−2.5	−3.5	−1.6	−1.1	+1.0	+0.8	−0.2	−2.1	−0.5	−2.2	−2.7	−2.3	0.0	−0.6	−1.4	+0.2	+0.8	+3.6	+1.8	+3.3	−0.6	+2.4	+4.7
PS ISR	+0.5	−0.6	−0.9	+1.4	+0.9	+1.1	+1.3	+1.0	+1.1	+1.8	+1.0	0.0	+3.7	−2.4	+0.8	−6.2	−2.1	−1.3	+0.4	+0.8	−0.6	−2.5	+0.2	−0.7
	+0.4	−1.7	−2.4	−1.6	−0.6	+0.5	+0.1	−0.5	−1.5	−1.3	−1.7	−1.0	+1.5	+1.0	0.0	−1.7	+0.8	+0.2	+1.8	+2.3	+2.1	−0.4	+3.1	+2.5
PS FSR	−1.7	−4.5	−4.0	−2.5	−0.4	+0.5	+0.9	−0.5	−1.5	−0.9	−1.4	−0.3	+2.7	+2.6	+2.9	+1.3	+0.8	+1.4	+3.1	+1.9	+1.1	−0.1	+0.9	+1.0
	+4.4	+1.3	+1.6	+0.8	−0.5	−0.4	−0.1	−0.6	+0.7	+0.9	+0.1	−0.5	−0.9	+1.0	−0.9	−2.9	−1.0	−1.7	+0.1	−0.3	+0.2	−1.1	+0.4	+0.6
UE tune	+3.9	−1.7	−4.2	+0.2	−1.0	+1.2	+0.9	−0.5	0.0	−0.2	−0.9	−1.8	+3.7	+3.3	+2.8	−2.9	−2.0	−1.6	+1.8	+1.8	+0.7	−1.0	+0.5	+1.3
	+2.8	−0.2	−2.9	−1.0	+0.2	+0.4	+1.1	−0.4	−0.6	+1.0	−1.5	+0.5	−0.7	+1.4	−3.2	−2.5	+0.2	+0.3	+0.1	+2.4	+0.2	−0.7	+1.2	+0.9
colour reconnection	+1.3	+0.5	0.0	−0.7	−0.6	−0.8	+0.1	−0.5	+0.1	+0.3	−1.2	−0.7	+2.6	+2.0	−1.5	−2.2	−0.3	−1.0	+0.3	+1.5	+0.9	−0.9	+0.8	+2.3
	+3.0	+0.4	+1.0	+0.6	0.0	+1.7	+1.8	+0.6	+0.6	+2.1	+0.2	+0.6	+2.6	+0.6	−2.3	−3.1	−2.8	−3.0	−2.1	−0.6	+0.1	−2.6	+0.7	−0.1
	+2.8	−1.9	−1.1	0.0	+0.1	+0.5	+0.9	+0.6	−0.5	+1.7	−0.7	−0.1	+1.2	+0.6	0.0	−1.6	−2.2	−1.5	−0.3	+0.1	+0.6	−0.3	+0.8	+0.2
fragmentation b → B	+1.3	+0.8	+1.3	+0.6	+0.4	+0.2	+0.4	−0.5	+0.2	−0.4	−0.3	−1.0	0.0	+0.8	+0.2	−0.3	+0.1	+0.2	+0.1	−0.8	−0.1	−0.4	−0.7	−0.7
	−0.6	−0.6	−0.7	−0.3	−0.2	0.0	0.0	+0.2	−0.1	+0.2	+0.1	+0.6	0.0	−0.5	−0.3	0.0	−0.2	−0.1	0.0	+0.4	+0.1	+0.3	+0.4	+0.4
	+0.2	+0.2	+0.2	+0.1	+0.1	0.0	0.0	−0.1	0.0	0.0	0.0	−0.2	−0.1	+0.1	0.0	−0.1	0.0	0.0	0.0	−0.2	0.0	−0.1	−0.1	−0.1
	+1.5	+0.9	+1.2	+0.8	+0.3	+0.2	+0.3	−0.4	−0.1	−0.4	−0.5	−1.0	+1.2	+1.2	+1.0	+0.6	+0.1	+0.1	0.0	−0.5	−0.5	−0.8	−1.1	−1.0
branching ratio $B \to \mu$	−0.2	−0.2	−0.2	−0.2	+0.1	+0.1	+0.2	0.0	+0.1	0.0	+0.1	+0.1	−0.4	−0.4	−0.2	−0.1	+0.2	0.0	+0.1	0.0	0.0	0.0	+0.1	0.0
	+0.4	+0.4	+0.4	+0.2	−0.1	−0.2	−0.2	−0.1	−0.1	−0.1	−0.1	−0.2	+0.6	+0.5	+0.4	+0.2	−0.1	−0.2	−0.1	−0.1	−0.1	0.0	−0.1	−0.1

Table A.41: The measured $[N_{\text{jet}}^{0,1,2+}, M(\text{t}\bar{\text{t}}), y(\text{t}\bar{\text{t}})]$ cross sections, along with their relative statistical and systematic uncertainties, and NP corrections (see Section 9).

N_{jet}	$M(\text{t}\bar{\text{t}})$ [GeV]	$\lvert y(\text{t}\bar{\text{t}})\rvert$	$\frac{1}{\sigma(\text{t}\bar{\text{t}})}\frac{\text{d}\sigma}{\text{d}\lvert y(\text{t}\bar{\text{t}})\rvert}$	stat. [%]	syst. [%]	$\mathcal{C}_{\text{NP}}$	bin
0	300–400	0.00–0.35	8.235×10^{-2}	4.2	$^{+12.1}_{-8.0}$	0.973	1
0	300–400	0.35–0.75	8.580×10^{-2}	3.3	$^{+6.6}_{-10.7}$	0.974	2
0	300–400	0.75–1.15	7.629×10^{-2}	3.7	$^{+6.0}_{-12.6}$	0.973	3
0	300–400	1.15–2.50	3.578×10^{-2}	3.5	$^{+6.9}_{-8.2}$	0.975	4
0	400–500	0.00–0.35	1.361×10^{-1}	2.5	$^{+1.8}_{-3.1}$	0.971	5
0	400–500	0.35–0.75	1.231×10^{-1}	2.2	$^{+5.2}_{-1.8}$	0.971	6
0	400–500	0.75–1.15	1.030×10^{-1}	2.6	$^{+5.3}_{-1.5}$	0.972	7
0	400–500	1.15–2.50	4.724×10^{-2}	2.0	$^{+4.2}_{-3.0}$	0.974	8
0	500–1500	0.00–0.35	1.598×10^{-1}	1.7	$^{+2.6}_{-4.2}$	0.976	9
0	500–1500	0.35–0.75	1.402×10^{-1}	1.9	$^{+4.9}_{-2.6}$	0.978	10
0	500–1500	0.75–1.15	1.102×10^{-1}	2.3	$^{+2.7}_{-4.5}$	0.977	11
0	500–1500	1.15–2.50	3.225×10^{-2}	3.3	$^{+5.5}_{-6.4}$	0.982	12
1	300–400	0.00–0.35	4.219×10^{-2}	7.0	$^{+13.9}_{-6.0}$	1.031	13
1	300–400	0.35–0.75	4.211×10^{-2}	5.9	$^{+11.9}_{-5.3}$	1.031	14
1	300–400	0.75–1.15	3.709×10^{-2}	6.5	$^{+5.1}_{-13.3}$	1.035	15
1	300–400	1.15–2.50	1.619×10^{-2}	5.7	$^{+9.1}_{-14.9}$	1.034	16
1	400–500	0.00–0.35	7.864×10^{-2}	3.7	$^{+2.8}_{-9.7}$	1.036	17
1	400–500	0.35–0.75	7.203×10^{-2}	3.2	$^{+2.5}_{-7.0}$	1.033	18
1	400–500	0.75–1.15	5.572×10^{-2}	4.1	$^{+6.0}_{-3.7}$	1.034	19
1	400–500	1.15–2.50	2.186×10^{-2}	3.6	$^{+10.8}_{-2.8}$	1.034	20
1	500–1500	0.00–0.35	1.003×10^{-1}	2.5	$^{+7.8}_{-2.7}$	1.029	21
1	500–1500	0.35–0.75	8.991×10^{-2}	2.5	$^{+1.9}_{-8.1}$	1.032	22
1	500–1500	0.75–1.15	6.298×10^{-2}	3.5	$^{+8.0}_{-3.2}$	1.033	23
1	500–1500	1.15–2.50	1.796×10^{-2}	4.7	$^{+10.8}_{-8.7}$	1.027	24
$\geq$2	300–400	0.00–0.35	2.241×10^{-2}	13.4	$^{+24.6}_{-8.9}$	1.037	25
$\geq$2	300–400	0.35–0.75	2.132×10^{-2}	12.2	$^{+14.6}_{-12.7}$	1.031	26
$\geq$2	300–400	0.75–1.15	1.872×10^{-2}	12.8	$^{+27.3}_{-6.2}$	1.035	27
$\geq$2	300–400	1.15–2.50	8.949×10^{-3}	10.0	$^{+11.2}_{-20.8}$	1.045	28
$\geq$2	400–500	0.00–0.35	4.412×10^{-2}	6.7	$^{+8.1}_{-12.6}$	1.036	29
$\geq$2	400–500	0.35–0.75	3.703×10^{-2}	6.5	$^{+7.9}_{-14.4}$	1.035	30
$\geq$2	400–500	0.75–1.15	2.985×10^{-2}	8.1	$^{+12.6}_{-10.9}$	1.040	31
$\geq$2	400–500	1.15–2.50	1.069×10^{-2}	8.1	$^{+10.3}_{-15.6}$	1.044	32
$\geq$2	500–1500	0.00–0.35	5.843×10^{-2}	3.2	$^{+8.0}_{-7.5}$	1.017	33
$\geq$2	500–1500	0.35–0.75	4.772×10^{-2}	4.3	$^{+9.0}_{-9.1}$	1.013	34
$\geq$2	500–1500	0.75–1.15	3.761×10^{-2}	4.9	$^{+9.7}_{-8.6}$	1.012	35
$\geq$2	500–1500	1.15–2.50	9.239×10^{-3}	7.0	$^{+10.9}_{-8.1}$	1.014	36

Table A.42: The correlation matrix of statistical uncertainties for the measured $[N_{\text{jet}}^{0,1,2+}, M(\text{t}\bar{\text{t}}), y(\text{t}\bar{\text{t}})]$ cross sections. The values are expressed as percentages. For bin indices see Table A.41.

bin	2	3	4	5	6	7	8	9	10	11	12	13	14	15	16	17	18	19	20	21	22	23	24	25	26	27	28	29	30	31	32	33	34	35	36
1	−14	−18	+1	−33	−22	+6	+2	−8	+5	+1	−5	−5	−10	+1	0	−14	+1	+7	−2	+6	+1	−3	−2	−10	+3	+2	−1	+9	+3	−3	−1	−3	−3	0	+1
2		+20	−23	−20	−6	−28	−6	+7	−12	+1	+4	−10	+6	−9	−1	+2	−10	−7	+6	+2	+2	+5	−1	+4	−11	−1	+2	+2	+4	+6	−2	−3	0	−2	−2
3			+2	+5	−28	−14	−25	+1	0	−11	−1	+1	−9	+4	−13	+6	−9	−12	−10	−3	+4	+5	+5	+2	−2	−9	0	−3	+5	+6	+5	0	−2	−2	−4
4				−1	−4	−22	+3	−9	−1	−2	−29	−1	−1	−11	+7	−4	+4	−7	−24	−5	−6	+2	−1	−2	+1	+1	−17	−2	−4	+3	+6	−2	−3	−5	+3
5					+5	−9	−5	−16	−10	+2	−1	−20	−2	+6	−3	+5	−5	0	−1	−5	+2	+2	−1	+10	+3	−2	−1	−12	−1	+1	+1	+5	+1	−1	−1
6						+24	−13	−10	−3	−14	−3	−2	−14	−11	+4	−5	+10	−3	−1	+2	−5	−1	+1	+4	+3	+6	−1	−1	−10	−2	+1	+2	+2	+3	−1
7							+13	+3	−12	−6	−10	+7	−11	−16	−12	−1	−2	+10	−3	+2	0	−6	−3	−3	+6	+6	+5	+1	−3	−10	−2	−1	+2	+3	+2
8								−4	−4	−14	+3	−2	+6	−13	−28	−3	−2	−1	+12	−4	−1	−2	−16	−2	−1	+5	+2	0	−1	−3	−11	−2	−3	+1	+3
9									−19	−6	−1	+8	+3	−2	−4	−11	−1	+3	−1	−21	−6	+5	−1	0	−2	0	0	+4	+2	0	0	−3	+4	−1	−1
10										−3	−12	+3	+2	+5	−3	0	−9	−3	+1	−5	−9	−13	+3	−2	+1	−1	−2	+2	+1	+3	0	+4	−7	+4	0
11											−7	−2	+6	+4	+2	+2	−4	−9	−5	+5	−11	−12	−12	−1	−1	0	−2	0	+2	+2	+3	−1	+4	−6	+3
12												−2	−1	+5	−6	−1	+1	−2	−19	−3	+3	−8	−16	+1	−2	−2	+6	−1	−1	+1	0	−2	−2	+3	−10
13													−10	−13	+3	−30	−22	+5	+3	−8	+4	+2	−1	−6	−7	+3	0	−6	+6	+4	−2	+7	+1	−3	+1
14														+16	−17	−21	−4	−25	0	+4	−10	0	+4	−8	+3	−9	+1	+6	−9	−1	+6	+1	+3	+4	−4
15															+7	+4	−26	−11	−19	+2	+1	−10	0	+3	−9	−1	−6	+4	−1	−7	0	−3	+5	+5	+4
16																+2	−1	−18	+4	−3	+1	0	−21	0	+1	−6	+5	−3	+5	0	−21	−1	−4	+2	+9
17																	+5	−7	0	−12	−9	+2	+1	−16	+3	+4	−2	+4	−4	−1	+1	−2	+3	+1	−1
18																		+22	−9	−10	−1	−11	+1	+3	−13	−4	+5	−4	+7	−2	−2	+4	−5	+2	+1
19																			+11	+3	−10	−5	−9	+6	−4	−12	−2	−1	−2	+6	−1	+2	+1	−3	+1
20																				+1	+1	−10	0	−3	+7	−1	−27	0	−2	−1	+15	−1	+1	+3	−10
21																					−20	−5	+2	+7	+1	−3	0	−7	+1	+2	0	−20	−2	+5	−2
22																						−5	−8	+2	+3	+4	−2	+1	−7	−1	+2	0	−11	−7	+3
23																							−7	−3	+5	+4	+3	+2	0	−7	−1	+5	−5	−13	−6
24																								0	−2	+4	+5	0	+1	0	−12	−1	+4	−2	−16
25																									−24	−7	+3	−60	−17	+15	−1	+4	+9	−2	−2
26																										−4	−9	−13	−29	−32	+12	+9	−6	+9	−1
27																											−8	+12	−30	−40	−19	−3	+10	−3	+10
28																												−1	+12	−18	−50	−1	−2	+9	−10
29																													−2	−7	0	−28	−8	+5	0
30																														+11	−9	−8	−17	−13	+4
31																															+8	+5	−14	−20	−10
32																																0	+4	−9	−27
33																																	−35	+4	+1
34																																		−25	0
35																																			−24

Table A.43: Sources and values of the relative systematic uncertainties in percent of the measured $[N_{\text{jet}}^{0,1,2+}, M(\text{t}\bar{\text{t}}), y(\text{t}\bar{\text{t}})]$ cross sections. For bin indices see Table A.41.

source / bin	1	2	3	4	5	6	7	8	9	10	11	12	13	14	15	16	17	18	19	20	21	22	23	24	25	26	27	28	29	30	31	32	33	34	35	36
JER	+0.2	+0.6	+0.3	+0.6	0.0	+0.5	+0.4	+0.8	0.0	+0.3	+0.2	+0.9	−0.8	+0.9	+0.3	−0.6	−0.5	−0.2	+0.8	−0.6	0.0	+0.1	+0.1	−2.9	+0.3	−1.8	+0.3	−0.2	−0.5	−1.1	−0.2	−2.3	−0.9	−1.4	−1.3	+0.3
	−0.3	−1.1	−1.9	−0.6	−0.6	+0.2	−0.1	+0.2	−0.2	−0.2	+0.2	0.0	+2.2	+0.4	+0.3	−2.0	−0.5	−0.3	−0.1	+0.7	+0.6	+0.3	+0.1	+0.7	+2.4	−1.3	+0.5	+1.1	+1.5	−0.3	+2.0	+1.8	+0.3	+1.2	−0.4	−0.3
JESAbsoluteMPFBias	+0.7	+0.4	−0.1	+0.5	−0.1	+0.3	+0.3	+0.4	+0.1	−0.1	+0.1	−0.5	+1.4	+1.3	0.0	+0.4	−0.4	−0.4	−0.5	+0.5	+0.1	−0.1	+0.2	−1.0	+1.1	−0.6	+1.4	−0.3	−0.3	−0.7	−0.5	−1.8	−1.0	−0.8	−0.8	−0.6
	−0.7	−0.8	−1.4	−0.3	0.0	+0.2	+0.1	+0.2	−0.2	+0.2	+0.1	0.0	−0.3	−0.7	−0.2	−1.4	0.0	0.0	+0.3	+0.2	+0.8	+0.1	+0.4	+0.3	−0.1	−1.7	+1.3	−0.5	+1.2	+1.1	+0.4	+0.8	+0.1	+0.4	+0.3	+0.9
JESAbsoluteScale	+0.5	0.0	−0.1	+0.5	−0.2	+0.3	+0.2	+0.3	0.0	−0.1	+0.2	−0.1	+0.8	+0.9	−0.3	+0.8	−0.3	−0.4	−0.4	+0.6	−0.1	−0.4	+0.2	−1.5	−0.2	+0.3	+0.9	−1.2	+0.1	−0.5	−0.7	0.0	−0.6	−0.2	−1.0	−0.6
	−0.7	−0.7	−1.1	−0.5	−0.1	0.0	+0.2	+0.1	−0.1	+0.1	+0.2	0.0	−0.4	−0.4	−0.5	+0.3	+0.2	+0.1	+0.3	+1.2	+0.5	0.0	+0.2	+0.4	−0.1	−1.1	+2.7	+0.4	+0.8	+0.4	−1.4	−2.1	−0.2	+1.3	−0.3	+0.9
JESAbsoluteStat	+0.3	+0.9	−1.1	−0.4	−0.4	0.0	−0.2	+0.4	+0.1	+0.1	+0.6	+0.4	+1.1	+0.8	−0.6	+1.3	−0.5	−0.5	−0.4	+0.6	+0.2	+0.2	+0.7	−2.2	−0.2	+1.8	+1.7	+0.8	−1.0	−1.1	−1.5	−3.7	−0.1	+0.9	−0.8	+0.7
	−1.0	−0.3	−0.4	−0.3	+0.3	+0.1	+0.4	+0.2	−0.4	−0.3	−0.5	+0.3	−0.4	−0.3	−1.2	+2.4	−0.1	+0.2	+0.6	+1.4	+0.1	0.0	+0.1	−0.4	+2.9	−2.7	+2.2	+0.4	−0.2	+0.6	−0.1	−2.1	−0.6	+0.7	−0.7	−0.1
JESFlavourQCD	+2.9	+2.6	+1.2	+1.4	−0.2	+0.6	+0.1	+0.7	+0.8	+1.0	+0.9	+0.7	+2.3	+1.1	−0.1	+0.4	−1.7	−1.0	−0.9	−0.1	0.0	−0.3	−0.7	−1.6	+2.8	−0.2	−1.0	−5.7	−4.8	−5.1	−1.1	−2.4	−2.5	−2.2	−2.2	−2.4
	−3.0	−3.4	−3.1	−1.8	0.0	−0.1	+0.1	−0.3	−1.2	−0.6	−0.5	−0.3	−1.9	−0.5	−0.9	−1.2	+1.1	+1.0	+1.4	+2.1	+1.1	+0.1	+0.5	+0.3	+2.8	+1.9	+1.6	+1.7	+2.4	+2.3	+3.5	+3.8	+1.8	+3.5	+1.6	+2.3
JESFragmentation	+0.1	−0.2	−0.2	+0.2	+0.1	+0.4	+0.5	+0.4	+0.2	+0.2	−0.2	−0.4	+0.7	+0.8	+0.1	−0.2	−0.6	−0.4	−0.4	+0.7	+0.3	+0.4	+0.3	−1.1	+0.1	−0.4	+0.8	−0.5	−0.2	−1.3	−0.9	−2.4	−0.7	−0.2	+0.3	+0.4
	−0.4	−0.6	−1.1	−0.2	0.0	0.0	0.0	+0.1	−0.3	−0.2	−0.2	−0.3	−0.1	+0.1	−0.1	+0.3	+0.1	+0.1	+0.3	+1.4	+0.3	−0.1	+0.1	+0.3	+1.1	−0.5	+3.1	−0.1	+0.5	+0.9	−1.6	0.0	−0.1	+0.6	0.0	+0.4
JESPileUpDataMC	+0.5	0.0	−0.5	0.0	−0.1	+0.4	+0.4	+0.7	+0.2	+0.2	+0.1	+0.5	+0.4	+0.5	+0.1	−0.7	−0.5	−0.3	−0.1	−0.3	+0.3	+0.1	+1.0	−1.1	−0.5	−1.1	−0.2	+0.4	−0.4	−1.0	−0.2	−1.4	−0.5	−0.8	−0.9	−0.9
	−0.5	−0.9	−1.0	−0.5	+0.1	+0.1	+0.1	−0.1	−0.2	−0.4	−0.3	−0.6	0.0	+0.3	+0.4	−0.1	+0.4	+0.1	+0.4	+1.4	0.0	0.0	+0.5	+0.3	+1.2	+0.3	+2.3	+0.3	+0.7	+0.9	−0.9	−0.1	+0.3	+1.1	−0.9	+0.9
JESPileUpPtBB	0.0	−0.3	−0.4	+0.1	−0.2	+0.4	+0.5	+0.3	+0.4	+0.2	+0.4	+0.3	−0.3	−0.2	−0.1	−1.1	0.0	−0.2	−0.2	+0.3	+0.1	+0.1	+0.3	+0.4	−1.1	−1.7	0.0	−0.6	−0.4	−0.3	−0.8	−0.5	−0.2	0.0	−0.8	−0.5
	−0.2	−0.4	−0.4	−0.1	0.0	−0.1	−0.3	0.0	−0.3	−0.2	−0.2	0.0	−0.1	+1.9	+2.3	−0.6	0.0	−0.2	−0.2	−0.2	−0.1	−0.4	−0.1	−0.1	+1.7	+0.8	+1.0	−0.1	+0.5	+0.6	0.0	+1.9	−0.1	+1.0	−0.5	−0.3
JESPileUpPtEC1	+1.0	+1.4	−0.3	−0.1	+0.1	+0.4	+0.2	+0.1	+0.5	+0.7	+0.6	+0.2	+1.0	+1.2	−0.3	+0.3	−0.3	−0.2	−0.6	+0.2	−0.1	−0.2	+0.1	−1.0	+0.1	−0.4	+1.2	−5.9	−0.8	−1.9	−0.7	−2.1	−0.9	−0.5	−0.6	−0.8
	−0.9	−1.2	−1.2	−0.2	−0.6	−0.4	−0.2	+0.2	−0.5	−0.6	−0.7	−0.5	−0.2	−0.7	+0.1	+2.3	+0.1	+0.2	+0.4	+2.1	+0.2	+0.2	+0.3	+0.6	+0.4	−0.2	+2.0	+1.5	+0.6	0.0	+2.1	−0.7	+0.9	+0.9	+0.6	+0.9
JESPileUpPtEC2	0.0	0.0	0.0	0.0	0.0	0.0	0.0	0.0	0.0	0.0	0.0	0.0	0.0	0.0	0.0	0.0	0.0	0.0	0.0	0.0	0.0	0.0	0.0	0.0	0.0	0.0	0.0	0.0	0.0	0.0	0.0	0.0	0.0	0.0	0.0	0.0
	0.0	0.0	0.0	0.0	0.0	0.0	0.0	0.0	0.0	0.0	0.0	0.0	0.0	0.0	0.0	0.0	0.0	0.0	0.0	0.0	0.0	0.0	0.0	0.0	0.0	0.0	0.0	0.0	0.0	0.0	0.0	0.0	0.0	0.0	0.0	0.0
JESPileUpPtHF	0.0	0.0	0.0	0.0	0.0	0.0	0.0	0.0	0.0	0.0	0.0	0.0	0.0	0.0	0.0	0.0	0.0	0.0	0.0	0.0	0.0	0.0	0.0	0.0	0.0	0.0	0.0	0.0	0.0	0.0	0.0	0.0	0.0	0.0	0.0	0.0
	0.0	0.0	0.0	0.0	0.0	0.0	0.0	0.0	0.0	0.0	0.0	0.0	0.0	0.0	0.0	0.0	0.0	0.0	0.0	0.0	0.0	0.0	0.0	0.0	0.0	0.0	0.0	0.0	0.0	0.0	0.0	0.0	0.0	0.0	0.0	0.0
JESPileUpPtRef	+0.1	−0.1	−0.3	+0.3	+0.2	+0.5	+0.1	+0.5	+0.5	+0.5	0.0	+0.1	+0.3	−0.3	−0.6	−0.9	−0.4	−0.1	−0.2	−0.4	+0.2	+0.5	+0.7	−0.7	−1.1	−1.2	−1.2	−0.9	−0.8	−0.8	+0.5	−0.8	−0.1	−1.2	−0.4	−0.6
	−0.2	−0.6	−1.0	0.0	−0.2	+0.1	−0.2	−0.3	−0.6	−0.4	−0.7	−0.7	+0.1	+0.7	+0.8	+2.3	+0.1	0.0	0.0	+0.9	+0.1	−0.1	−0.1	+0.6	+1.2	−0.4	+1.3	+1.1	+1.7	+1.4	+1.0	−0.6	+0.2	+0.2	+0.6	−0.4
JESRelativeBal	+1.9	+2.2	+1.5	+1.6	−0.1	+0.3	−0.2	0.0	+0.3	+0.4	+0.2	−1.1	+1.6	+1.4	+0.7	+0.1	−0.7	−0.5	−0.6	−0.2	+0.2	−0.2	−0.5	−0.8	+2.5	−0.7	+1.5	−4.7	−1.9	−2.5	−0.9	−0.8	−1.8	−1.8	−1.8	−1.7
	−2.6	−2.7	−2.8	−1.7	−0.1	−0.2	+0.2	+0.7	−0.7	−0.4	−0.1	+1.1	−0.8	−0.1	−0.6	−1.7	+0.2	0.0	+1.1	+2.0	+0.9	+0.2	+1.2	+1.5	+0.9	+0.2	0.0	+2.2	+0.7	+1.4	+1.4	−0.3	+1.1	+2.1	+1.2	+1.4
JESRelativeFSR	−0.6	−0.9	−0.7	−0.1	+0.2	+0.1	+0.2	+0.2	−0.2	−0.2	−0.2	0.0	−0.5	−0.8	−0.5	−0.5	+0.2	+0.2	+0.5	−0.1	+0.5	0.0	+0.8	+0.2	+0.3	−0.4	+0.9	+0.5	+0.7	+0.8	−0.7	+1.5	0.0	+0.8	−0.5	−0.5
	+0.2	+0.5	+0.2	0.0	+0.1	+0.2	+0.1	+0.2	−0.1	−0.1	+0.3	0.0	+1.0	+0.8	+0.1	+0.7	−0.8	−0.5	−0.1	+0.9	+0.3	0.0	0.0	−0.9	−0.2	+1.1	+0.4	−0.1	−0.6	−0.5	−1.5	−0.9	−0.6	−0.4	−0.9	−1.0
JESRelativeJEREC1	0.0	0.0	−0.2	0.0	+0.1	0.0	0.0	+0.1	0.0	0.0	+0.2	−0.4	+0.1	−0.1	−0.1	+0.3	−0.1	0.0	+0.2	+1.0	+0.2	0.0	0.0	+0.5	+0.2	−0.4	+1.6	0.0	−0.2	+0.1	−1.0	−2.5	−0.2	+0.2	−0.9	+0.4
	0.0	0.0	−0.7	−0.1	0.0	0.0	−0.1	+0.2	0.0	−0.2	−0.3	−0.6	−0.1	+0.1	−0.2	+0.4	0.0	+0.1	+0.2	+1.3	+0.2	0.0	+0.1	+1.8	+1.0	−1.0	+2.1	−0.1	−0.6	+0.1	−0.8	−3.1	−0.2	+0.6	−0.2	+0.1

Table A.44: Table A.43 continued.

source / bin	1	2	3	4	5	6	7	8	9	10	11	12	13	14	15	16	17	18	19	20	21	22	23	24	25	26	27	28	29	30	31	32	33	34	35	36
JESRelativeJEREC2	0.0	0.0	0.0	0.0	0.0	0.0	0.0	0.0	0.0	0.0	0.0	0.0	0.0	0.0	0.0	0.0	0.0	0.0	0.0	0.0	0.0	0.0	0.0	0.0	0.0	0.0	0.0	0.0	0.0	0.0	0.0	0.0	0.0	0.0	0.0	0.0
	0.0	0.0	0.0	0.0	0.0	0.0	0.0	0.0	0.0	0.0	0.0	0.0	0.0	0.0	0.0	0.0	0.0	0.0	0.0	0.0	0.0	0.0	0.0	0.0	0.0	0.0	0.0	0.0	0.0	0.0	0.0	0.0	0.0	0.0	0.0	0.0
JESRelativeJERHF	0.0	0.0	0.0	0.0	0.0	0.0	0.0	0.0	0.0	0.0	0.0	0.0	0.0	0.0	0.0	0.0	0.0	0.0	0.0	0.0	0.0	0.0	0.0	0.0	0.0	0.0	0.0	0.0	0.0	0.0	0.0	0.0	0.0	0.0	0.0	0.0
	0.0	0.0	0.0	0.0	0.0	0.0	0.0	0.0	0.0	0.0	0.0	0.0	0.0	0.0	0.0	0.0	0.0	0.0	0.0	0.0	0.0	0.0	0.0	0.0	0.0	0.0	0.0	0.0	0.0	0.0	0.0	0.0	0.0	0.0	0.0	0.0
JESRelativePtBB	+0.2	+0.2	+0.2	+0.2	−0.2	−0.1	+0.2	+0.2	+0.1	+0.1	+0.1	−0.2	+0.6	+0.2	+0.1	−0.5	−0.3	−0.2	−0.4	+0.1	0.0	−0.3	+0.4	+0.7	+0.9	+0.1	+1.0	+0.3	−1.0	−0.4	−1.0	−0.6	−0.6	+0.9	−1.2	−0.4
	−0.5	−1.5	−0.8	+0.2	+0.3	+0.4	+0.4	0.0	−0.1	−0.1	0.0	0.0	−0.4	+1.0	+0.4	−1.1	+0.4	0.0	−0.1	−0.1	+0.5	−0.1	+0.2	+0.1	−0.7	−0.3	−0.1	−0.8	+0.9	+0.2	+0.4	+0.7	−0.3	+0.6	−0.3	−0.1
JESRelativePtEC1	0.0	+1.1	+0.2	+0.3	+0.3	+0.4	0.0	0.0	+0.3	+0.2	+0.2	−0.1	+0.3	+1.1	−0.1	+1.0	+0.2	0.0	−0.2	−0.1	−0.1	+0.1	−0.2	−2.3	+0.3	−0.3	+1.6	−4.6	0.0	−1.1	−0.6	+0.5	−0.5	−0.5	−0.5	−1.5
	−0.6	−0.8	−1.0	−0.4	−0.4	−0.4	+0.1	+0.7	−0.3	−0.4	−0.1	+0.7	−0.2	−0.9	−1.8	−0.3	−0.2	+0.2	+0.6	+0.8	+0.3	+0.2	+0.6	+0.5	+1.1	−0.8	+1.0	+1.6	−0.2	+0.1	−0.1	−0.1	+0.3	+0.9	+0.1	+0.9
JESRelativePtEC2	0.0	0.0	0.0	0.0	0.0	0.0	0.0	0.0	0.0	0.0	0.0	0.0	0.0	0.0	0.0	0.0	0.0	0.0	0.0	0.0	0.0	0.0	0.0	0.0	0.0	0.0	0.0	0.0	0.0	0.0	0.0	0.0	0.0	0.0	0.0	0.0
	0.0	0.0	0.0	0.0	0.0	0.0	0.0	0.0	0.0	0.0	0.0	0.0	0.0	0.0	0.0	0.0	0.0	0.0	0.0	0.0	0.0	0.0	0.0	0.0	0.0	0.0	0.0	0.0	0.0	0.0	0.0	0.0	0.0	0.0	0.0	0.0
JESRelativePtHF	0.0	0.0	0.0	0.0	0.0	0.0	0.0	0.0	0.0	0.0	0.0	0.0	0.0	0.0	0.0	0.0	0.0	0.0	0.0	0.0	0.0	0.0	0.0	0.0	0.0	0.0	0.0	0.0	0.0	0.0	0.0	0.0	0.0	0.0	0.0	0.0
	0.0	0.0	0.0	0.0	0.0	0.0	0.0	0.0	0.0	0.0	0.0	0.0	0.0	0.0	0.0	0.0	0.0	0.0	0.0	0.0	0.0	0.0	0.0	0.0	0.0	0.0	0.0	0.0	0.0	0.0	0.0	0.0	0.0	0.0	0.0	0.0
JESRelativeStatEC	0.0	+0.3	−0.1	+0.1	0.0	+0.2	+0.3	+0.2	+0.2	−0.1	+0.2	−0.5	+0.1	+0.4	−0.1	+1.0	0.0	+0.1	−0.2	+0.6	+0.1	−0.1	+0.2	−1.3	−0.1	−0.4	+1.9	+0.4	+0.1	−0.1	−1.5	−3.0	−0.4	+0.2	−0.6	+0.2
	−0.1	−0.4	−1.0	0.0	0.0	0.0	0.0	+0.3	−0.1	−0.1	0.0	0.0	+0.1	0.0	−0.3	−0.8	−0.2	−0.1	+0.1	+1.3	+0.2	−0.1	+0.2	+1.3	+0.7	−0.2	+2.0	+0.1	−0.3	+0.2	−0.7	−1.5	−0.3	+0.5	0.0	−0.5
JESRelativeStatFSR	0.0	+0.1	−0.2	+0.1	−0.2	0.0	+0.2	+0.2	+0.2	−0.2	+0.2	−0.1	+0.5	+0.1	+0.1	−0.5	0.0	0.0	−0.1	0.0	−0.2	+0.3	0.0	+0.3	−0.5	−1.0	+1.0	−0.1	+0.4	+0.3	−1.1	+0.4	−0.3	−0.1	−0.8	−0.3
	0.0	0.0	−0.7	0.0	−0.1	0.0	0.0	+0.2	0.0	−0.1	0.0	+0.1	−0.1	0.0	−0.2	−0.4	+0.1	0.0	+0.1	−0.1	0.0	+0.3	+0.1	+0.9	−0.2	−0.7	+1.2	−0.7	+0.3	+0.3	−0.9	+1.0	0.0	−0.1	−0.6	−0.7
JESRelativeStatHF	0.0	0.0	0.0	0.0	0.0	0.0	0.0	0.0	0.0	0.0	0.0	0.0	0.0	0.0	0.0	0.0	0.0	0.0	0.0	0.0	0.0	0.0	0.0	0.0	0.0	0.0	0.0	0.0	0.0	0.0	0.0	0.0	0.0	0.0	0.0	0.0
	0.0	0.0	0.0	0.0	0.0	0.0	0.0	0.0	0.0	0.0	0.0	0.0	0.0	0.0	0.0	0.0	0.0	0.0	0.0	0.0	0.0	0.0	0.0	0.0	0.0	0.0	0.0	0.0	0.0	0.0	0.0	0.0	0.0	0.0	0.0	0.0
JESSinglePionECAL	−0.6	−1.0	−0.7	0.0	+0.2	+0.2	0.0	0.0	−0.2	−0.3	−0.3	−0.1	+0.3	+0.3	+0.6	0.0	−0.3	−0.1	+0.4	+0.1	+0.2	+0.1	0.0	−0.1	+0.8	−0.9	+1.2	+0.3	+1.2	+1.0	+0.4	+0.1	−0.1	+0.7	+0.2	+0.7
	+0.3	0.0	−0.1	+0.3	0.0	+0.5	+0.4	+0.6	+0.5	+0.1	−0.3	−0.3	+0.3	+0.5	−0.4	−0.7	−0.2	−0.3	−0.1	+0.5	0.0	0.0	+0.6	−0.7	+0.3	+0.3	0.0	−0.8	−0.9	−1.4	−1.3	−0.4	−0.7	−0.5	−0.2	−0.8
JESSinglePionHCAL	−0.4	−0.6	−0.5	−0.1	−0.3	0.0	+0.1	0.0	−0.3	−0.2	−0.3	+0.1	−0.1	−0.3	+0.1	−0.2	+0.3	+0.2	+0.4	−0.1	+0.4	−0.2	+0.3	−0.1	+0.3	−1.5	+0.1	+0.8	+1.3	+1.3	+0.6	+0.4	−0.2	+0.8	0.0	+0.1
	+0.3	0.0	−0.5	+0.3	+0.1	+0.4	+0.4	+0.5	+0.3	+0.1	−0.1	−0.4	+0.5	+1.3	+0.1	−0.3	−0.5	−0.3	−0.6	+0.5	+0.2	0.0	+0.3	−0.8	+0.3	−0.5	+0.7	−0.7	−0.5	−1.0	−0.4	−1.6	−0.8	0.0	−0.3	−0.4
JESTimePtEta	−0.1	−0.1	−0.4	−0.1	−0.2	0.0	+0.3	0.0	+0.3	−0.1	+0.1	0.0	+0.3	−0.2	−0.2	0.0	−0.3	−0.1	0.0	+0.2	−0.2	0.0	+0.1	+0.3	−1.0	−0.3	+1.0	+1.0	+1.2	+0.7	−1.6	−0.6	−0.5	0.0	−0.3	+0.4
	−0.2	+0.2	0.0	0.0	0.0	+0.3	−0.1	−0.1	+0.1	−0.2	0.0	+0.2	+0.8	+0.2	−0.5	+1.0	−0.1	0.0	+0.1	+0.8	0.0	+0.3	+0.3	−1.4	−0.2	−0.2	+1.5	−0.4	+0.4	−0.5	+0.1	−1.6	−0.1	−0.1	−0.6	−1.1
$\vec{p}_{\mathrm{T}}^{\mathrm{miss}}$	−2.2	−0.4	−1.2	−0.2	+0.2	+0.2	−0.3	−0.2	+0.1	+0.2	+0.5	+0.2	+0.7	+0.8	−0.1	+0.9	−0.2	+0.1	+0.1	+0.4	+0.4	−0.1	+0.4	+0.5	+2.1	−1.1	+0.6	0.0	−0.6	+0.1	+0.1	−0.6	+0.3	+0.4	0.0	−0.6
	−0.1	−0.2	+0.8	+0.4	−0.1	−0.3	+0.2	+0.6	−0.1	+0.1	−0.6	−0.6	−0.2	+0.1	−0.6	+1.6	−0.2	+0.1	0.0	+0.5	−0.1	−0.3	−0.1	−0.1	−0.4	+1.2	0.0	0.0	+0.1	−0.4	+0.2	−1.4	−0.4	0.0	−0.3	+0.7
lepton ID/ISO	−0.2	−0.1	−0.5	−0.2	+0.1	+0.3	+0.2	+0.6	−0.1	0.0	−0.2	−0.6	−0.1	+0.1	−0.1	−0.3	+0.2	+0.3	+0.3	+0.5	−0.1	−0.1	−0.2	−0.7	+0.1	+0.2	0.0	+0.1	+0.3	+0.3	+0.4	+0.8	−0.1	−0.2	−0.1	−0.9
	+0.2	+0.1	+0.5	+0.1	−0.1	−0.3	−0.2	−0.6	+0.1	0.0	+0.2	+0.6	+0.1	0.0	+0.1	+0.3	−0.2	−0.3	−0.3	−0.5	+0.1	+0.1	+0.2	+0.7	−0.1	−0.2	0.0	−0.1	−0.3	−0.4	−0.4	−0.8	+0.1	+0.2	+0.2	+0.9
pileup	+0.6	−0.3	−0.5	−0.5	+0.1	+0.2	+0.3	+0.1	+0.3	+0.3	+0.2	+0.2	−0.5	+0.3	−0.3	−0.5	+0.2	−0.1	−0.2	+0.1	−0.2	−0.1	+0.2	−0.1	−0.8	+1.7	+0.4	−2.1	+0.9	−0.9	−0.9	+0.8	+0.2	−0.6	+0.2	−0.7
	−0.7	+0.2	+0.6	+0.5	−0.1	−0.2	−0.3	−0.1	−0.3	−0.3	−0.2	−0.1	+0.4	−0.1	+0.6	+0.3	−0.2	+0.1	+0.3	−0.1	+0.2	0.0	−0.2	+0.1	+0.8	−1.8	−0.2	+2.4	−1.0	+0.8	+0.7	−0.9	−0.1	+0.5	−0.1	+0.7
trigger	+0.1	+0.2	+0.1	−0.3	+0.2	+0.1	0.0	−0.1	+0.1	0.0	−0.1	−0.2	+0.1	+0.2	+0.2	−0.4	+0.2	+0.1	0.0	−0.2	+0.1	0.0	−0.1	−0.2	+0.1	+0.2	+0.3	−0.2	+0.2	+0.2	+0.1	−0.2	+0.1	0.0	−0.1	−0.2
	−0.1	−0.2	−0.1	+0.3	−0.2	−0.1	0.0	+0.1	−0.1	0.0	+0.1	+0.2	−0.1	−0.2	−0.2	+0.4	−0.2	−0.1	0.0	+0.2	−0.1	0.0	+0.1	+0.2	−0.1	−0.2	−0.3	+0.2	−0.2	−0.2	−0.1	+0.2	−0.1	0.0	+0.1	+0.2

Table A.45: Table A.43 continued.

source / bin	1	2	3	4	5	6	7	8	9	10	11	12	13	14	15	16	17	18	19	20	21	22	23	24	25	26	27	28	29	30	31	32	33	34	35	36
trigger (η)	−0.3	−0.2	−0.3	+0.7	−0.2	−0.2	−0.2	+0.4	0.0	−0.1	−0.2	+0.3	−0.2	−0.1	−0.3	+0.9	−0.3	−0.2	−0.2	+0.5	0.0	−0.1	−0.3	+0.2	−0.2	0.0	−0.4	+0.7	−0.3	−0.2	−0.2	+0.6	0.0	−0.1	−0.3	+0.2
	+0.3	+0.2	+0.3	−0.6	+0.2	+0.2	+0.2	−0.4	0.0	+0.1	+0.2	−0.3	+0.2	+0.1	+0.3	−0.9	+0.3	+0.2	+0.2	−0.5	0.0	+0.1	+0.3	−0.2	+0.2	0.0	+0.4	−0.7	+0.3	+0.2	+0.2	−0.6	0.0	+0.1	+0.3	−0.3
non-$t\bar{t}$ background	−0.9	−0.7	−1.8	−3.9	−0.2	−0.2	+0.2	0.0	+0.6	+0.3	+0.7	−0.3	+0.7	+1.1	+1.2	−3.7	0.0	+0.5	+0.5	+0.3	+0.8	+0.8	+0.6	+0.2	+2.9	+2.4	+3.0	+0.6	+0.9	+0.5	+0.3	+1.0	+1.2	+0.4	+1.3	−0.6
	+1.1	+0.5	+2.0	+3.7	+0.1	+0.1	−0.3	−0.2	−0.5	−0.3	−0.6	+0.3	−0.6	−0.8	−0.8	+3.4	−0.1	−0.5	−0.5	−0.6	−0.8	−0.8	−0.5	−0.1	−3.0	−2.5	−2.9	−0.1	−0.8	−0.4	−0.3	−1.0	−1.2	−0.3	−1.2	+0.5
b-tagging	0.0	0.0	−0.1	−0.1	−0.1	−0.1	−0.1	0.0	−0.1	0.0	0.0	0.0	−0.4	−0.4	−0.5	−0.2	+0.1	+0.1	+0.1	+0.1	+0.1	+0.1	+0.2	+0.2	−0.8	−0.7	−0.8	−0.3	+0.4	+0.4	+0.4	+0.3	+0.4	+0.4	+0.3	+0.5
	0.0	0.0	+0.1	+0.1	+0.1	+0.1	+0.1	0.0	+0.1	0.0	0.0	0.0	+0.4	+0.4	+0.5	+0.2	−0.1	−0.1	−0.1	−0.1	−0.1	−0.1	−0.2	−0.2	+0.8	+0.7	+0.9	+0.3	−0.4	−0.4	−0.4	−0.3	−0.4	−0.4	−0.3	−0.5
b-tagging (light jets)	−0.3	−0.3	−0.5	−0.9	+0.1	+0.1	+0.3	+0.2	+0.2	+0.2	+0.2	+0.1	+0.4	+0.3	0.0	−1.1	0.0	+0.1	+0.2	+0.2	+0.1	+0.1	+0.1	0.0	+0.5	+0.9	+0.7	−1.0	+0.3	−0.1	+0.2	+0.3	−0.1	−0.2	−0.2	−0.5
	+0.3	+0.3	+0.5	+0.9	−0.1	−0.2	−0.3	−0.2	−0.2	−0.2	−0.2	−0.1	−0.4	−0.3	+0.1	+1.1	−0.1	−0.1	−0.2	−0.2	−0.1	−0.1	−0.1	0.0	−0.5	−0.9	−0.7	+1.1	−0.3	+0.1	−0.2	−0.3	0.0	+0.2	+0.2	+0.5
luminosity	0.0	0.0	0.0	0.0	0.0	0.0	0.0	0.0	0.0	0.0	0.0	0.0	0.0	0.0	0.0	0.0	0.0	0.0	0.0	0.0	0.0	0.0	0.0	0.0	0.0	0.0	0.0	0.0	0.0	0.0	0.0	0.0	0.0	0.0	0.0	0.0
	0.0	0.0	0.0	0.0	0.0	0.0	0.0	0.0	0.0	0.0	0.0	0.0	0.0	0.0	0.0	0.0	0.0	0.0	0.0	0.0	0.0	0.0	0.0	0.0	0.0	0.0	0.0	0.0	0.0	0.0	0.0	0.0	0.0	0.0	0.0	0.0
branching ratio $t\bar{t} \to \ell\ell$	0.0	0.0	0.0	0.0	0.0	0.0	0.0	0.0	0.0	0.0	0.0	0.0	0.0	0.0	0.0	0.0	0.0	0.0	0.0	0.0	0.0	0.0	0.0	0.0	0.0	0.0	0.0	0.0	0.0	0.0	0.0	0.0	0.0	0.0	0.0	0.0
	0.0	0.0	0.0	0.0	0.0	0.0	0.0	0.0	0.0	0.0	0.0	0.0	0.0	0.0	0.0	0.0	0.0	0.0	0.0	0.0	0.0	0.0	0.0	0.0	0.0	0.0	0.0	0.0	0.0	0.0	0.0	0.0	0.0	0.0	0.0	0.0
PDF eigenvector 1	0.0	0.0	0.0	0.0	0.0	0.0	0.0	0.0	0.0	0.0	0.0	0.0	0.0	0.0	0.0	0.0	0.0	0.0	0.0	0.0	0.0	0.0	0.0	0.0	+0.1	+0.1	0.0	0.0	−0.1	−0.1	0.0	0.0	0.0	0.0	0.0	0.0
	0.0	0.0	0.0	0.0	0.0	0.0	0.0	−0.1	0.0	0.0	0.0	0.0	0.0	+0.1	0.0	0.0	0.0	0.0	−0.1	−0.1	0.0	0.0	0.0	0.0	0.0	+0.1	+0.1	0.0	0.0	0.0	−0.1	−0.1	0.0	+0.1	+0.1	+0.1
PDF eigenvector 2	0.0	−0.1	+0.1	+0.1	−0.3	−0.1	0.0	0.0	+0.2	+0.1	0.0	−0.1	+0.1	−0.1	+0.1	+0.1	−0.5	−0.2	+0.1	+0.1	+0.2	+0.1	0.0	−0.2	+0.4	0.0	+0.1	0.0	−0.6	−0.3	+0.1	+0.1	+0.3	+0.2	0.0	−0.1
	0.0	0.0	0.0	0.0	+0.1	0.0	0.0	+0.1	−0.1	−0.1	−0.1	+0.1	−0.1	−0.1	0.0	0.0	+0.2	+0.1	+0.1	+0.1	−0.1	−0.1	−0.1	+0.1	−0.3	−0.2	−0.1	0.0	+0.3	+0.2	+0.2	+0.2	−0.2	−0.2	−0.1	−0.1
PDF eigenvector 3	+0.1	+0.1	0.0	−0.1	+0.1	0.0	0.0	−0.2	+0.1	+0.1	+0.1	−0.2	+0.1	+0.1	+0.1	−0.1	+0.1	0.0	−0.1	−0.3	+0.1	+0.1	+0.1	0.0	+0.1	+0.2	+0.1	+0.1	0.0	0.0	−0.3	−0.4	+0.1	+0.1	+0.1	+0.2
	0.0	0.0	0.0	0.0	0.0	0.0	0.0	+0.1	0.0	0.0	−0.1	+0.1	0.0	−0.1	0.0	0.0	0.0	0.0	+0.1	+0.2	0.0	0.0	0.0	0.0	0.0	−0.1	−0.1	0.0	0.0	0.0	+0.1	+0.2	0.0	−0.1	−0.1	−0.1
PDF eigenvector 4	0.0	0.0	0.0	+0.1	−0.2	−0.1	0.0	0.0	+0.1	+0.1	0.0	0.0	+0.1	0.0	0.0	+0.1	−0.3	−0.2	0.0	+0.1	+0.1	+0.1	0.0	−0.1	+0.3	+0.1	0.0	0.0	−0.4	−0.2	0.0	+0.1	+0.2	+0.2	0.0	−0.1
	0.0	0.0	0.0	0.0	+0.1	0.0	0.0	0.0	0.0	0.0	0.0	0.0	0.0	0.0	0.0	0.0	+0.1	+0.1	0.0	0.0	0.0	0.0	0.0	0.0	−0.2	−0.1	0.0	0.0	+0.2	+0.1	0.0	−0.1	−0.1	−0.1	0.0	+0.1
PDF eigenvector 5	−0.1	−0.1	0.0	+0.1	0.0	0.0	+0.1	+0.3	−0.2	−0.2	−0.2	+0.4	−0.2	−0.2	−0.1	+0.1	+0.2	+0.2	+0.3	+0.4	−0.2	−0.2	−0.2	+0.1	−0.4	−0.4	−0.3	−0.1	+0.3	+0.3	+0.5	+0.5	−0.3	−0.4	−0.3	−0.3
	+0.1	+0.2	+0.1	−0.1	+0.1	+0.1	−0.1	−0.3	+0.2	+0.1	+0.1	−0.4	+0.1	+0.2	+0.2	−0.2	+0.1	0.0	−0.3	−0.5	+0.2	+0.1	+0.1	−0.1	+0.1	+0.3	+0.3	+0.1	0.0	0.0	−0.5	−0.7	+0.2	+0.3	+0.2	+0.4
PDF eigenvector 6	0.0	0.0	0.0	0.0	−0.1	0.0	−0.1	0.0	+0.1	+0.1	+0.1	0.0	+0.1	+0.1	0.0	0.0	−0.2	−0.1	−0.1	−0.1	+0.1	+0.1	+0.1	0.0	+0.2	+0.2	+0.1	0.0	−0.2	−0.2	−0.2	−0.1	+0.1	+0.1	+0.1	0.0
	0.0	0.0	0.0	0.0	0.0	0.0	0.0	0.0	0.0	−0.1	0.0	0.0	0.0	−0.1	0.0	0.0	+0.1	0.0	+0.1	0.0	0.0	0.0	0.0	0.0	−0.1	−0.1	0.0	0.0	+0.1	+0.1	+0.1	+0.1	−0.1	−0.1	0.0	0.0
PDF eigenvector 7	−0.2	−0.2	0.0	+0.2	+0.1	+0.1	+0.2	+0.4	−0.3	−0.3	−0.3	+0.5	−0.3	−0.4	−0.1	+0.2	+0.3	+0.3	+0.6	+0.6	−0.4	−0.3	−0.4	0.0	−0.6	−0.7	−0.4	−0.1	+0.6	+0.5	+0.9	+0.8	−0.6	−0.6	−0.6	−0.5
	+0.1	+0.1	0.0	−0.1	0.0	0.0	−0.1	−0.3	+0.2	+0.2	+0.2	−0.3	+0.2	+0.2	+0.1	−0.1	−0.2	−0.1	−0.3	−0.4	+0.2	+0.2	+0.2	0.0	+0.3	+0.4	+0.2	+0.1	−0.3	−0.3	−0.5	−0.5	+0.3	+0.3	+0.3	+0.2
PDF eigenvector 8	−0.1	0.0	−0.1	0.0	0.0	+0.1	0.0	+0.2	−0.1	0.0	−0.1	+0.1	−0.1	0.0	0.0	0.0	0.0	+0.1	+0.1	+0.1	−0.1	−0.1	−0.1	0.0	−0.1	0.0	0.0	0.0	+0.1	+0.1	0.0	+0.2	−0.1	−0.1	−0.1	0.0
	+0.1	0.0	+0.1	0.0	0.0	−0.1	0.0	−0.1	+0.1	0.0	+0.1	0.0	0.0	0.0	0.0	0.0	0.0	−0.1	−0.1	−0.1	0.0	+0.1	0.0	0.0	+0.1	0.0	0.0	−0.1	−0.1	−0.1	0.0	−0.1	+0.1	0.0	0.0	0.0
PDF eigenvector 9	0.0	0.0	+0.1	+0.1	0.0	0.0	0.0	0.0	0.0	0.0	0.0	−0.2	+0.1	0.0	0.0	+0.1	0.0	0.0	+0.1	0.0	0.0	0.0	0.0	−0.1	+0.1	0.0	0.0	0.0	0.0	0.0	0.0	0.0	0.0	0.0	0.0	−0.1
	0.0	0.0	−0.1	−0.1	0.0	0.0	−0.1	0.0	0.0	0.0	0.0	+0.2	−0.1	0.0	0.0	−0.1	0.0	0.0	−0.1	0.0	0.0	0.0	0.0	+0.1	−0.1	0.0	0.0	0.0	0.0	0.0	0.0	0.0	0.0	0.0	0.0	+0.1
PDF eigenvector 10	+0.1	+0.1	0.0	−0.1	0.0	0.0	−0.1	−0.2	+0.1	+0.1	+0.1	−0.2	+0.2	+0.2	0.0	−0.1	−0.2	−0.1	−0.3	−0.3	+0.2	+0.2	+0.2	0.0	+0.3	+0.4	+0.2	+0.1	−0.3	−0.3	−0.4	−0.4	+0.3	+0.3	+0.3	+0.2
	−0.1	−0.1	0.0	+0.1	0.0	0.0	+0.1	+0.2	−0.1	−0.2	−0.2	+0.2	−0.2	−0.2	0.0	+0.1	+0.2	+0.2	+0.3	+0.3	−0.2	−0.2	−0.2	0.0	−0.4	−0.4	−0.2	−0.1	+0.3	+0.3	+0.5	+0.4	−0.3	−0.3	−0.3	−0.2

Table A.46: Table A.43 continued.

source / bin	1	2	3	4	5	6	7	8	9	10	11	12	13	14	15	16	17	18	19	20	21	22	23	24	25	26	27	28	29	30	31	32	33	34	35	36
PDF eigenvector 11	0.0	0.0	0.0	0.0	0.0	0.0	0.0	0.0	0.0	0.0	0.0	−0.1	0.0	+0.1	0.0	0.0	0.0	0.0	−0.1	−0.1	0.0	0.0	0.0	0.0	+0.1	+0.1	0.0	0.0	−0.1	0.0	−0.1	−0.1	+0.1	+0.1	+0.1	0.0
	0.0	0.0	0.0	0.0	0.0	0.0	0.0	+0.1	−0.1	−0.1	−0.1	+0.2	−0.1	−0.1	0.0	0.0	+0.1	0.0	+0.1	+0.2	−0.1	−0.1	−0.1	0.0	−0.1	−0.2	−0.1	−0.1	+0.1	+0.1	+0.2	+0.2	−0.1	−0.1	−0.1	−0.1
PDF eigenvector 12	−0.1	0.0	0.0	0.0	0.0	0.0	0.0	+0.1	−0.1	−0.1	−0.1	+0.1	−0.1	−0.1	0.0	0.0	+0.1	+0.1	+0.2	+0.2	−0.1	−0.1	−0.1	0.0	−0.2	−0.2	−0.1	0.0	+0.1	+0.1	+0.2	+0.2	−0.2	−0.2	−0.2	−0.1
	+0.1	0.0	0.0	0.0	0.0	0.0	0.0	−0.1	+0.1	+0.1	+0.1	−0.1	+0.1	+0.1	0.0	0.0	−0.1	−0.1	−0.1	−0.2	+0.1	+0.1	+0.1	0.0	+0.2	+0.2	+0.1	0.0	−0.1	−0.1	−0.2	−0.2	+0.1	+0.2	+0.1	+0.1
PDF eigenvector 13	0.0	0.0	0.0	−0.1	+0.1	+0.1	0.0	0.0	−0.1	0.0	0.0	0.0	−0.1	0.0	0.0	−0.1	+0.2	+0.1	0.0	−0.1	−0.1	0.0	0.0	0.0	−0.2	0.0	0.0	0.0	+0.3	+0.2	0.0	−0.1	−0.1	−0.1	0.0	+0.1
	0.0	0.0	0.0	+0.1	−0.1	−0.1	0.0	0.0	+0.1	0.0	0.0	0.0	+0.1	0.0	0.0	+0.1	−0.2	−0.1	0.0	+0.1	+0.1	0.0	0.0	0.0	+0.1	0.0	0.0	0.0	−0.3	−0.2	0.0	+0.1	+0.1	+0.1	0.0	−0.1
PDF eigenvector 14	0.0	0.0	0.0	0.0	0.0	0.0	0.0	+0.1	0.0	0.0	0.0	0.0	−0.1	0.0	0.0	0.0	+0.1	+0.1	+0.1	+0.1	−0.1	−0.1	−0.1	0.0	−0.1	−0.1	0.0	0.0	+0.1	+0.1	+0.1	+0.1	−0.1	−0.1	−0.1	0.0
	0.0	0.0	0.0	0.0	0.0	0.0	0.0	−0.1	+0.1	+0.1	+0.1	0.0	+0.1	+0.1	0.0	0.0	−0.1	−0.1	−0.1	−0.1	+0.1	+0.1	+0.1	0.0	+0.1	+0.1	0.0	0.0	−0.2	−0.1	−0.2	−0.1	+0.1	+0.1	+0.1	0.0
PDF eigenvector 15	0.0	0.0	0.0	0.0	+0.1	0.0	0.0	+0.1	−0.1	−0.1	−0.1	0.0	−0.1	−0.1	0.0	0.0	+0.1	+0.1	+0.1	+0.1	−0.1	−0.1	−0.1	0.0	−0.2	−0.1	0.0	0.0	+0.2	+0.2	+0.2	0.0	−0.1	−0.1	−0.1	0.0
	0.0	0.0	0.0	0.0	0.0	0.0	0.0	0.0	0.0	0.0	0.0	0.0	0.0	0.0	0.0	0.0	0.0	0.0	0.0	0.0	0.0	0.0	0.0	0.0	+0.1	+0.1	0.0	0.0	−0.1	−0.1	−0.1	0.0	0.0	+0.1	0.0	0.0
PDF eigenvector 16	0.0	0.0	0.0	0.0	0.0	0.0	0.0	0.0	0.0	0.0	0.0	0.0	0.0	0.0	0.0	0.0	0.0	0.0	0.0	0.0	0.0	0.0	0.0	0.0	0.0	+0.1	0.0	0.0	0.0	0.0	−0.1	0.0	0.0	0.0	0.0	0.0
	0.0	0.0	0.0	0.0	0.0	0.0	0.0	0.0	0.0	0.0	0.0	0.0	0.0	0.0	0.0	0.0	0.0	0.0	+0.1	0.0	0.0	0.0	0.0	0.0	−0.1	−0.1	0.0	0.0	0.0	0.0	+0.1	+0.1	0.0	0.0	−0.1	0.0
PDF eigenvector 17	0.0	0.0	0.0	0.0	0.0	0.0	0.0	0.0	0.0	0.0	0.0	0.0	0.0	0.0	0.0	0.0	0.0	0.0	+0.1	+0.1	0.0	0.0	0.0	0.0	−0.1	−0.1	0.0	0.0	0.0	0.0	+0.1	+0.1	0.0	0.0	−0.1	0.0
	0.0	0.0	0.0	−0.1	0.0	0.0	0.0	−0.1	0.0	+0.1	0.0	0.0	+0.1	+0.1	0.0	−0.1	0.0	0.0	−0.1	−0.1	0.0	+0.1	+0.1	+0.1	+0.1	+0.2	0.0	0.0	−0.1	−0.1	−0.2	−0.1	+0.1	+0.1	+0.1	+0.1
PDF eigenvector 18	0.0	0.0	0.0	0.0	−0.1	−0.1	−0.1	−0.1	+0.1	+0.1	+0.1	0.0	+0.2	+0.1	0.0	0.0	−0.3	−0.2	−0.1	0.0	+0.2	+0.1	+0.1	+0.1	+0.3	+0.2	+0.1	0.0	−0.4	−0.4	−0.2	0.0	+0.3	+0.2	+0.2	0.0
	0.0	0.0	0.0	0.0	+0.1	+0.1	0.0	+0.1	−0.1	−0.1	−0.1	0.0	−0.1	0.0	0.0	0.0	+0.3	+0.2	+0.1	0.0	−0.1	−0.1	−0.1	0.0	−0.3	−0.2	0.0	0.0	+0.4	+0.3	+0.2	0.0	−0.2	−0.2	−0.2	0.0
PDF eigenvector 19	+0.1	+0.1	0.0	0.0	−0.1	0.0	0.0	−0.2	+0.1	+0.1	+0.1	−0.2	+0.1	+0.1	0.0	0.0	−0.2	−0.1	−0.2	−0.2	+0.1	+0.1	+0.2	0.0	+0.2	+0.3	+0.1	0.0	−0.2	−0.2	−0.3	−0.2	+0.2	+0.2	+0.2	+0.1
	−0.1	−0.1	0.0	0.0	+0.1	+0.1	+0.1	+0.3	−0.2	−0.2	−0.2	+0.3	−0.2	−0.2	0.0	0.0	+0.2	+0.2	+0.3	+0.3	−0.2	−0.2	−0.2	0.0	−0.4	−0.4	−0.2	0.0	+0.4	+0.3	+0.5	+0.3	−0.3	−0.4	−0.3	−0.2
PDF eigenvector 20	0.0	0.0	0.0	0.0	0.0	0.0	0.0	−0.1	0.0	0.0	+0.1	0.0	0.0	+0.1	−0.1	0.0	0.0	0.0	−0.1	0.0	0.0	0.0	+0.1	0.0	−0.1	−0.1	−0.3	0.0	−0.1	0.0	+0.1	0.0	+0.1	+0.1	0.0	−0.4
	0.0	0.0	0.0	0.0	0.0	0.0	0.0	+0.1	−0.1	−0.1	−0.1	0.0	−0.1	−0.1	0.0	0.0	+0.1	+0.1	+0.1	+0.1	−0.1	−0.1	−0.1	0.0	−0.1	−0.1	0.0	0.0	+0.1	+0.1	+0.1	+0.1	−0.1	−0.1	−0.1	0.0
PDF eigenvector 21	0.0	−0.1	0.0	+0.1	−0.1	−0.1	0.0	+0.1	0.0	0.0	0.0	+0.1	0.0	−0.1	0.0	+0.1	−0.2	−0.1	0.0	+0.2	0.0	0.0	0.0	0.0	+0.1	0.0	0.0	0.0	−0.2	−0.2	+0.1	+0.2	+0.1	0.0	0.0	−0.1
	0.0	+0.1	0.0	−0.1	+0.1	+0.1	0.0	−0.1	0.0	0.0	0.0	−0.1	0.0	+0.1	0.0	−0.1	+0.2	+0.1	−0.1	−0.2	0.0	0.0	0.0	0.0	−0.1	+0.1	+0.1	0.0	+0.2	+0.1	−0.1	−0.2	0.0	0.0	+0.1	+0.1
PDF eigenvector 22	0.0	−0.1	0.0	+0.2	−0.3	−0.2	0.0	+0.2	0.0	0.0	0.0	+0.2	+0.1	−0.1	−0.1	+0.2	−0.4	−0.3	0.0	+0.4	+0.1	+0.1	0.0	0.0	+0.3	0.0	−0.2	−0.1	−0.5	−0.4	+0.2	+0.6	+0.2	+0.1	0.0	−0.4
	+0.1	+0.1	0.0	−0.2	+0.2	+0.1	0.0	−0.2	0.0	0.0	+0.1	−0.2	−0.1	+0.1	+0.1	−0.2	+0.4	+0.2	−0.1	−0.3	−0.1	0.0	0.0	0.0	−0.2	+0.1	+0.1	+0.1	+0.4	+0.3	−0.3	−0.5	−0.1	0.0	+0.1	+0.3
PDF eigenvector 23	−0.1	+0.1	+0.1	−0.1	+0.2	+0.2	+0.1	+0.1	−0.1	−0.1	−0.1	−0.2	−0.2	−0.1	+0.1	−0.1	+0.5	+0.4	+0.2	−0.1	−0.1	−0.2	−0.2	−0.1	−0.5	−0.3	0.0	+0.1	+0.6	+0.6	+0.2	−0.3	−0.3	−0.3	−0.3	+0.1
	0.0	0.0	0.0	0.0	0.0	0.0	0.0	0.0	0.0	0.0	0.0	+0.2	0.0	0.0	−0.1	0.0	0.0	−0.1	0.0	+0.1	0.0	0.0	0.0	+0.1	0.0	0.0	−0.1	0.0	0.0	−0.1	0.0	+0.2	0.0	0.0	0.0	−0.1
PDF eigenvector 24	0.0	0.0	0.0	0.0	0.0	0.0	0.0	+0.1	−0.1	−0.1	0.0	+0.2	−0.1	−0.1	−0.1	0.0	+0.1	0.0	+0.1	+0.1	−0.1	−0.1	0.0	+0.1	−0.2	−0.1	−0.1	0.0	+0.2	+0.1	+0.1	+0.2	−0.2	−0.2	−0.1	−0.1
	−0.1	−0.1	+0.1	+0.1	−0.1	0.0	+0.1	+0.1	0.0	−0.1	−0.1	−0.1	−0.1	−0.2	+0.1	+0.1	−0.1	+0.1	+0.3	+0.1	+0.1	0.0	−0.2	−0.2	−0.1	−0.3	0.0	0.0	0.0	+0.1	+0.3	0.0	0.0	−0.1	−0.2	−0.1
PDF eigenvector 25	−0.1	0.0	+0.1	+0.1	0.0	0.0	+0.1	+0.1	0.0	−0.1	−0.1	−0.1	−0.1	−0.2	+0.1	0.0	0.0	+0.1	+0.2	0.0	0.0	−0.1	−0.2	−0.2	−0.2	−0.3	0.0	0.0	+0.1	+0.2	+0.3	0.0	−0.1	−0.1	−0.2	−0.1
	−0.1	−0.1	0.0	+0.1	+0.1	0.0	+0.1	+0.2	−0.2	−0.2	−0.1	+0.4	−0.2	−0.2	−0.1	+0.1	+0.2	+0.1	+0.2	+0.4	−0.2	−0.2	−0.1	+0.2	−0.4	−0.3	−0.3	−0.1	+0.3	+0.2	+0.3	+0.5	−0.3	−0.3	−0.2	−0.2
PDF eigenvector 26	0.0	0.0	0.0	0.0	0.0	0.0	0.0	0.0	0.0	0.0	0.0	0.0	0.0	0.0	0.0	0.0	+0.1	+0.1	0.0	0.0	0.0	0.0	0.0	0.0	0.0	−0.1	0.0	0.0	0.0	+0.1	+0.1	+0.1	0.0	−0.1	0.0	−0.1	0.0
	0.0	0.0	0.0	0.0	0.0	0.0	0.0	0.0	0.0	0.0	0.0	+0.1	0.0	0.0	0.0	0.0	0.0	0.0	0.0	+0.1	0.0	0.0	0.0	0.0	−0.1	0.0	0.0	0.0	0.0	0.0	+0.1	+0.1	0.0	0.0	0.0	−0.1

Table A.47: Table A.43 continued.

source / bin	1	2	3	4	5	6	7	8	9	10	11	12	13	14	15	16	17	18	19	20	21	22	23	24	25	26	27	28	29	30	31	32	33	34	35	36
PDF eigenvector 27	+0.1	0.0	+0.2	+0.1	−0.1	−0.1	+0.1	−0.3	+0.1	+0.1	+0.1	−0.3	+0.2	0.0	+0.1	+0.2	−0.1	−0.1	0.0	−0.2	+0.2	+0.1	0.0	−0.1	+0.2	+0.1	+0.1	0.0	−0.2	−0.1	−0.1	−0.2	+0.2	+0.2	0.0	−0.1
	0.0	0.0	0.0	0.0	0.0	0.0	0.0	0.0	0.0	0.0	0.0	+0.1	0.0	0.0	0.0	0.0	0.0	0.0	0.0	0.0	0.0	0.0	0.0	0.0	0.0	0.0	0.0	0.0	0.0	0.0	0.0	0.0	0.0	0.0	0.0	0.0
PDF eigenvector 28	0.0	0.0	0.0	0.0	0.0	0.0	0.0	0.0	0.0	0.0	0.0	0.0	0.0	0.0	0.0	0.0	+0.1	0.0	0.0	0.0	0.0	0.0	0.0	0.0	−0.1	−0.1	0.0	0.0	+0.1	+0.1	+0.1	0.0	0.0	0.0	0.0	0.0
	0.0	0.0	−0.1	0.0	0.0	0.0	0.0	+0.1	0.0	0.0	0.0	+0.1	0.0	0.0	0.0	0.0	−0.1	0.0	0.0	+0.1	0.0	0.0	0.0	0.0	+0.1	+0.1	0.0	0.0	−0.1	−0.1	−0.1	+0.1	0.0	0.0	0.0	0.0
α_S	+0.1	0.0	+0.1	0.0	0.0	0.0	0.0	−0.2	0.0	0.0	0.0	−0.1	0.0	0.0	+0.1	+0.1	0.0	0.0	0.0	−0.1	+0.1	0.0	0.0	0.0	0.0	0.0	+0.1	0.0	0.0	0.0	−0.1	−0.2	+0.1	+0.1	0.0	0.0
	−0.1	0.0	−0.1	0.0	0.0	0.0	0.0	+0.2	−0.1	0.0	0.0	+0.2	−0.1	0.0	−0.1	−0.1	0.0	0.0	0.0	+0.2	−0.1	0.0	0.0	0.0	0.0	0.0	−0.1	0.0	0.0	0.0	+0.1	+0.2	−0.1	−0.1	−0.1	0.0
m_t^{MC}	+1.6	−0.1	+0.5	−0.8	−0.6	+0.1	−0.2	−0.3	+0.2	+0.6	+0.1	+0.1	+1.2	+0.4	−1.9	−1.5	−1.2	−0.5	0.0	+0.2	+0.7	−0.5	0.0	+0.5	+1.2	−0.6	+0.5	0.0	+0.1	+1.3	+0.7	−0.3	+0.3	+0.4	−0.3	+0.4
	+0.5	−1.6	−0.9	+0.9	+0.5	+0.9	+0.7	−0.2	−0.5	+0.1	−0.6	−0.3	−0.5	+1.0	−0.8	−0.9	−0.1	+0.2	+0.3	+0.9	+0.3	−1.1	−0.7	+0.6	+0.1	+1.1	−1.4	+1.2	+0.2	−0.4	+1.0	+0.5	+0.1	−0.4	+0.7	−0.4
$\mu_{r,f}$	+0.7	+0.2	+1.3	+0.6	−0.1	−0.3	+0.3	−1.2	+0.4	−0.1	−0.2	−1.8	+0.8	−0.1	+0.7	+0.8	−0.6	−0.5	−0.1	−0.8	+0.5	+0.2	0.0	−0.9	+1.7	+0.9	+1.1	+0.1	−1.2	−1.2	−1.3	−0.7	+1.9	+2.0	+1.6	+0.7
	−0.9	−0.3	−1.5	−0.8	+0.1	+0.2	−0.4	+1.2	−0.3	+0.1	+0.5	+2.7	−1.0	+0.1	−0.8	−0.7	+0.7	+0.6	+0.2	+0.9	−0.5	−0.2	+0.2	+1.4	−2.0	−0.6	−1.3	−0.2	+1.3	+1.1	+1.0	+0.2	−2.4	−2.5	−2.2	−1.2
h_{damp}	+1.4	+0.8	−1.6	−1.0	−0.8	+0.1	−0.4	−0.6	−0.1	+1.4	−0.6	+1.2	+0.5	+4.4	+0.3	−2.3	−3.2	−0.9	+1.3	+0.3	+1.1	−2.1	−0.6	+3.6	+12.0	+2.0	+3.0	+0.7	−3.1	−1.8	+0.3	−2.7	+1.2	−1.5	−2.2	+2.1
	+2.4	−1.7	−2.7	−1.0	−0.4	+1.5	+1.5	+0.6	−1.3	+0.2	−1.3	−1.4	−2.9	−1.8	−4.7	−3.9	−0.6	−0.5	+2.0	+0.4	+2.0	−2.1	+1.4	+2.4	−0.2	+1.1	+2.9	+0.7	−0.3	+0.9	+4.8	+1.2	+3.0	0.0	+1.1	+4.8
PS ISR	−0.2	−1.0	−1.7	−0.1	−0.5	0.0	+0.4	−0.2	−0.7	+0.3	−0.3	−1.7	+6.2	+0.5	−1.2	−1.1	+0.1	−0.6	+0.8	+3.3	+3.7	−0.3	+4.2	+3.2	−0.1	−5.5	+8.7	−9.2	−2.3	+0.2	+0.1	+1.1	−1.6	−2.5	−1.6	−2.6
	+0.8	−1.2	−1.6	−0.9	+0.3	+1.4	+1.5	+0.3	−0.1	+0.1	−0.2	+0.4	+2.0	−2.4	−4.1	−3.3	−0.5	−1.0	−0.2	+0.8	−1.4	−3.4	−0.9	−0.2	−1.0	+5.5	+4.6	−2.4	+1.7	−1.5	+1.0	+3.5	+3.1	+1.3	+5.3	+2.3
PS FSR	−1.8	−3.9	−3.3	−1.7	−0.3	+0.6	+1.3	+0.1	−1.3	−0.6	−1.0	−0.3	+1.9	+2.6	−1.0	−2.4	+0.4	+0.7	+1.8	+1.3	+1.1	−1.5	+0.8	+2.0	+5.0	−1.0	+8.5	+5.1	+1.0	+2.5	+4.5	+0.5	+0.3	+1.5	−0.2	−0.6
	+4.1	+1.3	+1.5	+0.4	−0.5	−0.1	+0.2	−0.5	+0.6	+0.8	+0.2	−0.3	+0.9	+1.1	−2.1	−2.4	−1.8	−2.3	−0.3	+0.2	+0.5	−1.0	0.0	−0.7	−3.9	+2.1	+0.5	−1.6	+0.4	−1.8	+0.9	−2.5	0.0	−0.9	+0.3	+2.6
UE tune	+3.6	−1.2	−3.5	0.0	−0.8	+1.1	+1.0	−0.2	0.0	−0.2	−0.8	−1.9	+3.9	+2.8	−2.3	−3.9	−3.0	−1.4	+1.5	+2.2	+1.3	−1.3	+0.8	+2.6	+4.5	+3.9	+11.7	−1.8	−0.7	−3.7	+2.1	+1.2	0.0	−0.3	0.0	−0.9
	+2.7	0.0	−2.7	−1.1	+0.4	+0.6	+1.1	−0.2	−0.5	+1.1	−1.0	+0.4	−1.1	+1.8	−4.7	−2.8	−0.9	−0.7	−1.2	+2.6	+0.1	−1.0	−0.4	+1.3	+0.4	−0.3	−1.1	−2.8	+1.3	+1.4	+1.4	+2.6	−0.1	−0.7	+2.6	−0.2
colour reconnection	+1.1	+0.6	+0.1	−0.9	−0.6	−0.7	+0.1	−0.1	+0.1	+0.4	−1.1	−0.8	+1.6	+2.7	−2.1	−4.4	+0.2	−1.8	−0.3	+2.1	+0.7	−1.6	+1.6	+2.5	+5.5	+1.1	−0.8	+2.2	−1.8	−0.2	+1.1	−1.3	+1.1	+0.1	−0.6	+2.3
	+3.0	+0.6	+1.0	+0.1	0.0	+1.5	+1.6	+0.5	+0.3	+1.8	+0.2	+0.2	+1.0	−0.4	−2.6	−3.8	−2.4	−2.7	−0.9	+0.7	+1.5	−2.5	+1.5	+0.9	+5.9	+3.9	−0.8	+0.9	−4.1	−4.4	−4.6	−4.4	−0.6	−2.3	+0.4	−0.5
	+2.5	−1.6	−1.1	−0.2	+0.1	+0.5	+0.9	+0.6	−0.2	+1.7	−0.5	−0.2	+2.4	+1.4	−0.8	−1.7	−3.2	−1.9	0.0	+1.1	−0.1	−1.2	+1.1	−0.4	−0.1	−1.9	+1.7	+0.1	−0.4	−1.2	−0.5	−2.8	+0.9	+1.2	−0.3	+1.7
fragmentation b → B	+1.3	+0.7	+1.2	+0.4	+0.3	+0.1	+0.3	−0.7	+0.1	−0.4	−0.4	−1.0	+0.5	+0.6	+0.4	+0.4	+0.1	+0.3	+0.2	−0.6	+0.2	−0.4	−0.5	−0.6	−1.1	+1.8	−0.3	−0.5	+0.5	+0.4	+0.1	−0.6	−0.3	−0.4	−0.9	−0.6
	−0.7	−0.4	−0.6	−0.3	−0.2	−0.1	−0.1	+0.3	0.0	+0.2	+0.3	+0.5	−0.2	−0.4	−0.4	−0.3	0.0	−0.2	0.0	+0.3	−0.1	+0.2	+0.3	+0.4	+0.4	−1.1	−0.1	+0.3	−0.3	−0.1	−0.1	+0.1	+0.2	+0.2	+0.6	+0.4
	+0.2	+0.1	+0.2	+0.1	0.0	0.0	0.0	−0.1	0.0	0.0	−0.1	−0.2	0.0	0.0	0.0	+0.1	0.0	0.0	0.0	−0.1	+0.1	−0.1	−0.1	−0.1	−0.3	+0.3	−0.1	−0.1	+0.1	+0.1	0.0	−0.2	0.0	−0.1	−0.1	−0.1
	+1.4	+0.8	+1.2	+0.6	+0.1	+0.1	+0.1	−0.6	−0.3	−0.5	−0.6	−1.1	+1.6	+1.0	+1.1	+1.1	+0.2	+0.3	+0.4	−0.2	−0.3	−0.5	−0.9	−0.8	+0.5	+1.7	+0.8	+1.0	+0.3	+0.4	−0.2	−0.7	−0.5	−1.1	−1.1	−0.9
branching ratio B → μ	−0.2	−0.2	−0.2	−0.1	+0.1	+0.1	+0.1	0.0	+0.1	0.0	+0.1	+0.1	−0.4	−0.3	−0.3	−0.2	+0.2	+0.1	+0.1	+0.1	0.0	+0.1	0.0	0.0	−0.4	−0.4	0.0	0.0	+0.3	−0.1	+0.1	−0.2	0.0	0.0	+0.1	0.0
	+0.4	+0.3	+0.4	+0.2	−0.1	−0.1	−0.2	−0.1	−0.1	−0.1	−0.1	−0.1	+0.6	+0.4	+0.5	+0.3	−0.2	−0.2	−0.2	−0.2	−0.1	−0.1	−0.1	0.0	+0.7	+0.7	+0.4	+0.2	−0.1	−0.2	−0.2	−0.1	−0.1	0.0	−0.1	−0.1

B Additional details and plots for α_S and m_t^{pole} extraction using external PDFs

The $\alpha_S(m_Z)$ scans performed using altered scale and m_t^{pole} settings, and CT14, HERAPDF2.0, and ABMP16 PDF sets are shown in Fig. B.1.

The m_t^{pole} scans for the same variations are shown in Fig. B.2.

The extracted values of $\alpha_S(m_Z)$ and m_t^{pole} obtained using single-differential cross sections as a function of N_{jet}, $M(t\bar{t})$, and $|y(t\bar{t})|$ are shown in Fig. B.3.

The extracted values of $\alpha_S(m_Z)$ and m_t^{pole} obtained using $[N_{jet}^{0,1,2+}, M(t\bar{t}), y(t\bar{t})]$ triple-differential cross sections are shown in Fig. B.4.

B.1 The α_S and m_t^{pole} extraction using $[p_T(t\bar{t}), M(t\bar{t}), y(t\bar{t})]$ cross sections with two $p_T(t\bar{t})$ bins.

The NLO calculations for inclusive $t\bar{t}$ and $t\bar{t}+1$ jet production with an appropriate jet p_T threshold are used to describe the distribution in the two $p_T(t\bar{t})$ bins. Because the final state of the NLO calculation for $t\bar{t}$ and at least one jet consists of at most two light partons, there can be up to two jets built from these partons, which balance the $t\bar{t}$ transverse momentum. Therefore e.g. for $p_T(t\bar{t}) > 100\,\text{GeV}$ there is at least one jet with $p_T > 50\,\text{GeV}$ in the NLO calculation, and one can use the $t\bar{t}+1$ jet calculation requiring $p_T(t\bar{t}) > 100\,\text{GeV}$ without any requirement on the extra jet (if the jet p_T threshold is not larger than 50 GeV). In this analysis, the jet $p_T > 30\,\text{GeV}$ was found to correspond approximately to $p_T(t\bar{t}) \gtrsim 50\,\text{GeV}$, therefore the boundary of 50 GeV was chosen to split the data into two $p_T(t\bar{t})$ bins. The minimum jet p_T of 25 GeV was used in the NLO calculation for $t\bar{t}+1$ jet production (no selection on jet $|\eta|$), and the predicted events were required to have $p_T(t\bar{t}) > 50\,\text{GeV}$. This calculation was used for the bin with $p_T(t\bar{t}) > 50\,\text{GeV}$, while for the bin with $p_T(t\bar{t}) < 50\,\text{GeV}$ the difference of the predictions for inclusive $t\bar{t}$ production and $t\bar{t}+1$ jet production was used. The extracted values of $\alpha_S(m_Z)$ and m_t^{pole} are shown in Fig. B.5. They are consistent with the nominal ones (shown in Fig. 18) but have slightly larger uncertainties.

C Dependence of measured cross sections on m_t^{MC}

The dependence of the measured $[N_{jet}^{0,1+}, M(t\bar{t}), y(t\bar{t})]$ cross sections on the m_t^{MC} value is shown in Fig. C.1. The cross sections are compared to the same theoretical predictions as in Fig. 16 with different values of m_t^{pole}. Compared to the sensitivity of the theoretical predictions to m_t^{pole}, the dependence of the measured cross sections on m_t^{MC} is negligible.

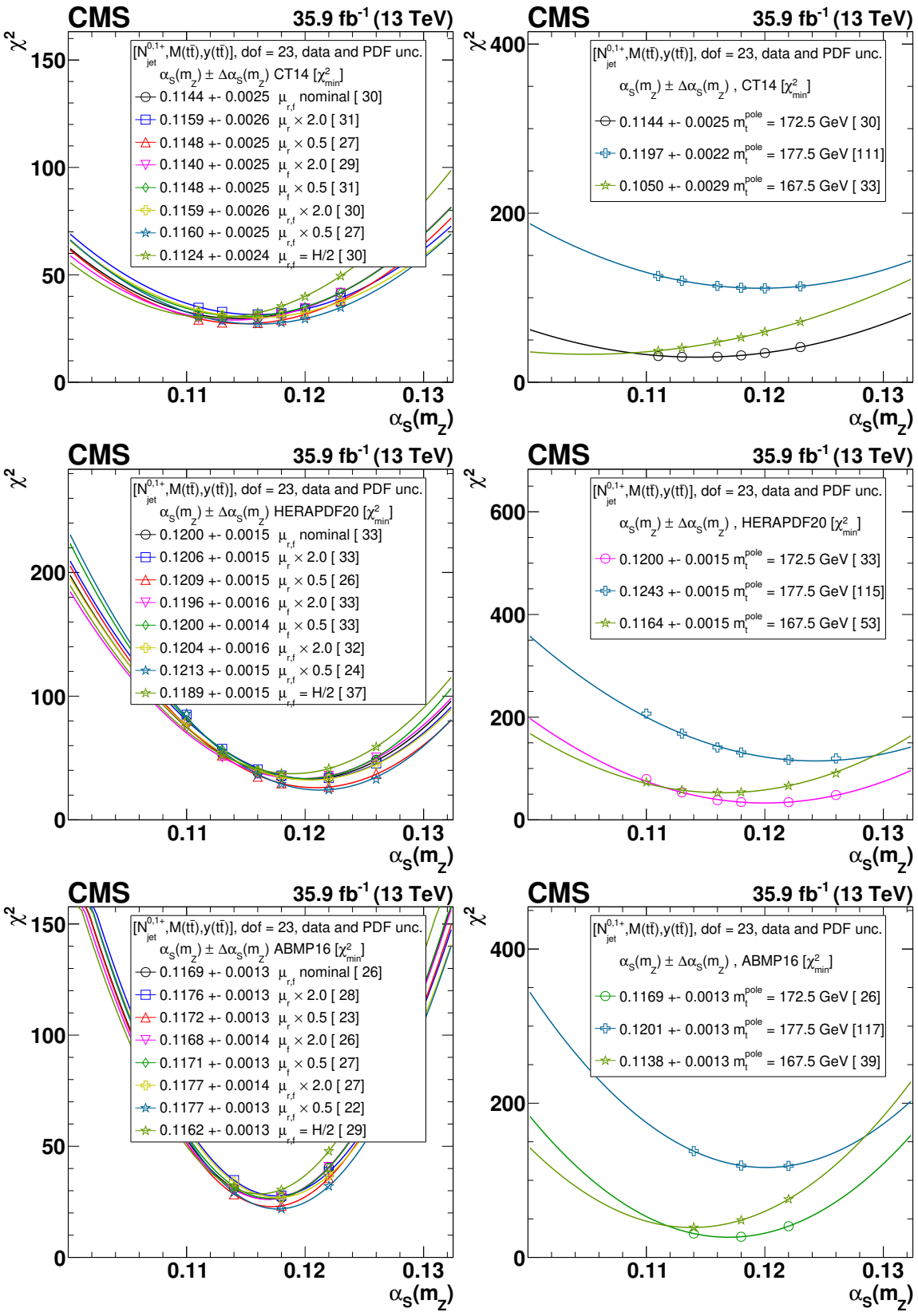

Figure B.1: The $\alpha_S(m_Z)$ extraction from the measured $[N_{jet}^{0,1+}, M(t\bar{t}), y(t\bar{t})]$ cross sections using varied scale and m_t^{pole} settings, and CT14 (upper), HERAPDF2.0 (middle), and ABMP16 (lower) PDF sets. Details can be found in the caption of Fig. 17.

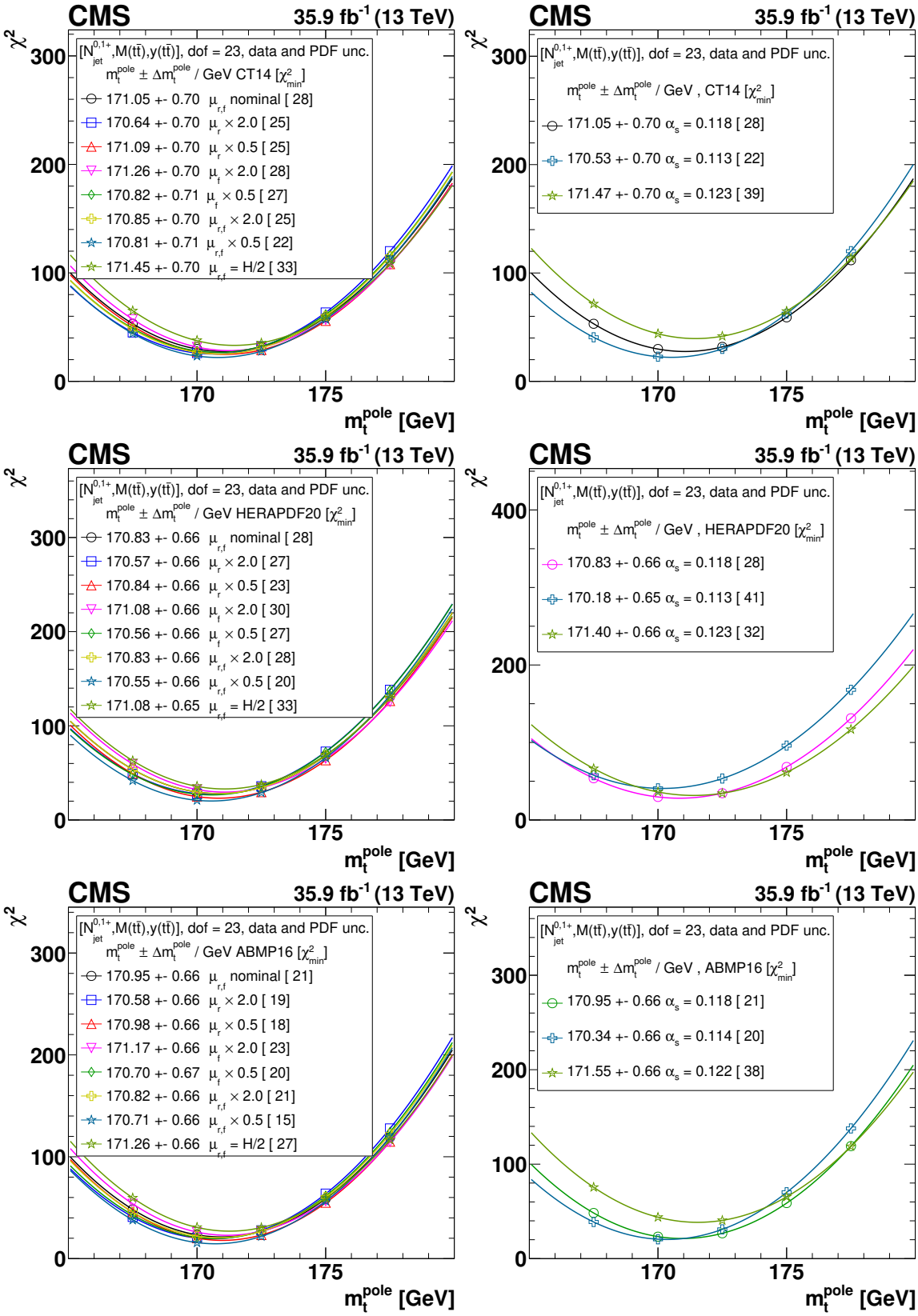

Figure B.2: The m_t^{pole} extraction from the measured $[N_{jet}^{0,1+}, M(t\bar{t}), y(t\bar{t})]$ cross sections using varied scale and $\alpha_S(m_Z)$ settings, and CT14 (upper), HERAPDF2.0 (middle), and ABMP16 (lower) PDF sets. Details can be found in the caption of Fig. 17.

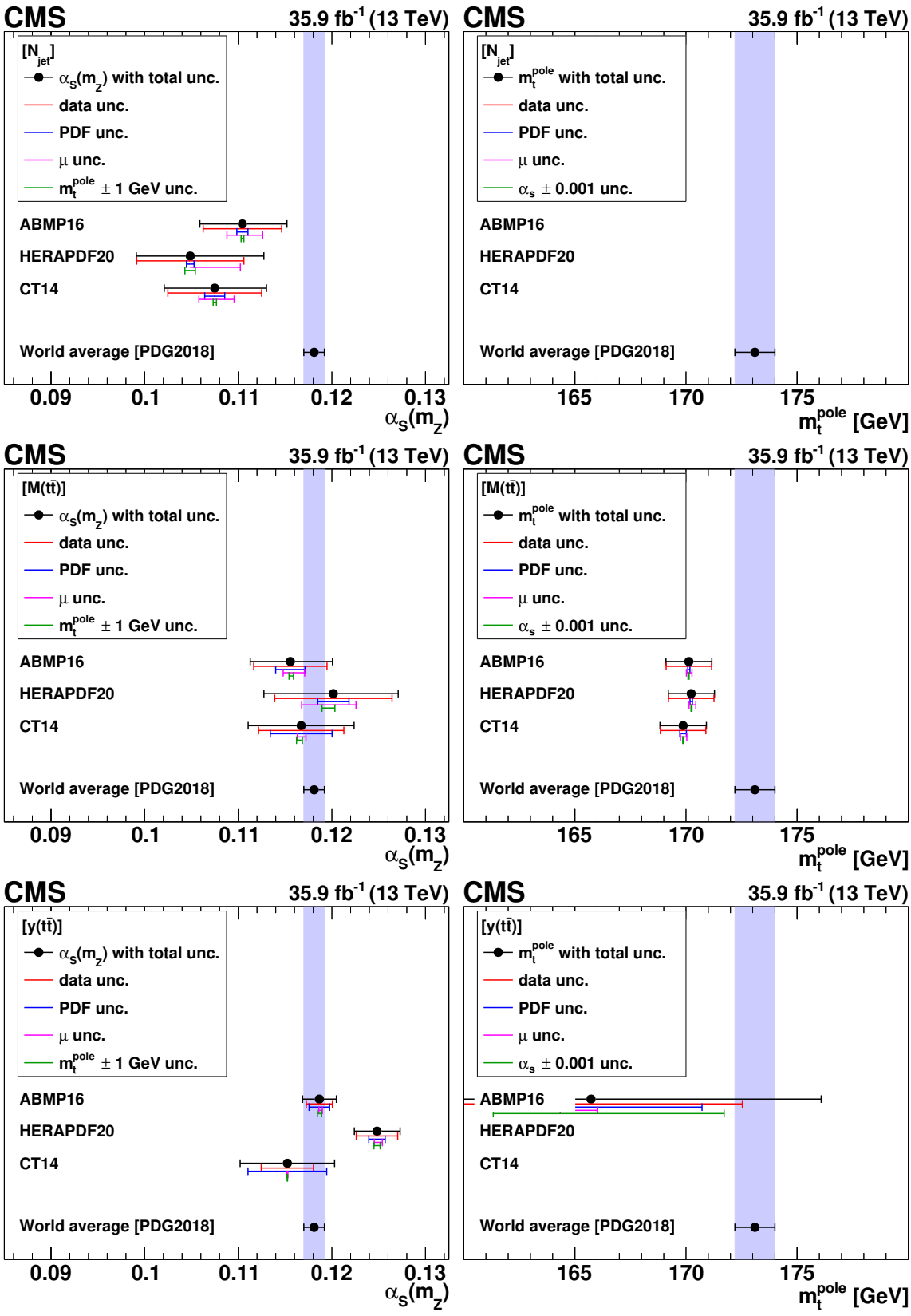

Figure B.3: The $\alpha_S(m_Z)$ (left) and m_t^{pole} (right) values extracted using different single-differential cross sections, for N_{jet} (upper), $M(t\bar{t})$ (middle), and $|y(t\bar{t})|$ (lower) measurements. For central values outside the displayed m_t^{pole} range, no result is shown. Details can be found in the caption of Fig. 18.

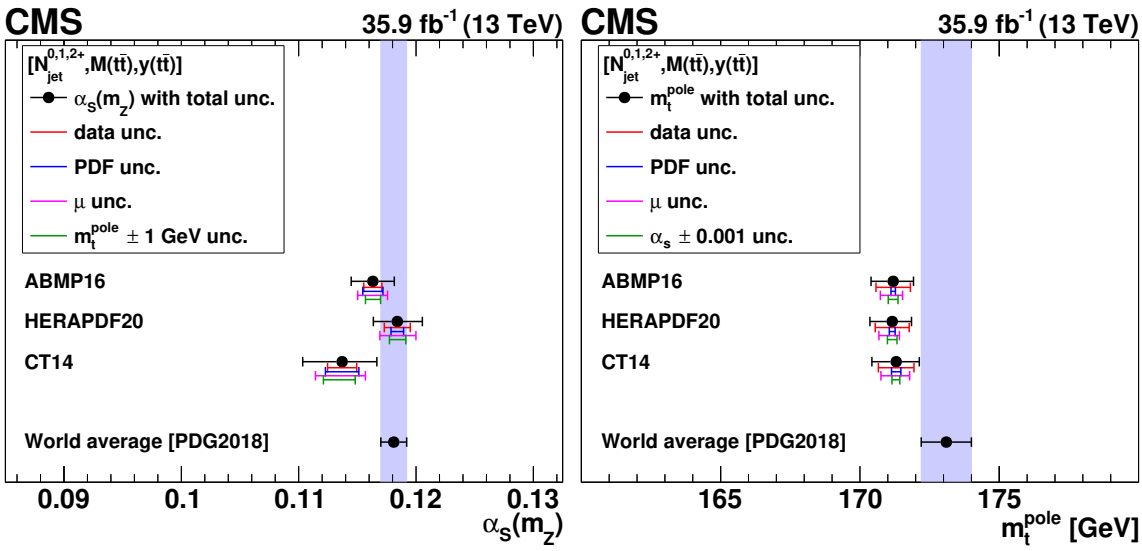

Figure B.4: The $\alpha_S(m_Z)$ (left) and m_t^{pole} (right) values extracted from the triple-differential $[N_{jet}^{0,1,2+}, M(t\bar{t}), y(t\bar{t})]$ cross sections. Details can be found in the caption of Fig. 18.

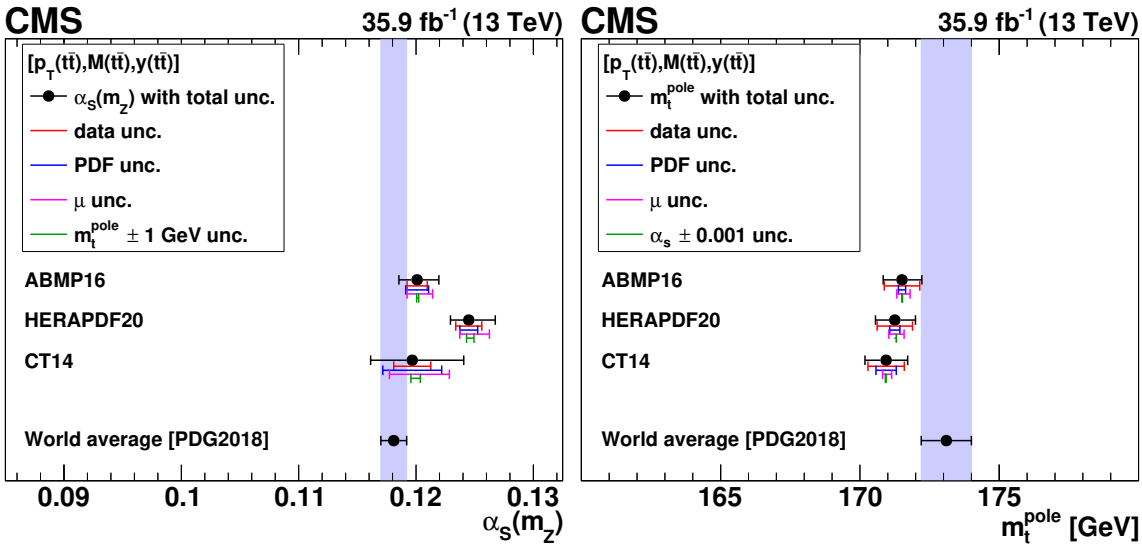

Figure B.5: The $\alpha_S(m_Z)$ (left) and m_t^{pole} (right) values extracted from the triple-differential $[p_T(t\bar{t}), M(t\bar{t}), y(t\bar{t})]$ cross sections. Details can be found in the caption of Fig. 18.

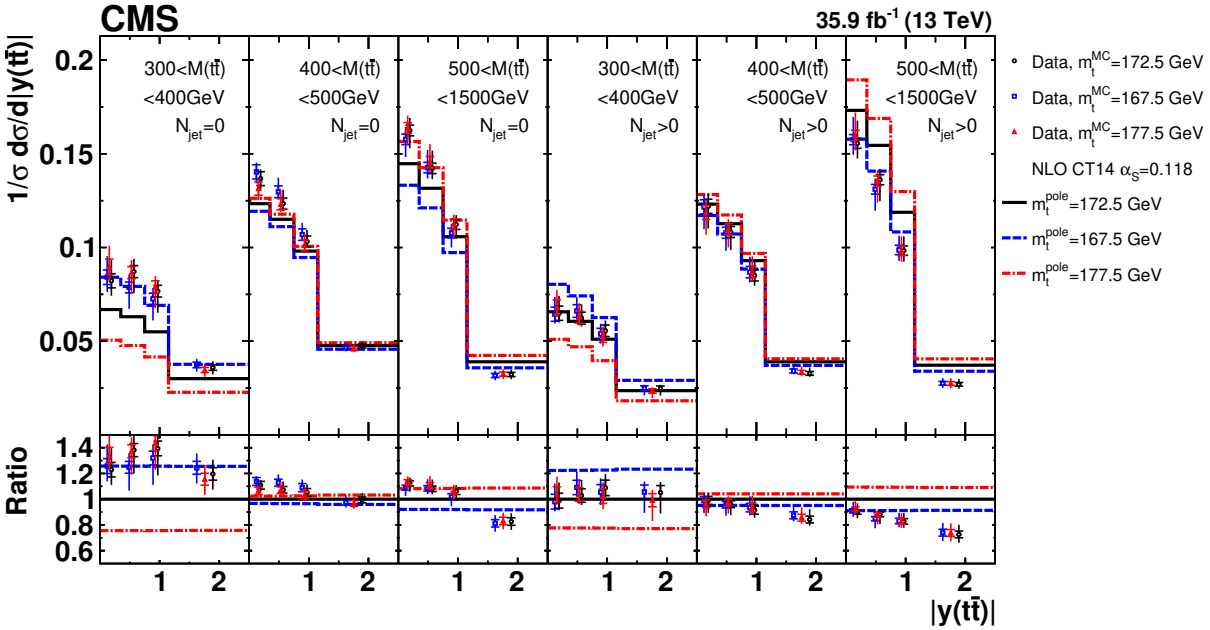

Figure C.1: Comparison of the measured $[N_{\text{jet}}^{0,1+}, M(\text{t}\bar{\text{t}}), y(\text{t}\bar{\text{t}})]$ cross sections obtained using different values of m_{t}^{MC} to NLO predictions obtained using different $m_{\text{t}}^{\text{pole}}$ values (further details can be found in Fig. 3).

D The CMS Collaboration

Yerevan Physics Institute, Yerevan, Armenia
A.M. Sirunyan, A. Tumasyan

Institut für Hochenergiephysik, Wien, Austria
W. Adam, F. Ambrogi, E. Asilar, T. Bergauer, J. Brandstetter, M. Dragicevic, J. Erö, A. Escalante Del Valle, M. Flechl, R. Frühwirth[1], V.M. Ghete, J. Hrubec, M. Jeitler[1], N. Krammer, I. Krätschmer, D. Liko, T. Madlener, I. Mikulec, N. Rad, H. Rohringer, J. Schieck[1], R. Schöfbeck, M. Spanring, D. Spitzbart, W. Waltenberger, J. Wittmann, C.-E. Wulz[1], M. Zarucki

Institute for Nuclear Problems, Minsk, Belarus
V. Chekhovsky, V. Mossolov, J. Suarez Gonzalez

Universiteit Antwerpen, Antwerpen, Belgium
E.A. De Wolf, D. Di Croce, X. Janssen, J. Lauwers, A. Lelek, M. Pieters, H. Van Haevermaet, P. Van Mechelen, N. Van Remortel

Vrije Universiteit Brussel, Brussel, Belgium
F. Blekman, J. D'Hondt, J. De Clercq, K. Deroover, G. Flouris, D. Lontkovskyi, S. Lowette, I. Marchesini, S. Moortgat, L. Moreels, Q. Python, K. Skovpen, S. Tavernier, W. Van Doninck, P. Van Mulders, I. Van Parijs

Université Libre de Bruxelles, Bruxelles, Belgium
D. Beghin, B. Bilin, H. Brun, B. Clerbaux, G. De Lentdecker, H. Delannoy, B. Dorney, G. Fasanella, L. Favart, A. Grebenyuk, A.K. Kalsi, J. Luetic, A. Popov[2], N. Postiau, E. Starling, L. Thomas, C. Vander Velde, P. Vanlaer, D. Vannerom, Q. Wang

Ghent University, Ghent, Belgium
T. Cornelis, D. Dobur, A. Fagot, M. Gul, I. Khvastunov[3], C. Roskas, D. Trocino, M. Tytgat, W. Verbeke, B. Vermassen, M. Vit, N. Zaganidis

Université Catholique de Louvain, Louvain-la-Neuve, Belgium
O. Bondu, G. Bruno, C. Caputo, P. David, C. Delaere, M. Delcourt, A. Giammanco, G. Krintiras, V. Lemaitre, A. Magitteri, K. Piotrzkowski, A. Saggio, M. Vidal Marono, P. Vischia, J. Zobec

Centro Brasileiro de Pesquisas Fisicas, Rio de Janeiro, Brazil
F.L. Alves, G.A. Alves, G. Correia Silva, C. Hensel, A. Moraes, M.E. Pol, P. Rebello Teles

Universidade do Estado do Rio de Janeiro, Rio de Janeiro, Brazil
E. Belchior Batista Das Chagas, W. Carvalho, J. Chinellato[4], E. Coelho, E.M. Da Costa, G.G. Da Silveira[5], D. De Jesus Damiao, C. De Oliveira Martins, S. Fonseca De Souza, L.M. Huertas Guativa, H. Malbouisson, D. Matos Figueiredo, M. Melo De Almeida, C. Mora Herrera, L. Mundim, H. Nogima, W.L. Prado Da Silva, L.J. Sanchez Rosas, A. Santoro, A. Sznajder, M. Thiel, E.J. Tonelli Manganote[4], F. Torres Da Silva De Araujo, A. Vilela Pereira

Universidade Estadual Paulista [a], Universidade Federal do ABC [b], São Paulo, Brazil
S. Ahuja[a], C.A. Bernardes[a], L. Calligaris[a], T.R. Fernandez Perez Tomei[a], E.M. Gregores[b], P.G. Mercadante[b], S.F. Novaes[a], SandraS. Padula[a]

Institute for Nuclear Research and Nuclear Energy, Bulgarian Academy of Sciences, Sofia, Bulgaria
A. Aleksandrov, R. Hadjiiska, P. Iaydjiev, A. Marinov, M. Misheva, M. Rodozov, M. Shopova, G. Sultanov

University of Sofia, Sofia, Bulgaria
A. Dimitrov, L. Litov, B. Pavlov, P. Petkov

Beihang University, Beijing, China
W. Fang[6], X. Gao[6], L. Yuan

Department of Physics, Tsinghua University, Beijing, China
Y. Wang

Institute of High Energy Physics, Beijing, China
M. Ahmad, J.G. Bian, G.M. Chen, H.S. Chen, M. Chen, Y. Chen, C.H. Jiang, D. Leggat, H. Liao, Z. Liu, S.M. Shaheen[7], A. Spiezia, J. Tao, E. Yazgan, H. Zhang, S. Zhang[7], J. Zhao

State Key Laboratory of Nuclear Physics and Technology, Peking University, Beijing, China
Y. Ban, G. Chen, A. Levin, J. Li, L. Li, Q. Li, Y. Mao, S.J. Qian, D. Wang

Universidad de Los Andes, Bogota, Colombia
C. Avila, A. Cabrera, C.A. Carrillo Montoya, L.F. Chaparro Sierra, C. Florez, C.F. González Hernández, M.A. Segura Delgado

Universidad de Antioquia, Medellin, Colombia
J.D. Ruiz Alvarez

University of Split, Faculty of Electrical Engineering, Mechanical Engineering and Naval Architecture, Split, Croatia
N. Godinovic, D. Lelas, I. Puljak, T. Sculac

University of Split, Faculty of Science, Split, Croatia
Z. Antunovic, M. Kovac

Institute Rudjer Boskovic, Zagreb, Croatia
V. Brigljevic, D. Ferencek, K. Kadija, B. Mesic, M. Roguljic, A. Starodumov[8], T. Susa

University of Cyprus, Nicosia, Cyprus
M.W. Ather, A. Attikis, M. Kolosova, G. Mavromanolakis, J. Mousa, C. Nicolaou, F. Ptochos, P.A. Razis, H. Rykaczewski

Charles University, Prague, Czech Republic
M. Finger[9], M. Finger Jr.[9]

Escuela Politecnica Nacional, Quito, Ecuador
E. Ayala

Universidad San Francisco de Quito, Quito, Ecuador
E. Carrera Jarrin

Academy of Scientific Research and Technology of the Arab Republic of Egypt, Egyptian Network of High Energy Physics, Cairo, Egypt
H. Abdalla[10], M.A. Mahmoud[11,12], A. Mohamed[13]

National Institute of Chemical Physics and Biophysics, Tallinn, Estonia
S. Bhowmik, A. Carvalho Antunes De Oliveira, R.K. Dewanjee, K. Ehataht, M. Kadastik, M. Raidal, C. Veelken

Department of Physics, University of Helsinki, Helsinki, Finland
P. Eerola, H. Kirschenmann, J. Pekkanen, M. Voutilainen

Helsinki Institute of Physics, Helsinki, Finland
J. Havukainen, J.K. Heikkilä, T. Järvinen, V. Karimäki, R. Kinnunen, T. Lampén, K. Lassila-Perini, S. Laurila, S. Lehti, T. Lindén, P. Luukka, T. Mäenpää, H. Siikonen, E. Tuominen, J. Tuominiemi

Lappeenranta University of Technology, Lappeenranta, Finland
T. Tuuva

IRFU, CEA, Université Paris-Saclay, Gif-sur-Yvette, France
M. Besancon, F. Couderc, M. Dejardin, D. Denegri, J.L. Faure, F. Ferri, S. Ganjour, A. Givernaud, P. Gras, G. Hamel de Monchenault, P. Jarry, C. Leloup, E. Locci, J. Malcles, J. Rander, A. Rosowsky, M.Ö. Sahin, A. Savoy-Navarro[14], M. Titov

Laboratoire Leprince-Ringuet, CNRS/IN2P3, Ecole Polytechnique, Institut Polytechnique de Paris
C. Amendola, F. Beaudette, P. Busson, C. Charlot, B. Diab, R. Granier de Cassagnac, I. Kucher, A. Lobanov, J. Martin Blanco, C. Martin Perez, M. Nguyen, C. Ochando, G. Ortona, P. Paganini, J. Rembser, R. Salerno, J.B. Sauvan, Y. Sirois, A.G. Stahl Leiton, A. Zabi, A. Zghiche

Université de Strasbourg, CNRS, IPHC UMR 7178, Strasbourg, France
J.-L. Agram[15], J. Andrea, D. Bloch, G. Bourgatte, J.-M. Brom, E.C. Chabert, V. Cherepanov, C. Collard, E. Conte[15], J.-C. Fontaine[15], D. Gelé, U. Goerlach, M. Jansová, A.-C. Le Bihan, N. Tonon, P. Van Hove

Centre de Calcul de l'Institut National de Physique Nucleaire et de Physique des Particules, CNRS/IN2P3, Villeurbanne, France
S. Gadrat

Université de Lyon, Université Claude Bernard Lyon 1, CNRS-IN2P3, Institut de Physique Nucléaire de Lyon, Villeurbanne, France
S. Beauceron, C. Bernet, G. Boudoul, N. Chanon, R. Chierici, D. Contardo, P. Depasse, H. El Mamouni, J. Fay, S. Gascon, M. Gouzevitch, G. Grenier, B. Ille, F. Lagarde, I.B. Laktineh, H. Lattaud, M. Lethuillier, L. Mirabito, S. Perries, V. Sordini, G. Touquet, M. Vander Donckt, S. Viret

Georgian Technical University, Tbilisi, Georgia
A. Khvedelidze[9]

Tbilisi State University, Tbilisi, Georgia
Z. Tsamalaidze[9]

RWTH Aachen University, I. Physikalisches Institut, Aachen, Germany
C. Autermann, L. Feld, M.K. Kiesel, K. Klein, M. Lipinski, M. Preuten, M.P. Rauch, C. Schomakers, J. Schulz, M. Teroerde, B. Wittmer

RWTH Aachen University, III. Physikalisches Institut A, Aachen, Germany
A. Albert, M. Erdmann, S. Erdweg, T. Esch, R. Fischer, S. Ghosh, T. Hebbeker, C. Heidemann, K. Hoepfner, H. Keller, L. Mastrolorenzo, M. Merschmeyer, A. Meyer, P. Millet, S. Mukherjee, A. Novak, T. Pook, A. Pozdnyakov, M. Radziej, H. Reithler, M. Rieger, A. Schmidt, A. Sharma, D. Teyssier, S. Thüer

RWTH Aachen University, III. Physikalisches Institut B, Aachen, Germany
G. Flügge, O. Hlushchenko, T. Kress, T. Müller, A. Nehrkorn, A. Nowack, C. Pistone, O. Pooth, D. Roy, H. Sert, A. Stahl[16]

Deutsches Elektronen-Synchrotron, Hamburg, Germany
M. Aldaya Martin, T. Arndt, C. Asawatangtrakuldee, I. Babounikau, H. Bakhshiansohi, K. Beernaert, O. Behnke, U. Behrens, A. Bermúdez Martínez, D. Bertsche, A.A. Bin Anuar, K. Borras[17], V. Botta, A. Campbell, P. Connor, C. Contreras-Campana, V. Danilov, A. De Wit, M.M. Defranchis, C. Diez Pardos, D. Domínguez Damiani, G. Eckerlin, T. Eichhorn, A. Elwood, E. Eren, E. Gallo[18], A. Geiser, J.M. Grados Luyando, A. Grohsjean, M. Guthoff, M. Haranko, A. Harb, N.Z. Jomhari, H. Jung, M. Kasemann, J. Keaveney, C. Kleinwort, J. Knolle, D. Krücker, W. Lange, T. Lenz, J. Leonard, K. Lipka, W. Lohmann[19], R. Mankel, I.-A. Melzer-Pellmann, A.B. Meyer, M. Meyer, M. Missiroli, G. Mittag, J. Mnich, V. Myronenko, S.K. Pflitsch, D. Pitzl, A. Raspereza, A. Saibel, M. Savitskyi, P. Saxena, P. Schütze, C. Schwanenberger, R. Shevchenko, A. Singh, H. Tholen, O. Turkot, A. Vagnerini, M. Van De Klundert, G.P. Van Onsem, R. Walsh, Y. Wen, K. Wichmann, C. Wissing, O. Zenaiev

University of Hamburg, Hamburg, Germany
R. Aggleton, S. Bein, L. Benato, A. Benecke, V. Blobel, T. Dreyer, A. Ebrahimi, E. Garutti, D. Gonzalez, P. Gunnellini, J. Haller, A. Hinzmann, A. Karavdina, G. Kasieczka, R. Klanner, R. Kogler, N. Kovalchuk, S. Kurz, V. Kutzner, J. Lange, D. Marconi, J. Multhaup, M. Niedziela, C.E.N. Niemeyer, D. Nowatschin, A. Perieanu, A. Reimers, O. Rieger, C. Scharf, P. Schleper, S. Schumann, J. Schwandt, J. Sonneveld, H. Stadie, G. Steinbrück, F.M. Stober, M. Stöver, B. Vormwald, I. Zoi

Karlsruher Institut fuer Technologie, Karlsruhe, Germany
M. Akbiyik, C. Barth, M. Baselga, S. Baur, T. Berger, E. Butz, R. Caspart, T. Chwalek, W. De Boer, A. Dierlamm, K. El Morabit, N. Faltermann, M. Giffels, M.A. Harrendorf, F. Hartmann[16], U. Husemann, I. Katkov[2], S. Kudella, S. Mitra, M.U. Mozer, Th. Müller, M. Musich, G. Quast, K. Rabbertz, M. Schröder, I. Shvetsov, H.J. Simonis, R. Ulrich, M. Weber, C. Wöhrmann, R. Wolf

Institute of Nuclear and Particle Physics (INPP), NCSR Demokritos, Aghia Paraskevi, Greece
G. Anagnostou, G. Daskalakis, T. Geralis, A. Kyriakis, D. Loukas, G. Paspalaki

National and Kapodistrian University of Athens, Athens, Greece
A. Agapitos, G. Karathanasis, P. Kontaxakis, A. Panagiotou, I. Papavergou, N. Saoulidou, K. Vellidis

National Technical University of Athens, Athens, Greece
G. Bakas, K. Kousouris, I. Papakrivopoulos, G. Tsipolitis

University of Ioánnina, Ioánnina, Greece
I. Evangelou, C. Foudas, P. Gianneios, P. Katsoulis, P. Kokkas, S. Mallios, K. Manitara, N. Manthos, I. Papadopoulos, E. Paradas, J. Strologas, F.A. Triantis, D. Tsitsonis

MTA-ELTE Lendület CMS Particle and Nuclear Physics Group, Eötvös Loránd University, Budapest, Hungary
M. Bartók[20], M. Csanad, N. Filipovic, P. Major, K. Mandal, A. Mehta, M.I. Nagy, G. Pasztor, O. Surányi, G.I. Veres

Wigner Research Centre for Physics, Budapest, Hungary
G. Bencze, C. Hajdu, D. Horvath[21], Á. Hunyadi, F. Sikler, T.Á. Vámi, V. Veszpremi, G. Vesztergombi[†]

Institute of Nuclear Research ATOMKI, Debrecen, Hungary
N. Beni, S. Czellar, J. Karancsi[20], A. Makovec, J. Molnar, Z. Szillasi

Institute of Physics, University of Debrecen, Debrecen, Hungary
P. Raics, Z.L. Trocsanyi, B. Ujvari

Indian Institute of Science (IISc), Bangalore, India
S. Choudhury, J.R. Komaragiri, P.C. Tiwari

National Institute of Science Education and Research, HBNI, Bhubaneswar, India
S. Bahinipati[23], C. Kar, P. Mal, A. Nayak[24], S. Roy Chowdhury, D.K. Sahoo[23], S.K. Swain

Panjab University, Chandigarh, India
S. Bansal, S.B. Beri, V. Bhatnagar, S. Chauhan, R. Chawla, N. Dhingra, R. Gupta, A. Kaur, M. Kaur, S. Kaur, P. Kumari, M. Lohan, M. Meena, K. Sandeep, S. Sharma, J.B. Singh, A.K. Virdi, G. Walia

University of Delhi, Delhi, India
A. Bhardwaj, B.C. Choudhary, R.B. Garg, M. Gola, S. Keshri, Ashok Kumar, S. Malhotra, M. Naimuddin, P. Priyanka, K. Ranjan, Aashaq Shah, R. Sharma

Saha Institute of Nuclear Physics, HBNI, Kolkata, India
R. Bhardwaj[25], M. Bharti[25], R. Bhattacharya, S. Bhattacharya, U. Bhawandeep[25], D. Bhowmik, S. Dey, S. Dutt[25], S. Dutta, S. Ghosh, M. Maity[26], K. Mondal, S. Nandan, A. Purohit, P.K. Rout, A. Roy, G. Saha, S. Sarkar, T. Sarkar[26], M. Sharan, B. Singh[25], S. Thakur[25]

Indian Institute of Technology Madras, Madras, India
P.K. Behera, A. Muhammad

Bhabha Atomic Research Centre, Mumbai, India
R. Chudasama, D. Dutta, V. Jha, V. Kumar, D.K. Mishra, P.K. Netrakanti, L.M. Pant, P. Shukla, P. Suggisetti

Tata Institute of Fundamental Research-A, Mumbai, India
T. Aziz, M.A. Bhat, S. Dugad, G.B. Mohanty, N. Sur, RavindraKumar Verma

Tata Institute of Fundamental Research-B, Mumbai, India
S. Banerjee, S. Bhattacharya, S. Chatterjee, P. Das, M. Guchait, Sa. Jain, S. Karmakar, S. Kumar, G. Majumder, K. Mazumdar, N. Sahoo

Indian Institute of Science Education and Research (IISER), Pune, India
S. Chauhan, S. Dube, V. Hegde, A. Kapoor, K. Kothekar, S. Pandey, A. Rane, A. Rastogi, S. Sharma

Institute for Research in Fundamental Sciences (IPM), Tehran, Iran
S. Chenarani[27], E. Eskandari Tadavani, S.M. Etesami[27], M. Khakzad, M. Mohammadi Najafabadi, M. Naseri, F. Rezaei Hosseinabadi, B. Safarzadeh[28], M. Zeinali

University College Dublin, Dublin, Ireland
M. Felcini, M. Grunewald

INFN Sezione di Bari [a], Università di Bari [b], Politecnico di Bari [c], Bari, Italy
M. Abbrescia[a,b], C. Calabria[a,b], A. Colaleo[a], D. Creanza[a,c], L. Cristella[a,b], N. De Filippis[a,c], M. De Palma[a,b], A. Di Florio[a,b], F. Errico[a,b], L. Fiore[a], A. Gelmi[a,b], G. Iaselli[a,c], M. Ince[a,b], S. Lezki[a,b], G. Maggi[a,c], M. Maggi[a], G. Miniello[a,b], S. My[a,b], S. Nuzzo[a,b], A. Pompili[a,b], G. Pugliese[a,c], R. Radogna[a], A. Ranieri[a], G. Selvaggi[a,b], L. Silvestris[a], R. Venditti[a], P. Verwilligen[a]

INFN Sezione di Bologna [a], Università di Bologna [b], Bologna, Italy
G. Abbiendi[a], C. Battilana[a,b], D. Bonacorsi[a,b], L. Borgonovi[a,b], S. Braibant-Giacomelli[a,b], R. Campanini[a,b], P. Capiluppi[a,b], A. Castro[a,b], F.R. Cavallo[a], S.S. Chhibra[a,b], G. Codispoti[a,b], M. Cuffiani[a,b], G.M. Dallavalle[a], F. Fabbri[a], A. Fanfani[a,b], E. Fontanesi, P. Giacomelli[a], C. Grandi[a], L. Guiducci[a,b], F. Iemmi[a,b], S. Lo Meo[a,29], S. Marcellini[a], G. Masetti[a], A. Montanari[a], F.L. Navarria[a,b], A. Perrotta[a], F. Primavera[a,b], A.M. Rossi[a,b], T. Rovelli[a,b], G.P. Siroli[a,b], N. Tosi[a]

INFN Sezione di Catania [a], Università di Catania [b], Catania, Italy
S. Albergo[a,b,30], A. Di Mattia[a], R. Potenza[a,b], A. Tricomi[a,b,30], C. Tuve[a,b]

INFN Sezione di Firenze [a], Università di Firenze [b], Firenze, Italy
G. Barbagli[a], K. Chatterjee[a,b], V. Ciulli[a,b], C. Civinini[a], R. D'Alessandro[a,b], E. Focardi[a,b], G. Latino, P. Lenzi[a,b], M. Meschini[a], S. Paoletti[a], L. Russo[a,31], G. Sguazzoni[a], D. Strom[a], L. Viliani[a]

INFN Laboratori Nazionali di Frascati, Frascati, Italy
L. Benussi, S. Bianco, F. Fabbri, D. Piccolo

INFN Sezione di Genova [a], Università di Genova [b], Genova, Italy
F. Ferro[a], R. Mulargia[a,b], E. Robutti[a], S. Tosi[a,b]

INFN Sezione di Milano-Bicocca [a], Università di Milano-Bicocca [b], Milano, Italy
A. Benaglia[a], A. Beschi[b], F. Brivio[a,b], V. Ciriolo[a,b,16], S. Di Guida[a,b,16], M.E. Dinardo[a,b], S. Fiorendi[a,b], S. Gennai[a], A. Ghezzi[a,b], P. Govoni[a,b], M. Malberti[a,b], S. Malvezzi[a], D. Menasce[a], F. Monti, L. Moroni[a], M. Paganoni[a,b], D. Pedrini[a], S. Ragazzi[a,b], T. Tabarelli de Fatis[a,b], D. Zuolo[a,b]

INFN Sezione di Napoli [a], Università di Napoli 'Federico II' [b], Napoli, Italy, Università della Basilicata [c], Potenza, Italy, Università G. Marconi [d], Roma, Italy
S. Buontempo[a], N. Cavallo[a,c], A. De Iorio[a,b], A. Di Crescenzo[a,b], F. Fabozzi[a,c], F. Fienga[a], G. Galati[a], A.O.M. Iorio[a,b], L. Lista[a], S. Meola[a,d,16], P. Paolucci[a,16], C. Sciacca[a,b], E. Voevodina[a,b]

INFN Sezione di Padova [a], Università di Padova [b], Padova, Italy, Università di Trento [c], Trento, Italy
P. Azzi[a], N. Bacchetta[a], D. Bisello[a,b], A. Boletti[a,b], A. Bragagnolo, R. Carlin[a,b], P. Checchia[a], M. Dall'Osso[a,b], P. De Castro Manzano[a], T. Dorigo[a], U. Dosselli[a], F. Gasparini[a,b], U. Gasparini[a,b], A. Gozzelino[a], S.Y. Hoh, S. Lacaprara[a], P. Lujan, M. Margoni[a,b], A.T. Meneguzzo[a,b], J. Pazzini[a,b], M. Presilla[b], P. Ronchese[a,b], R. Rossin[a,b], F. Simonetto[a,b], A. Tiko, E. Torassa[a], M. Tosi[a,b], M. Zanetti[a,b], P. Zotto[a,b], G. Zumerle[a,b]

INFN Sezione di Pavia [a], Università di Pavia [b], Pavia, Italy
A. Braghieri[a], A. Magnani[a], P. Montagna[a,b], S.P. Ratti[a,b], V. Re[a], M. Ressegotti[a,b], C. Riccardi[a,b], P. Salvini[a], I. Vai[a,b], P. Vitulo[a,b]

INFN Sezione di Perugia [a], Università di Perugia [b], Perugia, Italy
M. Biasini[a,b], G.M. Bilei[a], C. Cecchi[a,b], D. Ciangottini[a,b], L. Fanò[a,b], P. Lariccia[a,b], R. Leonardi[a,b], E. Manoni[a], G. Mantovani[a,b], V. Mariani[a,b], M. Menichelli[a], A. Rossi[a,b], A. Santocchia[a,b], D. Spiga[a]

INFN Sezione di Pisa [a], Università di Pisa [b], Scuola Normale Superiore di Pisa [c], Pisa, Italy
K. Androsov[a], P. Azzurri[a], G. Bagliesi[a], L. Bianchini[a], T. Boccali[a], L. Borrello, R. Castaldi[a], M.A. Ciocci[a,b], R. Dell'Orso[a], G. Fedi[a], F. Fiori[a,c], L. Giannini[a,c], A. Giassi[a], M.T. Grippo[a], F. Ligabue[a,c], E. Manca[a,c], G. Mandorli[a,c], A. Messineo[a,b], F. Palla[a], A. Rizzi[a,b], G. Rolandi[32], A. Scribano[a], P. Spagnolo[a], R. Tenchini[a], G. Tonelli[a,b], A. Venturi[a], P.G. Verdini[a]

INFN Sezione di Roma [a], Sapienza Università di Roma [b], Rome, Italy
L. Barone[a,b], F. Cavallari[a], M. Cipriani[a,b], D. Del Re[a,b], E. Di Marco[a,b], M. Diemoz[a], S. Gelli[a,b], E. Longo[a,b], B. Marzocchi[a,b], P. Meridiani[a], G. Organtini[a,b], F. Pandolfi[a], R. Paramatti[a,b], F. Preiato[a,b], C. Quaranta[a,b], S. Rahatlou[a,b], C. Rovelli[a], F. Santanastasio[a,b]

INFN Sezione di Torino [a], Università di Torino [b], Torino, Italy, Università del Piemonte Orientale [c], Novara, Italy
N. Amapane[a,b], R. Arcidiacono[a,c], S. Argiro[a,b], M. Arneodo[a,c], N. Bartosik[a], R. Bellan[a,b], C. Biino[a], A. Cappati[a,b], N. Cartiglia[a], F. Cenna[a,b], S. Cometti[a], M. Costa[a,b], R. Covarelli[a,b], N. Demaria[a], B. Kiani[a,b], C. Mariotti[a], S. Maselli[a], E. Migliore[a,b], V. Monaco[a,b], E. Monteil[a,b], M. Monteno[a], M.M. Obertino[a,b], L. Pacher[a,b], N. Pastrone[a], M. Pelliccioni[a], G.L. Pinna Angioni[a,b], A. Romero[a,b], M. Ruspa[a,c], R. Sacchi[a,b], R. Salvatico[a,b], K. Shchelina[a,b], V. Sola[a], A. Solano[a,b], D. Soldi[a,b], A. Staiano[a]

INFN Sezione di Trieste [a], Università di Trieste [b], Trieste, Italy
S. Belforte[a], V. Candelise[a,b], M. Casarsa[a], F. Cossutti[a], A. Da Rold[a,b], G. Della Ricca[a,b], F. Vazzoler[a,b], A. Zanetti[a]

Kyungpook National University, Daegu, Korea
D.H. Kim, G.N. Kim, M.S. Kim, J. Lee, S.W. Lee, C.S. Moon, Y.D. Oh, S.I. Pak, S. Sekmen, D.C. Son, Y.C. Yang

Chonnam National University, Institute for Universe and Elementary Particles, Kwangju, Korea
H. Kim, D.H. Moon, G. Oh

Hanyang University, Seoul, Korea
B. Francois, J. Goh[33], T.J. Kim

Korea University, Seoul, Korea
S. Cho, S. Choi, Y. Go, D. Gyun, S. Ha, B. Hong, Y. Jo, K. Lee, K.S. Lee, S. Lee, J. Lim, S.K. Park, Y. Roh

Sejong University, Seoul, Korea
H.S. Kim

Seoul National University, Seoul, Korea
J. Almond, J. Kim, J.S. Kim, H. Lee, K. Lee, S. Lee, K. Nam, S.B. Oh, B.C. Radburn-Smith, S.h. Seo, U.K. Yang, H.D. Yoo, G.B. Yu

University of Seoul, Seoul, Korea
D. Jeon, H. Kim, J.H. Kim, J.S.H. Lee, I.C. Park

Sungkyunkwan University, Suwon, Korea
Y. Choi, C. Hwang, J. Lee, I. Yu

Riga Technical University, Riga, Latvia
V. Veckalns[34]

Vilnius University, Vilnius, Lithuania
V. Dudenas, A. Juodagalvis, J. Vaitkus

National Centre for Particle Physics, Universiti Malaya, Kuala Lumpur, Malaysia
Z.A. Ibrahim, M.A.B. Md Ali[35], F. Mohamad Idris[36], W.A.T. Wan Abdullah, M.N. Yusli, Z. Zolkapli

Universidad de Sonora (UNISON), Hermosillo, Mexico
J.F. Benitez, A. Castaneda Hernandez, J.A. Murillo Quijada

Centro de Investigacion y de Estudios Avanzados del IPN, Mexico City, Mexico
H. Castilla-Valdez, E. De La Cruz-Burelo, M.C. Duran-Osuna, I. Heredia-De La Cruz[37], R. Lopez-Fernandez, J. Mejia Guisao, R.I. Rabadan-Trejo, G. Ramirez-Sanchez, R. Reyes-Almanza, A. Sanchez-Hernandez

Universidad Iberoamericana, Mexico City, Mexico
S. Carrillo Moreno, C. Oropeza Barrera, M. Ramirez-Garcia, F. Vazquez Valencia

Benemerita Universidad Autonoma de Puebla, Puebla, Mexico
J. Eysermans, I. Pedraza, H.A. Salazar Ibarguen, C. Uribe Estrada

Universidad Autónoma de San Luis Potosí, San Luis Potosí, Mexico
A. Morelos Pineda

University of Montenegro, Podgorica, Montenegro
N. Raicevic

University of Auckland, Auckland, New Zealand
D. Krofcheck

University of Canterbury, Christchurch, New Zealand
S. Bheesette, P.H. Butler

National Centre for Physics, Quaid-I-Azam University, Islamabad, Pakistan
A. Ahmad, M. Ahmad, M.I. Asghar, Q. Hassan, H.R. Hoorani, W.A. Khan, M.A. Shah, M. Shoaib, M. Waqas

National Centre for Nuclear Research, Swierk, Poland
H. Bialkowska, M. Bluj, B. Boimska, T. Frueboes, M. Górski, M. Kazana, M. Szleper, P. Traczyk, P. Zalewski

Institute of Experimental Physics, Faculty of Physics, University of Warsaw, Warsaw, Poland
K. Bunkowski, A. Byszuk[38], K. Doroba, A. Kalinowski, M. Konecki, J. Krolikowski, M. Misiura, M. Olszewski, A. Pyskir, M. Walczak

Laboratório de Instrumentação e Física Experimental de Partículas, Lisboa, Portugal
M. Araujo, P. Bargassa, C. Beirão Da Cruz E Silva, A. Di Francesco, P. Faccioli, B. Galinhas, M. Gallinaro, J. Hollar, N. Leonardo, J. Seixas, G. Strong, O. Toldaiev, J. Varela

Joint Institute for Nuclear Research, Dubna, Russia
S. Afanasiev, P. Bunin, M. Gavrilenko, I. Golutvin, I. Gorbunov, A. Kamenev, V. Karjavine, A. Lanev, A. Malakhov, V. Matveev[39,40], P. Moisenz, V. Palichik, V. Perelygin, S. Shmatov, S. Shulha, N. Skatchkov, V. Smirnov, N. Voytishin, A. Zarubin

Petersburg Nuclear Physics Institute, Gatchina (St. Petersburg), Russia
V. Golovtsov, Y. Ivanov, V. Kim[41], E. Kuznetsova[42], P. Levchenko, V. Murzin, V. Oreshkin, I. Smirnov, D. Sosnov, V. Sulimov, L. Uvarov, S. Vavilov, A. Vorobyev

Institute for Nuclear Research, Moscow, Russia
Yu. Andreev, A. Dermenev, S. Gninenko, N. Golubev, A. Karneyeu, M. Kirsanov, N. Krasnikov, A. Pashenkov, A. Shabanov, D. Tlisov, A. Toropin

Institute for Theoretical and Experimental Physics named by A.I. Alikhanov of NRC 'Kurchatov Institute', Moscow, Russia
V. Epshteyn, V. Gavrilov, N. Lychkovskaya, V. Popov, I. Pozdnyakov, G. Safronov, A. Spiridonov, A. Stepennov, V. Stolin, M. Toms, E. Vlasov, A. Zhokin

Moscow Institute of Physics and Technology, Moscow, Russia
T. Aushev

National Research Nuclear University 'Moscow Engineering Physics Institute' (MEPhI), Moscow, Russia
R. Chistov[43], M. Danilov[43], D. Philippov, E. Tarkovskii

P.N. Lebedev Physical Institute, Moscow, Russia
V. Andreev, M. Azarkin, I. Dremin[40], M. Kirakosyan, A. Terkulov

Skobeltsyn Institute of Nuclear Physics, Lomonosov Moscow State University, Moscow, Russia
A. Baskakov, A. Belyaev, E. Boos, V. Bunichev, M. Dubinin[44], L. Dudko, A. Ershov, V. Klyukhin, I. Lokhtin, S. Obraztsov, M. Perfilov, V. Savrin, P. Volkov

Novosibirsk State University (NSU), Novosibirsk, Russia
A. Barnyakov[45], V. Blinov[45], T. Dimova[45], L. Kardapoltsev[45], Y. Skovpen[45]

Institute for High Energy Physics of National Research Centre 'Kurchatov Institute', Protvino, Russia
I. Azhgirey, I. Bayshev, S. Bitioukov, V. Kachanov, A. Kalinin, D. Konstantinov, P. Mandrik, V. Petrov, R. Ryutin, S. Slabospitskii, A. Sobol, S. Troshin, N. Tyurin, A. Uzunian, A. Volkov

National Research Tomsk Polytechnic University, Tomsk, Russia
A. Babaev, S. Baidali, A. Iuzhakov, V. Okhotnikov

University of Belgrade: Faculty of Physics and VINCA Institute of Nuclear Sciences
P. Adzic[46], P. Cirkovic, D. Devetak, M. Dordevic, P. Milenovic[47], J. Milosevic

Centro de Investigaciones Energéticas Medioambientales y Tecnológicas (CIEMAT), Madrid, Spain
J. Alcaraz Maestre, A. Álvarez Fernández, I. Bachiller, M. Barrio Luna, J.A. Brochero Cifuentes, M. Cerrada, N. Colino, B. De La Cruz, A. Delgado Peris, C. Fernandez Bedoya, J.P. Fernández Ramos, J. Flix, M.C. Fouz, O. Gonzalez Lopez, S. Goy Lopez, J.M. Hernandez, M.I. Josa, D. Moran, A. Pérez-Calero Yzquierdo, J. Puerta Pelayo, I. Redondo, L. Romero, S. Sánchez Navas, M.S. Soares, A. Triossi

Universidad Autónoma de Madrid, Madrid, Spain
C. Albajar, J.F. de Trocóniz

Universidad de Oviedo, Instituto Universitario de Ciencias y Tecnologías Espaciales de Asturias (ICTEA), Oviedo, Spain
J. Cuevas, C. Erice, J. Fernandez Menendez, S. Folgueras, I. Gonzalez Caballero, J.R. González Fernández, E. Palencia Cortezon, V. Rodríguez Bouza, S. Sanchez Cruz, J.M. Vizan Garcia

Instituto de Física de Cantabria (IFCA), CSIC-Universidad de Cantabria, Santander, Spain
I.J. Cabrillo, A. Calderon, B. Chazin Quero, J. Duarte Campderros, M. Fernandez, P.J. Fernández Manteca, A. García Alonso, J. Garcia-Ferrero, G. Gomez, A. Lopez Virto,

J. Marco, C. Martinez Rivero, P. Martinez Ruiz del Arbol, F. Matorras, J. Piedra Gomez, C. Prieels, T. Rodrigo, A. Ruiz-Jimeno, L. Scodellaro, N. Trevisani, I. Vila, R. Vilar Cortabitarte

University of Ruhuna, Department of Physics, Matara, Sri Lanka
N. Wickramage

CERN, European Organization for Nuclear Research, Geneva, Switzerland
D. Abbaneo, B. Akgun, E. Auffray, G. Auzinger, P. Baillon, A.H. Ball, D. Barney, J. Bendavid, M. Bianco, A. Bocci, C. Botta, E. Brondolin, T. Camporesi, M. Cepeda, G. Cerminara, E. Chapon, Y. Chen, G. Cucciati, D. d'Enterria, A. Dabrowski, N. Daci, V. Daponte, A. David, A. De Roeck, N. Deelen, M. Dobson, M. Dünser, N. Dupont, A. Elliott-Peisert, F. Fallavollita[48], D. Fasanella, G. Franzoni, J. Fulcher, W. Funk, D. Gigi, A. Gilbert, K. Gill, F. Glege, M. Gruchala, M. Guilbaud, D. Gulhan, J. Hegeman, C. Heidegger, Y. Iiyama, V. Innocente, G.M. Innocenti, A. Jafari, P. Janot, O. Karacheban[19], J. Kieseler, A. Kornmayer, M. Krammer[1], C. Lange, P. Lecoq, C. Lourenço, L. Malgeri, M. Mannelli, A. Massironi, F. Meijers, J.A. Merlin, S. Mersi, E. Meschi, F. Moortgat, M. Mulders, J. Ngadiuba, S. Nourbakhsh, S. Orfanelli, L. Orsini, F. Pantaleo[16], L. Pape, E. Perez, M. Peruzzi, A. Petrilli, G. Petrucciani, A. Pfeiffer, M. Pierini, F.M. Pitters, D. Rabady, A. Racz, M. Rovere, H. Sakulin, C. Schäfer, C. Schwick, M. Selvaggi, A. Sharma, P. Silva, P. Sphicas[49], A. Stakia, J. Steggemann, D. Treille, A. Tsirou, A. Vartak, M. Verzetti, W.D. Zeuner

Paul Scherrer Institut, Villigen, Switzerland
L. Caminada[50], K. Deiters, W. Erdmann, R. Horisberger, Q. Ingram, H.C. Kaestli, D. Kotlinski, U. Langenegger, T. Rohe, S.A. Wiederkehr

ETH Zurich - Institute for Particle Physics and Astrophysics (IPA), Zurich, Switzerland
M. Backhaus, P. Berger, N. Chernyavskaya, G. Dissertori, M. Dittmar, M. Donegà, C. Dorfer, T.A. Gómez Espinosa, C. Grab, D. Hits, T. Klijnsma, W. Lustermann, R.A. Manzoni, M. Marionneau, M.T. Meinhard, F. Micheli, P. Musella, F. Nessi-Tedaldi, F. Pauss, G. Perrin, L. Perrozzi, S. Pigazzini, M. Reichmann, C. Reissel, T. Reitenspiess, D. Ruini, D.A. Sanz Becerra, M. Schönenberger, L. Shchutska, V.R. Tavolaro, K. Theofilatos, M.L. Vesterbacka Olsson, R. Wallny, D.H. Zhu

Universität Zürich, Zurich, Switzerland
T.K. Aarrestad, C. Amsler[51], D. Brzhechko, M.F. Canelli, A. De Cosa, R. Del Burgo, S. Donato, C. Galloni, T. Hreus, B. Kilminster, S. Leontsinis, V.M. Mikuni, I. Neutelings, G. Rauco, P. Robmann, D. Salerno, K. Schweiger, C. Seitz, Y. Takahashi, S. Wertz, A. Zucchetta

National Central University, Chung-Li, Taiwan
T.H. Doan, C.M. Kuo, W. Lin, S.S. Yu

National Taiwan University (NTU), Taipei, Taiwan
P. Chang, Y. Chao, K.F. Chen, P.H. Chen, W.-S. Hou, Y.F. Liu, R.-S. Lu, E. Paganis, A. Psallidas, A. Steen

Chulalongkorn University, Faculty of Science, Department of Physics, Bangkok, Thailand
B. Asavapibhop, N. Srimanobhas, N. Suwonjandee

Çukurova University, Physics Department, Science and Art Faculty, Adana, Turkey
A. Bat, F. Boran, S. Cerci[52], S. Damarseckin[53], Z.S. Demiroglu, F. Dolek, C. Dozen, I. Dumanoglu, G. Gokbulut, EmineGurpinar Guler[54], Y. Guler, I. Hos[55], C. Isik, E.E. Kangal[56], O. Kara, A. Kayis Topaksu, U. Kiminsu, M. Oglakci, G. Onengut, K. Ozdemir[57], S. Ozturk[58], D. Sunar Cerci[52], B. Tali[52], U.G. Tok, S. Turkcapar, I.S. Zorbakir, C. Zorbilmez

Middle East Technical University, Physics Department, Ankara, Turkey
B. Isildak[59], G. Karapinar[60], M. Yalvac, M. Zeyrek

Bogazici University, Istanbul, Turkey
I.O. Atakisi, E. Gülmez, M. Kaya[61], O. Kaya[62], Ö. Özçelik, S. Ozkorucuklu[63], S. Tekten, E.A. Yetkin[64]

Istanbul Technical University, Istanbul, Turkey
A. Cakir, K. Cankocak, Y. Komurcu, S. Sen[65]

Institute for Scintillation Materials of National Academy of Science of Ukraine, Kharkov, Ukraine
B. Grynyov

National Scientific Center, Kharkov Institute of Physics and Technology, Kharkov, Ukraine
L. Levchuk

University of Bristol, Bristol, United Kingdom
F. Ball, J.J. Brooke, D. Burns, E. Clement, D. Cussans, O. Davignon, H. Flacher, J. Goldstein, G.P. Heath, H.F. Heath, L. Kreczko, D.M. Newbold[66], S. Paramesvaran, B. Penning, T. Sakuma, D. Smith, V.J. Smith, J. Taylor, A. Titterton

Rutherford Appleton Laboratory, Didcot, United Kingdom
K.W. Bell, A. Belyaev[67], C. Brew, R.M. Brown, D. Cieri, D.J.A. Cockerill, J.A. Coughlan, K. Harder, S. Harper, J. Linacre, K. Manolopoulos, E. Olaiya, D. Petyt, T. Reis, T. Schuh, C.H. Shepherd-Themistocleous, A. Thea, I.R. Tomalin, T. Williams, W.J. Womersley

Imperial College, London, United Kingdom
R. Bainbridge, P. Bloch, J. Borg, S. Breeze, O. Buchmuller, A. Bundock, D. Colling, P. Dauncey, G. Davies, M. Della Negra, R. Di Maria, P. Everaerts, G. Hall, G. Iles, T. James, M. Komm, C. Laner, L. Lyons, A.-M. Magnan, S. Malik, A. Martelli, V. Milosevic, J. Nash[68], A. Nikitenko[8], V. Palladino, M. Pesaresi, D.M. Raymond, A. Richards, A. Rose, E. Scott, C. Seez, A. Shtipliyski, G. Singh, M. Stoye, T. Strebler, S. Summers, A. Tapper, K. Uchida, T. Virdee[16], N. Wardle, D. Winterbottom, J. Wright, S.C. Zenz

Brunel University, Uxbridge, United Kingdom
J.E. Cole, P.R. Hobson, A. Khan, P. Kyberd, C.K. Mackay, A. Morton, I.D. Reid, L. Teodorescu, S. Zahid

Baylor University, Waco, USA
K. Call, J. Dittmann, K. Hatakeyama, H. Liu, C. Madrid, B. McMaster, N. Pastika, C. Smith

Catholic University of America, Washington, DC, USA
R. Bartek, A. Dominguez

The University of Alabama, Tuscaloosa, USA
A. Buccilli, O. Charaf, S.I. Cooper, C. Henderson, P. Rumerio, C. West

Boston University, Boston, USA
D. Arcaro, T. Bose, Z. Demiragli, D. Gastler, S. Girgis, D. Pinna, C. Richardson, J. Rohlf, D. Sperka, I. Suarez, L. Sulak, D. Zou

Brown University, Providence, USA
G. Benelli, B. Burkle, X. Coubez, D. Cutts, M. Hadley, J. Hakala, U. Heintz, J.M. Hogan[69], K.H.M. Kwok, E. Laird, G. Landsberg, J. Lee, Z. Mao, M. Narain, S. Sagir[70], R. Syarif, E. Usai, D. Yu

University of California, Davis, Davis, USA
R. Band, C. Brainerd, R. Breedon, D. Burns, M. Calderon De La Barca Sanchez, M. Chertok, J. Conway, R. Conway, P.T. Cox, R. Erbacher, C. Flores, G. Funk, W. Ko, O. Kukral, R. Lander, M. Mulhearn, D. Pellett, J. Pilot, M. Shi, D. Stolp, D. Taylor, K. Tos, M. Tripathi, Z. Wang, F. Zhang

University of California, Los Angeles, USA
M. Bachtis, C. Bravo, R. Cousins, A. Dasgupta, A. Florent, J. Hauser, M. Ignatenko, N. Mccoll, S. Regnard, D. Saltzberg, C. Schnaible, V. Valuev

University of California, Riverside, Riverside, USA
E. Bouvier, K. Burt, R. Clare, J.W. Gary, S.M.A. Ghiasi Shirazi, G. Hanson, G. Karapostoli, E. Kennedy, O.R. Long, M. Olmedo Negrete, M.I. Paneva, W. Si, L. Wang, H. Wei, S. Wimpenny, B.R. Yates

University of California, San Diego, La Jolla, USA
J.G. Branson, P. Chang, S. Cittolin, M. Derdzinski, R. Gerosa, D. Gilbert, B. Hashemi, A. Holzner, D. Klein, G. Kole, V. Krutelyov, J. Letts, M. Masciovecchio, S. May, D. Olivito, S. Padhi, M. Pieri, V. Sharma, M. Tadel, J. Wood, F. Würthwein, A. Yagil, G. Zevi Della Porta

University of California, Santa Barbara - Department of Physics, Santa Barbara, USA
N. Amin, R. Bhandari, C. Campagnari, M. Citron, V. Dutta, M. Franco Sevilla, L. Gouskos, R. Heller, J. Incandela, H. Mei, A. Ovcharova, H. Qu, J. Richman, D. Stuart, S. Wang, J. Yoo

California Institute of Technology, Pasadena, USA
D. Anderson, A. Bornheim, J.M. Lawhorn, N. Lu, H.B. Newman, T.Q. Nguyen, J. Pata, M. Spiropulu, J.R. Vlimant, R. Wilkinson, S. Xie, Z. Zhang, R.Y. Zhu

Carnegie Mellon University, Pittsburgh, USA
M.B. Andrews, T. Ferguson, T. Mudholkar, M. Paulini, M. Sun, I. Vorobiev, M. Weinberg

University of Colorado Boulder, Boulder, USA
J.P. Cumalat, W.T. Ford, F. Jensen, A. Johnson, E. MacDonald, T. Mulholland, R. Patel, A. Perloff, K. Stenson, K.A. Ulmer, S.R. Wagner

Cornell University, Ithaca, USA
J. Alexander, J. Chaves, Y. Cheng, J. Chu, A. Datta, K. Mcdermott, N. Mirman, J. Monroy, J.R. Patterson, D. Quach, A. Rinkevicius, A. Ryd, L. Skinnari, L. Soffi, S.M. Tan, Z. Tao, J. Thom, J. Tucker, P. Wittich, M. Zientek

Fermi National Accelerator Laboratory, Batavia, USA
S. Abdullin, M. Albrow, M. Alyari, G. Apollinari, A. Apresyan, A. Apyan, S. Banerjee, L.A.T. Bauerdick, A. Beretvas, J. Berryhill, P.C. Bhat, K. Burkett, J.N. Butler, A. Canepa, G.B. Cerati, H.W.K. Cheung, F. Chlebana, M. Cremonesi, J. Duarte, V.D. Elvira, J. Freeman, Z. Gecse, E. Gottschalk, L. Gray, D. Green, S. Grünendahl, O. Gutsche, J. Hanlon, R.M. Harris, S. Hasegawa, J. Hirschauer, Z. Hu, B. Jayatilaka, S. Jindariani, M. Johnson, U. Joshi, B. Klima, M.J. Kortelainen, B. Kreis, S. Lammel, D. Lincoln, R. Lipton, M. Liu, T. Liu, J. Lykken, K. Maeshima, J.M. Marraffino, D. Mason, P. McBride, P. Merkel, S. Mrenna, S. Nahn, V. O'Dell, K. Pedro, C. Pena, O. Prokofyev, G. Rakness, F. Ravera, A. Reinsvold, L. Ristori, B. Schneider, E. Sexton-Kennedy, A. Soha, W.J. Spalding, L. Spiegel, S. Stoynev, J. Strait, N. Strobbe, L. Taylor, S. Tkaczyk, N.V. Tran, L. Uplegger, E.W. Vaandering, C. Vernieri, M. Verzocchi, R. Vidal, M. Wang, H.A. Weber

University of Florida, Gainesville, USA
D. Acosta, P. Avery, P. Bortignon, D. Bourilkov, A. Brinkerhoff, L. Cadamuro, A. Carnes, D. Curry, R.D. Field, S.V. Gleyzer, B.M. Joshi, J. Konigsberg, A. Korytov, K.H. Lo, P. Ma, K. Matchev, N. Menendez, G. Mitselmakher, D. Rosenzweig, K. Shi, J. Wang, S. Wang, X. Zuo

Florida International University, Miami, USA
Y.R. Joshi, S. Linn

Florida State University, Tallahassee, USA
T. Adams, A. Askew, S. Hagopian, V. Hagopian, K.F. Johnson, R. Khurana, T. Kolberg, G. Martinez, T. Perry, H. Prosper, A. Saha, C. Schiber, R. Yohay

Florida Institute of Technology, Melbourne, USA
M.M. Baarmand, V. Bhopatkar, S. Colafranceschi, M. Hohlmann, D. Noonan, M. Rahmani, T. Roy, M. Saunders, F. Yumiceva

University of Illinois at Chicago (UIC), Chicago, USA
M.R. Adams, L. Apanasevich, D. Berry, R.R. Betts, R. Cavanaugh, X. Chen, S. Dittmer, O. Evdokimov, C.E. Gerber, D.A. Hangal, D.J. Hofman, K. Jung, C. Mills, M.B. Tonjes, N. Varelas, H. Wang, X. Wang, Z. Wu, J. Zhang

The University of Iowa, Iowa City, USA
M. Alhusseini, B. Bilki[54], W. Clarida, K. Dilsiz[71], S. Durgut, R.P. Gandrajula, M. Haytmyradov, V. Khristenko, O.K. Köseyan, J.-P. Merlo, A. Mestvirishvili, A. Moeller, J. Nachtman, H. Ogul[72], Y. Onel, F. Ozok[73], A. Penzo, C. Snyder, E. Tiras, J. Wetzel

Johns Hopkins University, Baltimore, USA
B. Blumenfeld, A. Cocoros, N. Eminizer, D. Fehling, L. Feng, A.V. Gritsan, W.T. Hung, P. Maksimovic, J. Roskes, U. Sarica, M. Swartz, M. Xiao

The University of Kansas, Lawrence, USA
A. Al-bataineh, P. Baringer, A. Bean, S. Boren, J. Bowen, A. Bylinkin, J. Castle, S. Khalil, A. Kropivnitskaya, D. Majumder, W. Mcbrayer, M. Murray, C. Rogan, S. Sanders, E. Schmitz, J.D. Tapia Takaki, Q. Wang

Kansas State University, Manhattan, USA
S. Duric, A. Ivanov, K. Kaadze, D. Kim, Y. Maravin, D.R. Mendis, T. Mitchell, A. Modak, A. Mohammadi

Lawrence Livermore National Laboratory, Livermore, USA
F. Rebassoo, D. Wright

University of Maryland, College Park, USA
A. Baden, O. Baron, A. Belloni, S.C. Eno, Y. Feng, C. Ferraioli, N.J. Hadley, S. Jabeen, G.Y. Jeng, R.G. Kellogg, J. Kunkle, A.C. Mignerey, S. Nabili, F. Ricci-Tam, M. Seidel, Y.H. Shin, A. Skuja, S.C. Tonwar, K. Wong

Massachusetts Institute of Technology, Cambridge, USA
D. Abercrombie, B. Allen, V. Azzolini, A. Baty, R. Bi, S. Brandt, W. Busza, I.A. Cali, M. D'Alfonso, G. Gomez Ceballos, M. Goncharov, P. Harris, D. Hsu, M. Hu, M. Klute, D. Kovalskyi, Y.-J. Lee, P.D. Luckey, B. Maier, A.C. Marini, C. Mcginn, C. Mironov, S. Narayanan, X. Niu, C. Paus, D. Rankin, C. Roland, G. Roland, Z. Shi, G.S.F. Stephans, K. Sumorok, K. Tatar, D. Velicanu, J. Wang, T.W. Wang, B. Wyslouch

University of Minnesota, Minneapolis, USA
A.C. Benvenuti[†], R.M. Chatterjee, A. Evans, P. Hansen, J. Hiltbrand, Sh. Jain, S. Kalafut, M. Krohn, Y. Kubota, Z. Lesko, J. Mans, R. Rusack, M.A. Wadud

University of Mississippi, Oxford, USA
J.G. Acosta, S. Oliveros

University of Nebraska-Lincoln, Lincoln, USA
E. Avdeeva, K. Bloom, D.R. Claes, C. Fangmeier, L. Finco, F. Golf, R. Gonzalez Suarez, R. Kamalieddin, I. Kravchenko, J.E. Siado, G.R. Snow, B. Stieger

State University of New York at Buffalo, Buffalo, USA
A. Godshalk, C. Harrington, I. Iashvili, A. Kharchilava, C. Mclean, D. Nguyen, A. Parker, S. Rappoccio, B. Roozbahani

Northeastern University, Boston, USA
G. Alverson, E. Barberis, C. Freer, Y. Haddad, A. Hortiangtham, G. Madigan, D.M. Morse, T. Orimoto, A. Tishelman-charny, T. Wamorkar, B. Wang, A. Wisecarver, D. Wood

Northwestern University, Evanston, USA
S. Bhattacharya, J. Bueghly, T. Gunter, K.A. Hahn, N. Odell, M.H. Schmitt, K. Sung, M. Trovato, M. Velasco

University of Notre Dame, Notre Dame, USA
R. Bucci, N. Dev, R. Goldouzian, M. Hildreth, K. Hurtado Anampa, C. Jessop, D.J. Karmgard, K. Lannon, W. Li, N. Loukas, N. Marinelli, F. Meng, C. Mueller, Y. Musienko[39], M. Planer, R. Ruchti, P. Siddireddy, G. Smith, S. Taroni, M. Wayne, A. Wightman, M. Wolf, A. Woodard

The Ohio State University, Columbus, USA
J. Alimena, L. Antonelli, B. Bylsma, L.S. Durkin, S. Flowers, B. Francis, C. Hill, W. Ji, A. Lefeld, T.Y. Ling, W. Luo, B.L. Winer

Princeton University, Princeton, USA
S. Cooperstein, G. Dezoort, P. Elmer, J. Hardenbrook, N. Haubrich, S. Higginbotham, A. Kalogeropoulos, S. Kwan, D. Lange, M.T. Lucchini, J. Luo, D. Marlow, K. Mei, I. Ojalvo, J. Olsen, C. Palmer, P. Piroué, J. Salfeld-Nebgen, D. Stickland, C. Tully, Z. Wang

University of Puerto Rico, Mayaguez, USA
S. Malik, S. Norberg

Purdue University, West Lafayette, USA
A. Barker, V.E. Barnes, S. Das, L. Gutay, M. Jones, A.W. Jung, A. Khatiwada, B. Mahakud, D.H. Miller, G. Negro, N. Neumeister, C.C. Peng, S. Piperov, H. Qiu, J.F. Schulte, J. Sun, F. Wang, R. Xiao, W. Xie

Purdue University Northwest, Hammond, USA
T. Cheng, J. Dolen, N. Parashar

Rice University, Houston, USA
Z. Chen, K.M. Ecklund, S. Freed, F.J.M. Geurts, M. Kilpatrick, Arun Kumar, W. Li, B.P. Padley, J. Roberts, J. Rorie, W. Shi, Z. Tu, A. Zhang

University of Rochester, Rochester, USA
A. Bodek, P. de Barbaro, R. Demina, Y.t. Duh, J.L. Dulemba, C. Fallon, T. Ferbel, M. Galanti, A. Garcia-Bellido, J. Han, O. Hindrichs, A. Khukhunaishvili, E. Ranken, P. Tan, R. Taus

Rutgers, The State University of New Jersey, Piscataway, USA
B. Chiarito, J.P. Chou, Y. Gershtein, E. Halkiadakis, A. Hart, M. Heindl, E. Hughes, S. Kaplan, S. Kyriacou, I. Laflotte, A. Lath, R. Montalvo, K. Nash, M. Osherson, H. Saka, S. Salur, S. Schnetzer, D. Sheffield, S. Somalwar, R. Stone, S. Thomas, P. Thomassen

University of Tennessee, Knoxville, USA
H. Acharya, A.G. Delannoy, J. Heideman, G. Riley, S. Spanier

Texas A&M University, College Station, USA
O. Bouhali[74], A. Celik, M. Dalchenko, M. De Mattia, A. Delgado, S. Dildick, R. Eusebi, J. Gilmore, T. Huang, T. Kamon[75], S. Luo, D. Marley, R. Mueller, D. Overton, L. Perniè, D. Rathjens, A. Safonov

Texas Tech University, Lubbock, USA
N. Akchurin, J. Damgov, F. De Guio, P.R. Dudero, S. Kunori, K. Lamichhane, S.W. Lee, T. Mengke, S. Muthumuni, T. Peltola, S. Undleeb, I. Volobouev, Z. Wang, A. Whitbeck

Vanderbilt University, Nashville, USA
S. Greene, A. Gurrola, R. Janjam, W. Johns, C. Maguire, A. Melo, H. Ni, K. Padeken, F. Romeo, P. Sheldon, S. Tuo, J. Velkovska, M. Verweij, Q. Xu

University of Virginia, Charlottesville, USA
M.W. Arenton, P. Barria, B. Cox, R. Hirosky, M. Joyce, A. Ledovskoy, H. Li, C. Neu, Y. Wang, E. Wolfe, F. Xia

Wayne State University, Detroit, USA
R. Harr, P.E. Karchin, N. Poudyal, J. Sturdy, P. Thapa, S. Zaleski

University of Wisconsin - Madison, Madison, WI, USA
J. Buchanan, C. Caillol, D. Carlsmith, S. Dasu, I. De Bruyn, L. Dodd, B. Gomber[76], M. Grothe, M. Herndon, A. Hervé, U. Hussain, P. Klabbers, A. Lanaro, K. Long, R. Loveless, T. Ruggles, A. Savin, V. Sharma, N. Smith, W.H. Smith, N. Woods

†: Deceased
1: Also at Vienna University of Technology, Vienna, Austria
2: Also at Skobeltsyn Institute of Nuclear Physics, Lomonosov Moscow State University, Moscow, Russia
3: Also at IRFU, CEA, Université Paris-Saclay, Gif-sur-Yvette, France
4: Also at Universidade Estadual de Campinas, Campinas, Brazil
5: Also at Federal University of Rio Grande do Sul, Porto Alegre, Brazil
6: Also at Université Libre de Bruxelles, Bruxelles, Belgium
7: Also at University of Chinese Academy of Sciences, Beijing, China
8: Also at Institute for Theoretical and Experimental Physics named by A.I. Alikhanov of NRC 'Kurchatov Institute', Moscow, Russia
9: Also at Joint Institute for Nuclear Research, Dubna, Russia
10: Also at Cairo University, Cairo, Egypt
11: Also at Fayoum University, El-Fayoum, Egypt
12: Now at British University in Egypt, Cairo, Egypt
13: Also at Zewail City of Science and Technology, Zewail, Egypt
14: Also at Purdue University, West Lafayette, USA
15: Also at Université de Haute Alsace, Mulhouse, France
16: Also at CERN, European Organization for Nuclear Research, Geneva, Switzerland
17: Also at RWTH Aachen University, III. Physikalisches Institut A, Aachen, Germany

18: Also at University of Hamburg, Hamburg, Germany
19: Also at Brandenburg University of Technology, Cottbus, Germany
20: Also at Institute of Physics, University of Debrecen, Debrecen, Hungary, Debrecen, Hungary
21: Also at Institute of Nuclear Research ATOMKI, Debrecen, Hungary
22: Also at MTA-ELTE Lendület CMS Particle and Nuclear Physics Group, Eötvös Loránd University, Budapest, Hungary, Budapest, Hungary
23: Also at IIT Bhubaneswar, Bhubaneswar, India, Bhubaneswar, India
24: Also at Institute of Physics, Bhubaneswar, India
25: Also at Shoolini University, Solan, India
26: Also at University of Visva-Bharati, Santiniketan, India
27: Also at Isfahan University of Technology, Isfahan, Iran
28: Also at Plasma Physics Research Center, Science and Research Branch, Islamic Azad University, Tehran, Iran
29: Also at Italian National Agency for New Technologies, Energy and Sustainable Economic Development, Bologna, Italy
30: Also at Centro Siciliano di Fisica Nucleare e di Struttura Della Materia, Catania, Italy
31: Also at Università degli Studi di Siena, Siena, Italy
32: Also at Scuola Normale e Sezione dell'INFN, Pisa, Italy
33: Also at Kyung Hee University, Department of Physics, Seoul, Korea
34: Also at Riga Technical University, Riga, Latvia, Riga, Latvia
35: Also at International Islamic University of Malaysia, Kuala Lumpur, Malaysia
36: Also at Malaysian Nuclear Agency, MOSTI, Kajang, Malaysia
37: Also at Consejo Nacional de Ciencia y Tecnología, Mexico City, Mexico
38: Also at Warsaw University of Technology, Institute of Electronic Systems, Warsaw, Poland
39: Also at Institute for Nuclear Research, Moscow, Russia
40: Now at National Research Nuclear University 'Moscow Engineering Physics Institute' (MEPhI), Moscow, Russia
41: Also at St. Petersburg State Polytechnical University, St. Petersburg, Russia
42: Also at University of Florida, Gainesville, USA
43: Also at P.N. Lebedev Physical Institute, Moscow, Russia
44: Also at California Institute of Technology, Pasadena, USA
45: Also at Budker Institute of Nuclear Physics, Novosibirsk, Russia
46: Also at Faculty of Physics, University of Belgrade, Belgrade, Serbia
47: Also at University of Belgrade: Faculty of Physics and VINCA Institute of Nuclear Sciences, Belgrade, Serbia
48: Also at INFN Sezione di Pavia [a], Università di Pavia [b], Pavia, Italy, Pavia, Italy
49: Also at National and Kapodistrian University of Athens, Athens, Greece
50: Also at Universität Zürich, Zurich, Switzerland
51: Also at Stefan Meyer Institute for Subatomic Physics, Vienna, Austria, Vienna, Austria
52: Also at Adiyaman University, Adiyaman, Turkey
53: Also at Şırnak University, Sirnak, Turkey
54: Also at Beykent University, Istanbul, Turkey, Istanbul, Turkey
55: Also at Istanbul Aydin University, Application and Research Center for Advanced Studies (App. & Res. Cent. for Advanced Studies), Istanbul, Turkey
56: Also at Mersin University, Mersin, Turkey
57: Also at Piri Reis University, Istanbul, Turkey
58: Also at Gaziosmanpasa University, Tokat, Turkey
59: Also at Ozyegin University, Istanbul, Turkey

60: Also at Izmir Institute of Technology, Izmir, Turkey
61: Also at Marmara University, Istanbul, Turkey
62: Also at Kafkas University, Kars, Turkey
63: Also at Istanbul University, Istanbul, Turkey
64: Also at Istanbul Bilgi University, Istanbul, Turkey
65: Also at Hacettepe University, Ankara, Turkey
66: Also at Rutherford Appleton Laboratory, Didcot, United Kingdom
67: Also at School of Physics and Astronomy, University of Southampton, Southampton, United Kingdom
68: Also at Monash University, Faculty of Science, Clayton, Australia
69: Also at Bethel University, St. Paul, Minneapolis, USA, St. Paul, USA
70: Also at Karamanoğlu Mehmetbey University, Karaman, Turkey
71: Also at Bingol University, Bingol, Turkey
72: Also at Sinop University, Sinop, Turkey
73: Also at Mimar Sinan University, Istanbul, Istanbul, Turkey
74: Also at Texas A&M University at Qatar, Doha, Qatar
75: Also at Kyungpook National University, Daegu, Korea, Daegu, Korea
76: Also at University of Hyderabad, Hyderabad, India